11-12-2019 2:00 PM

The Role of Connexin and Pannexin Large-Pore Channels in Hearing

Julia Abitbol
The University of Western Ontario

Supervisor
Laird, Dale W.
The University of Western Ontario

Graduate Program in Anatomy and Cell Biology
A thesis submitted in partial fulfillment of the requirements for the degree in Doctor of Philosophy

Abstract

Connexin and pannexin large-pore channels allow the regulated passage of small molecules at sites of cell-cell contacts, and from the cytosol to the extracellular milieu, respectively. Since it has been known for many years that Cx26 and Cx30 gap junction proteins are crucial in hearing we propose that Cx43 might also be important in hearing. Here we used two different genetically modified mouse lines that contain systemic Cx43 gene mutations that reduces gap junctional intercellular communication (GJIC) to examine whether Cx43 is also important for proper hearing function. Furthermore, since pannexins have also been postulated to be involved in auditory function we used three different Panx global knock-out mice to evaluate their hearing profiles. We showed that Cx43 mutant mice that had severe loss of Cx43 channel function had hearing loss, while mutant mice with a modest loss of Cx43 function exhibited normal hearing. Surprisingly, $Panx1^{-/-}$, $Panx3^{-/-}$, and double knock-out (dKO) mice did not have hearing loss, suggesting that pannexins do not play an important role in hearing. To evaluate whether large-pore channels played a role in noise-induced hearing loss (NIHL), we challenged Cx43 mutant and pannexin knock-out mice with a loud noise-exposure and examined their permanent hearing loss. Interestingly, only $Panx3^{-/-}$ and Panx dKO mice were slightly protected against permanent hearing damage. Finally, organotypic cochlear cultures from Cx43 mutant mice and a CRISPR Cas9 Cx43 ablated cochlear-derived cell line, revealed that GJIC does not exacerbate drug-induced hearing loss but does cause supporting cell reorganization. Collectively, our results highlight the importance of Cx43 GJIC in hearing function, but not noise- or drug-induced ototoxicity. Furthermore, our studies support the notion that Panxs are not involved in baseline hearing, but loss of Panx3 may lead to slight protection against permanent NIHL.

Keywords

Connexin, Gap Junction, Pannexin, Connexin26, Connexin43, Pannexin1, Pannexin3, Cochlea, Hearing, Hearing Loss, Noise-Induced Hearing Loss, Auditory Brainstem Response, Noise-Exposure, Mouse Models, Drug-induced hearing loss, Ototoxicity, Cisplatin

Lay Summary

The cells of our body are in constant communication with each other to facilitate tissue health. Gap junction channels form the basis of direct cell to cell communication allowing the transfer of ions and small signaling molecules in a process known as gap junctional intercellular communication (GJIC). It has been known for many years now that GJIC is essential for proper hearing as many mutations in genes that encode connexin (Cx) gap junction proteins cause the majority of inherited hearing loss. Another large-pore channel type found in the inner ear that has been proposed to be important in hearing is made from pannexins (Panx) that allow small molecules to exit the cell. We evaluated the importance of Cx43, a poorly studied gap junction protein found in the auditory track, as well as Panx channels in baseline hearing and in noise-induced hearing loss. In mice, we found that Cx43 function was important in baseline hearing function, however, moderate levels of Cx43 function was enough to maintain proper hearing. In addition, Panxs were not found to be involved in hearing function. Loss of either Cx43 or Panx1 did not result in more or less permanent noise-induced hearing loss. Interestingly, loss of Panx3 led to a slight protection of hearing loss after a loud noise-exposure, however, the mechanisms behind this remains unknown. Cisplatin, a commonly used therapeutic agent, is effectively used to treat solid cancer tumors but results in permanent hearing loss in 75-100% of patients. Blocking and/or loss of GJIC with cisplatin treatment did not result in any differences in inner ear cell death, however, gap junction proteins were reorganized after cisplatin treatment. Overall, we examined the importance of large-pore channels in the context of three different kinds of hearing impairments including genetics, noise, and drug induced hearing loss. Interestingly, we found that Cx43 was essential for baseline hearing, but not NIHL or cisplatin-induced hearing loss. Further Panxs were not involved in any type of hearing function. These studies will directly contribute to gaining insight into molecular therapy treatments for hearing loss.

Abbreviations

°C - Degrees Celsius

µg - Micrograms

µM- Micromolar

µV- Microvolt

ABR- Auditory Brainstem Response

ANOVA- Analysis of Variance

ATP- Adenosine Triphosphate

BSA- Bovine Serum Albumin

CO_2- Carbon Dioxide

Ca^{2+}- Calcium

CM- Cochlear Microphonic

CN- Cochlear Nerve

Cx26- Connexin26

Cx43- Connexin43

DMEM- Dulbecco's Modified Eagle Medium

DNA- Deoxyribonucleic Acid

DPOAE- Distortion Product Otoacoustic Emission

dB- Decibel

dKO- Double Knock-out

E- Embryonic day

EDTA- Ethylenediaminetetraacetic Acid

EP- Endocochlear potential

ENU- *N*-ethyl-*N*-nitrosourea

FBS- Fetal Bovine Serum

g- Grams

GAPDH- Glyceraldehyde 3-phosphate dehydrogenase

G60S- Glycine to Serine substitution at amino acid position 60

Gja1- Mouse Gene Encoding Connexin43

GJA1- Human Gene Encoding Connexin43

Gjb2- Mouse Gene Encoding Connexin26

GJB2- Human Gene Encoding Connexin26

GJIC- Gap Junctional Intercellular Communication

Gly- Glycosylation State

hr- Hour

I130T- Isoleucine to Threonine substitution at amino acid position 130

IHC- Inner Hair Cell

IP- Intraperitoneal

IP_3- Inositol 1,4,5- Triphosphate

K^+- Potassium

kDa- KiloDalton

KD- Knock-down

kHz- Kilohertz

KID- Keratitis-ichthyosis-deafness Syndrome

KO- Knock-out

mRNA- Messenger Ribonucleic Acid

ms- millisecond

O_2- Oxygen

OC- Organ of Corti

ODDD- Oculodentodigital Dysplasia

OHC- Outer Hair Cell

P- Postnatal Day

Panx1- Pannexin1

Panx2- Pannexin2

Panx3- Pannexin3

Panx1- Mouse Gene Encoding Panx1

PANX1- Human Gene Encoding Panx1

PBS- Phosphate Buffered Saline

PBST- Phosphate Buffered Saline with Tween

PCR- Polymerase Chain Reaction

SDS- Sodium Dodecyl Sulfate

SEM- Standard Error of the Mean

SPL- Sound Pressure Level

SGN- Spiral Ganglion Neuron

TMX- Tamoxifen

WT- Wildtype

Co-Authorship Statement

The work contained herein was carried out by the author, under the supervision of Dr. Dale Laird and the collaboration and advice of Dr. Brian Allman. This includes conception, project design, implementation, data analysis and preparation of manuscripts.

Chapter 2

John J. Kelly assisted in technical training, analysis and interpretation of data.
Kevin Barr assisted in mouse breeding and maintenance of animal colonies.
Ashley L. Schormans assisted in set up of experimental apparatus.

Chapter 3

Brooke L. O'Donnell performed the expression analyses skin and hindlimb of Panxs (Figure 3), and histological analyses of the skin and paw (Figure 4).
Brent C. Wakefield performed qPCR and protein expression of Panxs in the skin (Figure 2).
Elizabeth Jewlal performed skull morphometric data collection and analysis (Figure 5) and histological analysis of bones (Figure 6).
John J. Kelly assisted in student training and western blot analysis of skin.
Kevin Barr assisted in mouse breeding and generated dKO mice by breeding $Panx1^{-/-}$ and $Panx3^{-/-}$ together then selecting for dKO mice.

Chapter 3 involved a collaboration between many labs including; the Penuela, Allman, and Willmore labs. Dr. Katherine Willmore provided funding and expertise on skull and bone morphometric data. Dr. Silvia Penuela was the corresponding author, provided expertise in skin and hindlimb studies, and provided funding. Dr. Brian Allman provided funding, and assisted in interpretation and analysis of hearing data.

Chapter 4

John J. Kelly assisted in training of organotypic cochlear techniques.
Kevin Barr assisted in mouse breeding and maintenance of mouse colonies.

Chapter 5

Rianne Beach performed all cell culture experiments of HEI-OC1 cells (Figure 5, and supplemental figures 4 and 5).
Jessica Esseltine assisted in the creation of Cx43-ablated HEI-OC1 cells.
Kevin Barr assisted in mouse breeding and maintenance of mouse colonies.

Acknowledgments

The past five years I've been blessed to have the most amazing support system from family and friends, during my graduate studies. First and foremost, I'd like to thanks my parents, Carmela and Emmanuel, for their unconditional love that they've given me throughout my life. Thank you for always being there for me and for your constant love, encouragement, and support. This would not have been possible without either of you.

I would like to thank my supervisor Dale Laird for his mentorship throughout my time in the Laird lab. Your mentorship, trust, and advice have truly let me grow as a scientist, as a leader in the community, and has helped me develop communication skills that I will use throughout my life. Thank you for always having an open door and helping me along the way with all of my successes. It truly was a privilege to be part of your lab.

I have also had the good fortune to collaborate with many labs throughout my studies and would like to thank Dr. Brian Allman for his willingness to allow me to conduct studies in his lab and for his dedication to assist in driving my research forward. I would also like to thank Dr. Silvia Penuela for the opportunity to collaborate and work with your lab, thank you for your expertise, time, and mentorship throughout my studies.

I would like to thank all past and present members of the Laird lab that I have had the pleasure of working with throughout the years. To Kevin and Cindy, thank you for being the backbones of the lab and your constant dedication. Thank you Kevin for all of your help from breeding mouse colonies to troubleshooting, and being my go-to person in the lab. I would also like to thank Dr. John Kelly who trained me in my early days in the lab, thank you for your patience, expertise, and your friendship throughout the past years.

Thank you to my supervisory committee; Dr. Brian Allman, Dr. Shawn Whitehead, Dr. Arthur Brown, and Dr. John Kelly for providing excellent feedback and advice that has always elevated my research. I would like to thank the Anatomy and Cell Biology department as well as both the past and present administrative staff for help throughout my studies. Finally, thank you to the Natural Science and Engineering Research Council for providing me with funding in the form of a doctoral scholarship for the past three years.

Table of Contents

List of Tables

List of Figures

List of Supplementary Figures

Chapter 1 Introduction

1.1. Hearing loss

Hearing loss remains one of the most prevalent chronic conditions faced worldwide. The World Health Organization estimated that as of 2019 approximately 466 million people worldwide have disabling hearing loss with a projection of reaching over 900 million people by 2050. The majority of hearing loss cases are sensorineural where the sensory receptors of the inner ear, the hair cells, or their connected auditory neurons are damaged [1]. Age-related hearing loss is extremely common where most people over 50 years old incur some degree of hearing loss [2]. Approximately 80% of congenital hearing loss is due to genetic mutations, while the other 20% is due to environmental factors, such as exposure to loud noises or ototoxic drugs that induce hearing loss [3]. In addition, 70% of hearing loss cases are non-syndromic, where the patient does not have any other symptoms other than hearing loss, and the other 30% of cases are syndromic, where patients will have other symptoms in addition to hearing loss such as skin disease or blindness [3]. Hearing loss can be encompassed by three broad categories; genetically acquired, noise-induced, and drug-induced, all of which are of particular interest in this thesis.

Hearing loss can be genetically inherited and identified at birth where mutations in many genes that are important for hearing (*SLC26A5* encoding Prestin, *Myo15A* encoding Myosin, and *OTOG* encoding Otogelin), including connexin encoding genes, cause hearing loss [4,5]. Collectively, there have been over one hundred different genes identified that underlie non-syndromic hearing loss [6]. When a child is first born with hearing loss they will be genotyped for mutations in common genes involved in hearing loss, such as *GJB2* encoding Cx26, *SLC26A4* encoding Pendrin, and *OTOF* encoding Otoferlin, to name a few; which can be used to help guide a treatment plan for the patient [4,7]. The most common hearing loss locus lies within chromosome 13q12 where DFNB1 is found. DFN refers to deafness, B refers to recessive, and 1 refers to the order the gene was identified. DFNB1 codes for *GJB2* (Cx26) where mutations account for approximately 50-60% of genetically acquired hearing loss [8]. In this thesis, we will focus on other connexin genes that are expressed in the inner ear and may also be involved in genetically inherited hearing loss.

Noise-induced and drug-induced hearing loss involves hearing impairment as a consequence of exposure to loud noise or ototoxic drugs, respectively, and will be discussed in more detail

in later sections. Generally, hearing loss treatment is limited to either hearing aids for mild to moderate hearing loss or cochlear implants for more severe cases [9,10]. Hearing aids are used to enhance the amplification of external sound into the inner ear and thus relies on a residual level of hair cell function [11]. For more severe hearing loss cochlear implants are used which directly bypasses the hair cells and stimulates auditory nerves, thus eliminating the need for functional hair cells [11]. Going forward the research community needs to understand the molecular mechanisms underpinning hearing loss in order to drive potential molecular therapies. This thesis will involve chapters examining genetic-based, noise, and drug-induced hearing loss with an emphasis on the role of large-pore channels that includes connexins and pannexins.

1.2. Anatomy of the inner ear

The intricate process of inner ear development leads to the formation of a mature organ of Corti; the sensory epithelium of the cochlea. In humans the onset of hearing is approximately 5-6 months *in utero* [12] while physiological hearing of mice is acquired at approximately P10-P14 [13,14]. The cochlea consists of approximately 3 turns; apical, middle, and basal regions which are tonotopically organized so that different frequency selectivity is represented at different regions along the length of the cochlea. Apical, middle, and basal regions represent low, mid, and high frequency ranges of hearing, respectively [15]. In examining a cross sectional area of the cochlea, key anatomical structures are observed (Figure 1.1). The cochlear lateral wall consists mostly of fibrocytes within the spiral ligament and the stria vascularis, an important structure in maintaining proper endolymphatic potential, (+100mV) in the endolymphatic space, that is necessary for proper hearing [16]. The stria vascularis houses three different cell layers; the marginal, intermediate, and basal cells which encompasses the blood vessels responsible for nourishing the cochlea [16]. The epithelial region of the organ of Corti (Figure 1.1B) consists of the sensory receptors of hearing, the hair cells, that are depolarized in response to K^+ influx through their mechanoelectrical transducer channels and relay information to the higher order auditory system [17].

Figure 1.1. Anatomical structure of the cochlea.

Cross sectional area of the inner ear. (A) Cross section of the cochlear duct showing the anatomical arrangement of the cochlea with all main structures labelled. Red cells represent cells of the connective tissue gap junction network and green cells represent cells of the epithelial gap junction network. Boxed area represents region highlighted in (B). Figure obtained with permission from Jagger et al. 2010. (B) Schematic of the epithelial region of the cochlea and all cell types associated within this region. Sensory receptor hair cells are shown in black and all cochlear supporting cells are annotated in different colors.

Figure 1.1.

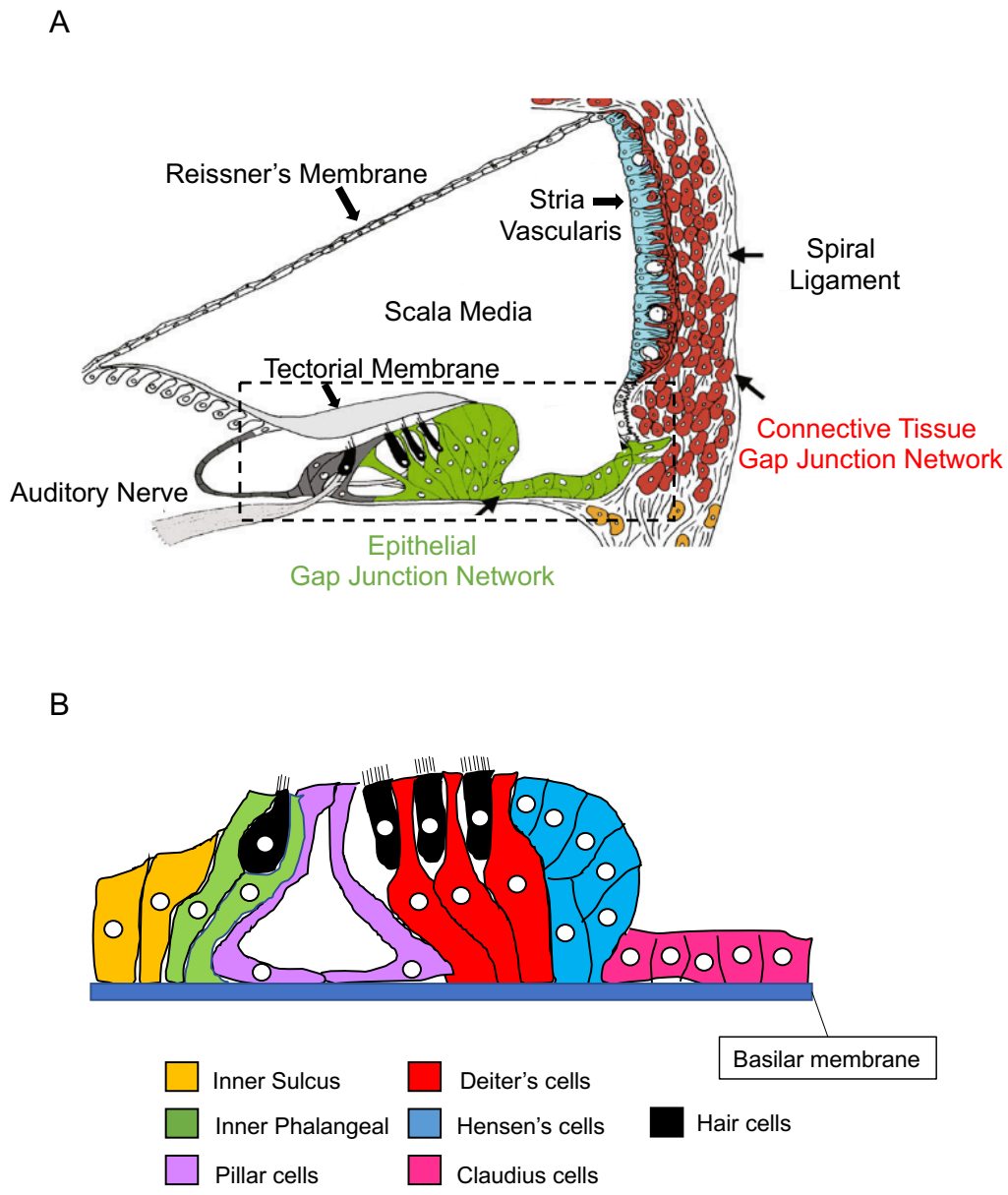
A
Reissner's Membrane
Stria Vascularis
Spiral Ligament
Scala Media
Tectorial Membrane
Connective Tissue Gap Junction Network
Auditory Nerve
Epithelial Gap Junction Network
B
Basilar membrane
Inner Sulcus
Deiter's cells
Inner Phalangeal
Hensen's cells
Hair cells
Pillar cells
Claudius cells

The hair cells are surrounded by many supporting cells which maintain the structure and integrity of the organ of Corti. Deiter's cells are located directly under the outer hair cells (at a 1:1 ratio) and have long phalangeal processes so they may stretch from the basilar membrane to the reticular lamina [18]. The pillar cells act as structural support to maintain the open tunnel of Corti as well as the thickness of the epithelium. Both inner and outer pillar cells are closely associated with the inner and outer hair cells, respectively, and act to provide structural support to the organ of Corti [19]. Hensen's cells, which are columnar in nature, as well as Claudius cells form the outer sulcus region of the epithelium and lie adjacent to the outer hair cells [19]. The inner phalangeal cells act as support to the inner hair cells and together with the inner border cells form the inner sulcus region of the epithelium [19]. Supporting cells of the cochlear epithelium act to give structure to the epithelium and to maintain metabolic support for the organ of Corti as well as the hair cells.

1.3. Connexins and gap junctions

Connexins (Cxs) are integral membrane proteins that form gap junctions which allow intercellular exchange of small members of the metabolome that are less than 1 kDa in size [20,21]. Each connexin subunit passes the plasma membrane four times and is comprised of two extracellular loops (E1, E2), one intracellular loop (IL), as well as an amino and carboxyl terminus that faces the cytosol. The topology of connexins is crucial for channel gating and selectivity of transjunctional molecules [22]. To date, 21 and 20 different connexin encoding genes have been identified in the human and mouse genomes, respectively, and each connexin is named according to their molecular weight (eg. Cx43= 43 kDa) [21,23]. Connexins are co-translationally integrated into the endoplasmic reticulum where they are then trafficked to the Golgi apparatus of the cell. Some connexins oligomerize in the ER (e.g., Cx26) while others, such as Cx43, oligomerize in the Golgi into hexameric structures called connexons that then traffic to the plasma membrane of the cell [24,25]. Once at the cell surface, it is thought that connexons typically remain closed under normal physiological healthy cell conditions [26,27]. However, recent evidence suggests that connexons can function as hemichannels in some dysregulated or pathological conditions allowing passage of small molecules between the cytosol and the extracellular space [28,29]. A gap junction channel is formed when a connexon from one cell docks with a compatible connexon from an adjacent cell establishing a point of

intercellular communication. The gap junction channels proceed to cluster together to form large gap junction plaques where hundreds to thousands of channels are found [21,30].

Gap junctional intercellular communication (GJIC) is critical in early embryonic development as well as in many important physiological processes such as cell proliferation, differentiation, and apoptosis [31–33]. Because of the complex nature of gap junctions and cell-cell communication, cells need to be able to regulate their ability to exchange molecules and ions in response to varying physiological processes. To do this, gap junctions are rapidly degraded after internalization as connexosomes by subsequently fusing with lysosomes [21,34]. Other pathways of connexin clearing from the cells surface may exist but these are not well elucidated. In most tissues, the half-life of connexins is approximately 1.5-5 hours which allows for the quick and dynamic regulation of gap junctions necessary for efficient and well-regulated cell-cell communication [35–38].

Another means of regulating GJIC is via rapid channel gating. For example, voltage gating mechanisms exist where the channel conductance is sensitive to transjunctional and transmembrane voltages [39,40]. It is also important to note that gap junction channels exhibit subconductance states where the channel can remain in a partially opened or partially closed state [40]. These subconductance states enable the gap junction channel to have different selective permeability properties where the passage of larger members of the metabolome, such as secondary messengers in some cases, is reduced [40]. In order to fully appreciate the complexity of gap junction channels it is important to note that most cells/tissues in the human body express multiple connexin isoforms allowing for the possibility of structural diversity in channel constituents. Gap junctions can be composed of homomeric or heteromeric oligomers which consists of either the same or different connexin isoforms, respectively [41,42] (Figure 1.2). For example, it has been well documented that Cx26 and Cx30 can form heteromeric channels in tissues co-expressing these connexins as seen in the inner ear [43–45].

Figure 1.2. The structure and oligomerization compatibility of connexins

(A) Structural topology of a connexin subunit with four α-helical transmembrane domains, two extracellular loops (ECL), an intracellular loop (IL), cytoplasmic amino terminal (AT), and carboxy termini (CT). (B) Connexins oligomerize to form hexameric channels and are categorized into different groups based on structural homology. Figure obtained with permission from Laird and Lampe, 2018.

Figure 1.2.

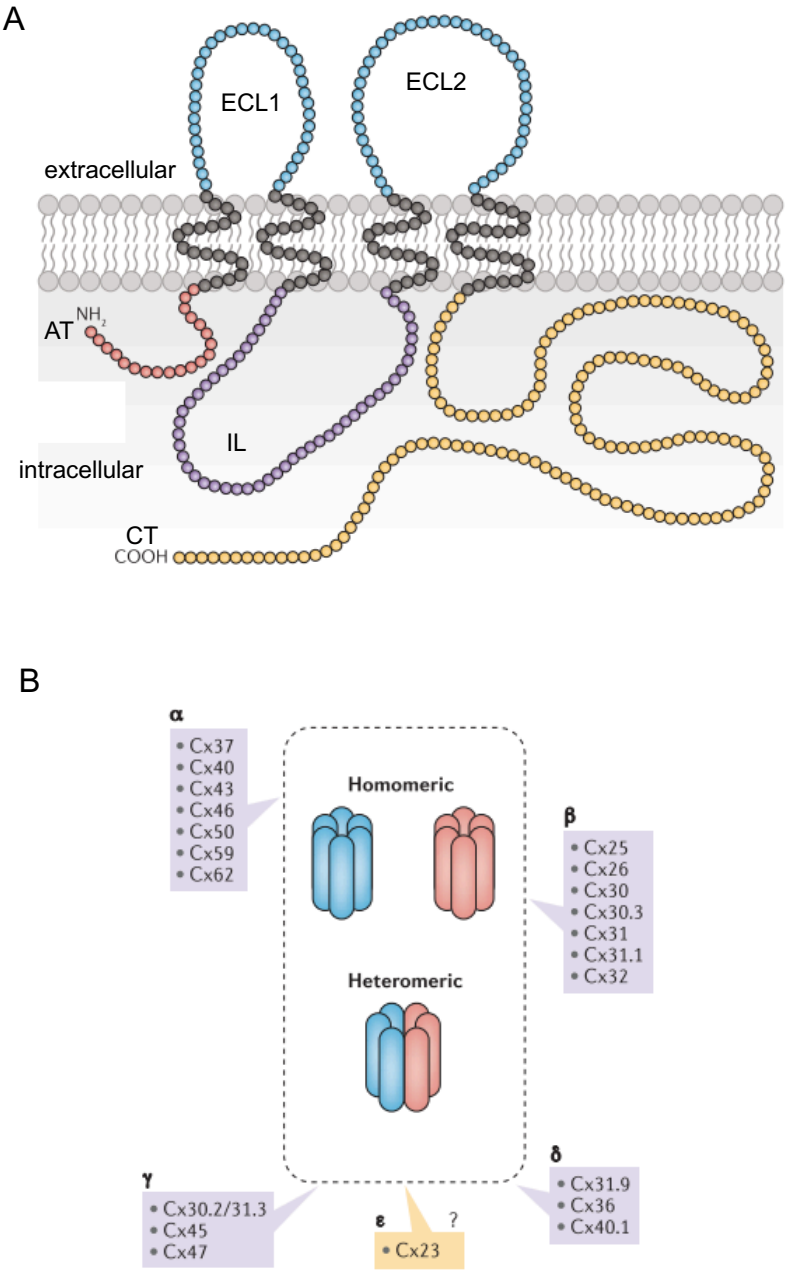
A
ECL1
ECL2
extracellular
AT
NH2
IL
intracellular
CT
COOH
B
α
• Cx37
• Cx40
• Cx43
• Cx46
• Cx50
• Cx59
• Cx62
Homomeric
Heteromeric
β
• Cx25
• Cx26
• Cx30
• Cx30.3
• Cx31
• Cx31.1
• Cx32
γ
• Cx30.2/31.3
• Cx45
• Cx47
ε
?
• Cx23
δ
• Cx31.9
• Cx36
• Cx40.1

Further, once connexons are formed they can also dock together to form a gap junction channel with different connexons from the opposing cell establishing heterotypic channels [42,46]. These different channel configurations can lead to distinct characteristics such as channels with unique conductance, gating properties, and transjunctional permeabilities [47].

1.4. Pannexin large pore channels

In the year 2000, a novel family of channel forming proteins called pannexins (Panxs) were discovered due to their sequence homology to the invertebrate gap junction proteins, innexins [49,51]. However, pannexins do not share similar sequence homology to the connexin gene family found in vertebrates [50]. Compared to connexins, the pannexin family is much smaller and comprised of only three members; pannexin1 (Panx1), pannexin2 (Panx2), and pannexin3 (Panx3) [51,52]. Structurally, pannexins pass the membrane four times and have two extracellular loops (EL1 and EL2), one intracellular loop (IL), transmembrane domains (TM1-TM4), and an amino and carboxy terminus that faces the cytosol (Figure 1.3A) [53,54]. Pannexins oligomerize and traffic to the cell surface where they can allow small molecules and ions of less than 1kDa in size to pass from the intracellular to the extracellular milieu (Figure 1.3B) [55,56]. Further, Panxs undergo posttranslational modification of glycosylation at asparagine residues present in their extracellular loops [57].

Panx1 is the most well characterized of the three family members and is ubiquitously expressed throughout the body including in the muscles, central nervous system, eye, inner ear, and olfactory epithelium [53,58–61]. Panx2 was originally shown to be mostly distributed in the central nervous system, however, recent studies have reported a wider distribution of Panx2 such as the skin, eye, small intestine, and heart [49,62,63]. Panx3 is mainly found in high abundance within the skin, cartilage, and bone, although recent studies have reported low levels of Panx3 mRNA transcripts in hippocampus and low levels of protein expression in the ventricles of the heart [49,64].

Figure 1.3. The structure of pannexin channels

(A) Prototypical topology of Panx1, Panx2, and Panx3 having four α-helical transmembrane domains, two extracellular loops (ECL), an intracellular loop (IL), cytoplasmic amino terminal (AT), and carboxy termini (CT). Figure obtained with permission from Penuela et al. 2013. (B) Upon arrival at the plasma membrane pannexin channels function as single membrane channels. Figure obtained with permission from Penuela et al. 2014.

Figure 1.3.

A

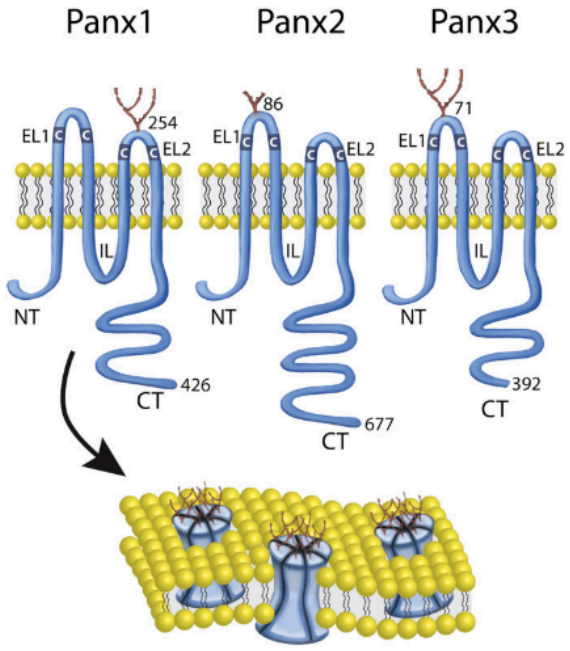

B

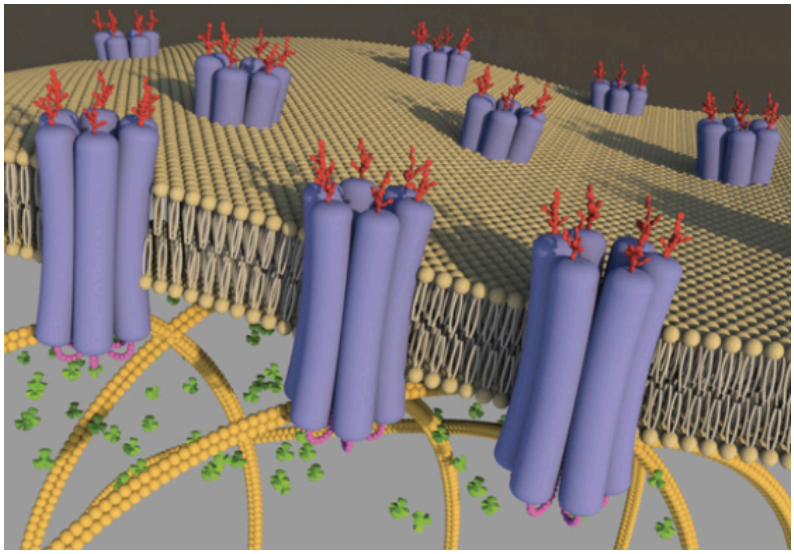

The majority of studies have shown that Panxs form single membrane channels. In fact, only a few reported cases have suggested that Panxs can form gap junction channels and these studies focused mainly on over-expression systems in non-mammalian cell cultures [65–67]. Most laboratories now concur that Panxs are unable to form gap junction channels, a conclusion based on a plethora of functional studies performed in various cell types such as MDCK, N2A, erythrocyte, neuronal, and glial cells [64,68–70]. The glycosylation of Panxs also makes it unlikely that they dock together to form gap junction channels due to the expected hindrance imposed by the glycosylated moieties [68,71]. Additionally, Panx channels do not cluster and pack to form semi-crystalline structures as seen in connexin gap junctions. Further, pannexins do not share the same complement of cysteine residues in the extracellular loops as seen in connexins suggesting that these differences may further impact pannexin folding and assembly properties [49,51,54,68,72]. Thus, most of the evidence points to Panxs forming single membrane channels at the plasma membrane that are tightly regulated in their ability to release small molecules from cells [73,74].

The regulation of Panx1 channel function has been shown to be activated through various mechanisms including: increased extracellular ATP, increased intracellular Ca^{2+}, increased extracellular K^{+}, cell depolarization, voltage changes, P2X7-mediated activation, and mechanical stimulation [75–80]. In addition, Panx1 channels can be irreversibly opened by the cleavage of the C-terminal tail by caspase3 [81,82]. Once opened, Panx1 channels have been shown to release ATP which can lead to purinergic signaling, Ca^{2+} wave propagation, and recruitment of macrophages to initiate apoptosis [52,81,83]. Panx1 channels also allow the passage of small molecules up to 1 kDa in size including UTP, and dyes such as To-Pro [81,84]. The channel is thought to be negatively regulated by a feedback loop where ATP can bind to the extracellular loop to prevent further ATP release [85]. One of the main goals of this thesis is to investigate the importance of Panxs in hearing function.

1.5. *GJB2* mutations in hearing loss

The ubiquitous expression of different connexin isoforms within the human body makes it unsurprising that there are many diseases caused by connexin gene mutations [86]. Currently, ten different connexin family members have mutations that cause twenty-eight different human-linked diseases that have been identified, with hearing loss being the most prevalent

[87]. Connexin gene mutations linked to hearing loss may be inherited in either an autosomal recessive or dominant manner, and may present with hearing loss as the only symptom (non-syndromic) or also be associated with additional phenotypes such as skin disease (syndromic) [88]. Clinically, mutations in *GJB2* (encoding Cx26) and *GJB6* (encoding Cx30) are responsible for nearly 50-60% of congenitally acquired sensorineural hearing loss [5,8]. In Canada, approximately 1-2 in 2000 children will be born with hearing impairment due to an inherited Cx26 gene mutation, leading to an estimated 35,000 Canadians that suffer from Cx-linked congenital hearing loss [8,87]. Consequently, in developed countries, if a child is born with a hearing impairment they will first be genotyped for both loss- and/or gain-of function *GJB2* gene mutations of which currently there are approximately 135 different ones [5,87]. The most common Cx26 mutation in European and North American populations is the 35delG deletion of a single guanine nucleotide resulting in a frameshift and premature termination of protein translation. This mutation has a carrier frequency of approximately 2-4% in the human population [8,89].

Hearing loss-linked Cx26 mutations can be placed into two broad categories where they may either produce a loss-of function or gain-of-function phenotype. First, loss-of-function mutants can result in defective trafficking to the plasma membrane, misfolding and retention in intracellular compartments, defective interactome binding, or the formation of non-functional hemichannels or gap junctions [90]. The majority of non-syndromic recessive Cx26 mutations that cause hearing loss are grouped into this category and many of these have been studied *in vitro*. For example, N14D, G59A, D66H, R143W, and R184P mutants are unable to form gap junction channels at the plasma membrane [91–95]. G12R, N14K, R75W, W77R, and L214P mutants are able to traffic to the plasma membrane but form non-functional gap junction channels [95-98]. N14Y, V84L, R127H, and N206S mutants alter the biochemical coupling of gap junction channels formed [99–102]. On the other hand, gain-of-function mutants can cause aberrant oligomerization with non-compatible connexins, interact with different binding partners, and increase hemichannel and/or gap junction channel function [87,90]. Interestingly, syndromic Cx26 mutants that are associated with skin diseases fall into this category such as the S17F, G45E, D50N, and M163L mutants where they have abnormal hemichannel opening [97, 103-104]. Although these studies have been conducted in overexpression systems *in vitro*, the trafficking patterns and function of these mutants has yet to be examined in a cochlear

relevant cell line. Collectively, each Cx26 mutation has a distinct mechanism of action on gap junction function, with the majority being loss-of function mutants either not trafficking to the plasma membrane or forming non-functional gap junction plaques. Discovery of how each mutation affects the fate of Cx26 will provide insight as to the possible types of intervention that can be implemented in human patients.

1.6. Cx43 and oculodentodigital dysplasia

Oculodentodigital dysplasia (ODDD) was the first human disease found to be linked to mutations in *GJA1*, encoding for Cx43 [105]. The ODDD locus was originally mapped to human chromosome 6q22-q24, close to where the *GJA1* gene is found on chromosome 6q21-23.2 [106]. Over 80 different Cx43 gene mutations have been linked to ODDD and most are inherited in an autosomal dominant manner, with the exception of a few cases that exhibit autosomal recessive inheritance [107,108]. Cx43 is the most ubiquitously expressed gap junction protein in the human body, thus it is not surprising that patients with ODDD have many different symptoms. Patients with ODDD generally present with more common symptoms such as cranial facial abnormalities, deformities of teeth and eyes, as well as syndactyly and fusion of digits [105,109]. In addition, patients may also exhibit more rare symptoms such as neuropathies, skin diseases, bladder incontinence, and hearing loss (which is of particular interest in this thesis) with a wide range of phenotypic variability [109–112]. Attempts to study the role of Cx43 in tissue and organ development have been hampered by the fact that Cx43 knock-out mice are embryonically lethal due to defects in the cardiovascular system [113]. However, novel insights into the role of Cx43 in organogenesis have benefited from the use of Cre-flox mice where Cx43 can be specifically and conditionally eliminated from targeted cells/tissues and organs. For the studies performed in this thesis we have relied on the use of mutant mice that model ODDD where Cx43-based gap junctional coupling is either moderately or severely compromised. Whether hearing loss is evident in mouse models of ODDD was evaluated in this thesis.

1.7. Inner ear development

In mice, the otic placode, a thickening of the ectoderm, is the structure that develops into the inner ear and begins to form at E8-8.5 [114]. During development, the otic placode proceeds to invaginate to form the otocyst which will pinch off from the ectodermal surface at E8.5-9.5.

In humans, the otic placode forms and subsequently invaginates at approximately 4 weeks in utero [114]. The developed otocyst must then differentiate into the different portions of the inner ear and the organ of Corti that harbours the sensory receptors of the inner ear. This process includes a period of cell proliferation within the prosensory domain followed by differentiation of the post-mitotic progenitor cells into hair cells and supporting cells [115].

At E12.5 in the mouse, the prosensory domain is established where Notch1, Jagged1, and Sox2 transcription factors are expressed in all cells of the cochlear epithelium [116,117]. P27Kip1, an inhibitor of cell proliferation, is expressed in the epithelium apex at E12.5 prior to being expressed at the epithelium base by E14, creating a wave of terminal cell cycle division [118,119]. This stage defines the "Zone of nonproliferating cells; ZNPC" [118] from which different transcription factors mediate their cell fate into either hair cells or supporting cells. The differentiation of both hair cells and supporting cells in the organ of Corti begins between E13 and E14 starting at the basal region of the cochlea and over the next 4 days spreads towards the apex [120,121]. Thus, the first cells that terminally exit the cell cycle (from apex) are the last to differentiate and vice versa. Fate mapping studies, creation of genetically modified mice, as well as recently acquired single cell analyses of the organ of Corti have provided an understanding of specific transcription factors that are involved in determining both hair cell and supporting cell specific factors [122–124]. The two different gap junction networks of the cochlea are developed at E16 and P0 within the mouse cochlea [125].

1.7.1. Specification of hair cell fate

ATOH1, a basic helix-loop-helix transcription factor, is the earliest and most crucial transcription factor involved in cells destined for a hair cell fate. Mice with loss of *Atoh1* do not develop hair cells [121] and Atoh1 overexpression in the inner ear is sufficient to induce ectopic hair cells [126,127]. Atoh1 mRNA is expressed at E13.5 in cells of the sensory epithelium and at E16.5-E18 the Atoh1 positive cells express Delta and Jagged2 mRNA, other hair cell specific markers [116,128–130]. At E17, only the four rows of hair cells express Atoh1 and the surrounding cells turn off Atoh1; a process that designates their fate as supporting cells [128]. Between P0-P3, hair cell fate genes *Atoh1*, *Delta*, and *Jagged1* are downregulated and by P7 are no longer expressed as progenitor cells are fully committed hair cells at this point [128, 130]. There is currently no evidence to suggest that connexins or pannexins are involved

in designating hair cell fate and they are not expressed in hair cells [132-135]. Additionally, there is no GJIC between hair cells and supporting cells [136].

1.7.2. Specification of supporting cell fate

As hair cell differentiation proceeds, expression of two Notch effectors *Hey1* and *Hey2* become restricted to supporting cells [137]. Supporting cell fate is initiated by inhibition of Notch signaling within lateral compartments of epithelial cells, where progenitor cells surrounding hair cells are prevented from becoming hair cells [116,128,138]. In the same manner, *Hey1* and *Hey2* act as transcriptional repressors to repress hair cell differentiation of progenitors, specifically the suppression of *Atoh1*; ultimately allowing for supporting cell fate determination [137,139]. At E16-E17, *notch1*, *Jagged1*, $p27^{kip1}$, *Prox1*, *Sox2*, and *Hes5* are localized specifically to supporting cells [117,131,140,141]. An important transcription factor in supporting cell fate determination, Sox2, is expressed in the initial prosensory domain of the epithelium and is retained exclusively in supporting cells of the mature cochlea [142]. Cx26 and Cx30 are first expressed around E16, after supporting cells have already been fated, where they start to form a gap junction network within supporting cells of the epithelium. Once hair cells and supporting cells are fated, they then undergo postnatal maturation. Although connexins and pannexins are not involved in designating supporting cell fate, connexins are crucial in postnatal inner ear development as conditionally ablating connexins in early postnatal development leads to malformation of the organ of Corti and hair cell loss [143–145].

Recent studies using tamoxifen inducible mouse models have highlighted the importance of Cx26 in early cochlear development as knocking down Cx26 at P0 and P7, led to severe hearing loss and cochlear malformation while knocking down Cx26 at P8 and P30 did not cause any hearing loss and produced a normal organ of Corti [145–147]. Further, a study using varying doses of tamoxifen to create “high”, “mid”, or “low” Cx26 knock-down groups showed that hearing loss was severe, mild, and not observable in each respective group [143]. Collectively, these key studies suggest that connexins are involved in early cochlear development after progenitor cells have already been fated, and that they are crucial for proper organ of Corti formation and hearing in early but not later postnatal developmental stages.

1.8. Connexin expression in the inner ear

Gap junctions of the mature inner ear assemble into two independent networks, the epithelial and the connective tissue gap junction networks, both predominantly expressing Cx26 and Cx30 [132,148]. The epithelial gap junction network is formed at E16 and is composed of all supporting cells of the organ of Corti whereas the connective tissue gap junction network (formed at P0) is localized in the cochlear lateral wall and includes strial basal and intermediate cells, and fibrocytes in the spiral limbus [132,149]. In addition, other Cx family members including Cx31, Cx30.3, Cx32, and Cx43 are expressed in the inner ear, albeit at lower levels then the predominant isoforms Cx26 and Cx30 [45,150]. The expression patterns of the less abundant Cx isoforms are as follows; Cx29 (a Cx isoform only found in mice) is expressed within supporting cells surrounding spiral ganglion neurons [151], Cx31 is expressed in fibrocytes of the spiral ligament [152], Cx30.3 has been reported in the spiral limbus and spiral ligament [153], and Cx32 is expressed in the cochlear nerve region [151]. Cx43 localization is described in the next section. Importantly Cx hemichannels composed of Cx26 and/or Cx30 in the inner ear have also been reported in the cochlea through the use of extracellular loop specific antibodies. Using this approach, both Cx26 and Cx30 have been localized to the apical regions of cochlear supporting cells of the organ of Corti facing the endolymph [154]. Although homomeric Cx26 and Cx30 gap junctions are found in the cochlea, immunoprecipitation and immunofluorescent studies have shown that Cx26 and Cx30 form heteromeric mixed channels [43,44,155,156]. However, a recent study showed that in the human cochlea Cx26 and Cx30 were mostly located in separate gap junction plaques [157].

1.8.1. Cx43 in the inner ear and hearing

Cx43 is the most ubiquitously expressed Cx found within the body and has been reported to be expressed in many different regions of the auditory system depending on developmental time point and species [158,159]. In the young mouse, Cx43 expression has been found in the spiral limbus, connective tissue gap junction network and weakly in the epithelial gap junction network up until approximately P7 [158,160]. In the adult mouse, Cx43 expression was mostly found in the cochlear bone and in the higher order auditory brainstem regions [158,159]. In rats, Cx43 has been documented in supporting cells of spiral ganglion neurons from P0-P14 [161] and then in adult rats is redistributed to supporting cells in the organ of Corti, in the stria vascularis, and the spiral limbus [162,163]. In guinea pigs, Cx43 was reported to be expressed

in cells surrounding spiral ganglion neurons [164], while in the human fetal cochlea Cx43 is found in fibrocytes of the cochlear lateral wall [165]. Taken together, these studies suggest that the localization profile of Cx43 may differ depending on species and age. With the hopes of elucidating the functional role of Cx43 in hearing, a study examining Cx43 in slice preparations of the inferior colliculus of the auditory brainstem tract found that Cx43 formed a glial like syncytium allowing for rapid dye transfer through Cx43 gap junctions, indicating GJIC within this region [166].

Although Cx43 is localized within distinct regions of the auditory tract, its role in physiological hearing was unknown at the beginning of my studies and is one of the central themes examined in this thesis. In a small cohort of patients two different Cx43 mutations, L11F and V24A were associated with non-syndromic hearing loss [160]. However, it was later identified that these mutations were found in the *GJA1* pseudogene on chromosome 5 [105], where other Cx43 hearing loss-linked mutations have also been found [167]. In a patient cohort from Taiwan, two patients with hearing loss were found to have a Cx43 T326S mutation [167]. Overall, these data suggest that both the localization and function of Cx43 in the auditory system warrants further investigation.

1.9. Mouse models used to assess connexins in hearing loss

Due to the fact that Cx26 knock-out mice exhibit embryonic lethality [168] and mutations in Cx26 cause the vast majority of congenital hearing loss, genetically modified mice from conditional knock-out mice or mice harbouring specific human linked missense mutations have greatly enhanced our knowledge of the importance of gap junctions in hearing. Table 1 includes a complete list of Cx26 conditional and missense mouse models created and their specific auditory phenotypes.

1.9.1. Conditional knock-outs using cochlear-specific Cre mice

Cre mice using different cochlear-specific transcription factors have been used to cross Cx26 floxed mice; creating Cx26 knock-out models specific to different cochlear regions. This approach alleviates the embryonic lethality of Cx26 knock-out mice by specifically deleting Cx26 in different cochlear regions while maintaining Cx26 expression elsewhere.

Table 1.1. Genetically-modified mice used to assess Cx26 in hearing

Mouse Model	Phenotype	ABR	EP/DPOAE	Reference
$Cx26^{fl/fl}$ x Otog-Cre	P14: IHC and SC loss P15-P16 onwards: OHC and SC loss, OC collapse	3-12 weeks: Elevated by ~30-40dB across frequencies	P12-P13: similar EPs Adult: EP decreased by 60%	[149]
$Cx26^{R75W/+}$	P14: OC collapse, deformed supporting cells 7 weeks: degeneration of OC, HCs and spiral ganglia	2 and 7 weeks: Elevated by ~70dB	No change	[169]
$Cx26^{fl/fl}$ x RosaCreER TMX at E19	P8 onwards: SC degeneration P14: OHC loss -Delayed postnatal development	P21: Elevated by ~30-50dB Further at 2 and 4 months	N/A	[170]
$Cx26^{fl/fl}$x Foxg1-Cre and $Cx26^{fl/fl}$ x Pax2-Cre	P8: degeneration of Claudius cells P13: dramatic cell death in OHCs and SCs, delayed OC development P30: cell death and SGN degeneration	Elevated by ~40-50dB	N/A	[171]
$Cx26^{S17F/+}$	No changes	Elevated by ~35dB	-129SV background reduced by 42mV -C57BL/6 background reduced by 25mV	[172]
$Cx26^{fl/fl}$ x Sox10-Cre	P30:Degeneration of sensory epithelium ,HC loss Loss of SGNs	Elevated by ~70dB across frequencies	Decreased by 66%	[173,174]
$Cx26^{fl/fl}$ x Pax2-Cre	P12, P18, and P21: Loss of OHC stereocilia and cuticular plate damaged	N/A	N/A	[175]
$Cx26^{fl/fl}$ x Prox1-CreER TMX at P0	No substantial HC loss, no SGN degeneration	Elevated by 10-50dB across frequencies and progressively	Normal EP DPOAE: Similar at 4kHz but decreased at 16 and 24kHz	(Zhu et al., 2013) [177]
$Cx26^{fl/fl}$ x Rosa-CreER TMX: P1, P6, P12	Malformed OC, hair cell loss only in P1 and P6 groups SGN loss in P1 and P6 groups	P1: 40dB elevation P6: 25dB elevation	N/A	[144]

		P12: 20dB elevation		
$Cx26^{fl/fl}$ x Foxg1-CreER TMX at different ages	E19 or P4: Degeneration of OC cells and spiral ganglia, closure of tunnel of Corti P0-P8 and >P8: Decreased ribbon synapses and increased spontaneous activity	E19 and P4: Elevated by ~40dB across frequencies	N/A	[147]
$Cx26^{fl/fl}$ x P0-CreER	3 weeks: OHC morphology disrupted Disruption of gap junction plaques	N/A	N/A	[178] [179]
$Cx26^{V37I/+}$	1 year: normal cochlear morphology Minor loss of OHCs	6 weeks: 25-30dB elevation at 24 and 32kHz	N/A	[180]
$Cx26^{fl/fl}$ x Prox1-CreER TMX at E19	No cochlear abnormalities Tunnel of Corti remained open	N/A	DPOAE: similar at 13 and 22kHz but decreased at 33, 42, and 52kHz	[181]
$Cx26^{fl/fl}$ x Rosa-CreER TMX: P0 and P8	P0: Phalangeal structures of Deiter's cells did not develop properly Significant reduction of microtubules in Pillar cells Tunnel of Corti closed P8: No changes	P0: Elevated by ~40dB across frequencies P8: No changes	N/A	[145]
$Cx26^{fl/fl}$ xRosa26-CreER TMX: P0, random null group $Cx26^{fl/fl}$ x Lgr5-CreER TMX: P0, longitudinally null group	Random null group: No significant OHC loss Longitudinal null group: Significant OHC loss No significant Deiter cell or SGN loss was observed in either group	Random null group: Normal hearing Longitudinal null group: Late-onset hearing loss	N/A	[182]
$Cx26^{fl/fl}$ x Rosa-CreER TMX (different doses)	Deformed organ of Corti, and loss of Pillar cell microtubules in Mid and High knock-down groups No changes in low knock-down group	Low Cx26 KD: No change Mid Cx26 KD: 20-30dB elevation High Cx26 KD: 40-50dB elevation	DPOA: normal in Mid KD group	[143]

ABR-auditory brainstem response, DPOAE-distortion product otoacoustic emission, EP-endocochlear potential, IHC- inner hair cell, KD- knockdown, OC- organ of Corti, OHC- outer hair cell, SGN-spiral ganglion neurons, TMX- tamoxifen.

The transcription factors that have been used to create these mice include; *Otog, Foxg1, Pax2, Sox10, Prox1*, and the Protein0 (*P0*) gene transcription factors [183–187]. These transcription factors can be further divided into two subgroups where they are involved in (1) early embryonic develop of the cochlea or (2) expressed specifically in the cochlear epithelium. Foxg1, Pax2, and Protein0 transcription factors are crucial in proper embryonic development of the cochlea [183,185,187]. Foxg1 knock-out mice have shortened cochleae and multiple rows of hair cells, delineating the importance of this gene in early cochlear development [183]. Pax2 (Paired box gene 2) is also involved during embryonic development and is important for the outgrowth of the cochlear duct [185].

Protein0 is also expressed specifically in the otic vesicle and in the early development of the cochlea in rats has been shown in nonsensory areas of the embryonic inner ear [188]. Although expressed in the embryonic inner ear, it is important to note that these transcription factors are also involved in the development of other organ systems. For example, Foxg1 is essential for proper brain development especially of the telencephalon which will further develop into the brain [189]. These studies collectively show that when Cx26 is lost early on in postnatal development, the organ of Corti does not develop properly, leading to both hair cell and supporting cell loss causing hearing loss. However, when Cx26 is ablated from the inner ear in later stages of postnatal development these phenotypes are not observed, highlighting the importance of Cx26 in early cochlear development.

1.9.2. Mouse models of missense *GJB2* mutations causing hearing loss

To date three Cx26 mutant mouse models harboring human linked hearing loss mutations have been created to examine their auditory profile. First, the Cx26 R75W mutant which has been associated with Palmoplantar keratoderma-deafness (PPK) syndrome characterized by skin abnormalities (developing unusually thick skin on hands and soles of feet) and hearing loss (ranging from mild to profound in the human population) [190,191]. These mice, developed on a C57BL/6 background, had cochlear deformities including closure of the tunnel of Corti as well as severe broadband hearing loss, measured by a click stimulus, that was elevated by approximately 70 dB at both two and seven weeks of age [169]. At the functional level, the R75W mutant impairs gap junction plaque formation, which was associated with increased expression of caveolin1 and caveolin2 suggesting increased endocytosis [179]. This was found

to be a dominant negative mutant, where co-transfection of WT and Cx26 R75W into HeLa cells significantly hindered the function of WT Cx26 and WT Cx30 [93].

Next the Cx26 S17F mutation was examined in genetically-modified mice as this mutation causes keratitis ichthyosis deafness syndrome (KIDS) leading to defects of the cornea, skin defects that included red and rough thickened patches of skin, and severe hearing loss. This mutant mouse was created on both the C57BL/6 and 129Sv backgrounds and had poor survival; however, the few mutants that survived had epidermal barrier malformations, hyperproliferation of the skin, and moderate hearing loss of approximately 20-40 dB across a wide frequency range of 4 kHz to 32 kHz [172]. At the cellular level, this Cx26 mutation did not form functional gap junctions [172,192]. When co-expressed with WT Cx43, the Cx26 S17F formed functional hyperactive heteromeric hemichannels [192,193], of which under normal conditions are not compatible to oligomerize [46].

The V37I mouse was the first Cx26 mutant mouse created that is linked to recessive non-syndromic hearing loss in the human population [180]. Mutant mice, that were generated on a 129T2/SvEmsJ background, had significantly elevated hearing thresholds by approximately 15-35 dB across a wide range of frequencies from 4 kHz to 32 kHz [180]. This degree of hearing loss mimicked the degree of hearing loss found in patients harboring this mutation [194]. Hearing loss was found to be progressive over a 50 week period [180]. Interestingly, there were no cochlear morphology deficits and only minor outer hair cell loss in one year-old mice. HeLa cells transfected with this Cx26 mutation had significantly reduced coupling compared to WT Cx26 [195]; classifying this mutant as loss of function. Together, these mutant mice provide us with clinically-relevant models to study Cx26 linked hearing and show that each hearing loss-linked Cx26 mutant can have variable auditory phenotypes. As highlighted, the R75W mutant caused severe hearing loss, while the S17F and V37I mutants caused mild-moderate hearing loss. We anticipate that the evaluation of the severity and function of Cx26 mutants in mouse models will assist in providing insights into possible treatments for hearing loss in humans.

1.9.3. Mouse models of *GJB6* mutations causing hearing loss

Although the involvement of *GJB2* in hearing is crucial for hearing, the importance of *GJB6*, encoding for Cx30, in hearing has been controversial. Table 1.2 includes a list of mouse models used to study Cx30 in hearing. Currently, no *GJB6* mutations have been linked to recessively inherited hearing loss, however, three missense mutations have been associated with autosomal dominantly inherited hearing loss in the human population (T5M, G59A, A40V) [196–198]. The Cx30-T5M mutant mouse was found to have mild hearing loss and a significant decrease in Cx26 and Cx30 protein expression in the cochlea [199]. Further, dye transfer in cochlear supporting cells was reduced, suggesting that this mutant impacts GJIC within the cochlea [199].

Overexpression of Cx30-A40V mutant *in vitro* led to its retention in the Golgi apparatus and it had a dominant negative effect on both WT Cx30 and Cx26 function [198]. The trafficking pattern of the Cx30-G59A mutant has not yet been examined, however, the Cx26 G59A mutant was mostly retained within the Golgi apparatus with a small population trafficking to the plasma membrane forming defective channels [91]. Additionally, another *GJB6* mutant, A88V, causes Clouston syndrome which is an autosomal dominant disorder where patients present with alopecia, and skin deformities. However, patients with the A88V mutation do not typically present with hearing loss. In fact a mouse model for the Cx30-A88V mutant was generated and found to rescue age related high-frequency hearing loss in mutants compared to their WT controls [200–202]. Interestingly, when the Cx30-A88V mutant was overexpressed in *in vitro* systems, including a cochlear relevant cell line, it exhibited toxic effects and ultimately caused cell death [200,203]. The mechanisms by which A88V mice have improved hearing requires further investigation.

The original $Cx30^{-/-}$ mouse that was created had severe hearing loss with an approximately 50 dB hearing threshold shift in P18 mice [204]. $Cx30^{-/-}$ mice also lacked an endocochlear potential and had a significantly decreased endolymphatic K^+ concentration, both of which are necessary for proper hearing function [204].

Table 1.2. Genetically-modified mice used to assess Cx30 in hearing

Model	Phenotype	ABR	EP/DPOAE	Ref.
$Cx30^{-/-}$	Normal development up to P17 P18: Gradual loss of sensory cells 4 months: extensive HC loss	Het mice no difference P17-P18: 50dB elevation in nulls Adult nulls (4 months) had no detectable ABR	P13-P14: 74mV vs 0mV Adult: 83mV vs 3mV	[205]
$Cx30^{T5M/+}$	Reduced Cx30 expression by approx. 1/3 in T5M mice Normal morphology in adult mice Electrical coupling similar	Elevated by approx. 15dB	No difference 121.2mV vs. 122.2mV at P21-P28	[199]
$Cx30^{\Delta/\Delta}$	Normal gross cochlear anatomy	No change across frequencies	N/A	[206]
$Cx30^{A88V/+}$, $Cx30^{A88V/A88V}$ **Syndromic hearing loss**	Normal gross cochlear anatomy Reduced Cx30 expression in lateral wall of $Cx30^{A88V/A88V}$ mutant mice	6-9 weeks: homozygous mice approx. 20dB elevation at low freq. tones -High freq. approx. 40dB improvement in homozygotes also DPOAEs improved	N/A	[181,200,201]

ABR-auditory brainstem response, EP- endocochlear potential, DPOAE: distortion product otoacoustic emission.

Further, the barrier of endothelial cells within capillaries of the stria vascularis was disrupted, and hair cell loss was observed in $Cx30^{-/-}$ mice compared to controls [170, 207]. However, it was later shown that Cx26 was significantly downregulated at both the mRNA and protein levels within cochlear supporting cells in $Cx30^{-/-}$ mice, suggesting that their hearing loss may be attributed to the loss of Cx26 [208]. To address this hypothesis, a second Cx30 null mouse ($Cx30^{\Delta/\Delta}$) was created where Cx26 expression in the cochlea was preserved [206]. Interestingly, hearing was normal in $Cx30^{\Delta/\Delta}$ mice and indistinguishable from control mice, and no cochlear deficits were observed [206]. Taken together, these studies suggest that Cx26 and Cx30 are closely regulated within the cochlea and that loss of Cx30 does not lead to hearing loss as long as Cx26 expression is maintained.

1.10. Functions of connexins and gap junctions in the inner ear

1.10.1. Potassium recycling and buffering

The structural arrangement of two independent gap junction networks within the inner ear led to the original proposal that gap junctions were involved in maintaining proper potassium (K^+) homeostasis. K^+ is necessary for depolarization of hair cells in sound acquisition and thus K^+ ions that exit hair cells after sound stimulation are then taken up by supporting cells immediately surrounding hair cells [209]. In support of this, cochlear supporting cells express K^+ channels such as Kir4.1 [210,211]. Subsequently, the ions are then transferred through the epithelial gap junction network and are excreted to the connective tissue gap junction network through root cells where K^+ may then be taken up by fibrocytes of the spiral ligament and secreted back into the endolymph by marginal cells of the stria vascularis through KCNQ channels [209,212,213]. In this manner, K^+ ions are continuously being replenished in the endolymph region where it is necessary to maintain the positive endolymphatic potential. This arrangement is similar to what is observed in the glial network of the brain where connexins allow for spatial buffering of K^+ [214]. Like above, this model allows for the redistribution of K^+ ions from regions of high K^+ concentration to areas of low K^+ concentration in order to alleviate neural toxicity. To support this in the cochlea, it has been reported that shortly after birth cochlear supporting cells express glial fibrillary acidic protein (GFAP), a typical marker of glial cells, which after P15 is mostly restricted to supporting cells surrounding hair cells, suggesting that cochlear supporting cells have similarities to glial cells in the central nervous system which also express abundant GFAP [215]. However, it is important to note that this

hypothesis has been challenged due to the premise that not all Cx26 mutations cause decreased endolymphatic potential which would be expected if this was the sole function of gap junctions in the inner ear [216, 217].

1.10.2. Glucose and miRNA transport

The epithelium of the organ of Corti is avascular and as such it has been hypothesized that gap junctions play a role in nutrient transport and cell nourishment. In flattened cochlear preparation samples, Cx30 null mice had decreased dye transfer in cochlear supporting cells including a decrease in transfer of 2-NBDG, an analog of glucose [218]. To further support this hypothesis another study showed that 6-NBDG, another glucose analog, was rapidly distributed through the spiral ligament and stria vascularis where Cx26, Cx30, and glucose transporter 1 (GLUT1) were colocalized [219]. Transfer of 6-NBDG was inhibited by carbenoxolone and octanol gap junction blockers, suggesting the importance of gap junctions in glucose uptake in the lateral wall [219].

Micro RNAs (miRNAs) are small non-coding RNAs that have been reported to pass through gap junction channels where they can regulate gene expression by degrading mRNA targets [220, 221]. MiRNA-96 and -183 have been documented to be important in inner ear and hair cell development [222, 223]. For example, miRNA-183 is expressed during otic vesicle formation and involved in invagination to the otic placode [224]. In isolated preparations of cochlear supporting cells, miRNA-96 was found to transfer to neighbouring Hensen's cells which was further blocked by gap junctions blockers and eliminated in Cx26 knock-out mice [225]. Therefore, it is reasonable to suggest that connexins may play a functional role in cochlear development by allowing transport of miRNAs that are essential in hearing.

1.10.3. Connexin hemichannels: ATP release and purinergic signaling

Recent evidence suggests that connexins may not only traffic to the plasma membrane for the sole purpose of docking with an adjacent connexin to form a gap junction, but that connexins may remain functional as undocked transmembrane channels [226]. Connexin hemichannels have been documented to preferentially open under conditions of low extracellular Ca^{2+} concentrations or through K^{+} stimulation, conditions not normally seen in healthy tissues. Thus, connexin hemichannels have been mostly studied in the context of pathological disease

such as ischemia and cardiovascular injury [227, 228]. Interestingly, the cochlear endolymph houses a unique ionic composition including high K^+ and low Ca^{2+} (20 μM) concentrations, which would favour Cx hemichannel opening [229]. To support the hypothesis that Cx hemichannels are present in the inner ear, antibodies directed against the extracellular loop of Cx26 have been reported to bind to the apical domains of cochlear supporting cells in mouse organotypic cochlear cultures [154] suggesting that hemichannels exist in these cells. Further, with exposure to low Ca^{2+} concentration, guinea pig cochleae exhibited increased uptake of fluorescent dyes into supporting cells [230].

Connexin hemichannels can also release ATP that could bind to purinergic receptors on hair cells and supporting cells to initiate the propagation of Ca^{2+} waves. Cochlear cultures from mice lacking Cx26 failed to propagate calcium waves when ATP was applied [231]. Cx hemichannels can also release IP_3, which is expressed in the epithelium of the inner ear [232]. Before the onset of hearing, inner hair cells spontaneously release glutamate onto spiral ganglion neurons which is necessary for their maturation [233]. Spontaneous ATP release was increased when subjected to low extracellular Ca^{2+} concentrations and was blocked with the addition of gap junction blockers, carbenoxolone and octanol. Lastly, the importance of Cx hemichannels in hearing is supported by the notion that many Cx26 hearing loss linked mutations that cause syndromic hearing loss (with various skin disorders) have aberrant hemichannel function. For example, the S17F KID syndrome mutant which causes a gain of function phenotype through aberrant oligomerization of Cx26 and Cx43 ultimately causing enhanced hemichannel activation and cell death [192].

1.11. Pannexin expression and function in the inner ear

Increasing evidence has suggested a role for Panxs in proper auditory function in keeping with the fact that all three Panx isotypes have been found to be expressed along distinct regions of the auditory tract [135]. Specifically, Panx1 has been reported to be expressed centrally in neurons of the superficial and deep layers of the auditory cortex, and peripherally within the inner ear, including supporting cells of the organ of Corti [234, 235]. Panx2 is expressed in the cochlear lateral wall and in the boundary of the stria vascularis, and Panx3 is expressed in the cochlear bone [135, 235].

In the cochlea, ATP is found within both fluid filled spaces of the cochlea, the endolymph and the perilymph. Since Panx1 is known to act as an ATP release channel it was thought that pannexins served a role in ATP release within the inner ear, however, there have been contradictory reports on this conclusion. First, organotypic cochlear cultures from $Panx1^{-/-}$ mice had no effect on ATP release, suggesting that Panx1 was not necessarily the predominant ATP release channel in the cochlea [231]. However, a second study showed that mice with a conditional Panx1 ablation in the inner ear abolished ATP release in the cochlea [236]. ATP is an essential secondary messenger in the cochlea and can elevate intracellular Ca^{2+} concentration in hair cells modifying sound transduction, activating P2X receptors for various physiological processes such as EP generation, and synchronizing auditory nerve activity during development [233, 237, 238]. In addition, conditionally ablated Panx1 knock-out mice had decreased active cochlear amplification; a process that is required for outer hair cell motility [236]. The mechanisms behind these findings are unclear since Panx1 is not expressed in hair cells, and thus may be contributing to cochlear amplification in an indirect manner.

1.11.1. Mouse models used to assess pannexins in hearing

Shortly after pannexins were discovered to be expressed in the auditory system, various genetically-modified mice using either conditional ablation in the inner ear or global knock-out models have been evaluated. Table 1.3. summarizes a list of mouse models used to assess pannexins in hearing. The two conditional knock-out mice created were done by crossing $Panx1^{-/-}$ mice with Pax2-cre and Foxg1-cre mice where both these transcription factors are involved in otocyst and embryonic development.

Panx1 conditional knock-out mice using the $Pax2^{cre}$ and $Foxg1^{cre}$ mice were created on a C57BL/6 background. Both of these knock-out mice had mild-moderate (i.e. 10-30 dB threshold shift) sensorineural hearing loss at 8-, 16-, 24-, 32-, and 40 kHz tones and caused cell degeneration in the cochlea [236, 241]. They also showed that Panx1 is the predominant ATP release channel in the cochlea [236]. In contrast, it was previously shown that cochlear cultures from $Panx1^{-/-}$ mice were able to propagate intracellular calcium waves, suggesting no deficits in their calcium signaling [231]. It was further demonstrated that a global Panx1 knock-out mouse did not have auditory deficits even at high frequencies (32 kHz) [239].

Table 1.3. Genetically-modified mice used to assess pannexins in hearing

Mouse Model	Phenotype	ABR	EP/DPOAE	Reference
$Panx1^{-/-}$ global knock-out B6;129-$Panx1^{tm1.1Fama/Cnrm}$	Normal Ca^{2+} signal propagation in cochlear cultures	N/A	N/A	[231]
$Pax2^{Cre}$;$Panx1^{Fl/Fl}$	Cell degeneration in Pax2Cre-$Panx1^{-/-}$ mice	10dB threshold shift (low freq.) 20-30dB threshold shift (high freq.)	DPOAE significantly reduced in Pax2Cre-$Panx1^{-/-}$ mice	[241]
$Foxg1^{Cre}$;$Panx1^{Fl/Fl}$	No hair cell loss and decreased ATP release in Foxg1Cre-$Panx1^{-/-}$ mice	20-30dB threshold shift at all frequencies	EP and CM were significantly reduced in Foxg1Cre-$Panx1^{-/-}$ mice	[236]
$Panx1^{-/-}$ global knock-out B6;129-$Panx1^{tm1.1Fama/Cnrm}$	Normal cochlear morphology	Normal ABRs; no hearing loss	Normal DPOAEs	[239]
$Panx1^{-/-}$ global knock-out (Genentech)	No loss of hair cells	10-15dB threshold shift (low-mid freq.) 30-40dB threshold shift (high freq.)	DPOAEs and CM significantly reduced in $Panx1^{-/-}$ mice	[240]

ABR-auditory brainstem response, EP- endocochlear potential, DPOAE: distortion product otoacoustic emission. CM- cochlear microphonics.

However, one laboratory found that mice globally lacking Panx1 had mild hearing loss (i.e. 10-15dB threshold shift) in frequencies at or below 24kHz but this hearing loss was more pronounced at higher frequencies of 32- and 40kHz with approximately 20-30dB shift [240]. Based on these previous findings one of our main objectives was to assess the auditory phenotype of globally ablated Panx1 knock-out mice to address these discrepancies.

1.12. Pannexins and compensation

Since all three pannexin channels share similar topology to one another, current research suggests that global loss of one pannexin family member could be compensated by the upregulation of another family member. Panx1 and Panx3 channels are the most similar to each other sharing 73.3% similarity at the amino acid level [242,243]. The first reports of compensation were observed in $Panx1^{-/-}$ mice where Panx3 protein expression was significantly upregulated in both skin and thoracodorsal arteries compared to WT controls [244, 245].

Similar findings were also found in the vomeronasal organ (VNO) where Panx3 mRNA and protein expression was upregulated in the VNO of $Panx1^{-/-}$ mice [243]. In addition, these authors found that Panx1 and Panx3 had similar dye uptake and ATP release efficiencies in N2A cells *in vitro*, suggesting that Panx3 may compensate for Panx1 at the functional level [243]. Evidence of pannexin compensation led researchers to create double knock-out mice in an effort to minimize the effects pannexin compensation may play on a tissue phenotype.

The first pannexin double knock-out mouse created was $Panx1^{-/-}$;$Panx2^{-/-}$ mice with the purpose of studying brain ischemia. Interestingly, after recovery of middle cerebral artery occlusion to induce stroke, brains of $Panx1^{-/-}$;$Panx2^{-/-}$ mice had significantly smaller infarct sizes and better functional outcomes compared to both WT and both single pannexin knock-out mice [246]. These studies highlighted the fact that single pannexin knock-out mice, although informative, have limitations as other pannexin family members may serve a compensatory role; hence single knock-out mice may be inadequate in revealing certain phenotypes. Therefore, it was deemed important to examine auditory phenotypes of mice lacking both Panx1 and Panx3 which is the subject of chapter 3 of my thesis.

1.13. Noise-induced hearing loss

Intense and chronic exposure to loud sounds causing noise-induced hearing loss (NIHL), remains one of the most common causes of hearing loss. A large study in the United States showed that approximately 12.5% of American children and young adults had NIHL [247]. Hearing loss due to exposure to loud noises may be transient and temporary (i.e. temporary threshold shift) or if severe enough could lead to permanent hearing damage (i.e. permanent threshold shift) [248]. NIHL generally damages higher-frequency regions of 4 kHz as a primary target, that can then progress to neighboring frequencies of 3-6 kHz, which are especially important in daily speech recognition [249]. Many primary cochlear pathologies arise with NIHL including hair cell loss, spiral ganglion neuron degeneration, and swelling of the stria vascularis [250][251]. Spiral ganglion neuron degeneration can even last for months to years after noise-exposure [252].

The mechanisms of noise-induced hearing loss remains an active area of research and includes mechanical damage to the cochlea and biochemical pathways that induce cell death, particularly in the hair cells. Rodent studies have confirmed that NIHL increases apoptotic markers of cell death in the cochlea such as caspases, tumour necrosis factors, and morphological nuclear changes [253–255]. Noise-exposure causes an increase in the amount of cochlear ROS which peaks at approximately 7-10 days after noise-exposure, and then tends to decrease over time [256]. The transient increase in ROS leads to hair cell death and spiral ganglion neuron degeneration. To support the notion that ROS plays a critical role in NIHL, pre-administration of antioxidants to the cochlea have been shown to protect against noise damage [257]. In addition, the mitogen-activated protein kinase (MAPK) pathways, which can also be activated by ROS, are increased after noise-exposure in animal models [258, 259]. Additionally, noise damage causes an increase in the intracellular Ca^{2+} concentration of hair cells, particularly in the outer hair cells, which can trigger cell death [260]. Noise damage also causes a decrease in blood flow in the capillaries of the stria vascularis, which can lead to ischemia in this area and negatively impact the positive endolymphatic potential [261]. If the level of noise-exposure is sufficient enough to cause substantial hair cell death then hearing loss is irreversible.

On the other hand, the damage incurred by either shorter or less intense exposure to noise can result in a temporary hearing threshold shift (TTS). The result of a TTS is when hearing recovers to baseline levels in hours to weeks following the noise damage [248]. The mechanisms are distinct from permanent NIHL, and studies have found that loss of inner hair cell afferents may be the primary cause [262]. In fact, studies have shown swelling of inner hair cell afferents after noise exposure which is thought to be due to excessive release of glutamate at the synapse leading to excitotoxicity [263]. TTS can also be due to outer hair cells stereocilia breaking off from the tectorial membrane, which can be reversed subsequently leading to hair cells being saved [264]. In this manner, hair cells are not lost leading to hearing preservation in the long term. In a mouse model designed to induce only temporary noise-induced hearing loss, it was found that hair cell synapses between hair cells and cochlear neurons can be destroyed well before the hair cells are damaged and can cause a delay in cochlear nerve degeneration [252].

1.13.1. The role of connexins in noise-induced hearing loss

The link between NIHL and gap junctions was originally proposed when it was shown that rats exposed to loud noise had increased Cx26 protein expression in the cochlear lateral wall [265]. However, another study found that noise-exposure led to decreased Cx26 protein expression that also correlated with a decrease in Na/K ATPase [266]. No changes in mRNA and/or protein levels were detected in Cx30 or Cx43 after noise-exposure [266]. Using tamoxifen-inducible conditional knock-out mice, it was found that mice with reduced Cx26 expression at P30 and P45 had enhanced susceptibility to noise-induced hearing loss and increased hair cell loss as a consequence of noise exposure compared to WT controls [267]. Finally, after mice were exposed to a loud noise-exposure, GJIC was significantly reduced in dissociated spiral ligament cultures, suggesting that noise-exposure has a direct impact on gap junctions in the spiral ligament of the cochlear lateral wall [268]. Currently only one patient cohort study has examined the correlation between Cx26 mutations and NIHL. In a cohort of 703 patients, carriers of the most common Cx26 deletion involved in hearing loss, 35delG, did not have enhanced susceptibility to NIHL [269]; although future studies using larger cohorts may be needed to further evaluate a potential correlation between connexin mutations and NIHL.

1.14. Cisplatin-induced ototoxicity

One of the most effective and commonly used chemotherapy drugs to treat solid tumors in cancer treatment is cisplatin (*cis*-diamminedichloroplatinumII). This drug has been widely used in testicular, ovarian, bladder, cervical, lung, head and neck cancers in both young children and adults [270]. Side effects of cisplatin chemotherapy include nephrotoxicity, neurotoxicity, and ototoxicity causing hearing loss [271]. While nephrotoxicity can be routinely managed through saline fluid absorption and diuretics, there are currently no treatments for neuro- or ototoxicity. Cisplatin-induced hearing loss occurs in approximately 75-100% of patients that undergo treatment and can range from moderate to severe in nature [272]. Children in particular generally exhibit severe hearing loss as a consequence of cisplatin treatment which can significantly hinder their cognitive and speech skills throughout their development [273, 274].

Although cisplatin is a highly effective chemotherapeutic agent, it causes significant hearing loss in many patients which is usually progressive and irreversible [270,275]. Hearing impairment in individuals can be variable in its severity and can depend on the concentration and accumulation (one administration or multi-dose) of the drug [276]. Generally, cisplatin causes high frequency hearing loss in humans (approximately 6-8 kHz) [277,278]. Within the cochlea, cisplatin induces cell death in three main locations. The most studied consequence is hair cell loss and structural damage with the outer hair cells being more preferentially impacted [279, 280]. Since then studies have found that cisplatin first causes damage to the stria vascularis on the cochlear lateral wall, a structure that is essential for the transport of potassium ions to the endolymph as well as damage to supporting cells in the organ of Corti [281–283]. Finally, cisplatin causes degeneration of the spiral ganglion neurons as well as disorganization of their afferents to hair cells [284, 285]. GJIC has been postulated to play an important role in cisplatin-induced cell death through the “bystander effect” whereby gap junctions transfer toxic compounds from cell to cell [286]. Alternatively, gap junctions may also be involved in transferring beneficial compounds to neighboring cells, thereby diluting toxic compounds known as the “Good Samaritan” effect [287].

Although the exact molecular mechanisms are unknown, cisplatin produces reactive oxygen species (ROS) accumulation within cells [288, 289]. These free radicals can then bind to

protein, DNA, or nucleic acid to cause cell death. Cisplatin can also directly bind to mitochondrial DNA causing cisplatin-DNA adducts leading to mitochondrial dysfunction [290]. Generation of ROS triggers apoptosis within cells by altering the mitochondrial membrane potential and damaging the electron transport chain [291]. One of the enzymes that can produce superoxide radicals that can lead to the formation of hydrogen peroxide, in the cochlea is an isoform of nicotinamide adenine dinucleotide phosphate (NADPH) oxidase, NOX-3, which is specifically expressed in the cochlea [292]. Cisplatin activates NOX-3, leading to an increase in superoxide formation, which has been shown to be increased in cisplatin-treated rats [292].

The specific compounds and/or signals that pass through gap junctions as a consequence of cisplatin treatment are not fully known but could include reactive oxygen species, reactive nitrogen species, superoxide radicals, calcium, and/or IP_3 [293–295]. It is also important to note that based on the charge and size of cisplatin (300 Da), it too can theoretically pass through a gap junction channel. *In vitro* studies have suggested that Cx43 can act to enhance cisplatin-induced cell death of HEI-OC1 cells [296]. Further, downregulation of Cx43 in HEI-OC1 cells through siRNA or application of 18α-GA gap junction blocker, mildly protected auditory cells against cisplatin-induced ototoxicity [296]. It was also found that cisplatin treatment itself caused a decrease in GJIC and Cx expression in HEI-OC1 cells, which is due to direct interaction of cisplatin with Cx channels thereby reducing their expression levels [296–298]. To support these findings, *in vitro* studies have shown that cisplatin-induced cell death is most extensively observed when cells are plated at high density suggesting GJIC plays a key role in this process [299,300]. However, some cell death is still observed after cisplatin treatment in low density *in vitro* cultures of different cell lines, suggesting that there may also be some gap junction-independent functions involved [299, 300].

1.14.1. Structure/activation of cisplatin

Cisplatin is a platinum based compound surrounded by two chloride and two amine ligands, in turn having a square planar structure and a half-life between 1.5-3.6 hours [301]. Cisplatin concentrations in patient plasma levels ranges from approximately 10-25 μM [298, 302]. For cisplatin to take its chemotherapeutic effect it must first be taken up by the cell. Although some cisplatin may passively diffuse through the plasma membrane of the cell, the most efficient

and studied mechanism of uptake of cisplatin are copper transporter such as CTR1, CTR2, and organic cation transporters 1 and 2 (OCT1, OCT2) [279,303]. Once cisplatin enters the cell, it undergoes hydrolysis by replacement of a H_2O molecule for a chloride ion which is favored due to the low concentration of Cl^- ions inside the cell relative to the extracellular environment (100 μM) [304]. The hydrolyzed cisplatin then binds to a single nitrogen of a purine base of DNA. Subsequently, the other chloride ion gets replaced for another H_2O molecule and the platinum ion binds to another nitrogen of the DNA, thereby crosslinking DNA causing cell damage [270, 304].

1.14.2. Uptake/efflux of cisplatin from cochlear cells

The high incidence of cisplatin-induced hair cell loss is due to the fact that hair cells express an abundant amount of copper transporters that are involved in cisplatin uptake including Ctr1, OCT2, and OCT1 [303,305]. These transporters, located on the apical regions of hair cells, enable a rapid and efficient influx of cisplatin into hair cells where cisplatin will then elicit the DNA repair response ultimately leading to cell death [275]. Importantly, supporting cells and spiral ganglion neurons were reported to also express OCT2 copper transporter [306]. Cisplatin is moved out of the cell through two specific efflux transporters ATPase7A, expressed in hair cells, and ATPase 7B, expressed in pillar supporting cells [285].

1.15. Modelling the inner ear using organotypic cochlear cultures

The inner ear is extremely complex to study due its complex structure and encapsulation within the cochlear bone. One challenge that is faced in inner ear biology remains the inability of hair cells to be immortalized. Inner ear *ex vivo* explants from rodents have now been used for approximately 40 years and offer a method of maintaining the full organ of Corti including the hair cells, and supporting cells [307]. These organotypic cochlear cultures have been widely used to study the function and structure of the inner ear and have been extensively used to study ototoxicity of various drugs [308, 309]. Therefore, this thesis will make use of organotypic cochlear cultures derived from different connexin mutant mice in order to more readily examine molecular processess involved in ototoxicity. Figure 1.4 shows a diagram illustrating the structure and cell types within organotypic cochlear cultures that will be used in this thesis.

Figure 1.4. Schematic diagram of organotypic cochlear culture

(A) *Ex vivo* preparation of the organ of Corti in an organotypic cochlear culture. These cultures are ideal for assessing the effect of drug treatment in an *in vitro* environment.

Figure 1.4.

A

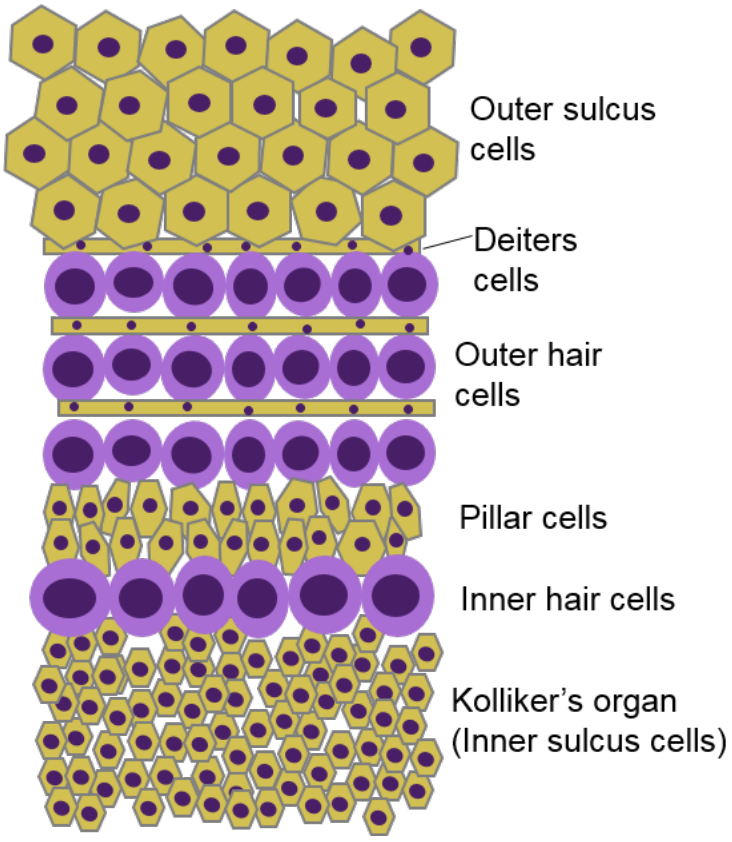
Outer sulcus cells
Deiters cells
Outer hair cells
Pillar cells
Inner hair cells
Kolliker's organ (Inner sulcus cells)

1.16. HEI-OC1 immortalized cochlear cells as a tool to model the *in vivo* cochlea

In depth functional studies of the inner ear are hindered by the small size and working availability of the cochlea making it difficult to evaluate complex *in vivo* cellular processes. To circumvent these obstacles Dr. Federico Kalinec and his group derived an immortalized cell line from organotypic cochlear cultures of the immortomouse, HEI-OC1 cells [310]. In this manner, the *in vitro* cell line can act as a tool to examine molecular functions, including connexin functions, that can be extrapolated to the *in vivo* mouse from which this cell line was derived. HEI-OC1 cells mimic cochlear progenitor cells of which, in the *in vivo* setting, would be later fated to become either sensory (hair cells) or non-sensory (supporting cells) [310, 311].

Due to the temperature sensitivity of cells obtained from the immortomouse, in permissive conditions these cells stay in a de-differentiated state as cochlear progenitors. However, under non-permissive conditions (33ºC, 10% CO_2), HEI-OC1 cells will differentiate into a "hair cell-like" phenotype expressing and upregulating markers that are expressed in hair cells such as myosinVI and prestin [310, 312]. Therefore, to evaluate cellular mechanisms of connexins in hearing, HEI-OC1 cells (generously obtained from Dr. Kalinec) will be used in this thesis as a tool to assess specific cellular processes that we would be otherwise unable to examine in the cochlea.

1.17. Mouse models used in this study

To examine the roles of Panx1, Panx3, and Cx43 in the auditory system, we have obtained and/or generated five different genetically modified mice. First, the $Panx1^{-/-}$ mice were originally obtained from Genentech [313]. Since then they have been backcrossed to C57BL6 mice for approximately 5 generations. Second, the $Panx3^{-/-}$ mice were generated in house and were previously characterized in regards to their gross phenotypes [314]. To eliminate the possibility of Panx1 and Panx3 compensating for one another, we generated the first Panx1 and Panx3 double knock-out mouse in house through crossing heterozygous $Panx1^{+/-}$ and $Panx3^{+/-}$ mice together and selecting for double null mice. The $Cx43^{I130T/+}$ mutant mice were generated by site-directed mutagenesis with mice maintained on a mixed C57BL/6 and CD1 background and backcrossed to C57BL/6 mice for over 5 generations [315]. These mice were generously obtained from Dr. Glen Fishman's laboratory. The $Cx43^{G60S/+}$ mutant mice were

generated by using an ENU mutagenesis approach whereby this mouse model phenotypically mimicked ODDD and has therefore been used as a mouse model to study this disease [316]. These mice were generously obtained from Dr. Janet Rossant's laboratory. Both the $Cx43^{I130T/+}$ and the $Cx43^{G60S/+}$ mutant mice have a moderate (50%) and severe (80%) reduction in Cx43 gap junctional intercellular communication, respectively, as has been demonstrated in different *in vitro* and *in vivo* tissue culture systems such as cardiomyocytes, mammary glands, and granulosa cells [315–319].

1.18. Rationale

It has been well known for two decades now that *GJB2* mutations cause the majority of congenitally acquired hearing loss. *GJA1* has also been documented within the literature to be expressed in the inner ear, however its expression pattern and function remains unclear. Importantly, the function of Cx43 in the auditory system remains unknown. Thus, we sought to further investigate the importance of Cx43 in hearing using two different Cx43 mutant mice that mimic a human linked disease, ODDD and examine their auditory phenotypes. Further, since Panx1 conditional knock-out mice have been documented to have hearing loss, we evaluated the auditory profiles of a global Panx1 and Panx3 knock-out mouse. Given that Panx1 and Panx3 may compensate for one another we further created a Panx1/Panx3 double knock-out mouse to eliminate the potential of compensation between these large pore channels and examined their auditory phenotypes. Finally, since Cx43 has been proposed to be involved in cisplatin-induced ototoxicity in cancer cell lines, Cx43 may also affect cisplatin induced cell death in cochlear relevant cells; including organotypic cochlear cultures from Cx43 mutant mice as well as an immortalized cochlear cell line.

1.19. Hypothesis

It is hypothesized that deletions of Panx1 and/or Panx3 will cause hearing loss, and Cx43 mutants will cause hearing impairment, and enhanced vulnerability to ototoxicity.

1.20. Objectives

The overall research objectives of this thesis are the following:

Objective 1 – Manuscript 1: Chapter 2

Determine the importance of Panx1 and Panx3 in mouse hearing before and after loud noise-exposure.

Objective 2 – Manuscript 3: Chapter 3

Characterize a novel Panx1 Panx3 double knock-out mouse and assess the impact on hearing.

Objective 3 – Manuscript 2: Chapter 4

Examine auditory function and susceptibility to noise-induced hearing loss in mice harboring a disease-linked Cx43 mutant.

Objective 4 – Manuscript 4: Chapter 5

Investigate the consequence of Cx43 mutations and gap junction blockage on the susceptibility of organotypic cochlear cultures to ototoxicity.

1.21. References

1 Morrill, S. and He, D. Z. Z. (2017) Apoptosis in inner ear sensory hair cells. J. Otol., Elsevier Ltd **12**, 151–164.

2 Fook, L. and Morgan, R. (2000) Hearing impairment in older people: A review. Postgrad. Med. J. **76**, 537–541.

3 Shearer, A. E., Hildebrand, M. S. and Smith, R. J. (1993) Hereditary Hearing Loss and Deafness Overview. GeneReviews® 1–27.

4 Egilmez, O. K. and Kalcioglu, M. T. (2016) Genetics of Nonsyndromic Congenital Hearing Loss. Scientifica (Cairo)., Hindawi Publishing Corporation **2016**.

5 Kelsell, D. P., Dunlop, J., Stevens, H. P., Lench, N. J., Liang, J. N., Parry, G., Mueller, R. F. and Leigh, I. M. (1997) Connexin 26 mutations in hereditary non-syndromic sensorineural deafness. Nature.

6 del Castillo, F. J. and del Castillo, I. (2017) DFNB1 Non-syndromic Hearing Impairment: Diversity of Mutations and Associated Phenotypes. Front. Mol. Neurosci. **10**, 1–18.

7 Hilgert, N., Smith, R. J. H. and Van Camp, G. (2009) Forty-six genes causing nonsyndromic hearing impairment: Which ones should be analyzed in DNA diagnostics? Mutat. Res. - Rev. Mutat. Res. **681**, 189–196.

8 Chan, D. K. and Chang, K. W. (2014) GJB2-associated hearing loss: Systematic review of worldwide prevalence, genotype, and auditory phenotype. Laryngoscope **124**, 34–53.

9 Papsin, B. C. and Gordon, K. A. (2007) Cochlear implants for children with severe-to-profound hearing loss. N. Engl. J. Med. **357**, 2380.

10 Gordon, K., Henkin, Y. and Kral, A. (2015) Asymmetric hearing during development: The aural preference syndrome and treatment options. Pediatrics **136**, 141–153.

11 Christopher W. Turner, Bruce J. Gantz, Sue Karsten, Jennifer Fowler, and L. A. R. A. (2010) The impact of hair cell preservation in cochlear implantation: Combined Electric and Acoustic Hearing Christopher. Otol Neurotol **31**, 1227–1232.

12 Hepper, P. G. and Shahidullah, B. S. (1994) Development of fetal hearing - Universität Wien 81–87.

13 Sanes, D. and Bao, S. (2009) Tuning up the developing CNS. Curr Opin Neurobiol **19**, 188–199.

14 Chang, A., Chen, P., Guo, S., Xu, N., Pan, W., Zhang, H., Li, C. and Tang, J. (2018) Specific Influences of Early Acoustic Environments on Cochlear Hair Cells in Postnatal Mice. Neural Plast., Hindawi **2018**.

15 Mann, Z. F. and Kelley, M. W. (2011) Development of tonotopy in the auditory periphery. Hear. Res., Elsevier B.V **276**, 2–15.

16 Trowe, M. O., Maier, H., Schweizer, M. and Kispert, A. (2008) Deafness in mice lacking the T-box transcription factor Tbx18 in otic fibrocytes. Development **135**, 1725–1734.

17 Fettiplace, R. (2017) Hair cell transduction, tuning and synaptic transmission in the mammalian cochlea. compr physiol. **7**, 1197–1227.

18 Arya Parsa, P. W. and F. K. (2012) Deiters Cells Tread a Narrow Path —The Deiters Cells-Basilar Membrane Junction. Hear Res **290**, 13–20.

19 Wan, Gabriel Corfas1, 2, 3, and J. S. S. 1F. M. (2013) Inner ear supporting cells: Rethinking the silent majority **24**, 448–459.

20 Bruzzone, R., White, T. W. and Paul, D. L. (1996) Connections with Connexins: the Molecular Basis of Direct Intercellular Signaling. Eur. J. Biochem. **238**, 1–27.

21 Laird, D. W. (2006) Life cycle of connexins in health and disease. Biochem. J. **394**, 527–543.

22 Goodenough, D. A. and Paul, D. L. (2003) Beyond the gap: Functions of unpaired connexon channels. Nat. Rev. Mol. Cell Biol. **4**, 285–294.

23 Söhl, G. and Willecke, K. (2004) Gap junctions and the connexin protein family. Cardiovasc. Res. **62**, 228–232.

24 Musil, L. S. and Goodenough, D. A. (1993) Multisubunit assembly of an integral plasma membrane channel protein, gap junction connexin43, occurs after exit from the ER. Cell **74**, 1065–1077.

25 Martin, P. E. M. and Evans, W. H. (2004) Incorporation of connexins into plasma membranes and gap junctions. Cardiovasc. Res. **62**, 378–387.

26 Loewenstein, W. R. (1981) Junctional intercellular communication: the cell-to-cell membrane channel. Physiol. Rev. **61**, 829–913.

27 Chow, I. and Young, S. H. (1987) Opening of single gap junction channels during formation of electrical coupling between embryonic muscle cells. Dev. Biol. **122**, 332–337.

28 Retamal, M. A., Reyes, E. P., GarcÃ-a, I. E., Pinto, B., Martanez, A. D. and Gonzalez, C. (2015) Diseases associated with leaky hemichannels. Front. Cell. Neurosci. **9**, 1–10.

29 Leybaert, L., Lampe, P. D., Dhein, S., Kwak, B. R., Ferdinandy, P., Beyer, E. C., Laird, D. W., Naus, C. C., Green, C. R. and Schulz, R. (2017) Connexins in Cardiovascular and Neurovascular Health and Disease: Pharmacological Implications. Pharmacol. Rev. **69**, 396–478.

30 Leybaert, L., Lampe, P. D., Dhein, S., Kwak, B. R., Ferdinandy, P., Beyer, E. C., Laird, D. W., Naus, C. C., Green, C. R. and Schulz, R. (2017) Connexins in cardiovascular and neurovascular health and disease: Pharmacological implications. Pharmacol. Rev. **69**, 396–478.

31 Vinken, M., Vanhaecke, T., Papeleu, P., Snykers, S., Henkens, T. and Rogiers, V. (2006) Connexins and their channels in cell growth and cell death. Cell. Signal. **18**, 592–600.

32 White, T. W. (2012) Connexins, cell proliferation and second messengers in the crystalline lens. J. Ophthalmic Vis. Res. **7**, 107–108.

33 Kameritsch, P., Khandoga, N., Pohl, U. and Pogoda, K. (2013) Gap junctional communication promotes apoptosis in a connexin-type- dependent manner. Cell Death

Dis., Nature Publishing Group **4**, e584-9.

34 Laird, D. W. (1996) The life cycle of a connexin: Gap junction formation, removal, and degradation. J. Bioenerg. Biomembr. **28**, 311–318.

35 Beardslee, M. A., Laing, J. G., Beyer, E. C. and Saffitz, J. E. (1998) Rapid turnover of connexin43 in the adult rat heart. Circ. Res. **83**, 629–635.

36 Fallon, R. F. and Goodenough, D. A. (1981) Five-hour half-life of mouse liver gap-junction protein. J. Cell Biol. **90**, 521–526.

37 Laird, D. W., Puranam, K. L. and Revel, J. (1991) Turnover and phosphorylation dynamics of. Biochem. J. **273**, 67–72.

38 Kelly, J. J., Shao, Q., Jagger, D. J. and Laird, D. W. (2015) Cx30 exhibits unique characteristics including a long half-life when assembled into gap junctions. J. Cell Sci. **128**, 3947–3960.

39 Spray, D. C. (1996) Molecular physiology of gap junction channels. 1038–1040.

40 Qu, Y. and Dahl, G. (2002) Function of the voltage gate of gap junction channels: Selective exclusion of molecules. Proc. Natl. Acad. Sci. U. S. A. **99**, 697–702.

41 Aasen, T., Mesnil, M., Naus, C. C., Lampe, P. D. and Laird, D. W. (2016) Gap junctions and cancer: Communicating for 50 years. Nat. Rev. Cancer **16**, 775–788.

42 Beyer, E. C., Gemel, J., Martínez, A., Berthoud, V. M., Valiunas, V., Moreno, A. P. and Brink, P. R. (2000) Heteromeric mixing of connexins: Compatibility of partners and functional consequences. Cell Adhes. Commun. **8**, 199–204.

43 Sun, J., Ahmad, S., Chen, S., Tang, W., Zhang, Y., Chen, P. and Lin, X. (2005) Cochlear gap junctions coassembled from Cx26 and 30 show faster intercellular Ca2+ signaling than homomeric counterparts. Am. J. Physiol. Cell Physiol. **288**, C613–C623.

44 Ahmad, S., Chen, S., Sun, J. and Lin, X. (2003) Connexins 26 and 30 are co-assembled to form gap junctions in the cochlea of mice. Biochem. Biophys. Res. Commun. **307**, 362–368.

45 Forge, A., Becker, D., Casalotti, S., Edwards, J., Marziano, N. and Nevill, G. (2003) Gap Junctions in the Inner Ear: Comparison of Distribution Patterns in Different Vertebrates and Assessment of Connexin Composition in Mammals. J. Comp. Neurol. **467**, 207–231.

46 Koval, M., Molina, S. A. and Burt, J. M. (2014) Mix and match: Investigating heteromeric and heterotypic gap junction channels in model systems and native tissues. FEBS Lett., Federation of European Biochemical Societies **588**, 1193–1204.

47 Kanaporis, G., Brink, P. R. and Valiunas, V. (2011) Gap junction permeability: Selectivity for anionic and cationic probes. Am. J. Physiol. - Cell Physiol. **300**, 600–609.

48 Roux, W., Biol, D. and Dev, G. (2000) A ubiquitous family of putative gap junction molecules Yuri Panchin, Ilya Kelmanson, Mikhail Usman and Sergey 473–474.

49 Baranova, A., Ivanova, D. V, Petrash, N., Pestova, A., Skoblov, M., Kelmanson, I., Shagin, D., Nazarenko, S., Geraymovych, E., Litvin, O., et al. (2004) The mammalian

pannexin family is homologous to the invertebrate innexin gap junction proteins. Genomics **83**, 706–716.

50 Panchin, Y. V. (2005) Evolution of gap junction proteins - the pannexin alternative. J. Exp. Biol. **208**, 1415–1419.

51 A ubiquitous family of putative gap junction molecules Panchin, Y., Kelmanson, I., Usman, M. and Sergey. A ubiquitous family of putative gap junction molecules Dev, G. (2000) Curr. Biol. 473–474.

52 Penuela, S., Gehi, R. and Laird, D. W. (2013) The biochemistry and function of pannexin channels. Biochim. Biophys. Acta, Elsevier B.V. **1828**, 15–22.

53 Penuela, S., Harland, L., Simek, J. and Laird, D. W. (2014) Pannexin channels and their links to human disease. Biochem. J. **461**, 371–381.

54 Barbe, M. T. (2006) Cell-Cell Communication Beyond Connexins: The Pannexin Channels. Physiology **21**, 103–114.

55 Gehi, R., Shao, Q. and Laird, D. W. (2011) Pathways regulating the trafficking and turnover of Pannexin1 protein and the role of the C-terminal domain. J. Biol. Chem. **286**, 27639–27653.

56 Penuela, S. and Laird, D. W. (2012) The cellular life of pannexins. Wiley Interdiscip. Rev. Membr. Transp. Signal. **1**, 621–632.

57 Penuela, S., Simek, J. and Thompson, R. J. (2014) Regulation of pannexin channels by post-translational modifications. FEBS Lett., Federation of European Biochemical Societies **588**, 1411–1415.

58 Cea, L. A., Riquelme, M. A., Vargas, A. A., Urrutia, C. and Sáez, J. C. (2014) Pannexin 1 channels in skeletal muscles. Front. Physiol. **5 APR**, 1–6.

59 Raslan, A., Hainz, N., Beckmann, A., Tschernig, T. and Meier, C. (2016) Pannexin-1 expression in developing mouse nervous system: new evidence for expression in sensory ganglia. Cell Tissue Res. **364**, 29–41.

60 Wang, X.-H., Streeter, M., Liu, Y.-P. and Zhao, H.-B. (2009) Identification and characterization of pannexin expression in the mammalian cochlea. J. Comp. Neurol. **512**, 336–46.

61 Zhang, H., Chen, Y. and Zhang, C. (2012) Patterns of heterogeneous expression of pannexin 1 and pannexin 2 transcripts in the olfactory epithelium and olfactory bulb. J. Mol. Histol. **43**, 651–660.

62 Bruzzone, R., Hormuzdi, S. G., Barbe, M. T., Herb, A. and Monyer, H. (2003) Pannexins, a family of gap junction proteins expressed in brain. Proc. Natl. Acad. Sci. **100**, 13644–13649.

63 Le Vasseur, M., Lelowski, J., Bechberger, J. F., Sin, W. C. and Naus, C. C. (2014) Pannexin 2 protein expression is not restricted to the CNS. Front. Cell. Neurosci. **8**, 1–13.

64 Penuela, S., Bhalla, R., Gong, X.-Q., Cowan, K. N., Celetti, S. J., Cowan, B. J., Bai, D., Shao, Q. and Laird, D. W. (2007) Pannexin 1 and pannexin 3 are glycoproteins that exhibit many distinct characteristics from the connexin family of gap junction

proteins. J. Cell Sci. **120**, 3772–3783.

65 Lai, C. P. K., Bechberger, J. F., Thompson, R. J., MacVicar, B. A., Bruzzone, R. and Naus, C. C. (2007) Tumor-suppressive effects of pannexin 1 in C6 glioma cells. Cancer Res. **67**, 1545–1554.

66 Bruzzone, R., Veronesi, V., Gomès, D., Bicego, M., Duval, N., Marlin, S., Petit, C., D'Andrea, P. and White, T. W. (2003) Loss-of-function and residual channel activity of connexin26 mutations associated with non-syndromic deafness. FEBS Lett. **533**, 79–88.

67 Sahu, G., Sukumaran, S. and Bera, A. K. (2014) Pannexins form gap junctions with electrophysiological and pharmacological properties distinct from connexins. Sci. Rep. **4**, 1–9.

68 Boassa, D., Ambrosi, C., Qiu, F., Dahl, G., Gaietta, G. and Sosinsky, G. (2007) Pannexin1 channels contain a glycosylation site that targets the hexamer to the plasma membrane. J. Biol. Chem. **282**, 31733–31743.

69 Locovei, S., Bao, L. and Dahl, G. (2006) Pannexin 1 in erythrocytes: Function without a gap. Proc. Natl. Acad. Sci. U. S. A. **103**, 7655–7659.

70 Huang, Grinspan, Abrams, Scherer (2007) Pannexin1 is Expressed by Neurons and Glia but Does Not Form Functional Gap Junctions. Glia **55**, 46–56.

71 Boassa, D., Qiu, F., Dahl, G. and Sosinsky, G. (2008) Trafficking dynamics of glycosylated pannexin1 proteins. Cell Commun. Adhes. **15**, 119–132.

72 Dahl, G., Levine, E., Rabadan-diehl, C. and Werner, R. (1991) Cell/cell channel formation involves disulfide exchange **144**, 141–144.

73 Thompson, R. J. and MacVicar, B. A. (2008) Connexin and pannexin hemichannels of neurons and astrocytes. Channels **2**, 81–86.

74 MacVicar, B. A. and Thompson, R. J. (2010) Non-junction functions of pannexin-1 channels. Trends Neurosci. **33**, 93–102.

75 Bao, L., Locovei, S. and Dahl, G. (2004) Pannexin membrane channels are mechanosensitive conduits for ATP. FEBS Lett. **572**, 65–68.

76 Thompson, R. J., Zhou, N. and Macvicar, B. a. (2006) Junction Hemichannels **851**, 924–927.

77 Locovei, S., Wang, J. and Dahl, G. (2006) Activation of pannexin 1 channels by ATP through P2Y receptors and by cytoplasmic calcium. FEBS Lett. **580**, 239–244.

78 Sandilos, J. K. and Bayliss, D. A. (2012) Physiological mechanisms for the modulation of pannexin 1 channel activity. J. Physiol. **590**, 6257–6266.

79 Chiu, Y. H., Schappe, M. S., Desai, B. N. and Bayliss, D. A. (2018) Revisiting multimodal activation and channel properties of Pannexin 1. J. Gen. Physiol. **150**, 19–39.

80 Chiu, Y. H., Jin, X., Medina, C. B., Leonhardt, S. A., Kiessling, V., Bennett, B. C., Shu, S., Tamm, L. K., Yeager, M., Ravichandran, K. S., et al. (2017) A quantized mechanism for activation of pannexin channels. Nat. Commun., Nature Publishing Group **8**, 1–15.

81 Chekeni, F. B., Elliott, M. R., Sandilos, J. K., Walk, S. F., Kinchen, J. M., Lazarowski, E. R., Armstrong, A. J., Penuela, S., Laird, D. W., Salvesen, G. S., et al. (2010) Pannexin 1 channels mediate "find-me" signal release and membrane permeability during apoptosis. Nature, Nature Publishing Group **467**, 863–7.

82 Sandilos, J. K., Chiu, Y. H., Chekeni, F. B., Armstrong, A. J., Walk, S. F., Ravichandran, K. S. and Bayliss, D. A. (2012) Pannexin 1, an ATP release channel, is activated by caspase cleavage of its pore-associated C-terminal autoinhibitory region. J. Biol. Chem. **287**, 11303–11311.

83 Locovei, S., Wang, J. and Dahl, G. (2006) Activation of pannexin 1 channels by ATP through P2Y receptors and by cytoplasmic calcium. FEBS Lett. **580**, 239–244.

84 Elliott, M. R., Chekeni, F. B., Trampont, P. C., Lazarowski, E. R., Kadl, A., Walk, S. F., Park, D., Woodson, R. I., Sharma, P., Lysiak, J. J., et al. (2010) Nucleotides released by apoptotic cells act as a find-me signal for phagocytic clearance. Nature **461**, 282–286.

85 Qiu, F. and Dahl, G. (2009) A permeant regulating its permeation pore: Inhibition of pannexin 1 channels by ATP. Am. J. Physiol. - Cell Physiol. **296**, 250–255.

86 Srinivas, M., Verselis, V. K. and White, T. W. (2018) Human diseases associated with connexin mutations. Biochim. Biophys. Acta - Biomembr., Elsevier B.V. **1860**, 192–201.

87 Laird, D. W., Naus, C. C. and Lampe, P. D. (2017) SnapShot: Connexins and Disease. Cell, Elsevier **170**, 1260-1260.e1.

88 Kenna, M. A., Feldman, H. A., Neault, M. W., Frangulov, A., Wu, B. L., Fligor, B. and Rehm, H. L. (2010) Audiologic phenotype and progression in GJB2 (connexin 26) hearing loss. Arch. Otolaryngol. - Head Neck Surg. **136**, 81–87.

89 Taniguchi, M., Matsuo, H., Shimizu, S., Nakayama, A., Suzuki, K., Hamajima, N., Shinomiya, N., Nishio, S., Kosugi, S., Usami, S. I., et al. (2015) Carrier frequency of the GJB2 mutations that cause hereditary hearing loss in the Japanese population. J. Hum. Genet., Nature Publishing Group **60**, 613–617.

90 Kelly, J. J., Simek, J. and Laird, D. W. (2015) Mechanisms linking connexin mutations to human diseases. Cell Tissue Res. **360**, 701–721.

91 Thomas, T., Telford, D. and Laird, D. W. (2004) Functional Domain Mapping and Selective Trans-dominant Effects Exhibited by Cx26 Disease-causing Mutations. J. Biol. Chem. **279**, 19157–19168.

92 Mani, R. S., Ganapathy, A., Jalvi, R., Srikumari Srisailapathy, C. R., Malhotra, V., Chadha, S., Agarwal, A., Ramesh, A., Rangasayee, R. R. and Anand, A. (2009) Functional consequences of novel connexin 26 mutations associated with hereditary hearing loss. Eur. J. Hum. Genet. **17**, 502–509.

93 Marziano, N. K., Casalotti, S. O., Portelli, A. E., Becker, D. L. and Forge, A. (2003) Mutations in the gene for connexin 26 (GJB2) that cause hearing loss have a dominant negative effect on connexin 30. Hum. Mol. Genet. **12**, 805–812.

94 Haack, B., Schmalisch, K., Palmada, M., Böhmer, C., Kohlschmidt, N., Keilmann, A., Zechner, U., Limberger, A., Beckert, S., Zenner, H. P., et al. (2006) Deficient

membrane integration of the novel p.N14D-GJB2 mutant associated with non-syndromic hearing impairment. Hum. Mutat. **27**, 1158–1159.

95 Meşe, G., Londin, E., Mui, R., Brink, P. R. and White, T. W. (2004) Altered gating properties of functional Cx26 mutants associated with recessive non-syndromic hearing loss. Hum. Genet. **115**, 191–199.

96 Chen, Y., Deng, Y., Bao, X., Reuss, L., Altenberg, G. A. and Biology, C. (2005) Mechanism of the defect in gap-junctional communication by expression of a connexin 26 mutant associated with dominant deafness. FASEB J. **16**, 9–12.

97 Lee, J.R,. DeRosa, A.M., and White, T. W. (2009) Connexin mutations causing skin disease and deafness increase hemichannel activity and cell death when expressed in Xenopus oocytes **129**, 870–878.

98 Martin, P. E. M., Coleman, S. L., Casalotti, S. O., Forge, A. and Evans, W. H. (1999) Properties of connexin26 gap junctional proteins derived from mutations associated with non-syndromal heriditary deafness. Hum. Mol. Genet. **8**, 2369–2376.

99 Arita, K., Akiyama, M., Aizawa, T., Umetsu, Y., Segawa, I., Goto, M., Sawamura, D., Demura, M., Kawano, K. and Shimizu, H. (2006) A novel N14Y mutation in connexin26 in keratitis-ichthyosis-deafness syndrome: Analyses of altered gap junctional communication and molecular structure of N terminus of mutated connexin26. Am. J. Pathol. **169**, 416–423.

100 Meşe, G., Valiunas, V., Brink, P. R. and White, T. W. (2008) Connexin26 deafness associated mutations show altered permeability to large cationic molecules. Am. J. Physiol. Cell Physiol. **295**, C966-74.

101 Wang, H. L., Chang, W. T., Li, A. H., Yeh, T. H., Wu, C. Y., Chen, M. S. and Huang, P. C. (2003) Functional analysis of connexin-26 mutants associated with hereditary recessive deafness. J. Neurochem. **84**, 735–742.

102 Beltramello, M., Piazza, V., Bukauskas, F. F., Pozzan, T. and Mammano, F. (2005) Impaired permeabilty to Ins(1,4,5)P3in a mutant connexin underlies recessive hereditary deafness. Nat. Cell Biol. **7**, 63–69.

103 Gerido, D. A., DeRosa, A. M., Richard, G. and White, T. W. (2007) Aberrant hemichannel properties of Cx26 mutations causing skin disease and deafness. Am. J. Physiol. Physiol. **293**, C337–C345.

104 Matos, T. D., Caria, H., Simões-Teixeira, H., Aasen, T., Dias, O., Andrea, M., Kelsell, D. P. and Fialho, G. (2008) A novel M163L mutation in connexin 26 causing cell death and associated with autosomal dominant hearing loss. Hear. Res. **240**, 87–92.

105 Paznekas, W. A., Boyadjiev, S. A., Shapiro, R. E., Daniels, O., Wollnik, B., Keegan, C. E., Innis, J. W., Dinulos, M. B., Christian, C., Hannibal, M. C., et al. (2003) Connexin 43 (GJA1) mutations cause the pleiotropic phenotype of oculodentodigital dysplasia. Am. J. Hum. Genet. **72**, 408–18.

106 Gladwin, A., Donnai, D., Metcalfe, K., Schrander-Stumpel, C., Brueton, L., Verloes, A., Aylsworth, A., Toriello, H., Winter, R. and Dixon, M. (1997) Localization of a gene for oculodentodigital syndrome to human chromosome 6q22-q24. Hum. Mol. Genet. **6**, 123–127.

107 Huang, T., Shao, Q., MacDonald, A., Xin, L., Lorentz, R., Bai, D. and Laird, D. W. (2013) Autosomal recessive GJA1 (Cx43) gene mutations cause oculodentodigital dysplasia by distinct mechanisms. J. Cell Sci. **126**, 2857–2866.

108 Hu, Y., Chen, I. P., de Almeida, S., Tiziani, V., Do Amaral, C. M. R., Gowrishankar, K., Passos-Bueno, M. R. and Reichenberger, E. J. (2013) A Novel Autosomal Recessive GJA1 Missense Mutation Linked to Craniometaphyseal Dysplasia. PLoS One **8**, 6–12.

109 Paznekas, W. A., Karczeski, B., Vermeer, S., Lowry, R. B., Delatycki, M., Laurence, F., Koivisto, P. A., Van Maldergem, L., Boyadjiev, S. A., Bodurtha, J. N., et al. (2009) GJA1 mutations, variants, and connexin 43 dysfunction as it relates to the oculodentodigital dysplasia phenotype. Hum. Mutat. **30**, 724–733.

110 Bock, M. De, Kerrebrouck, M., Wang, N. and Leybaert, L. (2013) Neurological manifestations of oculodentodigital dysplasia: A Cx43 channelopathy of the central nervous system? Front. Pharmacol. **4**, 1–21.

111 Loddenkemper, T., Grote, K., Evers, S., Oelerich, M. and Stögbauer, F. (2002) Neurological manifestations of the oculodentodigital dysplasia syndrome. J. Neurol. **249**, 584–595.

112 Gutmann, D. H., Zackai, E. H., McDonald-McGinn, D. M., Fischbeck, K. H. and Kamholz, J. (1991) Oculodentodigital dysplasia syndrome associated with abnormal cerebral white matter. Am J Med.Genet. **41**, 18–20.

113 Reaume, a G., de Sousa, P. a, Kulkarni, S., Langille, B. L., Zhu, D., Davies, T. C., Juneja, S. C., Kidder, G. M. and Rossant, J. (1995) Cardiac malformation in neonatal mice lacking connexin43. Science **267**, 1831–1834.

114 Sai, X. and Ladher, R. K. (2015) Early steps in inner ear development: Induction and morphogenesis of the otic placode. Front. Pharmacol. **6**, 1–8.

115 Magariños, M., Contreras, J. and Varela-Nieto, I. (2014) Early Development of the Vertebrate Inner Ear. Dev. Audit. Vestib. Syst. Fourth Ed. **1790**, 1–30.

116 Lanford, P. J., Lan, Y., Jiang, R., Lindsell, C., Weinmaster, G., Gridley, T. and Kelley, M. W. (1999) Notch signalling pathway mediates hair cell development in mammalian cochlea. Nat. Genet. **21**, 289–292.

117 Kiernan, A. E., Pelling, A. L., Leung, K. K. H., Tang, A. S. P., Bell, D. M., Tease, C., Lovell-Badge, R., Steel, K. P. and Cheah, K. S. E. (2005) Sox2 is required for sensory organ development in the mammalian inner ear. Nature **434**, 1031–1035.

118 Chen, P. and Segil, N. (1999) p27(Kip1) links cell proliferation to morphogenesis in the developing organ of Corti. Development **126**, 1581–1590.

119 Lee, Y. S., Liu, F. and Segil, N. (2006) A morphogenetic wave of p27Kip1 transcription directs cell cycle exit during organ of Corti development. Development **133**, 2817–2826.

120 Chen, P., Johnson, J. E., Zoghbi, H. Y. and Segil, N. (2002) The role of Math1 in inner ear development: Uncoupling the establishment of the sensory primordium from hair cell fate determination. Development **129**, 2495–2505.

121 Cai, T., Seymour, M. L., Zhang, H., Pereira, F. A. and Groves, A. K. (2013)

Conditional Deletion of Atoh1 Reveals Distinct Critical Periods for Survival and Function of Hair Cells in the Organ of Corti. J. Neurosci. **33**, 10110–10122.

122 Costa, A., Sanchez-Guardado, L., Juniat, S., Gale, J. E., Daudet, N. and Henrique, D. (2015) Generation of sensory hair cells by genetic programming with a combination of transcription factors. Dev. **142**, 1948–1959.

123 Li, Y., Liu, H., Barta, C. L., Judge, P. D., Zhao, L., Zhang, W. J., Gong, S., Beisel, K. W. and He, D. Z. Z. (2016) Transcription factors expressed in mouse cochlear inner and outer hair cells. PLoS One **11**, 1–16.

124 Waldhaus et al. (2016) Quantitative High-Resolution Cellular Map of the Organ of Corti **42**, 407–420.

125 Frenz, C. M. and Van De Water, T. R. (2000) Immunolocalization of connexin 26 in the developing mouse cochlea. Brain Res. Rev. **32**, 172–180.

126 Zheng, J. L. and Gao, W. Q. (2000) Overexpression of Math1 induces robust production of extra hair cells in postnatal rat inner ears. Nat. Neurosci. **3**, 580–586.

127 Izumikawa, M., Minoda, R., Kawamoto, K., Abrashkin, K. A., Swiderski, D. L., Dolan, D. F., Brough, D. E. and Raphael, Y. (2005) Auditory hair cell replacement and hearing improvement by Atoh1 gene therapy in deaf mammals. Nat. Med. **11**, 271–276.

128 Lanford, P. J., Shailam, R., Norton, C. R., Ridley, T. and Kelley, M. W. (2000) Expression of Math1 and HES5 in the cochleae of wildtype and Jag2 mutant mice. JARO - J. Assoc. Res. Otolaryngol. **1**, 161–171.

129 Woods, C., Montcouquiol, M. and Kelley, M. W. (2004) Math1 regulates development of the sensory epithelium in the mammalian cochlea. Nat. Neurosci. **7**, 1310–1318.

130 Morrison, A., Hodgetts, C., Gossler, A., Hrabě de Angelis, M. and Lewis, J. (1999) Expression of Delta1 and Serrate1 (Jagged1) in the mouse inner ear. Mech. Dev. **84**, 169–172.

131 Murata, J., Tokunaga, A., Okanu, H., and Kuboi, A. T. (2006) Mapping of Notch Activation during Cochlear Development in Mice: Implications for Determination of Prosensory Domain and Cell Fate Diversification **518**, 502–518.

132 Kikuchi, T., Kimura, R., Paul, D. and Adams, J. (1995) Gap junctions in the rat cochlea: immunohistochemical and ultrastructural analysis. Anat. Embryol. (Berl). **191**, 101–118.

133 Zhao, H. B. and Santos-Sacchl, J. (1999) Auditory collusion and a coupled couple of outer hair cells. Nature **399**, 359–362.

134 Zhao, H.B, and Yu, N. (2006) Distinct and Gradient Distributions of Connexin26 and Connexin30 in the Cochlear Sensory Epithelium of Guinea Pigs. J. Comp. Neurol. **499**, 506–518.

135 Wang, X.-H., Streeter, M., Liu, Y.-P. and Zhao, H.-B. (2009) Identification and characterization of pannexin expression in the mammalian cochlea. J. Comp. Neurol. **512**, 336–46.

136 Yu, N. and Zho, H. B. (2009) Modulation of outer hair cell electromotility by cochlear

supporting cells and gap junctions. PLoS One **4**.

137 Benito-Gonzalez, A. and Doetzlhofer, A. (2014) Hey1 and Hey2 control the spatial and temporal pattern of mammalian auditory hair cell differentiation downstream of hedgehog signaling. J. Neurosci. **34**, 12865–12876.

138 Kiernan, A. (2013) Notch signaling during cell fate determination in the inner ear. Semin. Cell Dev. Biol. **24**, 470–479.

139 Abdolazimi, Y., Stojanova, Z. and Segil, N. (2016) Selection of cell fate in the organ of Corti involves the integration of Hes/Hey signaling at the Atoh1 promoter. Dev. **143**, 841–850.

140 Cotanche, D. A. and Kaiser, C. L. (2011) NIH Public Access **266**, 18–25.

141 Slowik, A.D., and Bermingham-McDonogh,O. (2009) Notch signaling in mammalian hair cell regeneration **6**, 247–253.

142 Hume,C., Bratt D., and E. C. O. (2007) Expression of LHX3 and SOX2 during Mouse Inner Ear Development. Gene Expr. Patterns **7**, 798–807.

143 Xie, L., Chen, S., Xu, K., Cao, H.-Y., Du, A.-N., Bai, X., Sun, Y. and Kong, W.-J. (2019) Reduced postnatal expression of cochlear Connexin26 induces hearing loss and affects the developmental status of pillar cells in a dose-dependent manner. Neurochem. Int. **128**, 196–205.

144 Chen, S., Sun, Y., Lin, X. and Kong, W. (2014) Down regulated connexin26 at different postnatal stage displayed different types of cellular degeneration and formation of organ of Corti. Biochem. Biophys. Res. Commun., Elsevier Inc. **445**, 71–77.

145 Chen, S., Xie, L., Xu, K., Cao, H.-Y., Wu, X., Xu, X.-X., Sun, Y. and Kong, W.-J. (2018) Developmental abnormalities in supporting cell phalangeal processes and cytoskeleton in the *Gjb2* knockdown mouse model. Dis. Model. Mech. **11**, dmm033019.

146 Chen, S., Sun, Y., Lin, X. and Kong, W. (2014) Down regulated connexin26 at different postnatal stage displayed different types of cellular degeneration and formation of organ of Corti. Biochem. Biophys. Res. Commun., Elsevier Inc. **445**, 71–77.

147 Chang, Q., Tang, W., Kim, Y. and Lin, X. (2015) Timed conditional null of connexin26 in mice reveals temporary requirements of connexin26 in key cochlear developmental events before the onset of hearing. Neurobiol. Dis., Elsevier Inc. **73**, 418–427.

148 Nickel, R. and Forge, A. (2008) Gap junctions and connexins in the inner ear: Their roles in homeostasis and deafness. Curr. Opin. Otolaryngol. Head Neck Surg. **16**, 452–457.

149 Cohen-Salmon, M., Ott, T., Michel, V., Hardelin, J. P., Perfettini, I., Eybalin, M., Wu, T., Marcus, D. C., Wangemann, P., Willecke, K., et al. (2002) Targeted ablation of connexin26 in the inner ear epithelial gap junction network causes hearing impairment and cell death. Curr. Biol. **12**, 1106–1111.

150 Martínez, A. D., Acuña, R., Figueroa, V., Maripillan, J. and Nicholson, B. (2009)

Gap-Junction Channels Dysfunction in Deafness and Hearing Loss. Antioxid. Redox Signal. **11**, 309–322.

151 Tang, W., Zhang, Y., Chang, Q., Ahmad, S., Dahlke, I., Yi, H., Chen, P., Paul, D. L. and Lin, X. (2006) Connexin29 Is Highly Expressed in Cochlear Schwann Cells, and It Is Required for the Normal Development and Function of the Auditory Nerve of Mice. J. Neurosci. **26**, 1991.

152 Xia, J. H., Liu, C. Y., Tang, B. S., Pan, Q., Huang, L., Dai, H. P., Zhang, B. R., Xie, W., Hu, D. X., Zheng, D., et al. (1998) Mutations in the gene encoding gap junction protein beta-3 associated with autosomal dominant hearing impairment. Nat. Genet. **20**, 370–3.

153 Wang, W. H., Yang, J. J., Lin, Y. C., Yang, J. T. and Li, S. Y. (2010) Novel expression patterns of connexin 30.3 in adult rat cochlea. Hear. Res., Elsevier B.V. **265**, 77–82.

154 Majumder, P., Crispino, G., Rodriguez, L., Ciubotaru, C. D., Anselmi, F., Piazza, V., Bortolozzi, M. and Mammano, F. (2010) ATP-mediated cell-cell signaling in the organ of corti: The role of connexin channels. Purinergic Signal. **6**, 167–187.

155 Mohamed, V. P., Hashim, Y. Z. H., Amid, A., Mel, M., Kamarulzaman, A. R., Adil, M., Wahab, A., Ezrina, S. and Saberi, M. (2011) Chinese hamster ovary (CHO-K1) cells expressed native insulin-like growth factor-1 (IGF-1) gene towards efficient mammalian cell culture host system. African J. Biotechnol. **10**, 18716–18721.

156 Yum, S. W., Zhang, J., Valiunas, V., Kanaporis, G., Brink, P. R., White, T. W. and Scherer, S. S. (2007) Human connexin26 and connexin30 form functional heteromeric and heterotypic channels. AJP Cell Physiol. **293**, C1032–C1048.

157 Liu, W., Boström, M., Kinnefors, A. and Rask-Andersen, H. (2009) Unique expression of connexins in the human cochlea. Hear. Res., Elsevier B.V. **250**, 55–62.

158 Cohen-Salmon, M., Maxeiner, S., Krüger, O., Theis, M., Willecke, K. and Petit, C. (2004) Expression of the connexin43- and connexin45-encoding genes in the developing and mature mouse inner ear. Cell Tissue Res. **316**, 15–22.

159 Kim, A. H., Nahm, E., Sollas, A., Mattiace, L. and Rozental, R. (2013) Connexin 43 and hearing: Possible implications for retrocochlear auditory processing. Laryngoscope **123**, 3185–3193.

160 Liu, X. Z., Xia, X. J., Adams, J., Chen, Z. Y., Welch, K. O., Tekin, M., Ouyang, X. M., Kristiansen, A., Pandya, A., Balkany, T., et al. (2001) Mutations in GJA1 (connexin 43) are associated with non-syndromic autosomal recessive deafness. Hum. Mol. Genet. **10**, 2945–2951.

161 Liu, W. J. and Yang, J. (2015) Preferentially regulated expression of connexin 43 in the developing spiral ganglion neurons and afferent terminals in post-natal rat cochlea. Eur. J. Histochem. **59**, 17–29.

162 Suzuki, T., Takamatsu, T. and Oyamada, M. (2003) Expression of Gap Junction Protein Connexin43 in the Adult Rat Cochlea: Comparison with Connexin26. J. Histochem. Cytochem. **51**, 903–912.

163 Lautermann, J., Cate, W. F., Altenhoff, P., Grümmer, R., Traub, O., Klaus, H. F. and

Elke, J. (1998) Expression of the gap-junction connexins 26 and 30 in the rat cochlea 415–420.

164 Liu, W., Glueckert, R., Linthicum, F. H., Rieger, G., Blumer, M., Bitsche, M., Pechriggl, E., Rask-Andersen, H. and Schrott-Fischer, A. (2014) Possible role of gap junction intercellular channels and connexin 43 in satellite glial cells (SGCs) for preservation of human spiral ganglion neurons: A comparative study with clinical implications. Cell Tissue Res. **355**, 267–278.

165 Locher, H., de Groot, J. C. M. J., van Iperen, L., Huisman, M. A., Frijns, J. H. M. and Chuva de Sousa Lopes, S. M. (2015) Development of the stria vascularis and potassium regulation in the human fetal cochlea: Insights into hereditary sensorineural hearing loss. Dev. Neurobiol. **75**, 1219–1240.

166 Kelly K. Ball, Gautam K. Gandhi2, Jarrod Thrash1, Nancy F. Cruz1, and G. A. D. (2007) Astrocytic Connexin Distributions and Rapid, Extensive Dye Transfer Via Gap Junctions in the Inferior Colliculus: Implications for [14 C]Glucose Metabolite Trafficking. J Neurosci Res **85**, 1–29.

167 Yang, J. J., Huang, S. H., Chou, K. H., Liao, P. J., Su, C. C. and Li, S. Y. (2007) Identification of mutations in members of the connexin gene family as a cause of nonsyndromic deafness in Taiwan. Audiol. Neurotol. **12**, 198–208.

168 Gabriel, H. D., Jung, D., Bützler, C., Temme, A., Traub, O., Winterhager, E. and Willecke, K. (1998) Transplacental uptake of glucose is decreased in embryonic lethal connexin26-deficient mice. J. Cell Biol. **140**, 1453–1461.

169 Kudo, T., Kure, S., Ikeda, K., Xia, A. P., Katori, Y., Suzuki, M., Kojima, K., Ichinohe, A., Suzuki, Y., Aoki, Y., et al. (2003) Transgenic expression of a dominant-negative connexin26 causes degeneration of the organ of Corti and non-syndromic deafness. Hum. Mol. Genet. **12**, 995–1004.

170 Sun, Y., Tang, W., Chang, Q., Wang, Y., Kong, W. and Lin, X. (2009) Connexin30 null and conditional connexin26 null mice display distinct pattern and time course of cellular degeneration in the cochlea. J. Comp. Neurol. **516**, 569–579.

171 Wang, Y., Chang, Q., Tang, W., Sun, Y., Zhou, B., Li, H. and Lin, X. (2009) Targeted connexin26 ablation arrests postnatal development of the organ of Corti. Biochem. Biophys. Res. Commun., Elsevier Inc. **385**, 33–37.

172 Schütz, M., Auth, T., Gehrt, A., Bosen, F., Körber, I., Strenzke, N., Moser, T. and Willecke, K. (2011) The connexin26 S17F mouse mutant represents a model for the human hereditary keratitis-ichthyosis-deafness syndrome. Hum. Mol. Genet. **20**, 28–39.

173 Crispino, G., Di Pasquale, G., Scimemi, P., Rodriguez, L., Ramirez, F. G., de Siati, R. D., Santarelli, R. M., Arslan, E., Bortolozzi, M., Chiorini, J. A., et al. (2011) BAAV mediated GJB2 gene transfer restores gap junction coupling in cochlear organotypic cultures from deaf Cx26Sox10Cre mice. PLoS One **6**.

174 Takada, Y., Beyer, L. A., Swiderski, D. L., O'Neal, A. L., Prieskorn, D. M., Shivatzki, S., Avraham, K. B. and Raphael, Y. (2014) Connexin 26 null mice exhibit spiral ganglion degeneration that can be blocked by BDNF gene therapy. Hear. Res., Elsevier B.V. **309**, 124–135.

175 Zhang, Y., Zhang, X., Li, L., Sun, Y. and Sun, J. (2012) Apoptosis progression in the hair cells in the organ of Corti of GJB2 conditional knockout mice. Clin. Exp. Otorhinolaryngol. **5**, 132–138.

176 Zhu1 Y, Liang, C., Chen J.,, Zong L., Chen, G., andZhao, H.B. (2013) Active cochlear amplification is dependent on supporting cell gap junctions. Nat commun **52**, 566–584.

177 Zong, L., Chen, J., Zhu, Y. and Zhao, H. B. (2017) Progressive age-dependence and frequency difference in the effect of gap junctions on active cochlear amplification and hearing. Biochem. Biophys. Res. Commun., Elsevier Ltd **489**, 223–227.

178 Anzai, T., Fukunaga, I., Hatakeyama, K., Fujimoto, A., Kobayashi, K., Nishikawa, A., Aoki, T., Noda, T., Minowa, O., Ikeda, K., et al. (2015) Deformation of the outer hair cells and the accumulation of caveolin-2 in connexin 26 deficient mice. PLoS One **10**, 1–12.

179 Kamiya, K., Yum, S. W., Kurebayashi, N., Muraki, M., Ogawa, K., Karasawa, K., Miwa, A., Guo, X., Gotoh, S., Sugitani, Y., et al. (2014) Assembly of the cochlear gap junction macromolecular complex requires connexin 26. J. Clin. Invest. **124**, 1598–1607.

180 Chen, Y., Hu, L., Wang, X., Sun, C., Lin, X., li, L., Mei, L., Huang, Z., Yang, T. and Wu, H. (2016) Characterization of a knock-in mouse model of the homozygous p.V37I variant in Gjb2. Sci. Rep., Nature Publishing Group **6**, 33279.

181 Lukashkina, V. A., Yamashita, T., Zuo, J., Lukashkin, A. N. and Russell, I. J. (2017) Amplification mode differs along the length of the mouse cochlea as revealed by connexin 26 deletion from specific gap junctions. Sci. Rep., Springer US **7**, 1–11.

182 Chen, S., Xu, K., Xie, L., Cao, H.-Y., Wu, X., Du, A.-N., He, Z.-H., Lin, X., Sun, Y. and Kong, W.-J. (2018) The spatial distribution pattern of Connexin26 expression in supporting cells and its role in outer hair cell survival. Cell Death Dis. **9**, 1180.

183 Pauley, S., Lai, E. and Fritzsch, B. (2006) Foxg1 is required for morphogenesis and histogenesis of the mammalian inner ear. Dev. Dyn. **235**, 2470–2482.

184 El-Amraoui, A., Cohen-Salmon, M., Petit, C. and Simmler, M. C. (2001) Spatiotemporal expression of otogelin in the developing and adult mouse inner ear. Hear. Res. **158**, 151–159.

185 Burton, Q., Cole, L. K., Mulheisen, M., Chang, W. and Wu, D. K. (2004) The role of Pax2 in mouse inner ear development. Dev. Biol. **272**, 161–175.

186 Breuskin, I., Bodson, M., Thelen, N., Thiry, M., Borgs, L., Nguyen, L., Lefebvre, P. P. and Malgrange, B. (2009) Sox10 promotes the survival of cochlear progenitors during the establishment of the organ of Corti. Dev. Biol., Elsevier Inc. **335**, 327–339.

187 Hasegawa, S., Sato, T., Akazawa, H., Okada, H., Maeno, A., Ito, M., Sugitani, Y., Shibata, H., Miyazaki, J. I., Katsuki, M., et al. (2002) Apoptosis in neural crest cells by functional loss of APC tumor suppressor gene. Proc. Natl. Acad. Sci. U. S. A. **99**, 297–302.

188 Lee,M., Calle, L.,, Brennan, A., Ahmed, S., Sviderskawa, E., R. Jessen, K.R., 1 and Mirksy, A. R. (2001) In early development of the rat mRNA for the major myelin

protein P0 is expressed in nonsensory areas of the embryonic inner ear, notochord, enteric nervous system, and olfactory ensheathing cells. Dev. Dyn. **222**, 40–51.

189 Kumamoto, T. and Hanashima, C. (2017) Evolutionary conservation and conversion of Foxg1 function in brain development. Dev. Growth Differ. **59**, 258–269.

190 Lee, J. R. and White, T. W. (2009) Connexin-26 mutations in deafness and skin disease. Expert Rev. Mol. Med. **11**, 1–19.

191 Lee, J. Y., In, S. Il, Kim, H. J., Jeong, S. Y., Choung, Y. H. and Kim, Y. C. (2010) Hereditary palmoplantar keratoderma and deafness resulting from genetic mutation of connexin 26. J. Korean Med. Sci. **25**, 1539–1542.

192 García, I. E., Maripillán, J., Jara, O., Ceriani, R., Palacios-Muñoz, A., Ramachandran, J., Olivero, P., Perez-Acle, T., González, C., Sáez, J. C., et al. (2015) Keratitis-ichthyosis-deafness syndrome-associated Cx26 mutants produce nonfunctional gap junctions but hyperactive hemichannels when co-expressed with wild type Cx43. J. Invest. Dermatol. **135**, 1338–1347.

193 García, I. E., Bosen, F., Mujica, P., Pupo, A., Flores-Muñoz, C., Jara, O., González, C., Willecke, K. and Martínez, A. D. (2016) From Hyperactive Connexin26 Hemichannels to Impairments in Epidermal Calcium Gradient and Permeability Barrier in the Keratitis-Ichthyosis-Deafness Syndrome. J. Invest. Dermatol. **136**, 574–583.

194 Bason, L., Dudley, T., Lewis, K., Shah, U., Potsic, W., Ferraris, A., Fortina, P., Rappaport, E. and Krantz, I. D. (2002) Homozygosity for the V37I Connexin 26 mutation in three unrelated children with sensorineural hearing loss. Clin. Genet. **61**, 459–464.

195 Kim, J., Jung, J., Lee, M. G., Choi, J. Y. and Lee, K. A. (2015) Non-syndromic hearing loss caused by the dominant cis mutation R75Q with the recessive mutation V37I of the GJB2 (Connexin 26) gene. Exp. Mol. Med., Nature Publishing Group **47**, e169.

196 Grifa, A., A Wagner, C., D'Ambrosio, L., Melchionda, S., Bernardi, F., Lopez-Bigas, N., Rabionet, R., Arbones, M., Della Monica, M., Estivill, X., et al. (1999) Mutations in GJB6 cause nonsyndromic autosomal dominant deafness at DFNA3 locus. Nat. Genet. **23**, 16–18.

197 Nemoto-Hasebe, I., Akiyama, M., Kudo, S., Ishiko, A., Tanaka, A., Arita, K. and Shimizu, H. (2009) Novel mutation p.Gly59Arg in GJB6 encoding connexin 30 underlies palmoplantar keratoderma with pseudoainhum, knuckle pads and hearing loss. Br. J. Dermatol. **161**, 452–455.

198 Wang, W.-H., Liu, Y.-F., Su, C.-C., Su, M.-C., Li, S.-Y. and Yang, J.-J. (2011) A novel missense mutation in the connexin30 causes nonsyndromic hearing loss. PLoS One **6**, e21473.

199 Schütz, M., Scimemi, P., Majumder, P., de Siati, R. D., Crispino, G., Rodriguez, L., Bortolozzi, M., Santarelli, R., Seydel, A., Sonntag, S., et al. (2010) The human deafness-associated connexin 30 T5M mutation causes mild hearing loss and reduces biochemical coupling among cochlear non-sensory cells in knock-in mice. Hum. Mol. Genet. **19**, 4759–4773.

200 Kelly, J. J., Abitbol, J. M., Hulme, S., Press, E. R., Laird, D. W. and Allman, B. L. (2019) The connexin 30 A88V mutant reduces cochlear gap junction expression and confers long-term protection against hearing loss. J. Cell Sci. **132**.

201 Bosen, F., Schütz, M., Beinhauer, A., Strenzke, N., Franz, T. and Willecke, K. (2014) The Clouston syndrome mutation connexin30 A88V leads to hyperproliferation of sebaceous glands and hearing impairments in mice. FEBS Lett., Federation of European Biochemical Societies **588**, 1795–1801.

202 Lukashkina, V. A., Levic, S., Lukashkin, A. N., Strenzke, N. and Russell, I. J. (2017) A connexin30 mutation rescues hearing and reveals roles for gap junctions in cochlear amplification and micromechanics. Nat. Commun., Nature Publishing Group **8**, 1–9.

203 Berger, A. C., Kelly, J. J., Lajoie, P., Shao, Q. and Laird, D. W. (2014) Mutations in Cx30 that are linked to skin disease and non-syndromic hearing loss exhibit several distinct cellular pathologies. J. Cell Sci. **127**, 1751–1764.

204 Teubner, B., Michel, V., Pesch, J., Lautermann, J., Cohen-Salmon, M., Söhl, G., Jahnke, K., Winterhager, E., Herberhold, C., Hardelin, J. P., et al. (2003) Connexin30 (Gjb6)-deficiency causes severe hearing impairment and lack of endocochlear potential. Hum. Mol. Genet. **12**, 13–21.

205 Teubner, B., Michel, V., Pesch, J., Lautermann, J., Cohen-Salmon, M., Söhl, G., Jahnke, K., Winterhager, E., Herberhold, C., Hardelin, J. P., et al. (2003) Connexin30 (Gjb6)-deficiency causes severe hearing impairment and lack of endocochlear potential. Hum. Mol. Genet. **12**, 13–21.

206 Boulay, A.-C., Del Castillo, F. J., Giraudet, F., Hamard, G., Giaume, C., Petit, C., Avan, P. and Cohen-Salmon, M. (2013) Hearing Is Normal without Connexin30 **33**, 430–434.

207 Cohen-Salmon, M., Regnault, B., Cayet, N., Caille, D., Demuth, K., Hardelin, J.-P., Janel, N., Meda, P. and Petit, C. (2007) Connexin30 deficiency causes instrastrial fluid-blood barrier disruption within the cochlear stria vascularis. Proc. Natl. Acad. Sci. **104**, 6229–6234.

208 Ortolano, S., Di Pasquale, G., Crispino, G., Anselmi, F., Mammano, F. and Chiorini, J. A. (2008) Coordinated control of connexin 26 and connexin 30 at the regulatory and functional level in the inner ear. Proc. Natl. Acad. Sci. **105**, 18776–18781.

209 Kikuchi, T., Adams, J. C., Miyabe, Y., So, E. and Kobayashi, T. (2000) Potassium ion recycling pathway via gap junction systems in the mammalian cochlea and its interruption in hereditary nonsyndromic deafness. Med. Electron Microsc. **33**, 51–56.

210 Ando, M. and Takeuchi, S. (1999) Immunological identification of an inward rectifier K+ channel (Kir4.1) in the intermediate cell (melanocyte) of the cochlear stria vascularis of gerbils and rats. Cell Tissue Res. **298**, 179–183.

211 Hibino, H., Horio, Y., Inanobe, A., Doi, K., Ito, M., Yamada, M., Gotow, T., Uchiyama, Y., Kawamura, M., Kubo, T., et al. (1997) An ATP-dependent inwardly rectifying potassium channel, K(AB)-2 (Kir4.1), in cochlear stria vascularis of inner ear: Its specific subcellular localization and correlation with the formation of endocochlear potential. J. Neurosci. **17**, 4711–4721.

212 Jagger, D. J., Nevill, G. and Forge, A. (2010) The membrane properties of cochlear root cells are consistent with roles in potassium recirculation and spatial buffering. JARO - J. Assoc. Res. Otolaryngol. **11**, 435–448.

213 Jagger, D. J. and Forge, A. (2013) The enigmatic root cell - Emerging roles contributing to fluid homeostasis within the cochlear outer sulcus. Hear. Res., **303**, 1–11.

214 Kofugi, P., and Newman, E.A. (2004) Potassium buffering in the central nervous system. Neuroscience **129**, 1045–1056.

215 Rio, C., Dikkes, P., Liberman, C., and Corfas, A. G. (2002) Glial fibrillary acidic protein expression and promoter activity in the inner ear of developing and adult mice. J. Comp. Neurol. **442**, 156–162.

216 Zhao, H.-B. (2017) Hypothesis of K+-Recycling Defect Is Not a Primary Deafness Mechanism for Cx26 (GJB2) Deficiency. Front. Mol. Neurosci. **10**, 1–6.

217 Jagger, D. J. and Forge, A. (2015) Connexins and gap junctions in the inner ear--it's not just about K^+ recycling. Cell Tissue Res. **360**, 633–44.

218 Chang, Q., Tang, W., Ahmad, S., Zhou, B. and Lin, X. (2008) Gap junction mediated intercellular metabolite transfer in the cochlea is compromised in connexin30 null mice. PLoS One **3**, 2–11.

219 Suzuki, T., Matsunami, T., Hisa, Y., Takata, K., Takamatsu, T. and Oyamada, M. (2009) Roles of gap junctions in glucose transport from glucose transporter 1-positive to -negative cells in the lateral wall of the rat cochlea. Histochem. Cell Biol. **131**, 89–102.

220 Katakowski, M., Buller, B., Wang, X., Rogers, T. and Chopp, M. (2010) Functional microRNA is transferred between glioma cells. Cancer Res. **70**, 8259–8263.

221 Zong, L., Zhu, Y., Liang, R. and Zhao, H. B. (2016) Gap junction mediated miRNA intercellular transfer and gene regulation: A novel mechanism for intercellular genetic communication. Sci. Rep. **6**, 1–9.

222 Conte, I., Banfi, S. and Bovolenta, P. (2013) Non-coding RNAs in the development of sensory organs and related diseases. Cell. Mol. Life Sci. **70**, 4141–4155.

223 Friedman, L. M., Dror, A. A., Mor, E., Tenne, T., Toren, G., Satoh, T., Biesemeier, D. J., Shomron, N., Fekete, D. M., Hornstein, E., et al. (2009) MicroRNAs are essential forhttp://www.scielo.br/pdf/paideia/v10n19/03.pdf development and function of inner ear hair cells in vertebrates.http://www.scielo.br/pdf/paideia/v10n19/03.pdf. Proc. Natl. Acad. Sci. U. S. A. **106**, 7915–20.

224 Sacheli, R., Nguyen, L., Borgs, L., Vandenbosch, R., Bodson, M., Lefebvre, P. and Malgrange, B. (2009) Expression patterns of miR-96, miR-182 and miR-183 in the developing inner ear. Gene Expr. Patterns, Elsevier B.V. **9**, 364–370.

225 Zhu, Y., Zong, L., Mei, L. and Zhao, H. B. (2015) Connexin26 gap junction mediates miRNA intercellular genetic communication in the cochlea and is required for inner ear development. Sci. Rep., Nature Publishing Group **5**, 1–8.

226 Sáez, J. C. and Leybaert, L. (2014) Hunting for connexin hemichannels. FEBS Lett. **588**, 1205–1211.

227 Kim, Y., Davidson, J. O., Green, C. R., Nicholson, L. F. B., O'Carroll, S. J. and Zhang, J. (2018) Connexins and Pannexins in cerebral ischemia. Biochim. Biophys. Acta - Biomembr., Elsevier B.V. **1860**, 224–236.

228 Johnson, R. D. and Camelliti, P. (2018) Role of non-myocyte gap junctions and connexin hemichannels in cardiovascular health and disease: Novel therapeutic targets? Int. J. Mol. Sci. **19**.

229 Bosher, S. K. and Warren, R. L. (1978) Very low calcium content of cochlear endolymph, an extracellular fluid. Nature **273**, 377–378.

230 Zhao, H.-B., Yu, N. and Fleming, C. R. (2005) Gap junctional hemichannel-mediated ATP release and hearing controls in the inner ear. Proc. Natl. Acad. Sci. U. S. A. **102**, 18724–9.

231 Anselmi, F., Hernandez, V. H., Crispino, G., Seydel, A., Ortolano, S., Roper, S. D., Kessaris, N., Richardson, W., Rickheit, G., Filippov, M. A., et al. (2008) ATP release through connexin hemichannels and gap junction transfer of second messengers propagate Ca2+ signals across the inner ear. Proc. Natl. Acad. Sci. **105**, 18770–18775.

232 Zhao, G. and. (2008) Hemichannel-mediated inositol 1,4,5-tri- sphosphate (IP3) release in the cochlea: a novel mechanism of IP3 intercellular signaling. **18**, 386–392.

233 Tritsch, N. X., Yi, E., Gale, J. E., Glowatzki, E. and Bergles, D. E. (2007) The origin of spontaneous activity in the developing auditory system. Nature **450**, 50–55.

234 Cunningham, M. O., Whittington, M. A., Bibbig, A., Roopun, A., Fiona, E., Lebeau, N., Vogt, A., Monyer, H., Buhl, E. H., Traub, R. D., et al. (2004) A role for bursting neurons in cortical fast rhythmic in vitro gamma oscillations **i**.

235 Tang, W., Ahmad, S., Shestopalov, V. I. and Lin, X. (2008) Pannexins are new molecular candidates for assembling gap junctions in the cochlea. Neuroreport **19**, 1253–7.

236 Chen, J., Zhu, Y., Liang, C., Chen, J. and Zhao, H.-B. (2015) Pannexin1 channels dominate ATP release in the cochlea ensuring endocochlear potential and auditory receptor potential generation and hearing. Sci. Rep., Nature Publishing Group **5**, 10762.

237 Ashmore, J. F. and Ohmori, H. (1990) Control of intracellular calcium by ATP in isolated outer hair cells of the guinea-pig cochlea. J. Physiol. **428**, 109–131.

238 Housley, G. D., Morton-jones, R., Vlajkovic, S. M. and Telang, R. S. (2013) ATP-gated ion channels mediate adaptation to elevated sound levels 2–7.

239 Zorzi, V., Paciello, F., Ziraldo, G., Peres, C., Mazzarda, F., Nardin, C., Pasquini, M., Chiani, F., Raspa, M., Scavizzi, F., et al. (2017) Mouse Panx1 is dispensable for hearing acquisition and auditory function. Front. Mol. Neurosci. **10**, 379.

240 Chen, J., Liang, C., Zong, L., Zhu, Y. and Zhao, H. (2018) Knockout of Pannexin-1 Induces Hearing Loss 1–11.

241 Zhao, H.-B., Zhu, Y., Liang, C. and Chen, J. (2015) Pannexin 1 deficiency can induce hearing loss. Biochem. Biophys. Res. Commun. 1–5.

242 Penuela, S., Bhalla, R., Nag K.,, and Laird, D.W. (2009) Glycosylation Regulates

Pannexin Intermixing and Cellular Localization Silvia. Mol. Biol. Cell **20**, 4313–4323.

243 Whyte-fagundes, P., Kurtenbach, S., Zoidl, C., Shestopalov, V. I., Carlen, P. L. and Zoidl, G. (2018) A Potential Compensatory Role of Panx3 in the VNO of a Panx1 Knock Out Mouse Model **11**, 1–16.

244 Lohman, A.W. and Isakson, B.E. (2014) Differentiating connexin hemichannels and pannexin channels in cellular ATP release **588**, 1379–1388.

245 Penuela, S., Kelly, J. J., Churko, J. M., Barr, K. J., Berger, A. C. and Laird, D. W. (2014) Panx1 regulates cellular properties of keratinocytes and dermal fibroblasts in skin development and wound healing. J. Invest. Dermatol., Nature Publishing Group **134**, 2026–35.

246 Bargiotas, P., Krenz, A., Monyer, H., Schwaninger, M., Bargiotas, P., Krenz, A., Monyer, H. and Schwaninger, M. (2012) Functional outcome of pannexin-deficient mice after cerebral ischemia Functional outcome of pannexin-deficient mice after cerebral ischemia. Channels **6**, 453–456.

247 Niskar, A. S., Kieszak, S. M., Holmes, A. E., Esteban, E., Rubin, C. and Brody, D. J. (2001) Estimated prevalence of noise-induced hearing threshold shifts among children 6 to 19 years of age: The Third National Health and Nutrition Examination Survey, 1988-1994, United States. Pediatrics **108**, 40–43.

248 Ryan, A. F. (2016) Temporary and Permanent Noise-Induced Threshold Shifts: A Review of Basic and Clinical Observations **37**, 1–8.

249 Le, T. N., Straatman, L. V., Lea, J. and Westerberg, B. (2017) Current insights in noise-induced hearing loss: a literature review of the underlying mechanism, pathophysiology, asymmetry, and management options. J. Otolaryngol. - Head Neck Surg., Journal of Otolaryngology - Head & Neck Surgery **46**, 1–15.

250 Le Prell, C. G., Yamashita, D., Minami, S. B., Yamasoba, T. and Miller, J. M. (2007) Mechanisms of noise-induced hearing loss indicate multiple methods of prevention. Hear. Res. **226**, 22–43.

251 Kurabi, A., Keithley, E. M., Housley, G. D., Ryan, A. F. and Wong, A. C. Y. (2017) Cellular mechanisms of noise-induced hearing loss. Hear. Res., Elsevier B.V **349**, 129–137.

252 Kujawa, S. G. and Liberman, M. C. (2009) Adding Insult to Injurt: Cochlear Nerve Degeneration after “Temporary” Noise- Induced Hearing Loss. J. Neurosci. **29**, 14077-.

253 Hu, B. H., Henderson, D. and Nicotera, T. M. (2002) F-actin cleavage in apoptotic outer hair cells in chinchilla cochleas exposed to intense noise. Hear. Res. **172**, 1–9.

254 Nicotera, T. M., Hu, B. H. and Henderson, D. (2003) The Caspase Pathway in Noise-Induced Apoptosis of the Chinchilla Cochlea. JARO - J. Assoc. Res. Otolaryngol. **4**, 466–477.

255 Hu, B. H., Cai, Q., Manohar, S., Jiang, H., Ding, D., Coling, D. E., Zheng, G. and Salvi, R. (2009) Differential expression of apoptosis-related genes in the cochlea of noise-exposed rats. Neuroscience, IBRO **161**, 915–925.

256 Yamane, H., Nakai, Y., Takayama, M., Iguchi, H., Nakagawa, T. and Kojima, A.

(1995) Appearance of free radicals in the guinea pig inner ear after noise-induced acoustic trauma. Eur. Arch. Oto-Rhino-Laryngology **252**, 504–508.

257 Lu, J., Li, W., Du, X., Ewert, D. L., West, M. B., Stewart, C., Floyd, R. A. and Kopke, R. D. (2014) Antioxidants reduce cellular and functional changes induced by intense noise in the inner ear and cochlear nucleus. JARO - J. Assoc. Res. Otolaryngol. **15**, 353–372.

258 Wang, J., Ruel, J., Ladrech, S., Bonny, C., Van De Water, T. R. and Puel, J. L. (2007) Inhibition of the c-Jun N-terminal kinase-mediated mitochondrial cell death pathway restores auditory function in sound-exposed animals. Mol. Pharmacol. **71**, 654–666.

259 Lo, Y. Y. C., Wong, J. M. S. and Cruz, T. F. (1996) Reactive oxygen species mediate cytokine activation of c-Jun NH2- terminal kinases. J. Biol. Chem. **271**, 15703–15707.

260 Fridberger, A., Flock, Å., Ulfendahl, M. and Flock, B. (1998) Acoustic overstimulation increases outer hair cell Ca 2% concentrations and causes dynamic contractions of the hearing organ (noise-induced hearing lossguinea pigmicromechanicsimage analysiscochlear microphonic potential). Neurobiology **95**, 7127–7132.

261 Thorne, P. R. and Nuttall, A. L. (1987) Laser doppler measurements of cochlear blood flow during loud sound exposure in the guinea pig. Hear. Res. **27**, 1–10.

262 Liberman, M. C. and Kujawa, S. G. (2017) Cochlear synaptopathy in acquired sensorineural hearing loss: Manifestations and mechanisms. Hear. Res., Elsevier B.V.

263 Puel, R. Pujol. A. J.-L. (1999) Excitotoxicity, Synaptic Repair, and Functional Recovery in the Mammalian Cochlea: A Review of Recent Findings. Ann. New York Acad. Sci. 249–254.

264 Zhao, Y. D., Yamoah, E. N. and Gillespie, P. G. (1996) Regeneration of broken tip links and restoration of mechanical transduction in hair cells. Proc. Natl. Acad. Sci. U. S. A. **93**, 15469–15474.

265 Hsu, W. C., Wang, J. Der, Hsu, C. J., Lee, S. Y. and Yeh, T. H. (2004) Expression of connexin 26 in the lateral wall of the rat cochlea after acoustic trauma. Acta Otolaryngol. **124**, 459–463.

266 Yamaguchi, T., Nagashima, R., Yoneyama, M., Shiba, T. and Ogita, K. (2014) Disruption of ion-trafficking system in the cochlear spiral ligament prior to permanent hearing loss induced by exposure to intense noise: Possible involvement of 4-hydroxy-2-nonenal as a mediator of oxidative stress. PLoS One **9**.

267 Zhou, X. X., Chen, S., Xie, L., Ji, Y. Z., Wu, X., Wang, W. W., Yang, Q., Yu, J. T., Sun, Y., Lin, X., et al. (2016) Reduced connexin26 in the mature cochlea increases susceptibility to noise-induced hearing lossin mice. Int. J. Mol. Sci. **17**.

268 Yamaguchi, T., Yoneyama, M. and Ogita, K. (2017) Calpain inhibitor alleviates permanent hearing loss induced by intense noise by preventing disruption of gap junction-mediated intercellular communication in the cochlear spiral ligament. Eur. J. Pharmacol., Elsevier B.V. **803**, 187–194.

269 Van Eyken, E., Van Laer, L., Fransen, E., Topsakal, V., Hendrickx, J. J., Demeester, K., Van De Heyning, P., Mäki-Torkko, E., Hannula, S., Sorri, M., et al. (2007) The

contribution of GJB2 (Connexin 26) 35delG to age-related hearing impairment and noise-induced hearing loss. Otol. Neurotol. **28**, 970–975.

270 Rybak, L. P. (2007) Mechanisms of cisplatin ototoxicity and progress in otoprotection. Curr. Opin. Otolaryngol. Head Neck Surg. **15**, 364–369.

271 Oun, R., Moussa, Y. E. and Wheate, N. J. (2018) The side effects of platinum-based chemotherapy drugs: A review for chemists. Dalt. Trans., Royal Society of Chemistry **47**, 6645–6653.

272 McKeage, M. J. (1995) Comparative Adverse Effect Profiles of Platinum Drugs. Drug Saf. **13**, 228–244.

273 Brock, P. R., Knight, K. R., Freyer, D. R., Campbell, K. C. M., Steyger, P. S., Blakley, B. W., Rassekh, S. R., Chang, K. W., Fligor, B. J., Rajput, K., et al. (2012) Platinum-induced ototoxicity in children: A consensus review on mechanisms, predisposition, and protection, including a new International Society of Pediatric Oncology Boston ototoxicity scale. J. Clin. Oncol. **30**, 2408–2417.

274 Knight, K. R. G., Kraemer, D. F. and Neuwelt, E. A. (2005) Ototoxicity in children receiving platinum chemotherapy: Underestimating a commonly occurring toxicity that may influence academic and social development. J. Clin. Oncol. **23**, 8588–8596.

275 Rybak, L. P., Whitworth, C. A., Mukherjea, D. and Ramkumar, V. (2007) Mechanisms of cisplatin-induced ototoxicity and prevention. Hear. Res. **226**, 157–167.

276 Callejo, A., Sedó-Cabezón, L., Juan, I. and Llorens, J. (2015) Cisplatin-Induced Ototoxicity: Effects, Mechanisms and Protection Strategies. Toxics **3**, 268–293.

277 Frisina, R. D., Wheeler, H. E., Fossa, S. D., Kerns, S. L., Fung, C., Sesso, H. D., Monahan, P. O., Feldman, D. R., Hamilton, R., Vaughn, D. J., et al. (2016) Comprehensive audiometric analysis of hearing impairment and tinnitus after cisplatin-based chemotherapy in survivors of adult-onset cancer. J. Clin. Oncol. **34**, 2712–2720.

278 Fausti, S. A., Henry, J. A., Schaffer, H. I., Olson, D. J., Frey, R. H. and Bagby, G. C. (1993) High-Frequency Monitoring for Early Detection of Cisplatin Ototoxicity. Arch. Otolaryngol. Neck Surg. **119**, 661–666.

279 Sheth1, S. and , Debashree Mukherjea2 , Leonard P. Rybak1, 2 and Vickram Ramkumar1. (2017) Mechanisms of cisplatin-induced ototoxicity and prevention. Front. Cell. Neurosci. **11**, 157–167.

280 Van Ruijven, M. W. M., De Groot, J. C. M. J., Hendriksen, F. and Smoorenburg, G. F. (2005) Immunohistochemical detection of platinated DNA in the cochlea of cisplatin-treated guinea pigs. Hear. Res. **203**, 112–121.

281 Sluyter, S., Klis, S. F. L., De Groot, J. C. M. J. and Smoorenburg, G. F. (2003) Alterations in the stria vascularis in relation to cisplatin ototoxicity and recovery. Hear. Res. **185**, 49–56.

282 Meech, R. P., Campbell, K. C. M., Hughes, L. P. and Rybak, L. P. (1998) A semiquantitative analysis of the effects of cisplatin on the rat stria vascularis. Hear. Res. **124**, 44–59.

283 Breglio, A. M., Rusheen, A. E., Shide, E. D., Fernandez, K. A., Spielbauer, K. K.,

McLachlin, K. M., Hall, M. D., Amable, L. and Cunningham, L. L. (2017) Cisplatin is retained in the cochlea indefinitely following chemotherapy. Nat. Commun., Springer US **8**.

284 Van Ruijven, M. W. M., De Groot, J. C. M. J., Klis, S. F. L. and Smoorenburg, G. F. (2005) The cochlear targets of cisplatin: An electrophysiological and morphological time-sequence study. Hear. Res. **205**, 241–248.

285 Ding, D., Allman, B. L. and Salvi, R. (2012) Review: Ototoxic Characteristics of Platinum Antitumor Drugs. Anat. Rec. **295**, 1851–1867.

286 Dilber, M. S., Abedi, M. R., Christensson, B., Bjrkstrand, B., Kidder, G. M., Naus, C. C. G., Gahrton, G. and Smith, C. I. E. (1997) Gap junctions promote the bystander effect of herpes simplex virus thymidine kinase in vivo. Cancer Res. **57**, 1523–1528.

287 Prise, K. M. and Sullivan, J. M. O. (2009) Radiation-induced bystander signalling in cancer therapy. Nat Rev Cancer **9**, 351–360.

288 Poirrier, A.L., Pincemail, J., Van Den Ackerveken, P., P. Lefebvre, P. and Malgrange, B. (2010) Oxidative Stress in the Cochlea: An Update. Curr. Med. Chem. **17**, 3591–3604.

289 Marullo, R., Werner, E., Degtyareva, N., Moore, B., Altavilla, G., Ramalingam, S. S. and Doetsch, P. W. (2013) Cisplatin induces a mitochondrial-ros response that contributes to cytotoxicity depending on mitochondrial redox status and bioenergetic functions. PLoS One **8**, 1–15.

290 Yang, Z., Schumaker, L. M., Egorin, M. J., Zuhowski, E. G., Quo, Z. and Cullen, K. J. (2006) Cisplatin preferentially binds mitochondrial DNA and voltage-dependent anion channel protein in the mitochondrial membrane of head and neck squamous cell carcinoma: Possible role in apoptosis. Clin. Cancer Res. **12**, 5817–5825.

291 Ježek, P. and Hlavatá, L. (2005) Mitochondria in homeostasis of reactive oxygen species in cell, tissues, and organism. Int. J. Biochem. Cell Biol. **37**, 2478–2503.

292 Bánfi, B., Malgrange, B., Knisz, J., Steger, K., Dubois-Dauphin, M. and Krause, K. H. (2004) NOX3, a superoxide-generating NADPH oxidase of the inner ear. J. Biol. Chem. **279**, 46065–46072.

293 Cusato, K., Ripps, H., Zakevicius, J. and Spray, D. C. (2006) Gap junctions remain open during cytochrome c-induced cell death: Relationship of conductance to "bystander" cell killing. Cell Death Differ. **13**, 1707–1714.

294 Feine, I., Pinkas, I., Salomon, Y. and Scherz, A. (2012) Local oxidative stress expansion through endothelial cells - a key role for gap junction intercellular communication. PLoS One **7**.

295 Krysko, D. V., Leybaert, L., Vandenabeele, P. and D'Herde, K. (2005) Gap junctions and the propagation of cell survival and cell death signals. Apoptosis **10**, 459–469.

296 Kim, Y. J., Kim, J., Tian, C., Lim, H. J., Kim, Y. S., Chung, J. H. and Choung, Y. H. (2014) Prevention of cisplatin-induced ototoxicity by the inhibition of gap junctional intercellular communication in auditory cells. Cell. Mol. Life Sci. **71**, 3859–3871.

297 Choi, S. J., Kim, S. W., Lee, J. B., Lim, H. J., Kim, Y. J., Tian, C., So, H. S., Park, R. and Choung, Y. H. (2013) Gingko biloba extracts protect auditory hair cells from

cisplatin-induced ototoxicity by inhibiting perturbation of gap junctional intercellular communication. Neuroscience **244**, 49–61.

298 Wang, Q. You, T., Yuan, D., Han, X., Hong, X., He, B., Wang, L., Tong, W., Tao, L., and Harri, A.L. (2010) Cisplatin and Oxaliplatin Inhibit Gap Junctional Communication by Direct Action and by Reduction of Connexin Expression, Thereby Counteracting Cytotoxic Efficacy, J. Pharm Exp Ther, **333**, 903–911.

299 Jensen, R. and Glazer, P. M. (2004) Cell-interdependent cisplatin killing by Ku/DNA-dependent protein kinase signaling transduced through gap junctions. Proc. Natl. Acad. Sci. **101**, 6134–6139.

300 Tong, X., Hong, X., Yang, Y., Tao, L., Harris, A. L., Zheng, S., Zhang, S. and Wang, Q. (2011) Gap junctions propagate opposite effects in normal and tumor testicular cells in response to cisplatin. Cancer Lett., **317**, 165–171.

301 Shaloam Dasari and Paul Bernard Tchounwou. (2015) Cisplatin in cancer therapy : molecular mechanisms of action. Eur J Pharmacol **5**, 364–378.

302 Erdlenbruch, B., Nier, M., Kern, W., Hiddemann, W., Pekrun, A. and Lakomek, M. (2001) Pharmacokinetics of cisplatin and relation to nephrotoxicity in paediatric patients. Eur. J. Clin. Pharmacol. **57**, 393–402.

303 More, S. S., Akil, O., Ianculescu, A. G., Geier, E. G., Lustig, L. R. and Giacomini, K. M. (2010) Role of the copper transporter, CTR1, in platinum-induced ototoxicity. J. Neurosci. **30**, 9500–9.

304 Basu, A. and Krishnamurthy, S. (2010) Cellular responses to cisplatin-induced DNA damage. J. Nucleic Acids **2010**.

305 Ciarimboli, G., Deuster, D., Knief, A., Sperling, M., Holtkamp, M., Edemir, B., Pavenstädt, H., Lanvers-Kaminsky, C., Zehnhoff-Dinnesen, A. A., Schinkel, A. H., et al. (2010) Organic cation transporter 2 mediates cisplatin-induced oto- and nephrotoxicity and is a target for protective interventions. Am. J. Pathol. **176**, 1169–1180.

306 Hellberg, V., Gahm, C., Liu, W., Ehrsson, H., Rask-Andersen, H. and Laurell, G. (2015) Immunohistochemical localization of OCT2 in the cochlea of various species. Laryngoscope **125**, E320–E325.

307 Russell, I. J. and Richardson, G. P. (1987) The morphology and physiology of hair cells in organotypic cultures of the mouse cochlea. Hear. Res. **31**, 9–24.

308 Richardson, G. P. and Russell, I. J. (1991) Cochlear cultures as a model system for studying aminoglycoside induced ototoxicity. Hear. Res. **53**, 293–311.

309 Ding, D., He, J., Allman, B. L., Yu, D., Jiang, H., Seigel, G. M. and Salvi, R. J. (2011) Cisplatin ototoxicity in rat cochlear organotypic cultures. Hear. Res., Elsevier B.V. **282**, 196–203.

310 Kalinec, G. M., Webster, P., Lim, D. J. and Kalinec, F. (2003) A cochlear cell line as an in vitro system for drug ototoxicity screening. Audiol. Neuro-Otology **8**, 177–189.

311 Kalinec, G., Thein, P., Park, C. and Kalinec, F. (2016) HEI-OC1 cells as a model for investigating drug cytotoxicity. Hear. Res., Elsevier B.V **335**, 105–117.

312 Park, C., Thein, P., Kalinec, G. and Kalinec, F. (2016) HEI-OC1 cells as a model for investigating prestin function. Hear. Res., Elsevier B.V **335**, 9–17.

313 Qu, Y., Misaghi, S., Newton, K., Gilmour, L. L., Louie, S., Cupp, J. E., Dubyak, G. R., Hackos, D. and Dixit, V. M. (2011) Pannexin-1 is required for ATP release during apoptosis but not for inflammasome activation. J. Immunol. **186**, 6553–61.

314 Moon, P. M., Penuela, S., Barr, K., Khan, S., Pin, C. L., Welch, I., Attur, M., Abramson, S. B., Laird, D. W. and Beier, F. (2015) Deletion of Panx3 Prevents the Development of Surgically Induced Osteoarthritis. J. Mol. Med. 845–856.

315 Kalcheva, N., Qu, J., Sandeep, N., Garcia, L., Zhang, J., Wang, Z., Lampe, P. D., Suadicani, S. O., Spray, D. C. and Fishman, G. I. (2007) Gap junction remodeling and cardiac arrhythmogenesis in a murine model of oculodentodigital dysplasia. Proc. Natl. Acad. Sci. U. S. A. **104**, 20512–20516.

316 Flenniken, A. M., Osborne, L. R., Anderson, N., Ciliberti, N., Fleming, C., Gittens, J. E. I., Gong, X.-Q., Kelsey, L. B., Lounsbury, C., Moreno, L., et al. (2005) A Gja1 missense mutation in a mouse model of oculodentodigital dysplasia. Development **132**, 4375–86.

317 Stewart, M. K. G., Gong, X.-Q., Barr, K. J., Bai, D., Fishman, G. I. and Laird, D. W. (2013) The severity of mammary gland developmental defects is linked to the overall functional status of Cx43 as revealed by genetically modified mice. Biochem. J. **449**, 401–13.

318 Manias, J. L., Plante, I., Gong, X. Q., Shao, Q., Churko, J., Bai, D. and Laird, D. W. (2008) Fate of connexin43 in cardiac tissue harbouring a disease-linked connexin43 mutant. Cardiovasc. Res. **80**, 385–395.

319 Plante, I. and Laird, D. W. (2008) Decreased levels of connexin43 result in impaired development of the mammary gland in a mouse model of oculodentodigital dysplasia. Dev. Biol. **318**, 312–322.

Chapter 2 : Differential effects of pannexins in noise-induced hearing loss

Pannexins have previously been shown to be localized to distinct regions of the mammalian cochlea. Previous studies have shown controversial results whereby some mice with Panx1 ablation have hearing loss while others so not. The purpose of this study was to examine mice with global ablation of Panx1 to determine if these channels are important in auditory function. In addition, the second goal of this study was to examine the impacts of globally ablating Panx3 in a mouse model to determine whether Panx3 is important in hearing.

A version of this chapter is published:

Abitbol JM, Kelly JJ, Barr K, Schormans AL, Laird DW, Allman BL. Differential effects of pannexins on noise-induced hearing loss. *Biochem J.* 473(24):4665-4680, 2016.

2.1. Introduction

Hearing loss is one of the most disabling sensory deficits, affecting approximately 360 million people worldwide [1]. Currently, cochlear implants and hearing aids are the most commonly used interventions for managing hearing impairment. The lack of drug therapies for hearing loss hinges upon the fact that the molecular aspects and mechanisms that regulate the transduction of sound waves into electrical impulses along the auditory pathway are not fully understood.

Connexin (Cx) channels, which allow the passage of small molecules and ions between cells and their external environments, make up the two gap junction networks of the inner ear [2]. These networks are formed before hearing onset [3] and are essential for cochlear ionic and metabolic homeostasis and maintenance of the endocochlear potential [2, 4-6]. Although Cxs are not expressed in the sensory receptor hair cells of the cochlea [7-10], they are still critical for hearing as loss of Cx26 and Cx30 function mutations lead to deafness [2, 11, 12]. Recently, it was discovered that a unique family of glycoproteins that share similar topology to Cxs, called Pannexins (Panxs), are expressed in the cochlea and other resident cell types of the auditory pathway [13, 14]. Pannexins, of which there are three subtypes (Panx1, -2, and -3), are all proposed to form single membrane channels at the cell surface but they may also serve other roles that have yet to be characterized [15, 16]. These channels connect the extracellular and intracellular environments by allowing the passage of small members of the metabolome across the plasma membrane [17, 18]. By far, the most understood and studied member of the pannexin family is Panx1. Panx1 plays a role in many cellular processes, such as Ca^{2+} wave propagation, ATP release, and apoptosis [19-21].

Under normal conditions, Panx1 channels may be opened via mechanical stimulation, intracellular calcium, extracellular potassium, ATP, membrane depolarization, and caspase3 cleavage [19-23]. In contrast, Panx1 channels are blocked by the negative feedback of ATP, carbon dioxide-mediated acidification, or in the presence of channel blockers such as probenecid and carbenoxolone [23-26]. In the cochlea, Panx1 expression was found in the spiral limbus, the spiral prominence in the cochlear lateral wall, Reissner's membrane, spiral ganglion neurons, and supporting cells of the organ of Corti, including pillar cells, Hensen cells, Boettcher cells, and Claudius cells [13, 14, 27]. In addition, Panx1 mRNA expression

was found in neurons of the auditory cortex [28]. Similar to Cxs, Panx1 was not detected in the hair cells that are responsible for initiating the transduction of electrical impulses through the auditory pathway [14].

Recently, mice lacking Panx1 in a subset of cells in the cochlea were generated through the crossing of Panx1 floxed mice with Paired box 2 (Pax2) Cre mice and were shown to exhibit sensorineural hearing loss [29]. Another study crossed Panx1 floxed mice with a Forkhead box G1 (Foxg1, which is required for proper morphogenesis of the cochlea [30]) Cre mouse line and showed that these mice also exhibited hearing loss [31]. The hearing loss in these mice may be linked to the finding that Panx1 is reported to be a predominant ATP release channel in the cochlea [31]. ATP acts as a signalling molecule in the inner ear, regulates mechanoelectrical transduction processes, and maintains proper cochlear mechanics [32-35]. To further support a possible role for Panx1 in hearing, a human patient was recently identified that harbored a loss-of-function *PANX1* gene mutation. This patient exhibited sensorineural hearing loss, required bilateral cochlear implants from a young age, and had neurological deficits among multiple symptoms [36]. Therefore, increasing evidence suggests the importance of Panx1 in hearing when conditionally ablated within the inner ear. However, a conditional ablation does not account for expression of Panx1 along the entire auditory pathway, including its presence within the auditory cortex [28]. Therefore, it is important to assess the comprehensive and developmental role of Panx1 in the entire auditory pathway from hair cell transduction to the transmission of electrical impulses along the successive relay nuclei in the central auditory system.

Compared to Panx1, Panx3 appears to have a more restricted expression pattern, being found mostly in bone, skin, and cartilage tissues [22, 37-40]. Panx3 plays a role in the differentiation of chondrocytes and osteoblasts, and is involved in growth and development of bone [37, 38, 41]. Panx3 has recently been described in the cochlea, where it was found to be expressed in the cochlear bone and the modiolus of the inner ear [14]. Sound conduction through the middle ear bones and the cochlea can be impaired by improper bone growth, leading to otosclerosis [42]. Patients with otosclerosis often show signs of sensorineural hearing loss due to improper bone growth in the middle ear and/or the cochlear bone, which ultimately affects sound transduction to the hair cells and neurons within the inner ear [43]. In addition, loss of proteins

that assist in endochondral ossification in the ear lead to deafness in mice, and abnormalities in middle ear bone formation can leave them in a non-functioning state [44, 45]. Therefore, because Panx3 is important in bone, it may be essential for proper middle and inner ear bone formation and morphology, but this has yet to be examined.

Since Panxs have recently been implicated in baseline hearing, it is reasonable to predict that they may also be involved in noise-induced hearing loss. Approximately 5% of the population worldwide will suffer from industrial, military, or recreational noise-induced hearing loss, which is most commonly caused by loss of hair cells due to apoptosis [46, 47]. Hair cells as well as cochlear neurons do not regenerate, and as a consequence, excessive exposure to loud noise can result in permanent hearing loss. Currently, there are no completely-accepted pharmacological treatments for noise-induced hearing loss, thus emphasizing that the development of molecular targets to prevent or reduce noise-induced hearing loss is essential [46]. Due to the expression of Panx1 in the inner ear and its role in ATP release and Ca^{2+} propagation functions, as well as the expression of Panx3 in the cochlear bone; both Panx1 and Panx3 may be potential molecular candidates implicated in noise-induced hearing loss through cochlear homeostasis and/or sound conduction. Thus, we set out to evaluate the impact of Panx1 and Panx3 ablation on acute loud noise-damage and recovery.

To that end, we have obtained and/or generated Panx1 and Panx3 null mice, to account for the potentially broad distribution of both Panxs along the entire auditory pathway. In the present study, we assessed if these Panx channels are crucial in baseline hearing and/or noise-induced hearing loss, and we evaluated the importance of Panx3 in the development of the middle ear bones. In contrast to our expectations, we discovered that Panx1 and Panx3 are not necessary for baseline hearing. However, mice lacking Panx3, but not Panx1, are partially protected from acute loud noise-damage.

2.2. Materials and methods

2.2.1. Animals

Pannexin1 null mice (*Panx1*$^{-/-}$) were obtained from Genentech (San Francisco, CA) and were previously described [48]. Briefly, the targeting construct used loxP sites to flank exon2 and

its deletion was achieved by breeding to the ubiquitously active Cre deleter mouse, C57BL/6-*Gt(ROSA)26Sor*$^{tm16(Cre)Arte}$ (TaconicArtemis) and has since been backcrossed several times to C57BL/6 mice, allowing Cre recombinase to have been bred out. Mice were genotyped to confirm *Panx1* ablation using the following primers; Forward: 5'-GGA GAA GCA GCT TAT CTG G-3', Reverse: 5'-ACT GTG CAA TAC TAC ACG GA-3'. *Panx1* expression has been shown to be ablated in several organs of these mice including; muscle, lung, liver, kidney, tail, brain, heart, thymus, spleen and skin tissues, validating this mouse model as a *Panx1*$^{-/-}$ mouse [48-50]. *Panx3* null mice (*Panx3*$^{-/-}$) were bred in-house and were previously described [51]. Briefly, *Panx3* floxed mice were crossed with C57BL/6 Cre deleter mice (B6.C-Tg(CMV-cre)1Cgn/J; Jaxmice #006054). Cre recombinase was bred out following generation of the *Panx3*$^{-/-}$ mouse line. Mice bred on the same background (C57BL/6) were used as age and sex matched wildtype (WT) controls. Mice were genotyped to confirm *Panx3* ablation using the following primers; Forward: 5'-TGC CCT CCA CAG AAA GCT ACC-3', Reverse: 5`-GGC CAG CCT TGT CCT GCG TAT G-3'. All mice tested were male and 2-3 months of age (P60-P90) unless otherwise stated. Mice were housed in the animal care facility at the University of Western Ontario, and maintained on a 12/12- hour light/dark cycle and fed ad libitum. Animal experiments were approved by the Animal Care Committee on animal care of the University of Western Ontario.

2.2.2. RNA Extraction and RT-PCR

Following euthanasia by CO_2, cochleae were dissected from mice and flash frozen in liquid nitrogen. RNA was extracted from tissues using a Qiagen RNeasy mini kit (catalog #74104) and an RNAse Free Dnase kit (catalog #79254) or by a combination of Trizol reagent, Qiagen RNeasy mini kit, as well as RNase Free Dnase treatment modified from a previous publication [52]. A Nanodrop spectrophotometer was used to measure absorbance of RNA. Subsequently, one-step RT-PCR was performed using an RT-PCR Qiagen kit (catalog #210210). The PCR profile was as follows: 50°C for 30 minutes, 95°C for 15 minutes, 94°C for 30s, 64°C for 30s and 72°C for 1 minute for 30 cycles. *Panx1* specific primers (forward: 5'-ACA GGC TGC CTT TGT GGA TTC A-3' and reverse: 5'-GGG CAG GTA CAG GAG TAT C-3') and *Panx3* specific primers (forward: 5'-TTT CGC CCA GGA GTT CTC ATC-3' and reverse: 5'-CCT GCC TGA CAC TGA AGT TG-3') were used. *18s rRNA* was used as a control (forward: 5'-

GTA ACC CGT TGA ACC CCA TT-3' and reverse: 5'-CCA TCC AAT CGG TAG TAG CG-3'). The amplified products were run on a 2% agarose gel with ethidium bromide for visualization.

2.2.3. Quantitative RT-PCR

Following euthanasia by CO_2, cochleae were dissected from mice and flash frozen in liquid nitrogen. RNA was extracted as described above and converted into cDNA using a SuperScript VILO cDNA Synthesis kit (Thermo-Fisher catalog #11754050). Two-step qPCR reactions were performed using a SYBR Green PCR master mix by Life Technologies (catalog #4309155) in order to quantify Panx1 and Panx3 expression in the cochleae. The Panx1 PCR protocol was as follows: 50°C for 2 min, 95°C for 2 min, 95°C for 3 sec, 60°C for 30 sec, for 40 cycles followed by a melt curve. The Panx3 PCR protocol was as follows: 50°C for 2 min, 95°C for 2 min, 95°C for 3 sec, 65°C for 30 sec, for 40 cycles followed by a melt curve. Panx1 and Panx3 transcripts were normalized to *18S rRNA* transcript level. The same primers as mentioned above were used for *Panx1* and *Panx3*. The following primers were also used in this study; *Cx26*; (forward: 5'-CCGTCTTCATGTACGTCTTTTACAT- 3' and reverse: 5' ATACCTAACGAACAAATAGCACAGC- 3'), *Cx30*; (forward: 5'-GGCCGAGTTGTGTTACCTGCT- 3' and reverse: 5'- TCTCTTTCAGGGCATGGTTGG-3'), *Cx43*; (forward: 5'- ACAACAAGCAAGCCAGCGAG- 3' and reverse: 5'-TCGTCAGGGAAATCAAACGG- 3'), and *Panx2*; (forward: 5'-TGGTACCCATCCTGCTGGT- 3' and reverse: 5'- GGGTGAAGTTGTGCGGAGT- 3'). For all three Cxs and Panx2 the PCR profile was as follows: 50°C for 2 min, 95°C for 2 min, 95°C for 5 sec, 60°C for 15 sec, followed by a melt curve.

2.2.4. Immunoblotting

Following euthanasia by CO_2, cochleae and brain tissues were dissected from mice, flash frozen in liquid nitrogen, and stored at -80°C. For cochlear tissues, a litter of mice (approximately 6-10 cochleae) were pooled together for one lysate due to the small amount of tissue. Cochleae were crushed using a mortar and pestle with liquid nitrogen, and protein was

extracted using a Triton-X 100 based immunoprecipitation buffer as previously described [22]. Lysates (30 μg) were run on 10% polyacrylamide gels using SDS-PAGE and protein was transferred to a nitrocellulose membrane using an iBlot transfer machine (Invitrogen). Membranes were blocked with 3% bovine serum albumin (BSA) in Tween-PBS for one hour. Blots were probed overnight with custom-made site directed antibodies; anti-Panx1 (CT-295) at a 1:2500 dilution, and anti-Panx3 (CT-379) at a 1:5000 dilution as previously described [22]. Blots were then washed and stained with AlexaFluor 680 secondary antibody (1:5000 dilution, Life Technologies) for two hours and subsequently stained with anti-mouse GAPDH (1:10000 dilution, Chemicon) as a loading control. IRdye800 (1:5000 dilution, Rockland) was used as the secondary antibody for GAPDH. Membranes were visualized with an Odyssey infrared imaging system (LiCor).

2.2.5. Hearing Assessment with an Auditory Brainstem Response

Hearing levels were determined using the auditory brainstem response (ABR), which measured the electrical activity in the brainstem evoked by the repeated presentation of a given acoustic stimulus. Mice were anaesthetized using a combination of ketamine (100 mg/kg) and xylazine (10 mg/kg) administered via intraperitoneal injections (i.p.), and positioned in a double-walled sound-attenuating chamber. The electrical activity of the ABR was recorded by subdermal electrodes (27 gauge; Rochester Electro-Medical, Lutz, FL) that were positioned at the vertex (active electrode), over the mastoid of the stimulated (right) ear (reference electrode), and on the mid-back (ground electrode). Throughout the ABR recordings, body temperature was maintained at ~37°C using a homeothermic heating pad (507220F; Harvard Apparatus, Kent, UK).

Acoustic stimuli were generated by a Tucker-Davis Technologies (TDT, Alachua, FL) RZ6 processing module at 100 kHz sampling rate and delivered by a magnetic speaker (MF1; TDT) positioned 10 cm from the animal's right ear. The left ear was occluded with a custom foam earplug. Acoustic stimuli for the click ABR and noise exposure procedure (described below) were calibrated with custom Matlab software (The Mathworks, Natick, MA) using a ¼-inch microphone (2530; Larson Davis, Depew, NY) and preamplifier (2221; Larson Davis) and tonal acoustic stimuli were calibrated using BioSig software by Tucker-Davis Technologies

(TDT, Alachua, FL) using a ¼-inch microphone (2530; Larson Davis, Depew, NY) and preamplifier (2221; Larson Davis).

The auditory evoked activity of the ABR was collected using a low-impedance headstage (RA4L1; TDT), preamplified and digitized (RA16SD Medusa preamp; TDT), and sent to a RZ6 processing module via a fiber optic cable. The signal was filtered (300 – 3000 Hz) and averaged using BioSig software (TDT). Acoustic stimuli consisted of a click (0.1 ms) and four tones (4, 8, 16 and 24 kHz; 5 ms duration and 1 ms rise/fall time). The click stimulus served as an indicator of general hearing, as it encompasses a range of frequencies that stimulate the cochlea. Mouse hearing frequency ranges from approximately 1-100 kHz [53] and thus the different tonal stimuli tested provided a measure of frequency-specific hearing sensitivity, as each tonal frequency stimulates a restricted portion of the cochlea. The click and tonal stimuli were each presented 1000 times (11 times/second) at decreasing intensities from 90 to 50 dB sound pressure level (SPL) in 10 dB SPL steps. From 50 dB SPL to ~15 dB SPL, the successive steps were at 5 dB, with each sound level presented twice in order to best determine ABR threshold offline. Ultimately, for each of the stimuli (click and 4-24 kHz tones), an experimenter who was blinded to the animal cohort and treatment condition determined the ABR threshold using the criteria of just noticeable deflection of the averaged electrical activity within the 10-ms time window [54].

2.2.6. Noise Exposure

For a subset of mice, the initial ABR was followed immediately by a loud noise exposure while the mice were maintained under anesthesia. While positioned in the double-walled sound-attenuating chamber, mice were bilaterally exposed to a calibrated 12 kHz tone at 115 dB SPL for one hour. The tone was generated with TDT software and hardware (RPvdsEx; RZ6 module), and delivered by a super tweeter (T90A; Fostex, Tokyo, Japan) which was placed 10 cm in front of the mouse. A homeothermic heating pad was used to maintain body temperature at ~37 °C, and supplemental doses of ketamine and xylazine were administered as needed to maintain anesthesia. Immediately following the noise exposure, ABR thresholds were re-assessed. Mice were then given antipamezole (1 mg/kg) to reverse anesthesia effects, and allowed to recover in their home cage. Seven days after noise exposure, mice were once again anesthetized and a final ABR recording was performed to determine the extent of permanent

hearing damage incurred by the loud noise exposure. Upon completion of the final ABR recordings, mice were then euthanized by cervical dislocation while under deep anesthesia, and tissue samples were collected for further processing.

1.2.7 Auditory Ossicle Dissection and Imaging

In a subset of 2-3 month old WT and *Panx3*$^{-/-}$ mice, the three auditory ossicles (malleus, incus and stapes) contained within the middle ear were carefully microdissected. Ossicles were fixed in 4% PFA overnight and then imaged using a Zeiss light microscope. An experimenter blinded to the treatment groups used ImageJ software to make measurements of the ossicles, including the length of the malleus, distance between the tips of the incus, and length of the stapes window.

1.2.8 Statistical analysis

Two-tailed independent unpaired student T-tests were used for comparisons for ABR wave I analysis between WT and *Panx1*$^{-/-}$ as well as WT and *Panx3*$^{-/-}$ mice, and the measurements of middle ear bone morphology between WT and *Panx3*$^{-/-}$ mice. One-way analysis of variance (ANOVA) with a Tukey's posthoc test was used to compare *Panx1*, *Panx2*, *Panx3*, *Cx26*, *Cx30*, and *Cx43* expression by qPCR in WT, *Panx1*$^{-/-}$, and *Panx3*$^{-/-}$ cochleae. Two-way ANOVA was used to compare WT, *Panx1*$^{-/-}$ and *Panx3*$^{-/-}$ groups for ABR thresholds with a Sidak's post hoc test. Two-way repeated measure ANOVAs were used for noise exposure analysis (where each individual frequency was analyzed separately), followed by a Sidak's post hoc test. All statistical analyses were performed using GraphPad Prism 6.0, *$p<0.05$. $N\geq3$ for all experiments.

2.3. Results

2.3.1. Panx1 and Panx3 are expressed in the cochlea and are ablated in knock-out mice

To confirm that both Panx1 and Panx3 knock-out mice had pannexins ablated from the cochlea, we used RT-PCR and qRT-PCR to determine the mRNA levels for Panx1 and Panx3 in 2-3 month-old WT, Panx1$^{-/-}$, and Panx3$^{-/-}$ cochleae. We found that both Panx1 and Panx3 mRNA transcripts were expressed in the cochlea of WT mice and were ablated in their respective knock-out cochleae as revealed when normalized to 18S rRNA (Figure 2.1A-D). Interestingly, there was no evidence of Panx1 or Panx3 compensation in the cochleae of their reciprocal null mice (Figure 2.1C-D). Western blots for Panx1 at postnatal day 1 and 8 (P1 and P8), revealed the loss of Panx1 in mutant mice, where age and sex matched brains were also used as controls (Figure 2.1E).

2.3.2. Panx1$^{-/-}$ and Panx3$^{-/-}$ mice do not exhibit reduced hearing sensitivity or cochlear nerve deficits

To assess baseline hearing sensitivity in mice lacking Panx1 or Panx3, we measured ABR thresholds in response to various acoustic stimuli (click and 4-24 kHz tones). ABR trace recordings from a representative WT, Panx1$^{-/-}$, and Panx3$^{-/-}$ mouse had similar waveform characteristics in response to a click stimulus at decreasing sound levels (90 to 30 dB SPL; Figure 2.2A). To further validate the finding that mutant mice had normal hearing, the ABR waveform traces for a 90 dB SPL click stimulus were averaged for each group (WT: n=17, Panx1$^{-/-}$: n=17, Panx3$^{-/-}$: n=18) to create a composite ABR waveform for each group of mice (Figure 2.2B). There were no observable deficits in ABR waveforms in either Panx1$^{-/-}$ or Panx3$^{-/-}$ mice (Figure 2.2B). Furthermore, there were no significant differences in ABR thresholds between WT and Panx1$^{-/-}$ or Panx3$^{-/-}$ mice at any of the stimuli tested (click and 4-24 kHz tones; Figure 2.2C-D). Additionally, we examined the amplitudes and latencies of the first wave of the ABR (wave I), which is representative of the activity at the level of the cochlear nerve, in response to a click stimulus at 90 dB SPL as well as 20 dB above the animal's ABR threshold, to determine if there were any deficits in neuronal synchrony or speed, respectively, at this point in the auditory pathway. We found that there were no differences in cochlear nerve amplitude or latency between WT and Panx1$^{-/-}$ mice, indicating no neuronal deficits within this region (Figure 2.2E,G).

Figure 2.1. Panx1 and Panx3 are expressed in the cochlea and are ablated in knock-out mice

RT-PCR of cochlear RNA confirmed Panx1 (A) and Panx3 (B) mRNA transcript expression in wild-type (WT) cochleae and loss of expression in knock-out cochleae. 18S rRNA was used as a reference gene. NTC+ P= No template control + primer, NTC= No template control. Panx1 (C) and Panx3 (D) mRNA expression was quantified in WT, Panx1$^{-/-}$, and Panx3$^{-/-}$ cochleae using RT-qPCR (N=3 (biological replicates), n=9 (technical replicates)) for all groups; $P<0.01$; one-way ANOVA). (E) Postnatal day 1 (P1) and P8 brain and cochlear protein lysates showed Panx1 expression with the expected glycosylated banding pattern (Gly0, Gly1, and Gly2). There was no Panx1 expression in the brain or cochleae of Panx1$^{-/-}$ mice ($^{-/-}$). An unspecific band was observed above the Gly2 species (E). (F) Panx3 was developmentally regulated in the cochleae of P1, P8, P16, and 2 month (2M)-old wildtype and Panx1$^{-/-}$ mice.

Figure 2.1

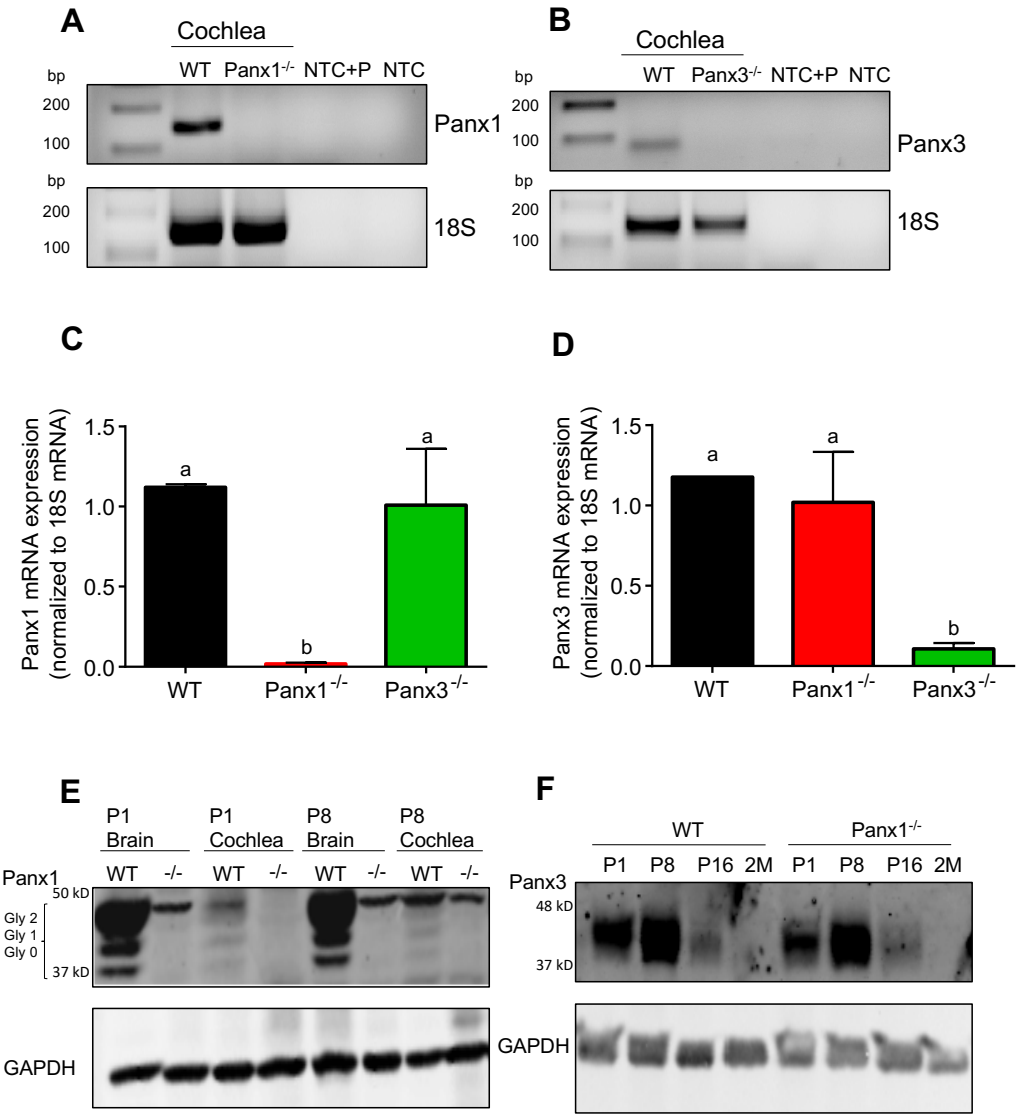
A
Cochlea
WT Panx1-/- NTC+P NTC
bp
200
100
Panx1
18S
B
Cochlea
WT Panx3-/- NTC+P NTC
Panx3
18S
C
Panx1 mRNA expression (normalized to 18S mRNA)
1.5
1.0
0.5
0.0
a
b
a
WT
Panx1-/-
Panx3-/-
D
Panx3 mRNA expression (normalized to 18S mRNA)
a
a
b
E
P1 Brain
P1 Cochlea
P8 Brain
P8 Cochlea
WT -/- WT -/- WT -/- WT -/-
Panx1
50 kD
Gly 2
Gly 1
Gly 0
37 kD
GAPDH
F
WT
Panx1-/-
P1 P8 P16 2M P1 P8 P16 2M
Panx3
48 kD
37 kD
GAPDH

Figure 2.2. Panx1$^{-/-}$ and Panx3$^{-/-}$ mice do not exhibit hearing or vestibulocochlear nerve deficits.

(A) Representative examples of a click stimulus for WT, Panx1$^{-/-}$, and Panx3$^{-/-}$ mice. (B) ABR waveforms for a click stimulus were averaged together to create a composite waveform for WT, Panx1$^{-/-}$, and Panx3$^{-/-}$ mice. (C) ABR thresholds showed no difference between WT and Panx1$^{-/-}$ mice for all stimuli tested. (D) Similarly, ABR thresholds showed no difference between WT and Panx3$^{-/-}$ mice for all stimuli tested. Amplitudes and latencies of wave I, the vestibulocochlear nerve, for a 90dB and 20dB above threshold click stimulus were analyzed. There were no differences in wave I amplitudes (E) or latencies (G) between WT and Panx1$^{-/-}$ mice. (F) At a 90dB click stimulus, Panx3$^{-/-}$ mice had a significant increase in the amplitude of the vestibulocochlear nerve compared to WT mice, (*$p<0.05$, unpaired *t* test). However, there was no difference at 20dB above threshold. (H) There were no differences observed in the latencies of ABR wave I at 90dB or 20dB above threshold between WT and Panx3$^{-/-}$ mice. WT: n=18, Panx1$^{-/-}$: n=17, Panx3$^{-/-}$: n=17. Bars represent mean ABR threshold ± SEM.

Figure 2.2

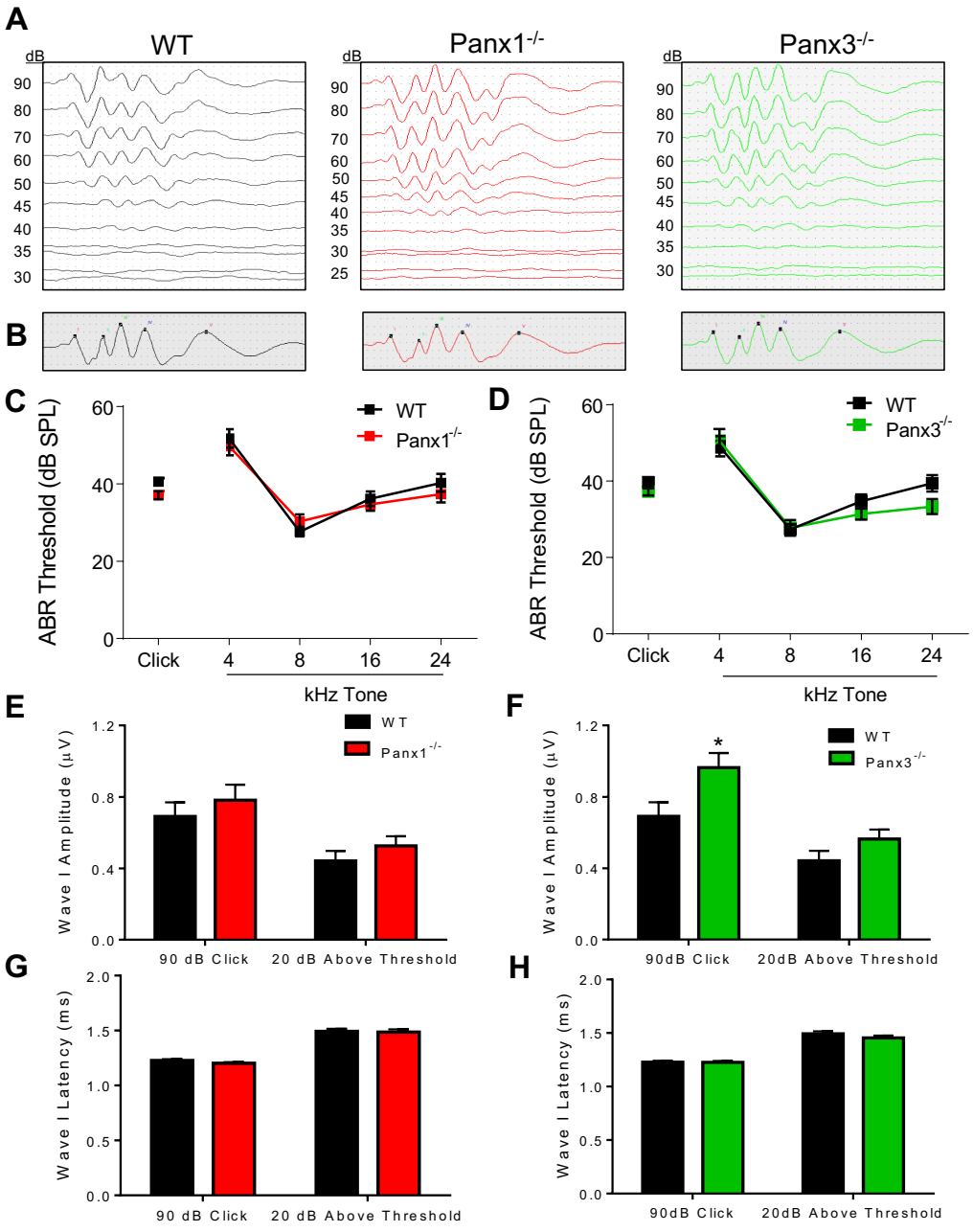
A
WT
Panx1-/-
Panx3-/-
dB
90
80
70
60
50
45
40
35
30
25
B
C
ABR Threshold (dB SPL)
WT
Panx1-/-
Click
4
8
16
24
kHz Tone
D
Panx3-/-
E
Wave I Amplitude (µV)
90 dB Click
20 dB Above Threshold
F
*
90dB Click
20dB Above Threshold
G
Wave I Latency (ms)
H

To our surprise, Panx3$^{-/-}$ mice had significantly increased wave I amplitudes compared to WTs in response to the 90 dB SPL click stimulus; however, there were no differences observed in wave I latencies (Figure 2.2F, H). Taken together, these results suggest that gene ablation of Panx1 or Panx3 does not lead to sensorineural hearing loss nor any deficits at the level of the cochlear nerve.

2.3.3. WT and Panx1$^{-/-}$ mice are equally susceptible to noise-induced hearing loss

To assess whether Panx1 channels play a role in noise-induced hearing loss, we exposed WT and Panx1$^{-/-}$ mice to a loud noise (12 kHz tone at 115 dB SPL for 1 hour) and let them recover for seven days following the exposure. ABR thresholds were recorded for each stimulus (click and 4-24 kHz tones) at three time points: (1) baseline, (2) immediately after noise exposure (Post NE) and (3) seven days after noise exposure, in an attempt to discern whether ablation of Panx1 channels would exacerbate or protect against acoustic trauma. At baseline, there were no differences observed in click, 4, 8, 16 or 24 kHz ABR thresholds between WT and Panx1$^{-/-}$ mice, (Figure 2.3A-D; 8 kHz data not shown). Immediately after noise exposure, ABR thresholds were significantly elevated in both WT and Panx1$^{-/-}$ mice compared to baseline (Figure 2.3A-D), with the most severe elevation in ABR threshold being at the higher frequencies, 16- and 24 kHz tones (Figure 2.3C-D). There were no differences between WT and Panx1$^{-/-}$ ABR thresholds immediately after noise exposure at any of the stimuli tested (Figure 2.3A-D), suggesting that a similar auditory insult occurred in both groups. Seven days after noise exposure, ABR thresholds recovered near baseline levels at the low-frequency stimuli (Figure 2.3A-B), with no difference between WT and Panx1$^{-/-}$ ABR thresholds. As expected after exposure to a loud 12 kHz tone for 1 hour, ABR thresholds were still elevated seven days later at the 16 kHz (WT: 86 ± 2 dB SPL; Panx1$^{-/-}$: 86.5 ± 3 dB SPL) and the 24 kHz (WT: 86 ± 1.6 dB SPL; Panx1$^{-/-}$: 86.5 ± 2 dB SPL) stimuli, but there were no differences found between WT and Panx1$^{-/-}$ mice. Collectively, these results suggest that ablation of Panx1 does not impact noise-induced hearing loss.

Figure 2.3. WT and Panx1$^{-/-}$ mice show similar susceptibility to noise-induced hearing loss.

Noise exposure caused a significant increase in ABR thresholds immediately after noise-exposure (Post NE) for (A) click, (B) 4 kHz, (C) 16 kHz, and (D) 24 kHz tonal stimuli, confirming auditory damage in both WT and Panx1$^{-/-}$ mice. The highest ABR thresholds Post NE were found at the higher frequency stimuli, (C) 16 kHz and (D) 24 kHz tones. However, there were no significant differences between WT mice 7 days after noise-exposure (7 days after NE). ABR thresholds recovered slightly but did not recover to baseline levels at any of the stimuli. At all three different time points, there were no significant differences between WT and Panx1$^{-/-}$ mice. Two-way repeated measures ANOVAs were performed for each individual stimuli. WT: n=10, Panx1$^{-/-}$: n=10. Bars represent mean ABR threshold ± SEM. $P<0.05$, ns = not significant.

Figure 2.3

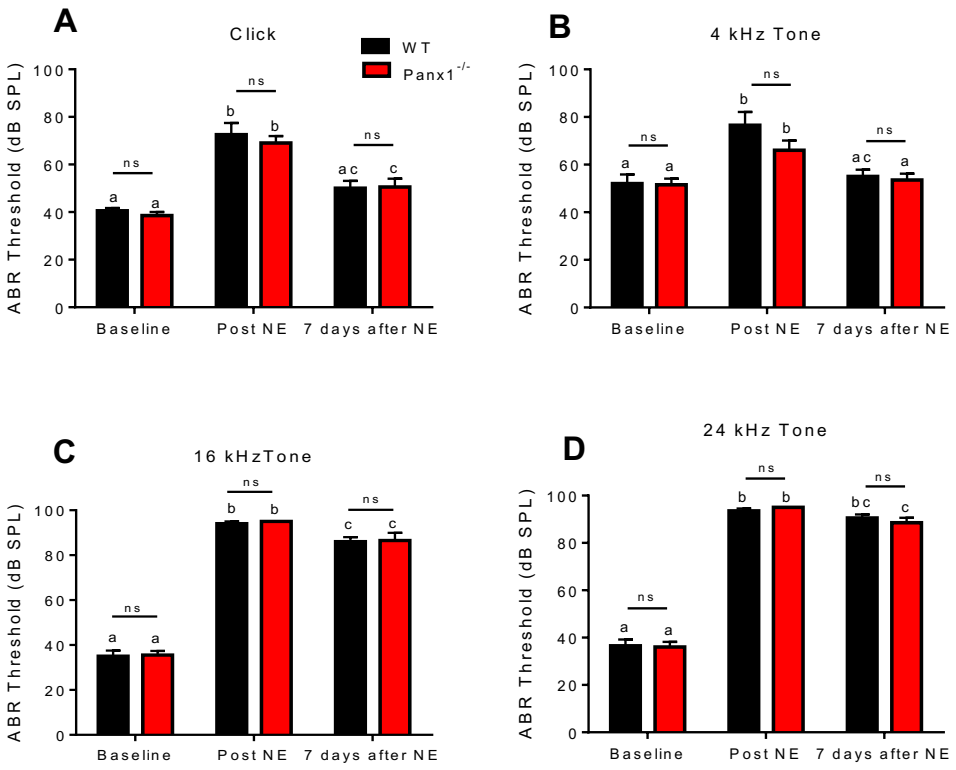
A
Click
WT
Panx1 -/-
ABR Threshold (dB SPL)
100
80
60
40
20
0
ns
a
a
b
b
ns
ac
c
ns
Baseline
Post NE
7 days after NE
B
4 kHz Tone
ns
a
a
b
b
ns
ac
a
ns
Baseline
Post NE
7 days after NE
C
16 kHzTone
ns
a
a
b
b
ns
c
c
ns
Baseline
Post NE
7 days after NE
D
24 kHz Tone
ns
a
a
b
b
ns
bc
c
ns
Baseline
Post NE
7 days after NE

2.3.4. Panx3$^{-/-}$ mice exhibit enhanced 16- and 24 kHz hearing recovery after loud noise exposure

Panx3$^{-/-}$ mice were exposed to a loud 12 kHz tone for 1 hour to assess whether Panx3 channels play an important role in noise-induced hearing loss. At baseline, there were no differences observed in ABR thresholds of click, 4, 8, 16 or 24 kHz tones between WT and Panx3$^{-/-}$ mice (Figure 2.4A-D; 8 kHz data not shown). Immediately after noise exposure, ABR thresholds were significantly elevated compared to baseline levels at all stimuli, with the most severe elevation occurring at the higher frequencies, 16- and 24 kHz tones (Figure 2.4C-D). WT and Panx3$^{-/-}$ mice showed a similar elevation of ABR threshold for all of the stimuli tested (Figure 2.4A-D). Seven days after noise exposure, ABR thresholds recovered to baseline levels at the lower frequencies, with no differences found between WT and Panx3$^{-/-}$ mice (Figure 2.4A-B). Interestingly, seven days after noise exposure, Panx3$^{-/-}$ mice had significantly less hearing loss at both the higher frequency stimuli (16- and 24 kHz) tested, as indicated by lower ABR thresholds than those observed in the WT mice (Figure 2.4C-D). The most profound enhancement of post-noise exposure recovery was found at the 16 kHz stimulus (WT: 86dB ± 2dB, Panx3$^{-/-}$: 66dB ± 5dB), where the Panx3$^{-/-}$ mice showed approximately a 20 dB improvement in hearing recovery compared to the WT mice (Figure 2.4C). Collectively, these data suggest that ablation of Panx3 has a protective function against exposure to a single bout of loud noise.

2.3.5. Panx3$^{-/-}$ mice have morphological changes of inner ear bones

We examined the morphological characteristics of the middle ear bones (malleus, incus, and stapes) to determine if ablation of Panx3 would alter their formation during development. Representative images of each middle ear bone from both WT and Panx3$^{-/-}$ mice revealed that there were no gross changes in anatomical structures (Figure 2.5A). However, analysis of the total length of the malleus (i.e. distance from the head of the malleus to the end of malleus) was significantly decreased in Panx3$^{-/-}$ mice (WT: 1.6 mm± 0.014, Panx3$^{-/-}$: 1.54 mm± 0.014; Figure 2.5A-B). In addition, the distance between the processes of the incus was significantly increased in Panx3$^{-/-}$ mice (WT: 0.59 mm ±0.009, Panx3$^{-/-}$: 0.62 mm ±0.006; Figures 2.5A-C).

Figure 2.4. Panx3$^{-/-}$ mice have enhanced recovery 7 days after auditory insult.

Noise-exposure caused a significant increase in ABR threshold immediately after noise-exposure (Post NE) for (A) click, (B) 4 kHz, (C) 16 kHz, and (D) 24 kHz tonal stimuli, confirming auditory damage in both WT and Panx3$^{-/-}$ mice. Following noise exposure, the highest ABR thresholds Post NE were found at the higher frequency stimuli, (C) 16 kHz and (D) 24 kHz tones. ABR thresholds for each stimulus recovered to some degree 7 days after noise-exposure but did not reach baseline ABR thresholds at any stimulus. At the lower frequencies, (A) click and (B) 4 kHz, there were no significant differences between ABR thresholds 7 days after noise-exposure between WT and Panx3$^{-/-}$ mice. However, at the higher frequencies (C) 16 kHz, and (D) 24 kHz, Panx3$^{-/-}$ mice had significantly decreased ABR thresholds compared to WTs 7 days after noise-exposure, suggesting better recovery after auditory insult, ($p< 0.0001$, $p<0.05$, respectively). Two-way repeated measures ANOVAs were performed for each individual stimulus, with a Sidak's post hoc test. WT: n=10, Panx3$^{-/-}$: n=10. Bars represent mean ABR threshold ± SEM. $P<0.05$, ns = not significant.

Figure 2.4

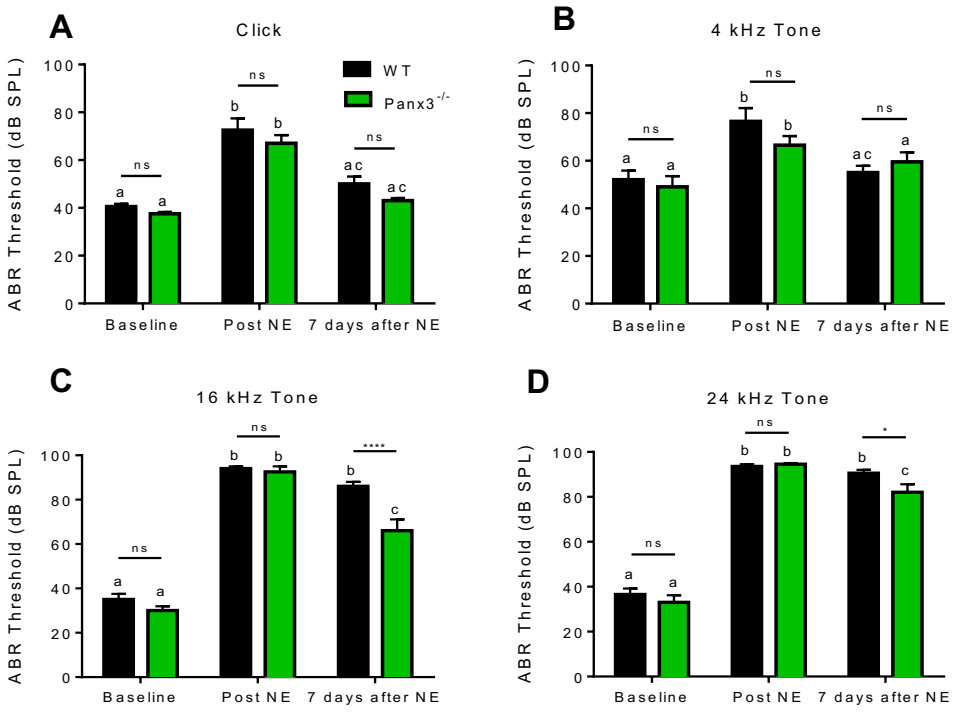
A
Click
WT
Panx3 -/-
ABR Threshold (dB SPL)
100
80
60
40
20
0
ns
b
b
ns
ac
ac
ns
a
a
Baseline
Post NE
7 days after NE
B
4 kHz Tone
ns
b
b
ns
ac
a
ns
a
a
C
16 kHz Tone
ns
b
b
****
b
c
ns
a
a
D
24 kHz Tone
ns
b
b
*
b
c
ns
a
a

Figure 2.5. Panx3$^{-/-}$ mice have morphological alterations of middle ear bones.

(A) Representative images of middle ear bones (malleus, incus, and stapes) from 2-3 month old WT and Panx3$^{-/-}$ mice. Middle ear bones were imaged and extensive measurements were taken. (B) The total length of the malleus was significantly decreased in Panx3$^{-/-}$ mice compared to WTs (n=17 and 24), respectively (**p<0.01, unpaired *t* test). (C) The distance between the tips of the incus bone was significantly increased in Panx3$^{-/-}$ mice compared to WTs (n=17 and 24), respectively (**p<0.01, unpaired *t* test). (D) The length of the stapes window was significantly decreased in Panx3$^{-/-}$ mice (n=13 and 19), respectively (*p< 0.05, unpaired *t* test). Bars represent mean length ± SEM.

Figure 2.5

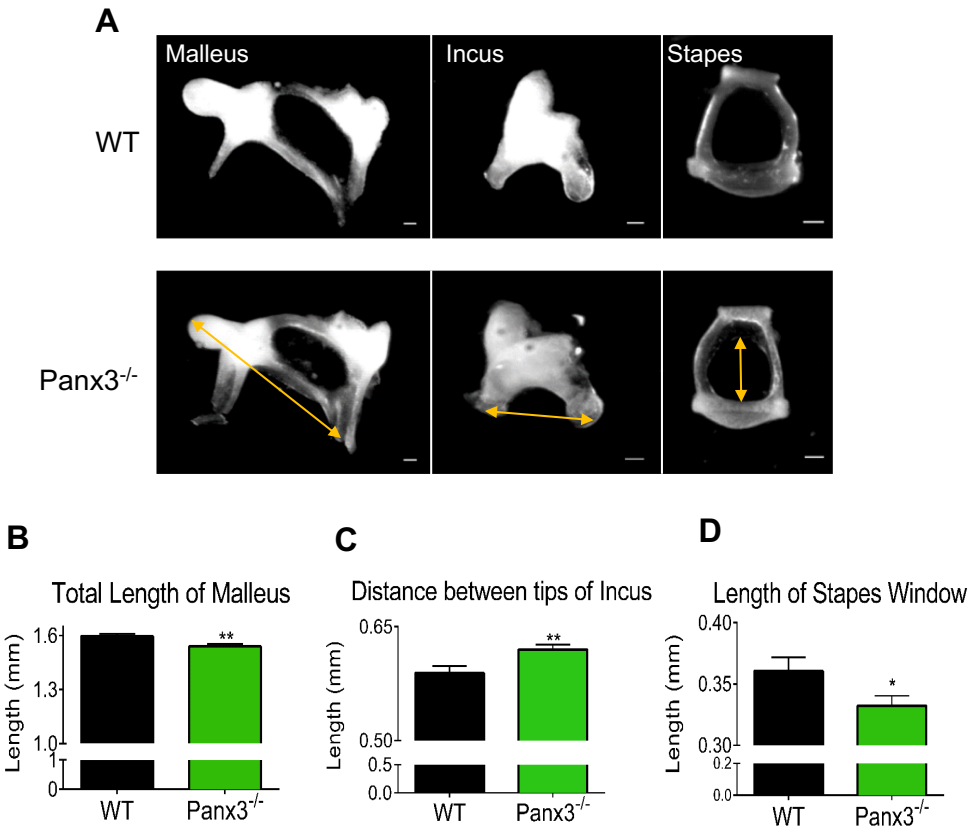
A
Malleus
Incus
Stapes
WT
Panx3-/-
B
Total Length of Malleus
Length (mm)
1.6
1.3
1.0
1
0
**
WT
Panx3-/-
C
Distance between tips of Incus
Length (mm)
0.65
0.50
0.5
0.0
**
WT
Panx3-/-
D
Length of Stapes Window
Length (mm)
0.40
0.35
0.30
0.2
0.0
*
WT
Panx3-/-

The length of the stapes window was significantly decreased in Panx3$^{-/-}$ mice (WT: 0.36 mm ±0.01, Panx3$^{-/-}$: 0.33 mm ±0.008; Figures 2.5A-C). Thus, the ablation of Panx3 leads to small morphological changes of middle ear bones.

2.3.6. Panx3$^{-/-}$ mice have enhanced Cx26, Cx30, Cx43, and Panx2 mRNA transcript levels

In order to assess for possible compensatory mechanisms that Cxs may be playing in Panx1 or Panx3 null mice, we examined Cx26, Cx30, and Cx43 mRNA expression levels in WT, Panx1$^{-/-}$, and Panx3$^{-/-}$ mice at two-three months of age. Interestingly, all three Cxs were upregulated in Panx3$^{-/-}$ mice compared to wild-type or Panx1$^{-/-}$ mice, while their expression in Panx1$^{-/-}$ remained similar to WT levels (Figure 2.6A-C). In addition, we assessed Panx2 mRNA expression in all three mice to determine if Panx2 may be upregulated in either Panx1 or Panx3 null mice. Panx2 mRNA expression was upregulated in Panx3$^{-/-}$ mice compared to Panx1$^{-/-}$ mice, however, no significant differences were observed in comparison to WT mice (Figure 2.6D). Panx1$^{-/-}$ mice had similar Panx2 expression to WT mice (Figure 2.6D).

Figure 2.6. Assessment of connexin and Panx2 mRNA transcript levels in Panx3$^{-/-}$ mice.

Using RT-qPCR, Cx26, Cx30, and Cx43 were all detected in 2-3 month old cochleae of WT, Panx1$^{-/-}$, and Panx3$^{-/-}$ mice (A-C). Cx30 and Cx43 were upregulated in Panx3$^{-/-}$ mice compared to both WT and Panx1$^{-/-}$ mice while Cx26 was only significantly higher than Panx1$^{-/-}$ mice (*$p<0.05$, **$p<0.01$ one way ANOVA with Tukey's multiple comparison test), N=5, n=15. However, no differences were found between WT and Panx1$^{-/-}$ mice. In addition, qPCR showed no upregulation of Panx2 transcript levels in Panx1$^{-/-}$ (D). However, although similar to WT mice, Panx3$^{-/-}$ mice had upregulation of Panx2 mRNA expression compared to Panx1$^{-/-}$ mice (*$p<0.05$, one way ANOVA with Tukey's multiple comparison test), N=4, n=12. Bars represent mean ± SEM.

Figure 2.6.

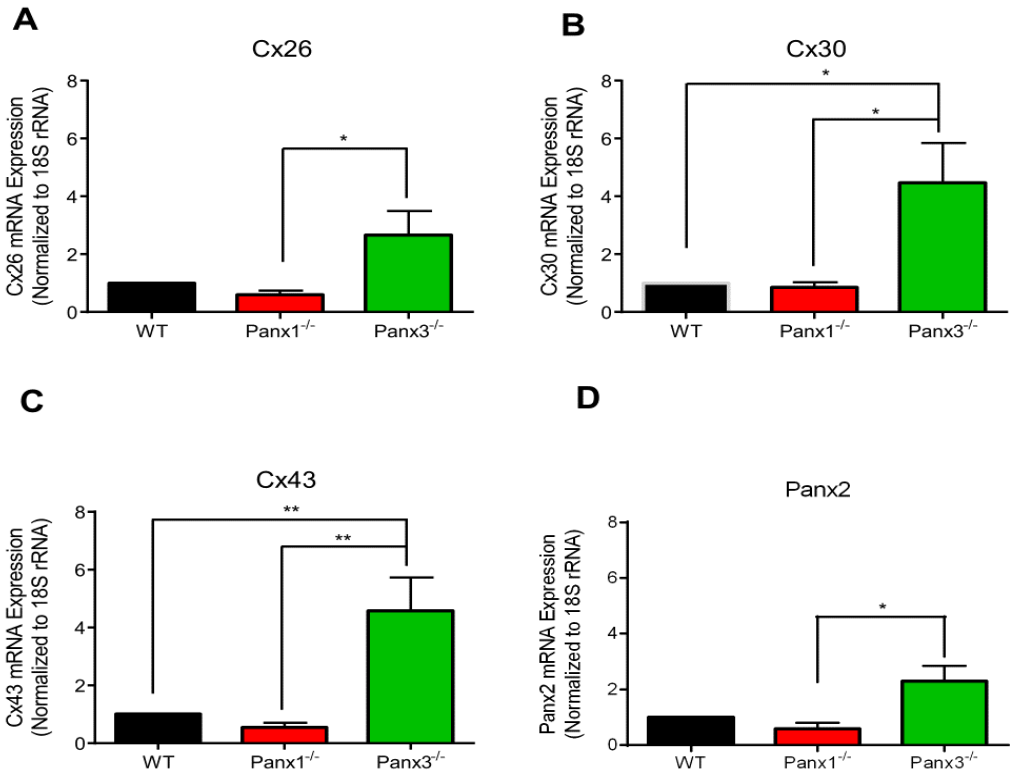
A
Cx26
Cx26 mRNA Expression (Normalized to 18S rRNA)
WT
Panx1-/-
Panx3-/-
B
Cx30
Cx30 mRNA Expression (Normalized to 18S rRNA)
C
Cx43
Cx43 mRNA Expression (Normalized to 18S rRNA)
D
Panx2
Panx2 mRNA Expression (Normalized to 18S rRNA)

2.4. Discussion

Since their discovery in 2000, Panx large-pore channels have been implicated in a large number of human diseases [15, 18, 55]. Most recently, Panx1 was found to be linked to hearing loss in two tissue-specific mouse models where Panx1 was selectively ablated from resident cells of the cochlea [29, 31]. In the current study, we addressed the possibility that Panx1 null mice, where Panx1 has been ablated throughout the entire animal, would exhibit even more severe hearing loss. Furthermore, we are the first group to assess if Panx3 is essential for normal hearing, and whether either Panx1 or Panx3 exacerbates or provides protection against noise-induced hearing loss. Surprisingly, $Panx1^{-/-}$ mice had normal hearing, and they exhibited no protection nor increased sensitivity to loud noise exposure. $Panx3^{-/-}$ mice also exhibited normal hearing but were partially protected from noise-induced hearing loss, possibly through morphological changes that were observed in the middle ear bone structures and/or compensatory upregulation of other large-pore channels found in the cochlea. Collectively, the present findings challenge the position that Panx1 ablation will lead to hearing impairment but support the concept that Panx3 ablation partially protects against loud noise-induced hearing loss.

Recently, it has been suggested that the most extensively studied Panx, Panx1, is the predominant ATP release channel in the cochlea [31], although connexin hemichannels have also been implicated in this process [56]. ATP acts as a signaling molecule in the cochlea and plays a role in the mechanoelectrical transduction processes throughout the auditory pathway [32] and in propagating Ca^{2+} waves in response to hair cell damage [57]. ATP also causes discrete bursts of action potentials in primary auditory neurons, an essential component in the development of central auditory pathways [32, 58, 59]. Pannexins have also been implicated in Ca^{2+} wave propagation, and Ca^{2+} is essential for inner hair cell development through its role in creating spontaneous Ca^{2+}-driven action potentials in early stages of development [60, 61]. Within the cochlea, Panx1 is expressed in the spiral limbus, supporting cells of the organ of Corti, the spiral prominence in the cochlear lateral wall, Reisner's membrane, and the spiral ganglion neurons [13, 14]. Moreover, Panx1 mRNA transcripts were detected in neurons of the auditory cortex [13, 14, 28]. Mounting evidence supports a role for Panx1 in hearing as a patient with a loss-of-function *PANX1* germline mutation exhibited multi-system defects, including severe hearing loss [36]. Perhaps more impacting, mutant mice lacking Panx1 in

Pax2 and Foxg1 expressing cells of the cochlear duct exhibited sensorineural hearing loss [29, 31]. Pax2 is a transcription factor expressed in the endolymphatic duct and in hair cells of the cochlea [62-64]. Foxg1 is part of a forkhead gene family and is required for morphogenesis of the cochlea and is expressed in most cell types of the inner ear [30]. To account for the potentially broad distribution of Panx1 within the peripheral and central auditory systems, we predicted that Panx1$^{-/-}$ mice would have even more severe hearing loss than mice lacking Panx1 in Pax2 or Foxg1 expressing cells only, but to our surprise both Panx1$^{-/-}$ and Panx3$^{-/-}$ mice did not exhibit sensorineural hearing loss. Moreover, the functional integrity of the auditory nerve was intact with no detrimental changes in neural transmission, which was observed by amplitude and latency analysis of ABR waveforms [65]. Consistent with Panx1 not playing a major role in the auditory pathway, Panx1 null mice were equally susceptible to noise-induced hearing damage compared to controls, further validating the conclusion that Panx1 does not contribute to impairments in hearing sensitivity of mice. Thus, the ablation of Panx1 does not lead to sensorineural hearing loss, cochlear nerve deficits, or altered susceptibility to noise-induced hearing loss.

Our findings were surprising and in contrast to previous studies that showed conditional ablation of Panx1 in the cochlea led to sensorineural hearing loss [29, 31]. On first pass, one might predict that a Panx1$^{-/-}$ mouse would have a more severe hearing loss phenotype than when Panx1 is only ablated from a subset of resident cochlea cells; however, systemic gene ablated mice have more opportunity for compensatory mechanisms to rescue a potential disease phenotype. For example, previous studies have shown that when Panx1 was ablated in mice, Panx3 was upregulated in dorsal skin and blood vessels; findings that support a compensatory mechanism [49, 66]. In the present study, we confirmed Panx1 ablation in the cochlea of Panx1$^{-/-}$ mice by assessing both mRNA transcripts and protein expression levels. We also showed that cochleae of Panx1$^{-/-}$ mice did not exhibit upregulation of Panx2 mRNA expression or Panx3 at either the mRNA transcript level, minimizing a potential compensatory role for the residual pannexins in the Panx1$^{-/-}$ mice. That said, we cannot exclude the possibility that baseline levels of Panx2 and/or Panx3 channels are hyperactive. Alternatively, it is worth noting that because Cx hemichannels have been proposed to have similar functions to Panx channels [67], it is possible that Cxs in the cochlea are acting to compensate for the loss of Panx1. However, no increase in the levels of Cx26, Cx30, or Cx43 was observed in Panx1$^{-/-}$

mice. Thus, the reasons for the phenotypic differences in hearing competence identified in the previously published conditional Panx1 ablation mouse models versus the present global ablation model remain elusive. It is interesting that a recent paper suggested that many genetically-modified mouse models harbor passenger mutations when bred back to different backgrounds, potentially influencing phenotypic outcomes [68]. It is unknown if this issue may be a complicating factor in Panx1 mouse ablation studies. In the human context, we recently discovered the first patient worldwide harboring a *PANX1* gene mutation linked to severe hearing loss [36]. This suggests a possible link between *PANX1* mutants and hearing loss that may be mechanistically distinct from cases where the *PANX1* gene is completely ablated. Future studies will need to resolve what findings in Panx1$^{-/-}$ mice best translates to the human condition.

Panx3, the second Panx examined in our study, is involved in proper bone formation and development. Panx3 is expressed in prehypertrophic chondrocytes and acts to accelerate their terminal differentiation through ATP release [38]. Recently, it was shown that Panx3$^{-/-}$ mice were protected against surgically-induced osteoarthritis and had alterations in their long bones [51, 69]. Panx3 is found mostly in bone and cartilage tissues, as well as in the cochlear bone and modiolus of the inner ear [14, 18]. In the present study, we found that Panx3 expression in WT cochleae was developmentally regulated peaking at P8 and there were morphological alterations to the middle ear bones. Interestingly, this finding correlates with previous findings that Panx3 regulates osteoblast differentiation [37], which our study suggests may be essential in the cochlear bone and auditory ossicles. The middle ear bones are essential for conveying sound from the external environment into the inner ear, as malformations of the middle ear bones can lead to hearing loss [45]. We found that Panx3$^{-/-}$ mice, despite having morphological alterations in the three ossicles, did not exhibit impaired hearing sensitivity. In fact, compared to WTs, Panx3$^{-/-}$ mice showed enhanced neural synchrony at the level of the cochlear nerve. At present, however, it is not possible to conclude the physiological mechanism underlying this finding. Since the developing cochlea is formed through signaling between the developing bone and sensorineural structures [70], and the auditory transduction pathway becomes embedded in bone, diseases changing bone remodeling can impact hearing. For example, patients with the human genetic condition cleidocranial dysplasia, resulting from RUNX2 haploinsufficiency, leads to bone deformities resulting in hearing loss, which can be

sensorineural, conductive or a combination of the two [71]. Interestingly, the Panx3 promoter can be trans-activated by RUNX2 [38]. This suggests that Panx3 expression could be regulated by RUNX2 and may explain some of the symptoms associated with cleidocranial dysplasia. Similarly, some patients with cochlear otosclerosis exhibit sensorineural hearing loss without morphological damage to the sensory tissues [43, 72]. Thus, the enhancement of cochlear nerve synchrony that was observed in Panx3$^{-/-}$ mice could be due to cochlear and/or middle ear bone shape changes. Alternatively, the enhanced neural synchrony observed in the cochlear nerve of Panx3$^{-/-}$ mice may be due to ablation of Panx3 in cell types that directly contribute to sensorineural processing. While Panx2 levels were increased in Panx3 ablated mice, this increase was not statistically significant compared to wild-type mice suggesting that the compensating role of Panx2 in assisting in neural synchrony remains to be firmly established. Finally, it is possible that the upregulation of cochlear connexins in Panx3$^{-/-}$ mice could be contributing to the increased synchrony observed in their cochlear nerve, as demonstrated by increased wave I amplitudes in response to the 90dB click stimulus.

To our surprise, when we challenged the auditory system of Panx3$^{-/-}$ mice with a loud noise exposure, they showed decreased susceptibility to 16- and 24 kHz hearing loss seven days after the acoustic insult. Similar to the enhanced neural synchrony in the auditory nerve of these mice, the mechanism by which Panx3 ablation allowed the auditory system to be more resilient to noise-induced hearing loss remains unknown and difficult to dissect. We suggest that various mechanisms, including morphological changes in the middle ear bones, and/or compensatory upregulation of Cxs may underlie the increased resistance to acoustic trauma observed in Panx3$^{-/-}$ mice in the present study. For example, since Panx3 is expressed in bone, the enhanced protection observed in Panx3$^{-/-}$ mice may also be due to differences in conveying mechanical sound through the middle ear bones during noise exposure. Furthermore, the morphological alterations observed in middle ear bones of Panx3$^{-/-}$ mice could perhaps contribute to the enhanced 16- and 24 kHz hearing protection through differences in sound conduction correlating to better tolerance of loud noise.

It is important to acknowledge that the hearing protection observed in the Panx3$^{-/-}$ mice may have occurred by mechanisms associated with Panx3 that extend beyond its expression in bone, such as Ca^{2+} or ATP release. It is well established that loud noise exposure causes an increase in metabolic activity that alters the cellular redox state of the cochlea, leading to reactive

oxygen species (ROS), that cause excessive cochlear damage [73, 74]. This damage can ultimately lead to hair cell death, which is associated with intracellular accumulation of potassium, as well as auditory nerve degeneration [75, 76]. Interestingly, dexamethasone administration in the cochlea was shown to have a protective function by preserving hair cell survival and reducing ototoxic injury through inhibition of Ca^{2+} entry in auditory cells [74, 77-79]. Since Panx3, among other functions, releases Ca^{2+}, it is reasonable to propose that ablation of Panx3 may have provided protection against noise-induced hearing loss in the present study, by reducing ototoxic injury through inhibition of Ca^{2+} release within the cochlea.

2.5. Conclusions

In considering the potential role that connexin compensation may play in $Panx3^{-/-}$mice, it is worth noting that previous studies have shown that reduced Cx26 expression leads to increased susceptibility to noise-induced hearing loss, and following a loud noise-exposure, Cx26 expression decreases [80, 81]. In the current study, we found that Cx26, Cx30, and Cx43 were all upregulated in $Panx3^{-/-}$ mice at baseline which could potentially act in a protective manner against an acute loud noise exposure. Alternatively, because the expression pattern of Panx3 in the auditory system is not fully characterized, it is possible that the hearing protection observed in the $Panx3^{-/-}$ mice occurred via mechanisms associated with Panx3 that extend beyond its expression in bone. Ultimately, future studies will be needed to uncover the mechanism(s) by which ablation of Panx3 provides hearing protection from excessive noise exposure, and thus, whether Panx3 could serve as a novel molecular target in the clinical protection against traumatic hearing loss.

2.6. Acknowledgements

The authors of this paper thank Dr. Silvia Penuela for consulting on this project.

2.7. References

1 Olusanya, B. O., Neumann, K. J. and Saunders, J. E. (2014) The global burden of disabling hearing impairment: a call to action. Bull World Health Organ. **92**, 367-373

2 Kikuchi, T., Kimura, R. S., Paul, D. L., Takasaka, T. and Adams, J. C. (2000) Gap junction systems in the mammalian cochlea. Brain Res Brain Res Rev. **32**, 163-166

3 Kelly, J. J., Forge, A. and Jagger, D. J. (2011) Development of gap junctional intercellular communication within the lateral wall of the rat cochlea. Neuroscience. **180**, 360-369

4 Zhao, H. B., Kikuchi, T., Ngezahayo, A. and White, T. W. (2006) Gap junctions and cochlear homeostasis. J Membr Biol. **209**, 177-186

5 Chang, Q., Tang, W., Ahmad, S., Zhou, B. and Lin, X. (2008) Gap junction mediated intercellular metabolite transfer in the cochlea is compromised in connexin30 null mice. PLoS One. **3**, e4088

6 Jagger, D. J. and Forge, A. (2015) Connexins and gap junctions in the inner ear--it's not just about K(+) recycling. Cell Tissue Res. **360**, 633-644

7 Forge, A., Becker, D., Casalotti, S., Edwards, J., Marziano, N. and Nevill, G. (2003) Gap junctions in the inner ear: comparison of distribution patterns in different vertebrates and assessement of connexin composition in mammals. J Comp Neurol. **467**, 207-231

8 Kikuchi, T., Kimura, R. S., Paul, D. L. and Adams, J. C. (1995) Gap junctions in the rat cochlea: immunohistochemical and ultrastructural analysis. Anat Embryol (Berl). **191**, 101-118

9 Zhao, H. B. and Yu, N. (2006) Distinct and gradient distributions of connexin26 and connexin30 in the cochlear sensory epithelium of guinea pigs. J Comp Neurol. **499**, 506-518

10 Jagger, D. J. and Forge, A. (2006) Compartmentalized and signal-selective gap junctional coupling in the hearing cochlea. J Neurosci. **26**, 1260-1268

11 Wingard, J. C. and Zhao, H. B. (2015) Cellular and Deafness Mechanisms Underlying Connexin Mutation-Induced Hearing Loss - A Common Hereditary Deafness. Front Cell Neurosci. **9**, 202

12 Chan, D. K. and Chang, K. W. (2014) GJB2-associated hearing loss: systematic review of worldwide prevalence, genotype, and auditory phenotype. Laryngoscope. **124**, E34-53

13 Tang, W., Ahmad, S., Shestopalov, V. I. and Lin, X. (2008) Pannexins are new molecular candidates for assembling gap junctions in the cochlea. Neuroreport. **19**, 1253-1257

14 Wang, X. H., Streeter, M., Liu, Y. P. and Zhao, H. B. (2009) Identification and characterization of pannexin expression in the mammalian cochlea. J Comp Neurol. **512**, 336-346

15 Panchin, Y., Kelmanson, I., Matz, M., Lukyanov, K., Usman, N. and Lukyanov, S. (2000) A ubiquitous family of putative gap junction molecules. Curr Biol. **10**, R473-474

16 Yen, M. R. and Saier, M. H., Jr. (2007) Gap junctional proteins of animals: the innexin/pannexin superfamily. Prog Biophys Mol Biol. **94**, 5-14

17 Bruzzone, R., White, T. W. and Paul, D. L. (1996) Connections with connexins: the molecular basis of direct intercellular signaling. Eur J Biochem. **238**, 1-27

18 Penuela, S., Gehi, R. and Laird, D. W. (2013) The biochemistry and function of pannexin channels. Biochim Biophys Acta. **1828**, 15-22

19 Bao, L., Locovei, S. and Dahl, G. (2004) Pannexin membrane channels are mechanosensitive conduits for ATP. FEBS Lett. **572**, 65-68

20 Locovei, S., Wang, J. and Dahl, G. (2006) Activation of pannexin 1 channels by ATP through P2Y receptors and by cytoplasmic calcium. FEBS Lett. **580**, 239-244

21 Chekeni, F. B., Elliott, M. R., Sandilos, J. K., Walk, S. F., Kinchen, J. M., Lazarowski, E. R., Armstrong, A. J., Penuela, S., Laird, D. W., Salvesen, G. S., Isakson, B. E., Bayliss, D. A. and Ravichandran, K. S. (2010) Pannexin 1 channels mediate 'find-me' signal release and membrane permeability during apoptosis. Nature. **467**, 863-867

22 Penuela, S., Bhalla, R., Gong, X. Q., Cowan, K. N., Celetti, S. J., Cowan, B. J., Bai, D., Shao, Q. and Laird, D. W. (2007) Pannexin 1 and pannexin 3 are glycoproteins that exhibit many distinct characteristics from the connexin family of gap junction proteins. J Cell Sci. **120**, 3772-3783

23 Silverman, W. R., de Rivero Vaccari, J. P., Locovei, S., Qiu, F., Carlsson, S. K., Scemes, E., Keane, R. W. and Dahl, G. (2009) The pannexin 1 channel activates the inflammasome in neurons and astrocytes. J Biol Chem. **284**, 18143-18151

24 Qiu, F. and Dahl, G. (2009) A permeant regulating its permeation pore: inhibition of pannexin 1 channels by ATP. Am J Physiol Cell Physiol. **296**, C250-255

25 Iglesias, R., Locovei, S., Roque, A., Alberto, A. P., Dahl, G., Spray, D. C. and Scemes, E. (2008) P2X7 receptor-Pannexin1 complex: pharmacology and signaling. Am J Physiol Cell Physiol. **295**, C752-760

26 Scemes, E., Suadicani, S. O., Dahl, G. and Spray, D. C. (2007) Connexin and pannexin mediated cell-cell communication. Neuron Glia Biol. **3**, 199-208

27 Zhao, H. B. (2016) Expression and function of pannexins in the inner ear and hearing. BMC Cell Biol. **17 Suppl 1**, 16

28 Cunningham, M. O., Whittington, M. A., Bibbig, A., Roopun, A., LeBeau, F. E., Vogt, A., Monyer, H., Buhl, E. H. and Traub, R. D. (2004) A role for fast rhythmic bursting neurons in cortical gamma oscillations in vitro. Proc Natl Acad Sci U S A. **101**, 7152-7157

29 Zhao, H. B., Zhu, Y., Liang, C. and Chen, J. (2015) Pannexin 1 deficiency can induce hearing loss. Biochem Biophys Res Commun. **463**, 143-147

30 Pauley, S., Lai, E. and Fritzsch, B. (2006) Foxg1 is required for morphogenesis and histogenesis of the mammalian inner ear. Dev Dyn. **235**, 2470-2482

31 Chen, J., Zhu, Y., Liang, C. and Zhao, H. B. (2015) Pannexin1 channels dominate ATP release in the cochlea ensuring endocochlear potential and auditory receptor potential generation and hearing. Sci Rep. **5**, 10762

32 Housley, G. D. (1998) Extracellular nucleotide signaling in the inner ear. Mol Neurobiol. **16**, 21-48

33 Thorne, P. R., Munoz, D. J., Nikolic, P., Mander, L., Jagger, D. J., Greenwood, D., Vlajkovic, S. and Housley, G. D. (2002) Potential role of purinergic signalling in cochlear pathology. Audiol Neurootol. **7**, 180-184

34 Zhu, Y. and Zhao, H. B. (2010) ATP-mediated potassium recycling in the cochlear supporting cells. Purinergic Signal. **6**, 221-229

35 Zhu, Y. and Zhao, H. B. (2012) ATP activates P2X receptors to mediate gap junctional coupling in the cochlea. Biochem Biophys Res Commun. **426**, 528-532

36 Shao, Q., Lindstrom, K., Shi, R., Kelly, J., Schroeder, A., Juusola, J., Levine, K. L., Esseltine, J. L., Penuela, S., Jackson, M. F. and Laird, D. W. (2016) A Germline Variant in the PANX1 Gene Has Reduced Channel Function and Is Associated with Multisystem Dysfunction. J Biol Chem. **291**, 12432-12443

37 Ishikawa, M., Iwamoto, T., Nakamura, T., Doyle, A., Fukumoto, S. and Yamada, Y. (2011) Pannexin 3 functions as an ER Ca(2+) channel, hemichannel, and gap junction to promote osteoblast differentiation. J Cell Biol. **193**, 1257-1274

38 Bond, S. R., Lau, A., Penuela, S., Sampaio, A. V., Underhill, T. M., Laird, D. W. and Naus, C. C. (2011) Pannexin 3 is a novel target for Runx2, expressed by osteoblasts and mature growth plate chondrocytes. J Bone Miner Res. **26**, 2911-2922

39 Celetti, S. J., Cowan, K. N., Penuela, S., Shao, Q., Churko, J. and Laird, D. W. (2010) Implications of pannexin 1 and pannexin 3 for keratinocyte differentiation. J Cell Sci. **123**, 1363-1372

40 Iwamoto, T., Nakamura, T., Doyle, A., Ishikawa, M., de Vega, S., Fukumoto, S. and Yamada, Y. (2010) Pannexin 3 regulates intracellular ATP/cAMP levels and promotes chondrocyte differentiation. J Biol Chem. **285**, 18948-18958

41 Ishikawa, M., Iwamoto, T., Fukumoto, S. and Yamada, Y. (2014) Pannexin 3 inhibits proliferation of osteoprogenitor cells by regulating Wnt and p21 signaling. J Biol Chem. **289**, 2839-2851

42 Rudic, M., Keogh, I., Wagner, R., Wilkinson, E., Kiros, N., Ferrary, E., Sterkers, O., Bozorg Grayeli, A., Zarkovic, K. and Zarkovic, N. (2015) The pathophysiology of otosclerosis: Review of current research. Hear Res. **330**, 51-56

43 Cureoglu, S., Baylan, M. Y. and Paparella, M. M. (2010) Cochlear otosclerosis. Curr Opin Otolaryngol Head Neck Surg. **18**, 357-362

44 Colvin, J. S., Bohne, B. A., Harding, G. W., McEwen, D. G. and Ornitz, D. M. (1996) Skeletal overgrowth and deafness in mice lacking fibroblast growth factor receptor 3. Nat Genet. **12**, 390-397

45 Duboeuf, F., Burt-Pichat, B., Farlay, D., Suy, P., Truy, E. and Boivin, G. (2015) Bone quality and biomechanical function: a lesson from human ossicles. Bone. **73**, 105-110

46 Oishi, N. and Schacht, J. (2011) Emerging treatments for noise-induced hearing loss. Expert Opin Emerg Drugs. **16**, 235-245

47 Hu, B. H., Cai, Q., Manohar, S., Jiang, H., Ding, D., Coling, D. E., Zheng, G. and Salvi, R. (2009) Differential expression of apoptosis-related genes in the cochlea of noise-exposed rats. Neuroscience. **161**, 915-925

48 Qu, Y., Misaghi, S., Newton, K., Gilmour, L. L., Louie, S., Cupp, J. E., Dubyak, G. R., Hackos, D. and Dixit, V. M. (2011) Pannexin-1 is required for ATP release during apoptosis but not for inflammasome activation. J Immunol. **186**, 6553-6561

49 Penuela, S., Kelly, J. J., Churko, J. M., Barr, K. J., Berger, A. C. and Laird, D. W. (2014) Panx1 regulates cellular properties of keratinocytes and dermal fibroblasts in skin development and wound healing. J Invest Dermatol. **134**, 2026-2035

50 Cone, A. C., Ambrosi, C., Scemes, E., Martone, M. E. and Sosinsky, G. E. (2013) A comparative antibody analysis of pannexin1 expression in four rat brain regions reveals varying subcellular localizations. Front Pharmacol. **4**, 6

51 Moon, P. M., Penuela, S., Barr, K., Khan, S., Pin, C. L., Welch, I., Attur, M., Abramson, S. B., Laird, D. W. and Beier, F. (2015) Deletion of Panx3 Prevents the Development of Surgically Induced Osteoarthritis. J Mol Med (Berl). **93**, 845-856

52 Vikhe Patil, K., Canlon, B. and Cederroth, C. R. (2015) High quality RNA extraction of the mammalian cochlea for qRT-PCR and transcriptome analyses. Hear Res. **325**, 42-48

53 Heffner, H. E. and Heffner, R. S. (2007) Hearing ranges of laboratory animals. J Am Assoc Lab Anim Sci. **46**, 20-22

54 Popelar, J., Grecova, J., Rybalko, N. and Syka, J. (2008) Comparison of noise-induced changes of auditory brainstem and middle latency response amplitudes in rats. Hear Res. **245**, 82-91

55 Penuela, S., Harland, L., Simek, J. and Laird, D. W. (2014) Pannexin channels and their links to human disease. Biochem J. **461**, 371-381

56 Anselmi, F., Hernandez, V. H., Crispino, G., Seydel, A., Ortolano, S., Roper, S. D., Kessaris, N., Richardson, W., Rickheit, G., Filippov, M. A., Monyer, H. and Mammano, F. (2008) ATP release through connexin hemichannels and gap junction transfer of second messengers propagate Ca2+ signals across the inner ear. Proc Natl Acad Sci U S A. **105**, 18770-18775

57 Lahne, M. and Gale, J. E. (2010) Damage-induced cell-cell communication in different cochlear cell types via two distinct ATP-dependent Ca waves. Purinergic Signal. **6**, 189-200

58 Tritsch, N. X., Yi, E., Gale, J. E., Glowatzki, E. and Bergles, D. E. (2007) The origin of spontaneous activity in the developing auditory system. Nature. **450**, 50-55

59 Mammano, F. (2013) ATP-dependent intercellular Ca2+ signaling in the developing cochlea: facts, fantasies and perspectives. Semin Cell Dev Biol. **24**, 31-39

60 Marcotti, W., Johnson, S. L., Rusch, A. and Kros, C. J. (2003) Sodium and calcium currents shape action potentials in immature mouse inner hair cells. J Physiol. **552**, 743-761

61 Tritsch, N. X. and Bergles, D. E. (2010) Developmental regulation of spontaneous activity in the Mammalian cochlea. J Neurosci. **30**, 1539-1550

62 Lawoko-Kerali, G., Rivolta, M. N. and Holley, M. (2002) Expression of the transcription factors GATA3 and Pax2 during development of the mammalian inner ear. J Comp Neurol. **442**, 378-391

63 Nornes, H. O., Dressler, G. R., Knapik, E. W., Deutsch, U. and Gruss, P. (1990) Spatially and temporally restricted expression of Pax2 during murine neurogenesis. Development. **109**, 797-809

64 Burton, Q., Cole, L. K., Mulheisen, M., Chang, W. and Wu, D. K. (2004) The role of Pax2 in mouse inner ear development. Dev Biol. **272**, 161-175

65 Rance, G. and Starr, A. (2015) Pathophysiological mechanisms and functional hearing consequences of auditory neuropathy. Brain. **138**, 3141-3158

66 Lohman, A. W., Billaud, M., Straub, A. C., Johnstone, S. R., Best, A. K., Lee, M., Barr, K., Penuela, S., Laird, D. W. and Isakson, B. E. (2012) Expression of pannexin isoforms in the systemic murine arterial network. J Vasc Res. **49**, 405-416

67 Lazarowski, E. R. (2012) Vesicular and conductive mechanisms of nucleotide release. Purinergic Signal. **8**, 359-373

68 Vanden Berghe, T., Hulpiau, P., Martens, L., Vandenbroucke, R. E., Van Wonterghem, E., Perry, S. W., Bruggeman, I., Divert, T., Choi, S. M., Vuylsteke, M., Shestopalov, V. I., Libert, C. and Vandenabeele, P. (2015) Passenger Mutations Confound Interpretation of All Genetically Modified Congenic Mice. Immunity. **43**, 200-209

69 Caskenette, D., Penuela, S., Lee, V., Barr, K., Beier, F., Laird, D. W. and Willmore, K. E. (2016) Global deletion of Panx3 produces multiple phenotypic effects in mouse humeri and femora. J Anat. **228**, 746-756

70 Driver, E. C. and Kelley, M. W. (2009) Specification of cell fate in the mammalian cochlea. Birth Defects Res C Embryo Today. **87**, 212-221

71 Chang, J. L., Brauer, D. S., Johnson, J., Chen, C. G., Akil, O., Balooch, G., Humphrey, M. B., Chin, E. N., Porter, A. E., Butcher, K., Ritchie, R. O., Schneider, R. A., Lalwani, A., Derynck, R., Marshall, G. W., Marshall, S. J., Lustig, L. and Alliston, T. (2010) Tissue-specific calibration of extracellular matrix material properties by transforming growth factor-beta and Runx2 in bone is required for hearing. EMBO Rep. **11**, 765-771

72 Akil, O., Hall-Glenn, F., Chang, J., Li, A., Chang, W., Lustig, L. R., Alliston, T. and Hsiao, E. C. (2014) Disrupted bone remodeling leads to cochlear overgrowth and hearing loss in a mouse model of fibrous dysplasia. PLoS One. **9**, e94989

73 Perlman, H. B. and Kimura, R. (1962) Cochlear blood flow in acoustic trauma. Acta Otolaryngol. **54**, 99-110

74 Le Prell, C. G., Yamashita, D., Minami, S. B., Yamasoba, T. and Miller, J. M. (2007) Mechanisms of noise-induced hearing loss indicate multiple methods of prevention. Hear Res. **226**, 22-43

75 Wong, A. C. and Ryan, A. F. (2015) Mechanisms of sensorineural cell damage, death and survival in the cochlea. Front Aging Neurosci. **7**, 58

76 Coordes, A., Groschel, M., Ernst, A. and Basta, D. (2012) Apoptotic cascades in the central auditory pathway after noise exposure. J Neurotrauma. **29**, 1249-1254

77 Lamm, K. and Arnold, W. (1998) The effect of prednisolone and non-steroidal anti-inflammatory agents on the normal and noise-damaged guinea pig inner ear. Hear Res. **115**, 149-161

78 Takemura, K., Komeda, M., Yagi, M., Himeno, C., Izumikawa, M., Doi, T., Kuriyama, H., Miller, J. M. and Yamashita, T. (2004) Direct inner ear infusion of dexamethasone attenuates noise-induced trauma in guinea pig. Hear Res. **196**, 58-68

79 Shirwany, N. A., Seidman, M. D. and Tang, W. (1998) Effect of transtympanic injection of steroids on cochlear blood flow, auditory sensitivity, and histology in the guinea pig. Am J Otol. **19**, 230-235

80 Zhou, X. X., Chen, S., Xie, L., Ji, Y. Z., Wu, X., Wang, W. W., Yang, Q., Yu, J. T., Sun, Y., Lin, X. and Kong, W. J. (2016) Reduced Connexin26 in the Mature Cochlea Increases Susceptibility to Noise-Induced Hearing Lossin Mice. Int J Mol Sci. **17**, 301

81 Yamaguchi, T., Nagashima, R., Yoneyama, M., Shiba, T. and Ogita, K. (2014) Disruption of ion-trafficking system in the cochlear spiral ligament prior to permanent hearing loss induced by exposure to intense noise: possible involvement of 4-hydroxy-2-nonenal as a mediator of oxidative stress. PLoS One. **9**, e102133

Chapter 3 : Double deletion of *Panx1* and *Panx3* affects skin and bone but not hearing

Both Panx1 and Panx3 are expressed in the inner ear and our previous study showed that single global knock-out mice of Panx1 or Panx3 did not cause any hearing deficits. To determine whether compensation of Panx channels was occurring in single knock-out mice, we created the first of its kind Panx1 and Panx3 double knock-out mouse and characterized the skin, bone, and hearing phenotypes.

Importantly this paper was strategically performed by the collaboration of three different labs (Penuela, Allman, and Willmore). My specific data contributions to this paper was all the hearing data, with the rest of the data being performed by others.

A version of this manuscript is published:

Abitbol JM, O'Donnell BL, Wakefield CB, Jewlal E, Kelly JJ, Barr K, Willmore KE, Allman BL, Penuela S. Double deletion of *Panx1* and *Panx3* affects skin and bone but not hearing. *J Mol. Med.* 2019. 97:723-736.

3.1. Introduction

Pannexins (Panxs; Panx1, Panx2, and Panx3), are a family of three glycoproteins that form large pore channels at the plasma membrane [1-3] to allow passage of ions and metabolites through the intracellular and extracellular space [4, 5]. Panx1 is expressed in most mammalian organs [2, 6-10], while Panx2 has a more restricted expression pattern [2, 11]. Panx3 is expressed predominantly in skin, cartilage and bone [2, 9, 12].

Panx1 plays a role in many cellular processes such as ATP release, Ca^{2+} wave propagation, and apoptosis [13-15]. Panx1 channels can be opened through mechanical stimulation, an increase in intracellular calcium concentration, extracellular potassium concentration, membrane depolarization, as well as caspase 3 cleavage. [13-16]. Panx1 is highly expressed in young mouse skin, but decreases in aged skin [17] and is important in keratinocyte differentiation [18]. We previously found that $Panx1^{-/-}$ (KO) mice had reduced dermal area, but increased hypodermal thickness in dorsal skin compared to wild-type (WT) mice [17]. $Panx1^{-/-}$ mice displayed increased fibrosis and delayed wound healing [17]. Panx3 is also expressed in adult human skin and embryonic mouse skin tissues and participates in wound healing [16, 18].

Panx3 is found in bone and cartilage tissues [19, 20] and is involved in the differentiation of osteoblasts [21]. Panx3 is also expressed in pre-hypertrophic chondrocytes and acts to accelerate their terminal differentiation through increased ATP release[19]. Our group previously generated a global $Panx3^{-/-}$ (KO) mouse that was shown to be less prone to surgically-induced osteoarthritis [22]. Although gross skeletal phenotypic changes were not observed in this global $Panx3^{-/-}$ mice, analyses of micro-CT images of long bones of adult $Panx3^{-/-}$ and WT mice revealed that KO mice had shorter long bone diaphyses, larger areas of muscle attachment, and greater cross-sectional areas at mid-diaphysis compared to WT mice [23].

Our group has recently shown that the global $Panx1^{-/-}$ mouse did not exhibit hearing loss nor changes in the timing/amplitude of the sound-evoked electrical activity recorded in the auditory brainstem [24]. In contrast, studies using conditional ablation of Panx1 in the cochlea exhibited severe hearing loss at all frequencies, reduced endocochlear potential, and reduced cochlear microphonics [25], [26]. In a recent study, we investigated the role of Panx1 and

Panx3 in noise-induced hearing loss. Although no differences were found between Panx1$^{-/-}$ mice and their WT littermates, Panx3$^{-/-}$ mice had slightly better hearing recovery after noise exposure than WT mice [24]. Illustrating the potential compensation between pannexins, single Panx1$^{-/-}$ and Panx2$^{-/-}$ mice were subjected to ischemic stroke and had similar degrees of infarcts compared to controls [27]. However, Panx1$^{-/-}$Panx2$^{-/-}$ double knock-out mice had smaller infarct sizes to the brain and better central nervous system functional outcomes, suggesting that ablation of both genes was necessary to observe the phenotype [27].

Panx1 and Panx3 share protein sequence homology, and thus, it is postulated that the lack of gross overt phenotypes observed in one Panx$^{-/-}$ mice could be due to functional compensation. In fact, Panx3 was upregulated in skin, blood vessels and the vomeronasal organ of Panx1$^{-/-}$ mice [17, 28, 29]. To address this compensation issue, we have generated the first Panx1 and Panx3 double knock-out mouse (dKO) and focused our characterization on the skin, bone, and the auditory system that are known to express both pannexins.

3.2. Materials and methods

3.2.1. Generation of dKO mice

Panx3$^{-/-}$ mice were generated in house [22]. Panx1$^{-/-}$ mice were a kind gift from Genentech Inc. (San Francisco, CA) and were previously described [30]. Panx3$^{-/-}$ mice were crossed with Panx1$^{-/-}$ mice to generate offspring heterozygous (HT) for both Panx. These mice were backcrossed with either Panx3$^{-/-}$ or Panx1$^{-/-}$ mice to generate Panx1$^{+/-}$/Panx3$^{-/-}$ or Panx1$^{-/-}$ /Panx3$^{+/-}$. The HT/KO and KO/HT mice were crossed, and mice null for both pannexins (dKO) were selected and kept in a closed colony. C57BL/6 mice were used as controls. Mice were maintained on a 12h-light-12h-dark cycle and fed *ad libitum*. All experiments followed the guidelines and protocols for animal care approved by the Animal Care Committee at the University of Western Ontario.

3.2.2. Genotyping

Tail tips from P4-5 were digested in EDTA in a protein kinase solution. PCR was used to verify the lack of exon 2 in both genes. Primers are listed in Suppl. Table 1. P anx1 #1 flank floxed exon 2 and yields a 662 bp WT DNA and a 450 bp Panx1 KO fragment. For Panx3, two reactions were needed. Reaction 1 uses Panx3 #1 primers flanking exon 2 and yield a 1326 bp

WT DNA fragment and a 600 bp DNA fragment indicates at least one mutant allele. To distinguish between a Panx3 HT or full KO, a second reaction is conducted using Panx3 #2 primers where WT and Panx3 HT mice produce a 770 bp band, not seen in a Panx3 KO.

3.2.3. Ribonucleic acid extraction and quantitative polymerase chain reaction

Two-to-three-month-old cochleae, P4-P5 skin, and P4-P5 hindlimb tissues were dissected from mice and flash-frozen in liquid nitrogen. Ribonucleic acid (RNA) was extracted using a combination of Trizol and a Qiagen RNeasy mini kit as was previously described [24]. A NanoDrop spectrophotometer was used to measure the absorbance of RNA and was converted to cDNA using Superscript VILO or high-capacity cDNA reverse transcription kit (Thermo Fisher). Two-step quantitative PCRs (qPCRs) were performed using a SYBR green PCR master mix by Life Technologies. The PCR protocol for all primers were as follows: 50°C for 2 min, 95°C for 2 min, 95°C for 5 s, 60°C for 15 s (except 65°C for Panx3), followed by a melt curve. Primers used are listed in Table 3.1. Normalized mRNA expression levels were analyzed using the delta-delta CT method which was calculated using BioRad CFX Manager Software. A WT sample was set as the control for all calculations.

3.2.4. Protein extraction and immunoblotting

Skin and limbs of P4-5 WT and dKO mice were pulverized in liquid nitrogen and digested using a RIPA buffer (50mM Tris-HCL pH 8.0, 150mM NaCl, 1% NP-40 (Igepal), 0.5% sodium deoxycholate) which contained 1mM sodium fluoride, 1 mM sodium orthovanadate and complete-mini EDTA-free protease inhibitor (Roche, Mannheim, Germany). Protein was quantified using the bicinchoninic acid (BCA) assay (Thermo Fisher Scientific), separated on a 10% SDS-PAGE gel (50 μg) and transferred onto a nitrocellulose membrane using an iBlotTM system (Invitrogen, USA). Membranes were blocked with 3% bovine serum albumin (BSA) in 1X phosphate buffered saline (PBS) with 0.05% Tween20 overnight and then incubated with either anti-Panx1 CT-395 (1:2000), anti-Panx2 CT-523 (1:500), or anti-Panx3 CT-379 (1:1000) overnight at 4˚C [2]. Anti-mouse GAPDH (Millipore Sigma, 1:5000) was used as a protein loading control.

Table 3.1. List of primers

	Forward Primer (5'-3')	Reverse Primer (5'-3')
Cx26	CCGTCTTCATGTACGTCTTTTACAT	ATACCTAACGAACAAATAGCACAGC
Cx30	GGCCGAGTTGTGTTACCTGCT	TCTCTTTCAGGGCATGGTTGG
Cx43	ACAACAAGCAAGCCAGCGAG	TCGTCAGGGAAATCAAACGG
Panx1	ACAGGCTGCCTTTGTGGATTCA	GGGCAGGTACAGGAGTATG
Panx3	TTTCGCCCAGGAGTTCTCATC	CCTGCCTGACACTGAAGTTG
Panx2	TGGTACCCATCCTGCTGGT	GGGTGAAGTTGTGCGGAGT
IL-6	CAAGCCAGAGTCCTTCAGAG	GAGCATTGGAAATTGGGGTA
TNF- α	CTGTGAAGGGAATGGGTGTT	GGTCACTGTCCCAGCATCTT
Hif1- α	GCAGCAGGAATTGGAACATT	GCATGCTAAATCGGAGGGTA
GluPx1	GTCCACCGTGTATGCCTTCT	CCTCAGAGAGACGCGACATT
MnSOD	GGCCAAGGGAGATGTTACAA	CCTTGGACTCCCACAGACAT
Caspase3	TGTCATCTCGCTCTGGTACG	AAATGACCCCTTCATCACCA
Bcl2	CCTGTGGATGACTGAGTACC	GAGACAGCCAGGAGAAATCA
18SrRNA	GTA ACCCGTTGAACCCCATT	CCATCCAATCGGTAGTAGCG

For detection, IRDye® – 8000CW and -680RD (Life Technologies, USA) were used as secondary antibodies at 1:10000 dilutions and blots were imaged using a Li-Cor Odyssey infrared imaging system (Li-Cor, USA). Expression levels of Panx1 and Panx3 were quantified and normalized to GAPDH and presented relative to the WT mean value. Panx1 and Panx3 overexpressed Human embryonic kidney cells (HEK 293T- ATCC) were used as positive controls as previously described [17].

3.2.5. Body mass composition

Fat and lean mass composition of 10-11 week old male mice, were measured using quantitative magnetic resonance (echo-MRI) analysis with an echo magnetic resonance imaging mobile unit (Avian Facility of Advanced Research, University of Western Ontario, London, ON, Canada) as described by (Guglielmo et al. 2011), with the modification of placing live mice in the apparatus and measuring on the 'small animal' setting omitting water content. Measurements were taken in triplicate to verify the results.

3.2.6. Histology

Histology assays were performed on skin samples collected from WT and dKO male mice at P0, P4, 4 weeks, and 2 years of age for dorsal skin and, P0, P5, 4 weeks, 9 weeks and 22 weeks of age for paw skin. Parallel tissue sections (5 μm) were deparaffinized using two 5-minute xylene treatments, rehydrated by immersion in an ethanol gradient (100%, 95% then 70% for 5 minutes each) and stained with hematoxylin (Sigma) for 2.5 minutes, followed by water rinses and stained with eosin (Lerner Laboratories) for 5 minutes. Samples were subjected to three changes of 95% and then 100% ethanol for 3 minutes each, followed by two xylene treatments in 5-minute intervals. Stained samples were mounted using Permount Mounting Medium (Electron Microscopy Sciences) and imaged on a Leica DMIL LED brightfield, inverted microscope using 5X (P4, 4 weeks and 2 years) and 20X (P0) magnifications for dorsal skin and a 20X magnification for all paw samples. Epidermal and dermal areas (excluding the stratum corneum) and hypodermal areas were manually segmented for dorsal skin and measured using ImageJ. Measurements from dKO and WT samples across each age were compared for each tissue type using unpaired sample t-tests (GraphPad Prism 7).

3.2.7. Skull shape and size comparisons- Imaging

Micro computed tomography (μ-CT) images were obtained from a sample of 11 dKO and 11 WT mice at P0, and 6 dKO and 5 WT at three months. Skulls were fixed in 4% paraformaldehyde overnight and embedded in 1% agarose in 50 mL Falcon tubes. Scans of P0 mice were conducted with a GE Locus RS-9 scanner (GE Healthcare, Waukesha, WI, USA). Scan parameters saw 900 views acquired each 0.4 degrees over a 360-degree rotation of the gantry. Each projection lasted for 4500 ms and two projections were averaged at each view angle. Potential was measured as 80 kVp and current as 450 μA. Images were obtained at an isotropic voxel size of 20 μm and reconstructed as 3D volumes. Scans of adult mouse skulls were conducted using the eXplore speCZT μCT scanner (GE Healthcare, Waukesha, WI, USA). Scan parameters followed those used for P0 mouse imaging except that each projection lasted 16 ms and images were obtained at 50 μm isotropic voxel size and reconstructed at 100 μm. Calibration of each scan to Hounsfield Units was done using a sample of air, water and cortical bone-mimicking epoxy (SB3, Gamex, Middleton, WI, USA) with density 1100 mg cm-3 [23, 31].

3.2.8. Data collection: Landmarking

Surface reconstructions were generated from μ-CT volumes of each skull, and 3D landmark coordinate data was collected using Checkpoint (Stratovan Corporation, Davis, CA, USA). A set of 45 and 53 homologous skull landmarks as well as 19 homologous mandibular landmarks were collected from P0 and three month-old mice, respectively [32, 33]. Two landmark trials were conducted by the same observer and deviations between the two trials were restricted to 0.05 mm [34] and then averaged for further analyses.

3.2.9. Geometric morphometric analyses- skull shape and size

Geometric morphometric statistical analyses were used for quantification and comparison of subtle shape and size differences. Landmark data underwent Procrustes superimposition using the R package *geomorph* [35] (R Foundation for Statistical Computing, Vienna, Austria, 2017) and subsequent analyses were conducted on Procrustes coordinate data. Due to the multivariate nature of geometric morphometric shape analyses, separate Procrustes superimpositions were necessary for the whole skull, face, cranial base, cranial vault and mandible Differences in each sections' shape were compared with a non-parametric MANOVA using the ProcD function in

the R package *geomorph*, R Foundation for Statistical Computing, Vienna, Austria, 2017); [36]. This function includes resampling of 10,000 iterations to create a probability distribution from which significance can be determined (α=0.05).

3.2.10. Principle component analyses

Differences in skull shape were compared using principal components analysis (PCA) performed on the variance/covariance matrix of Procrustes coordinates using the *geomorph* package in R; R Foundation for Statistical Computing, Vienna, Austria, 2017). Scores for each individual for PC1 and PC2 are presented as a scatterplot. Qualitative differences in shape are visualized by the density of the clustering of points and the separation between genotypes across the principal components. Visualization of shape changes between dKO and WT mice along PC1 was accomplished by morphing the Procrustes superimposed landmark data of the average WT and average dKO mouse for PC1 mice onto the mouse with a PC1 score closest to zero.

Differences in overall skull size as well as size of the cranial base, cranial vault, face, and mandible were compared using centroid size. Centroid size is measured as the square root of the sum of the squared distances between each landmark coordinate and the centroid of the landmark configuration [8]. Centroid size was calculated as part of the Procrustes superimposition, using the *geomorph* package in R [35]; R Foundation for Statistical Computing, Vienna, Austria, 2017). Differences in size were compared using ANOVA and Tukey's post-hoc test.

3.2.11. Limb bone length comparisons

Limb bones of P0 dKO and WT mice were double stained with alizarin red /alcian blue as previously described [37]. Briefly, mouse pups were placed in PBS and skin, fat and muscles were dissected. Dissected mice were then fixed overnight in 95% ethanol. The next day, mice were placed in acetone and left overnight. The following day, mice were stained in a solution of 0.015% alcian blue (Sigma-Aldrich, Cat. No. A25268), 0.05% alizarin red (Sigma-Aldrich, Cat. No. A5533) and 5% acetic acid in 70% ethanol for five days. Post-staining, remaining soft tissues were dissolved by placing mice in a solution of 2% potassium hydroxide in PBS for one day and then transferred to a solution of 1% potassium hydroxide and PBS until most of

the soft tissues were removed. Double stained limb bones were examined using a Leica S6-D stereomicroscope and a Leica EC3 camera (Leica Microsystems, Wetzlar, Germany). The length of the ossified portion of each bone was measured using ImageJ and then compared between genotypes using a MANOVA. Differences in length for specific bones were determined using Welch's t-tests with Bonferroni correction. All analyses were performed in R (R Foundation for Statistical Computing, Vienna, Austria, 2017).

3.2.12. Growth plate comparisons of P0 WT and dKO tibiae

Tibiae were dissected from a sample of six WT and five dKO P0 mice, fixed in 4% paraformaldehyde, decalcified, embedded in paraffin and sectioned length-wise. Safranin-O/Fast Green staining was used to visualize the growth plate. Length of the proximal growth plate, as well as the length of the proliferative and hypertrophic zones were measured using ImageJ and compared between WT and dKO mice using Welch's t-tests in R.

3.2.13. Cross-sectional geometric properties of humerus and femur

Cross-sectional measures were obtained from 20 μm thick cross-sections of the right humerus and femur from μ-CT scan data. Statistical comparison of each geometrical property was performed using Welch's two-sample t-tests in R (R Foundation for Statistical Computing, Vienna, Austria, 2017) with Bonferroni corrections for multiple comparisons.

3.2.14. Hearing assessment using the auditory brainstem response (ABR)

Hearing levels were determined using the ABR technique, which was previously described [24]. Hearing levels were determined using the ABR technique, which measures the electrical activity in the brainstem evoked by the repeated presentation of a given acoustic stimulus to ultimately assess hearing sensitivity. Mice were deeply anaesthetized with ketamine (100 mg/kg) and xylazine (10 mg/kg) administered via intraperitoneal injections, and electrical activity was recorded through subdermal electrodes placed at the vertex (active electrode), mastoid of the stimulated ear (reference electrode) and on the mid-back (ground electrode). Mice were maintained at ~37°C on a digital homeothermic heating pad throughout the duration of the experiment. Five individual acoustic stimuli were used in our studies which allowed us to test auditory function at various regions along the sensory epithelium in the cochlea which code for different sound frequencies. These stimuli included a broadband click stimulus which

comprises the 1- 10 kHz frequency region of the cochlea, and four tonal specific stimuli of 4-,8-, 16-, and 24 kHz to assess both broadband as well as tonal specific frequencies. In this manner, the low to midfrequency ranges spanning the apical and middle turns of the cochlea would be tested. For ABR waveform analysis, BioSig software program was used to measure the amplitudes and latencies of 90 dB sound pressure level (SPL) click stimuli for each wave and each mouse group tested.

3.2.15. Noise exposure

For a separate cohort of mice at one month of age, an initial ABR was followed immediately by exposure to a loud 12 kHz tonal stimulus at 115 dB SPL to both ears for a one hour time period, as has been previously described [24]. During the procedure, mice were deeply anaesthetized with ketamine (100 mg/kg) and xylazine (10 mg/kg), while noise exposures were performed in a sound attenuated chamber. Immediately following noise exposure, mice were reassessed with a second ABR to confirm elevation of thresholds at high frequencies. Mice were then administered antipamezole (1 mg/kg) to reverse the effects of anaesthesia and allowed to recover in their home cages. 7 days after the noise exposure, a third and final ABR was performed to determine the extent of permanent hearing damage incurred by the loud noise exposure.

3.3. Results

3.3.1. Characterization of dKO mice

Genotyping of dKO mice showed loss of both *Panx1* and *Panx3* (Figure 3.1A). Although gross morphology of $Panx1^{-/-}Panx3^{-/-}$ mice (dKO) did not show any major differences, adult dKO mice were slightly smaller than WT as evidenced in representative pictures (Figure 3.1B). Weaned litter sizes of dKO mice were significantly smaller compared to both WT and $Panx1^{-/-}$ weanlings (Figure 3.1C). Additionally, overall body weight of dKO mice were significantly decreased at postnatal day 0 (P0), 2-3 months, and 16 months of age compared to aged-matched WT controls (Figure 1D-F).

Figure 3.1. Characterization of dKO mice

Representative genotyping gels for dKO and WT mice for Panx1 and Panx3 exon 2 deletions. R1: reaction 1 (primers Panx3F1 and reverse Panx3R1) primers flank exon 2 and yield a 1326 bp WT DNA fragment and a 600 bp DNA fragment which shows the presence of at least one mutant allele. To distinguish between Panx3 HT or full KO, a second reaction (RT) is conducted using Panx3F1 and reverse Panx3RT that yields a 770 bp in the WT but not in the KO. Lines denote lanes from the same gel shown after removal of extra lanes (A). Representative pictures of WT and $Panx1^{-/-}Panx3^{-/-}$ mice at three months of age (B). Litter sizes of WT, $Panx1^{-/-}$, $Panx3^{-/-}$ and dKO mice at time of weaning where N= 71, 49, 45, and 36, respectively. One-way ANOVA followed by posthoc Tukey's test (C). Body weights of postnatal day 0 (P0) (WT: N=6, dKO: N=8), 2-3 months-old (WT: N=16, dKO: N=16) and 16-month-old (WT: N=4 and dKO: N=8) WT and dKO mice (D-F). Unpaired students t-tests **p<0.01, ***p<0.001, ****p<0.0001. N= number of biological replicates.

Figure 3.1.

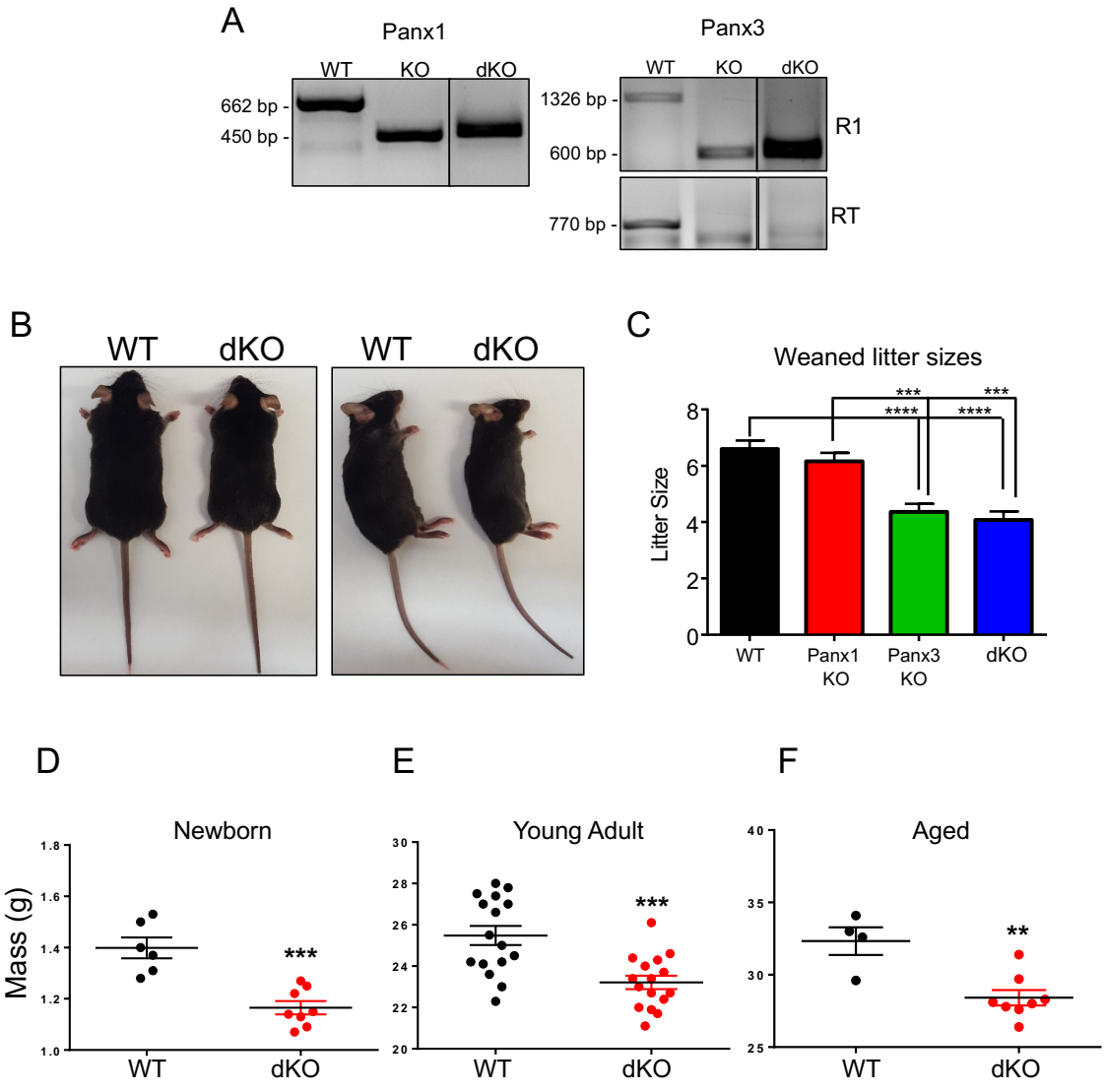
A
Panx1
WT
KO
dKO
662 bp -
450 bp -
Panx3
WT
KO
dKO
1326 bp -
600 bp -
R1
770 bp -
RT
B
WT
dKO
WT
dKO
C
Weaned litter sizes
***
****
***
****
Litter Size
8
6
4
2
0
WT
Panx1 KO
Panx3 KO
dKO
D
Newborn
Mass (g)
1.8
1.6
1.4
1.2
1.0
***
WT
dKO
E
Young Adult
30
28
26
24
22
20
***
WT
dKO
F
Aged
40
35
30
25
**
WT
dKO

However, qMRI tests revealed that the lean mass and fat mass normalized to body weight did not significantly change between WT and dKO mice at 2 months of age (Figure 3.S1).

3.3.2. Panx1 and Panx3 are ablated in skin, limb, and cochleae of dKO mice

Panx1 and Panx3 mRNA transcripts were present in skin, hindlimb, and cochleae of WT mice and absent in dKO (Figure 3.2A-C). At the protein level, low but detectable amounts of Panx1 and Panx3 were observed in skin tissues which was ablated in dKO mice (Figure 3.2A-C). In the hindlimb, Panx1 protein was undetectable in both WT and dKO, but high Panx3 protein expression was observed in WT mice (Figure 3.2A-C). Other immunoreactive bands are apparent at 50 and 70 kD, but are not ablated in the dKO, indicating that they are non-specific. We assessed the expression of Panx2 and other large pore channels in WT and dKO tissues. In skin, Panx2 full length was not detected, while Panx2 isoform X1 was observed at similar levels in WT and dKO mice (Figure 3.S2A). Cx26, Cx30, and Cx43 mRNA transcripts were also similarly detected in both WT and dKO mice (Figure 3.S2B). No differences in the expression of any of the tested Cxs or Panx2 channels were observed in WT and dKO hindlimbs or cochlear tissues (Figure 3.S3A,B).

3.3.3. Neonatal dKO mice exhibit decreased epidermal and dermal area in dorsal and paw skin

Analysis of dorsal skin showed a significant decrease in the epidermal and dermal area of dKO mice at P0 compared to WT (Figure 3.3). At P4, there was a significant increase in the hypodermal area of dKO compared to WT mice (Figure 3.3). However, no significant differences were seen at any other time point (Figure 3.3). dKO paw skin at P0 showed a significant decrease in epidermal area, however, no differences were found at any other age (Figure 3.4A-C).

3.3.4. Skull shape is significantly altered in neonatal but not adult dKO mice

Overall skull shape comparisons between dKO and WT mice at P0 was assessed using a MANOVA and found to be significant ($p=0.00165$). Significant shape changes between dKO and WT mice were detected for all regions of the skull: face ($p=0.00335$), base ($p=0.00035$), cranial vault ($p=0.00405$), and the mandible ($p=0.00045$) at P0.

Figure 3.2. Quantitative PCR confirms ablation of Panx1 and Panx3.

Skin (A), hindlimb (B), and cochleae (C), mRNA transcript levels for Panx1 and Panx3 were assessed using 18S rRNA or GAPDH to calculate normalized mRNA expression using the delta-delta CT method. No Panx mRNA was found in the dKO tissues. Panx1 and Panx3 western blots for P4 skin (A) and hindlimbs (B). Panx1 is glycosylated and runs in a multiple-banded pattern (Gly2, Gly1, Gly0) as shown in human embryonic kidney cells (HEK 293T) ectopically expressing Panx1 (bracket) and WT skin (not detectable in hindlimb). Panx3 protein (~43 kDa) shown in WT skin, bone and transfected HEK 293T cells (bracket). Unspecific bands are evident at ~50 and 70kDa (also in dKO). GAPDH was used as a loading control. Markers in kDa. Lines in blots indicate that positive control lanes (HEK Panx) are from the same blot but scanned at a lower intensity due to high ectopic expression. Bars: mean ± SEM. N=3 in skin and limbs and N=4 in cochleae.

Figure 3.2.

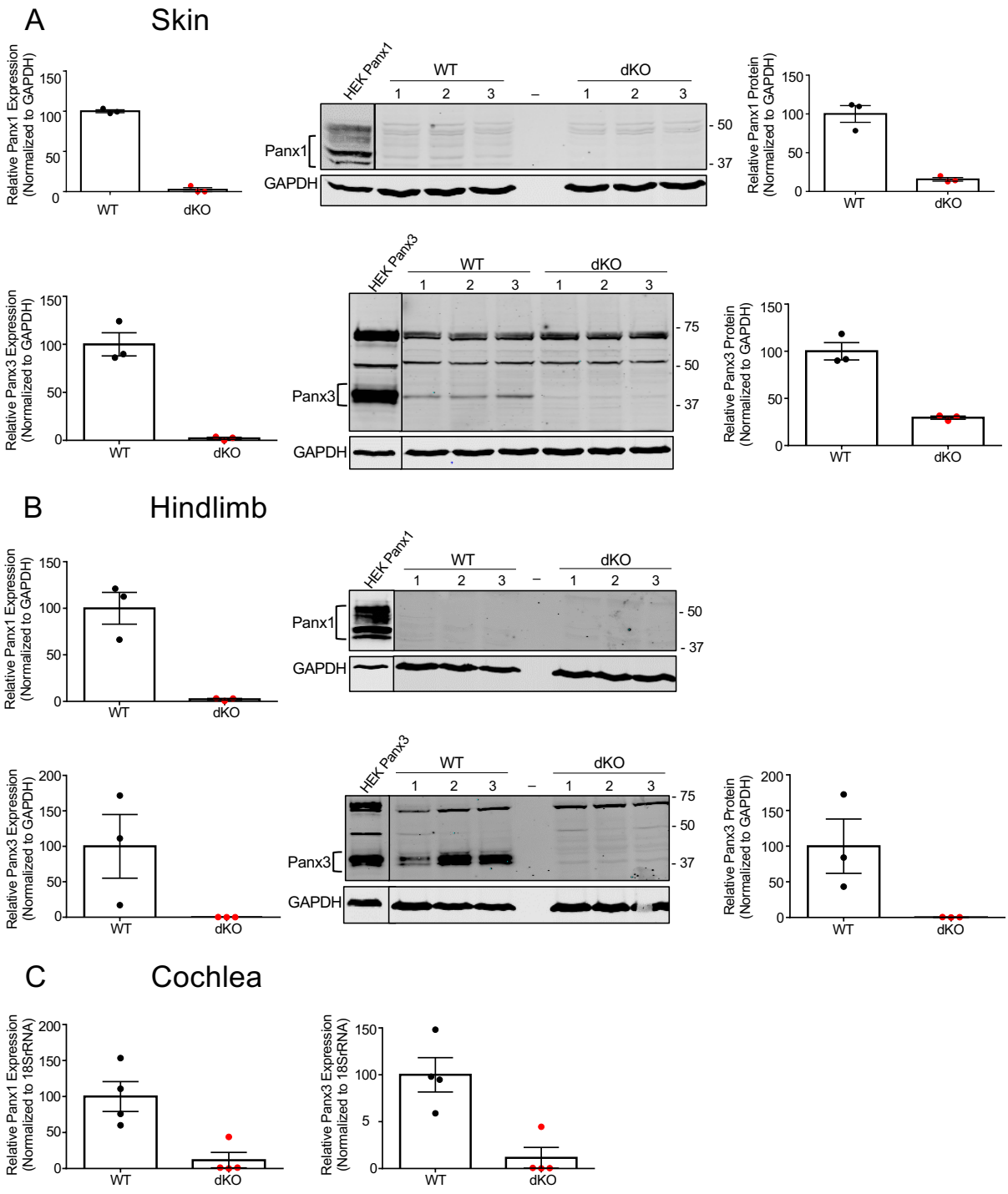
A
Skin
Relative Panx1 Expression (Normalized to GAPDH)
150
100
50
0
WT
dKO
HEK Panx1
WT
dKO
1 2 3 – 1 2 3
Panx1
GAPDH
50
37
Relative Panx1 Protein (Normalized to GAPDH)
Relative Panx3 Expression (Normalized to GAPDH)
HEK Panx3
75
Panx3
Relative Panx3 Protein (Normalized to GAPDH)
B
Hindlimb
200
C
Cochlea
Relative Panx1 Expression (Normalized to 18SrRNA)
Relative Panx3 Expression (Normalized to 18SrRNA)
5

Figure 3.3. dKO mice dorsal skin, epidermal and dermal area is decreased at P0 and hypodermal area is increased at P4 compared to WT mice.

Histological analysis of mouse dorsal skin at various ages showed the area of epidermal (excluding the highly variable stratum corneum) and dermal areas at P0, P4, 4 weeks, and 2 years of age in dKO and WT mice. N =3, n=9 for all time points and genotypes, except P0 (N=4, n=12). Error bars represent SEM. Scale bars represent 50μm at P0 and 100μm at P4, 4 weeks and 2 years. N= biological replicates, n= technical replicates. Independent student t-tests were performed. NS= no significance. ***$p < 0.001$, and ****$p < 0.0001$.

Figure 3.3.

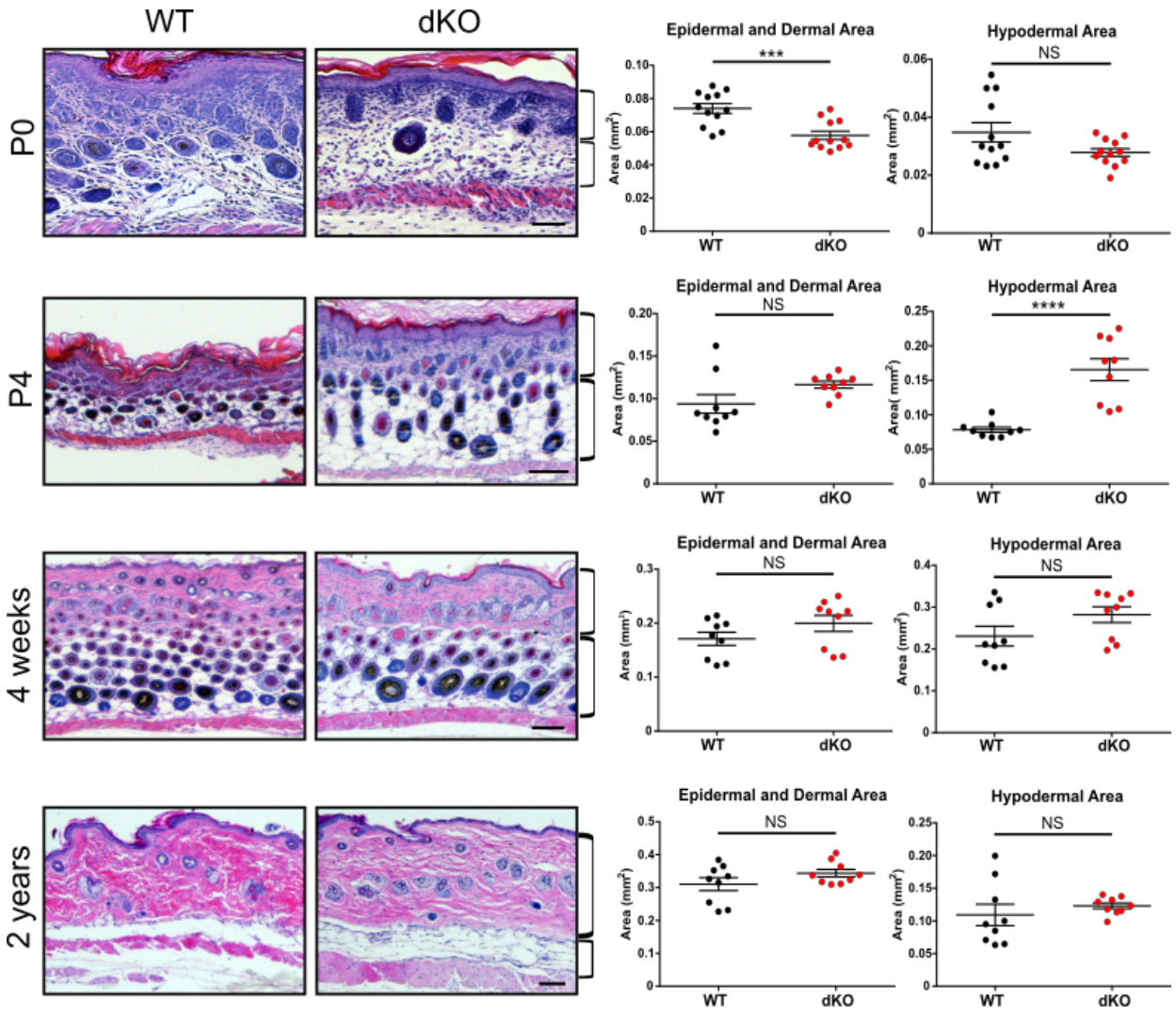
WT
dKO
P0
P4
4 weeks
2 years
Epidermal and Dermal Area
Hypodermal Area
***
NS
****
Area (mm²)
WT
dKO

Figure 3.4. Thick skin epidermal area is reduced in dKO paws of P0 mice.

Histological analysis and area of measurements in the epidermal area of mouse thick paw skin at P0, P5, 4, 9, and 22- weeks of age was quantified. N = 3, n=9, error bars represent SEM. Scale bars represent 25μm. Unpaired student t-tests were performed. NS= no significance, **p<0.01. N= biological replicates, n= technical replicates.

Figure 3.4.

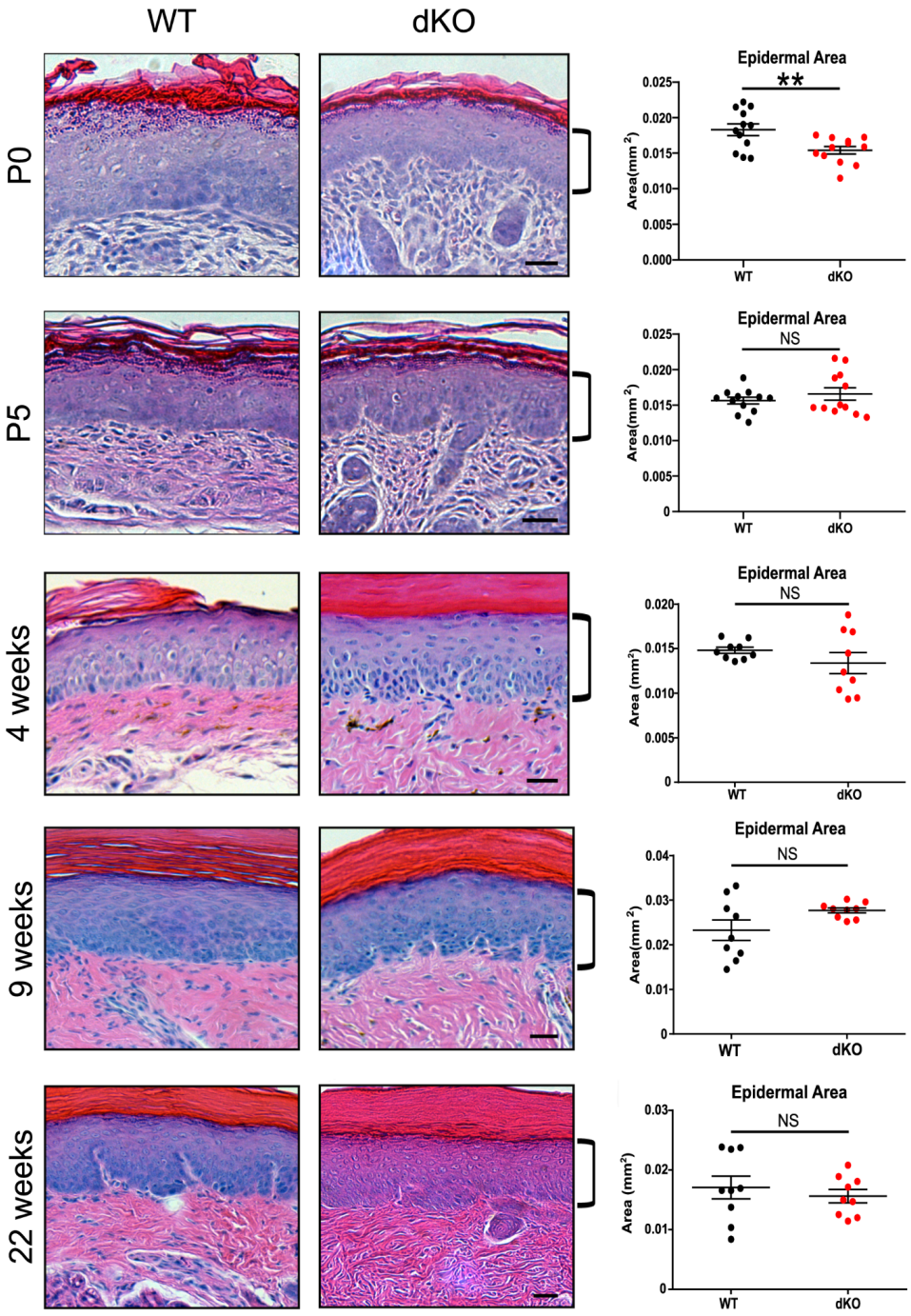
WT
dKO
P0
P5
4 weeks
9 weeks
22 weeks
Epidermal Area
**
NS
Area(mm 2)
Area (mm2)
WT
dKO

However, at three months, no statistically significant shape changes were observed. Skull shape differences were visualized using principal component analyses (PC). At P0 distinct separation was evident between WT and dKO mice across PC1 for the whole skull (Figure 3.5A) as well as for each region of the skull, particularly in the cranial base (Figure 3.5B). In contrast, in adult mice there was no separation between genotypes across PC1 and PC2 (Figure 3.5D,E). Heat morphs allow visualization of shape changes in P0 dKO across PC1 (Figure 3.5C,F).

3.3.5. dKO mice have significantly smaller mandibles, shorter hindlimbs, and altered femoral and humeral cross-sectional properties

Size of the whole skull, face, cranial base and cranial vault did not differ significantly between genotypes at P0 or in adult mice (Figure 3.5G). Mandible size was significantly smaller in dKO mice at P0 and at three months (Figure 3.5G). Lengths of the ossified portion of fore- and hind limb bones of P0 pups were measured and showed that P0 dKO mice have significantly shorter hind limb bones than WT (Figure 3.6A). Qualitative assessment revealed no differences in the general histomorphology of the tibial growth plate between WT and dKO P0 mice (Figure 3.6C). Measures of growth plate length were not statistically different between genotypes. Similarly, proportional lengths of the prehypertrophic and hypertrophic zones relative to total growth plate length were similar between genotypes (Figure 3.6D). At P0, polar second moment of area (J) ($p=0.0000034$) and cortical area (CA) ($p=0.0024$) of the humerus are larger in dKO than WT mice (Figure 3.6E). At three months, dKO mice have significantly larger %CA of the humerus than WT mice ($p=0.014$) and significantly larger femur Imax/Imin ($p=0.009$) (Figure 3.6E).

3.3.6. dKO mice have normal hearing

Representative ABR trace recordings of WT and dKO mice for a click stimulus showed that ABRs were similar in both genotypes (Figure 3.7A). No significant differences were observed between WT and dKO mice at any of the stimuli tested (Figure 3.7B). In addition to measuring hearing thresholds, analysis of ABR waveforms provided an indication of the integrity of neurotransmission throughout the auditory brainstem.

Figure 3.5. Skull shape is altered in dKO mice compared to WT mice at P0 but not in adult mice.

Principal components analyses (PCA) were used to visualize differences in shape between dKO and WT mice at P0 for the whole skull, face, cranial base, cranial vault and mandible. Small circles represent PC scores for PC1 and PC2 for each individual, large circles represent the average score for each genotype along PC1 and PC2. The two genotypes are clearly separated along PC1 for all regions of the skull at P0 (A, B). At three months (adult), no clear separation between genotypes was found for any of the regions analyzed (D, E). Specific shape changes associated with variation across PC1 are represented as heat morphs (C,F). Red colouration demonstrates regions of the skull that differ the most between the average dKO mouse and the group mean, whereas grey colouration represents differences between the average WT mouse and the group mean. At P0, the greatest shape differences in dKO mice are found in the cranial vault and cranial base (C), in agreement with our regional PC plots (B). At three months, the main differences in skull shape are concentrated on the inferior surface of the cranial base and face (F). Note that while these regions of the skull look markedly different due to the red colour, the actual difference (<0.5mm) is quite small for an adult mouse skull. Overall skull size, as well as face, cranial base, cranial vault and mandibular size were compared between dKO and WT mice at P0 and three months. For both age groups, WT mice have significantly larger mandibles than dKO mice (G), ** $p<0.01$.

Figure 3.5.

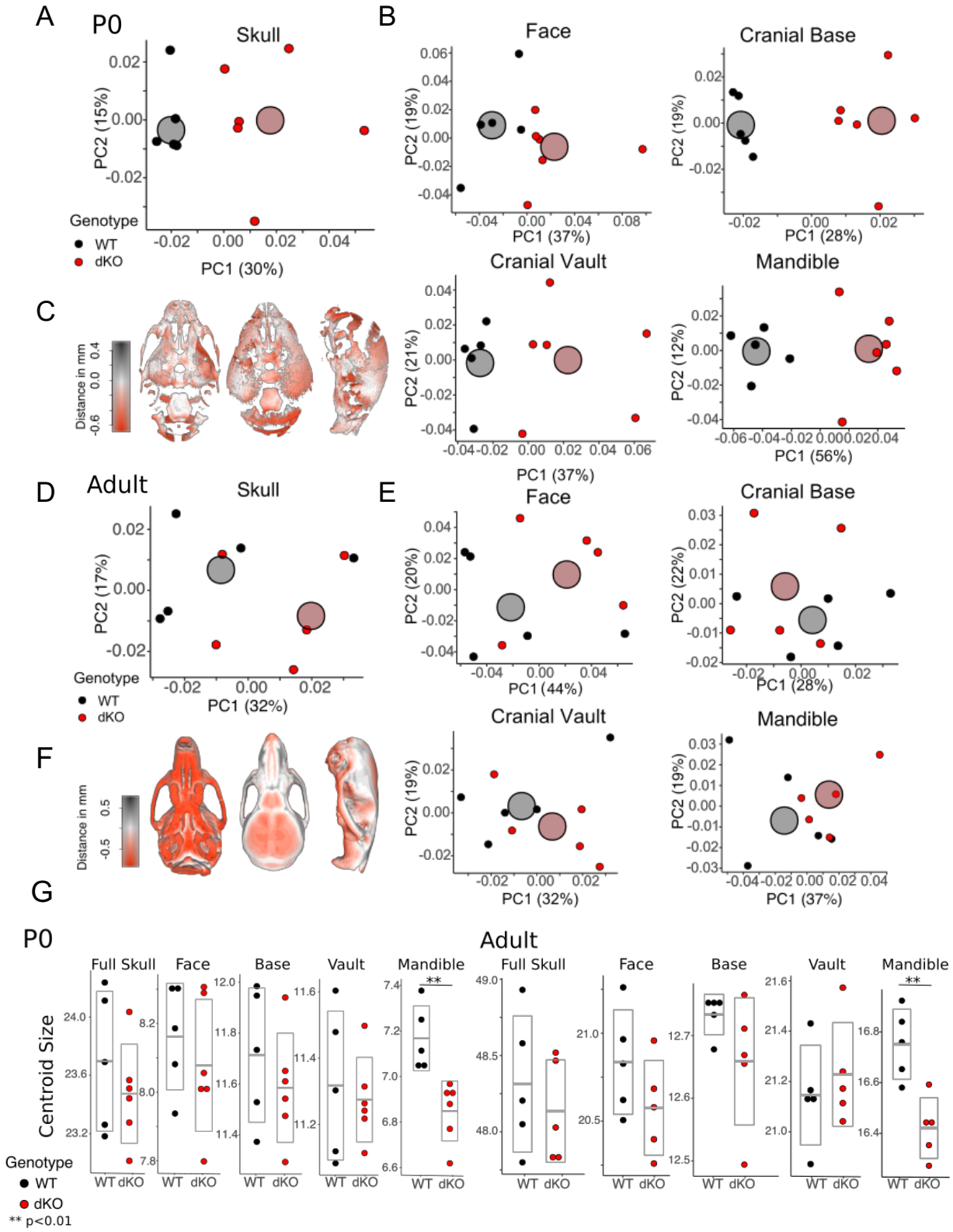
A
P0
Skull
PC2 (15%)
PC1 (30%)
Genotype
WT
dKO
B
Face
PC2 (19%)
PC1 (37%)
Cranial Base
PC2 (19%)
PC1 (28%)
C
Distance in mm
Cranial Vault
PC2 (21%)
PC1 (37%)
Mandible
PC2 (12%)
PC1 (56%)
D
Adult
Skull
PC2 (17%)
PC1 (32%)
E
Face
PC2 (20%)
PC1 (44%)
Cranial Base
PC2 (22%)
PC1 (28%)
F
Distance in mm
Cranial Vault
PC2 (19%)
PC1 (32%)
Mandible
PC2 (19%)
PC1 (37%)
G
P0
Adult
Full Skull
Face
Base
Vault
Mandible
Centroid Size
Genotype
WT
dKO
** p<0.01

Figure 3.6. dKO mice have significantly shorter hind limb bones than WT mice and altered femoral and humeral cross-sectional properties.

At P0, measures of femoral and tibial lengths are significantly shorter in dKO compared with WT mice (A). Geometric properties of the humerus and femur were calculated from diaphyseal cross-sections as shown (B). The general organization of the proximal tibial growth plate (GP), proliferative zone (PZ) and hypertrophic zone (HZ) is similar between genotypes at P0 (C) and no differences were found between dKO and WT mice for length measures of the total growth plate, or the prehypertrophic or hypertrophic zones as measured as percent of the total growth plate (D). Analysis of (B), showed that humeri of dKO mice have significantly larger cortical area (CA) and polar second moment of area (J) than WT mice at P0, while at three months percent cortical area (%CA) is significantly larger in dKO mice (E). No significant differences in femur cross-sectional measurements were detected at P0 between genotypes, but at three months dKO mice have significantly larger Imax/Imin values (E).* $p<0.05$, ** $p<0.001$, *** $p< 0001$.

Figure 3.6.

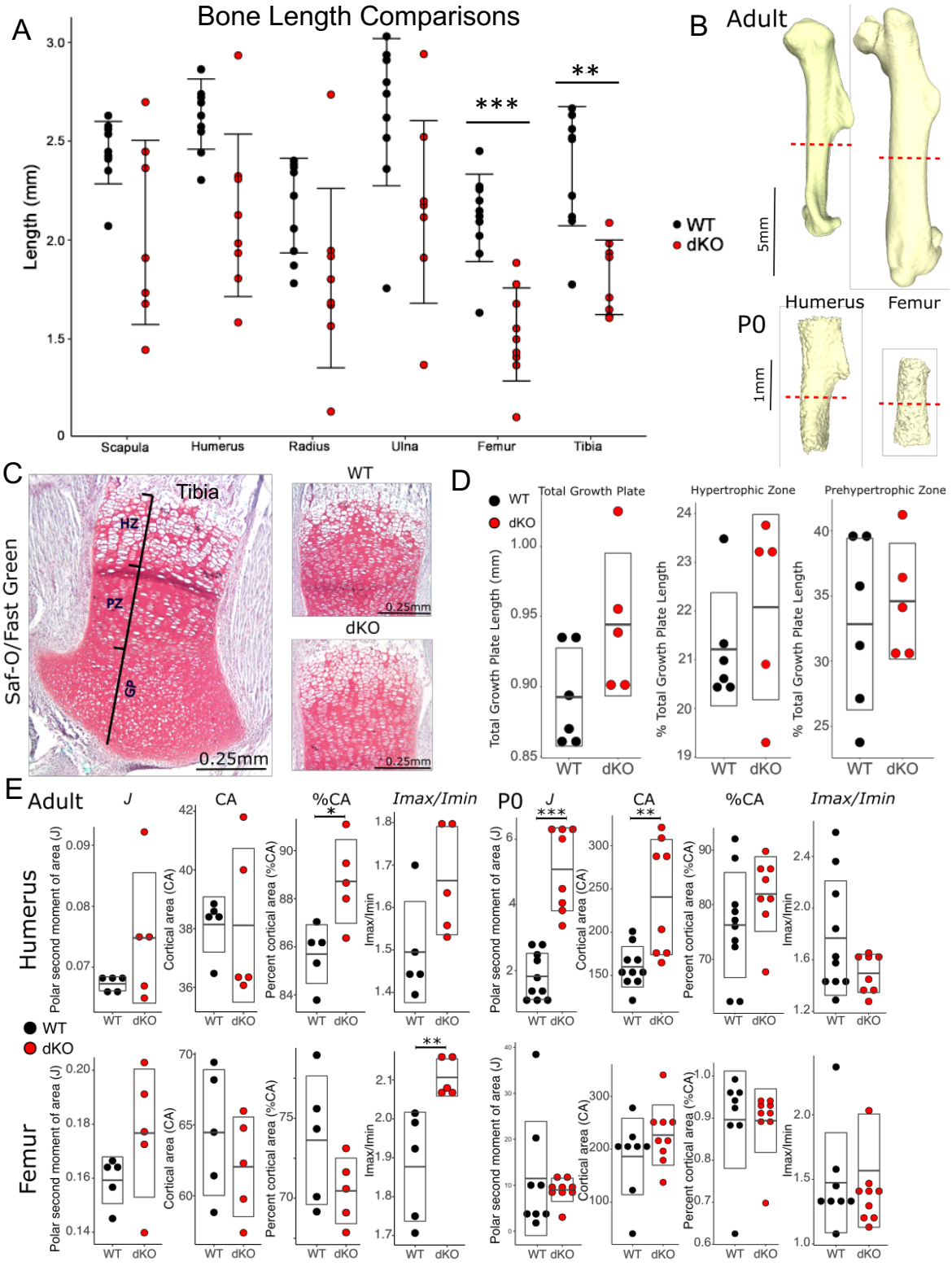
A
Bone Length Comparisons
Length (mm)
Scapula
Humerus
Radius
Ulna
Femur
Tibia
***
**
B
Adult
WT
dKO
5mm
Humerus
Femur
P0
1mm
C
Saf-O/Fast Green
Tibia
HZ
PZ
GP
0.25mm
WT
dKO
D
Total Growth Plate
Hypertrophic Zone
Prehypertrophic Zone
Total Growth Plate Length (mm)
% Total Growth Plate Length
E
Adult
P0
J
CA
%CA
Imax/Imin
Humerus
Femur
Polar second moment of area (J)
Cortical area (CA)
Percent cortical area (%CA)
Imax/Imin

dKO mice had significantly larger amplitudes in wave I (cochlear nerve), wave III (superior olivary complex), and wave IV (lateral lemniscus/inferior colliculus) of the ABR; findings which could result from a greater number of neurons along the auditory pathway being activated by the acoustic stimulus, and/or because the population of neurons in a given brainstem region discharged with more precise timing (Figure 3.7C). That said, no differences were detected in the latencies of ABR waveforms in dKO (Figure 3.7D), suggesting that the speed of neurotransmission was not affected by genotype. Collectively, these data suggest that dKO mice do not exhibit hearing deficits, and even have enhanced activation and/or neural synchrony in distinct auditory brainstem regions.

3.3.7. dKO mice have slightly decreased susceptibility to noise-induced hearing loss

As expected, ABR thresholds to all stimuli (click, 4-24 kHz tones) were elevated immediately after the noise exposure in both WT and dKO mice (Figure 3.8A-D), with the greatest degree of hearing impairment evident at the higher frequencies (Figure 3.8C-D). Interestingly, 7 days after the noise exposure, the 24 kHz hearing thresholds of dKO mice had recovered to a greater degree (i.e., lower ABR threshold values) than the WT mice; findings which show that the dKO mice were slightly less susceptible to permanent noise-induced hearing loss (Figure 3.8D).

Figure 3.7. Double knockout mice have normal hearing.

Representative auditory brainstem response (ABR) traces of a broadband click stimulus in both WT and dKO mice (A). Hearing assessment of 2-3-month-old mice through ABRs of WT and dKO mice for a broadband click stimulus and tonal specific frequencies (4, 8, 16, and 24 kHz tones) (B). ABR waveforms were further analyzed at the 90dB click stimulus by their amplitudes (C) and latencies (D), representing neural synchrony and speed, respectively. Bars represent mean ± SEM. *$p<0.05$, ****$p<0.0001$, One-way ANOVA followed by Sidak's post-hoc tests. Ns= no significance. WT: N=12, dKO: N=13. One outlier, as determined by GraphPad was removed from (B). N= number of biological replicates.

Figure 3.7.

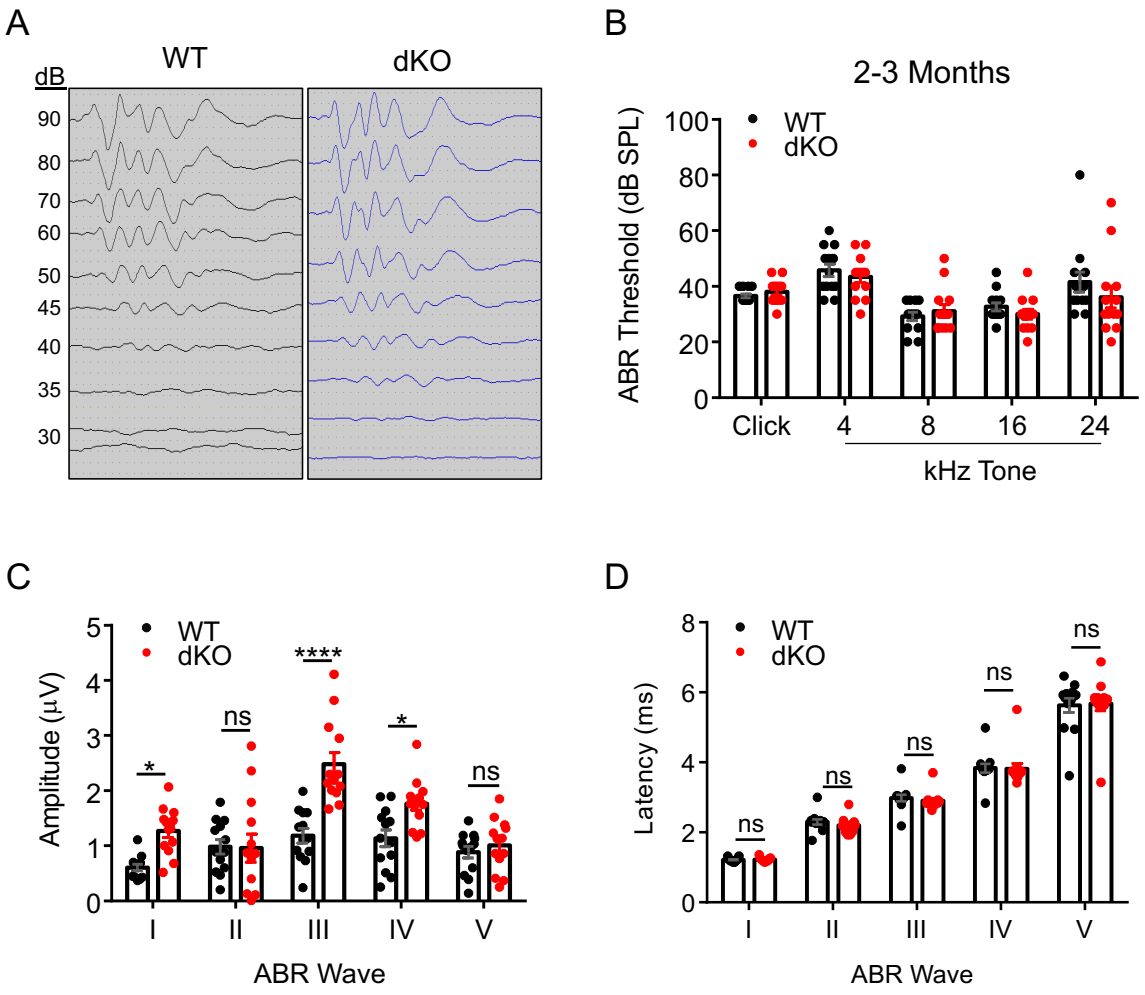
A
WT
dKO
dB
90
80
70
60
50
45
40
35
30
B
2-3 Months
WT
dKO
ABR Threshold (dB SPL)
100
80
60
40
20
0
Click
4
8
16
24
kHz Tone
C
WT
dKO
Amplitude (μV)
5
4
3
2
1
0
*
ns
****
*
ns
I
II
III
IV
V
ABR Wave
D
WT
dKO
Latency (ms)
8
6
4
2
0
ns
ns
ns
ns
ns
I
II
III
IV
V
ABR Wave

Figure 3.8. dKO mice exhibit slight protection against noise-induced hearing loss.

Noise exposure (NE) increased ABR thresholds immediately after NE (Post NE) for all stimuli tested, confirming auditory damage in both WT and dKO mice (A-D). The highest ABR thresholds were found at the higher frequency stimuli (C) 16 kHz and (D) 24 kHz tones. N=7 for each genotype. Bars represent mean ± SEM. Two-way repeated measures ANOVAs with Sidak's post-hoc tests were performed for each individual stimulus, ***$p<0.001$. N= number of biological replicates.

Figure 3.8.

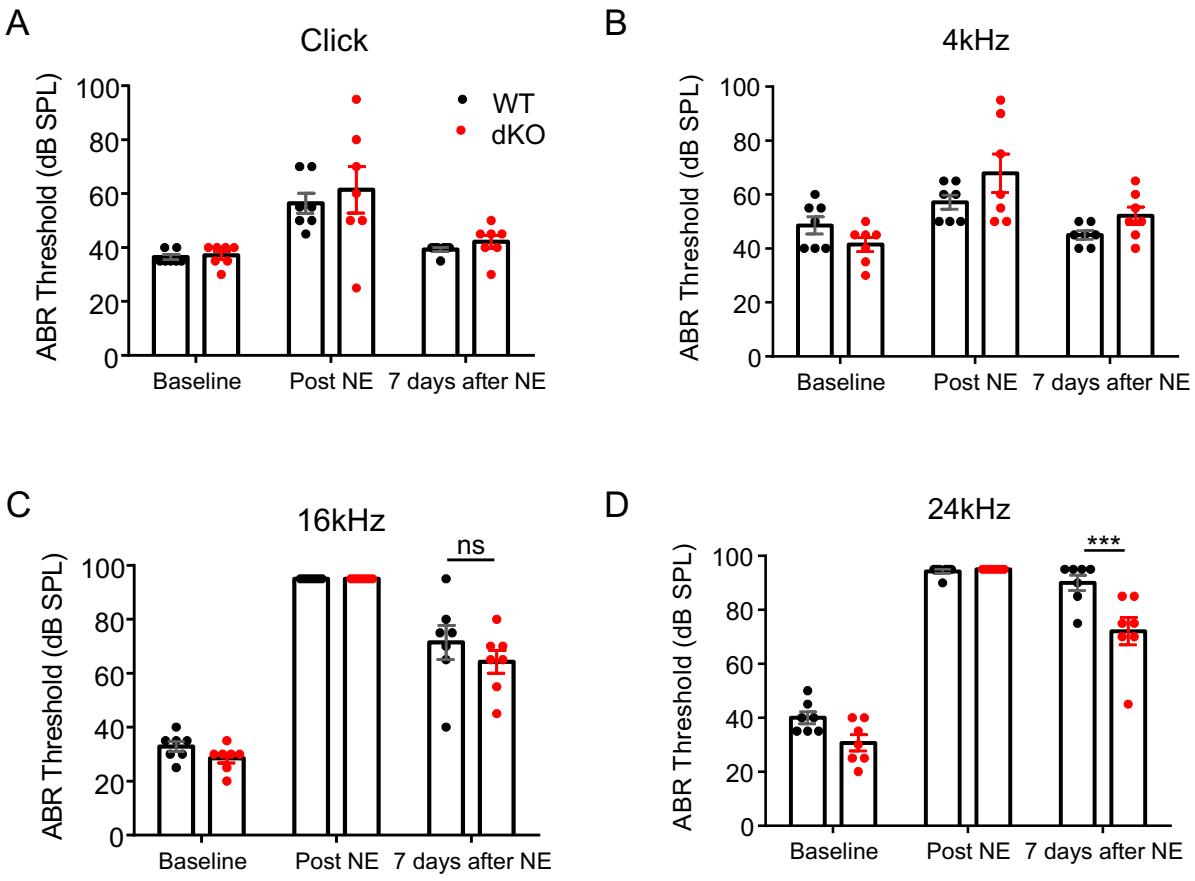
A
Click
ABR Threshold (dB SPL)
100
80
60
40
20
0
WT
dKO
Baseline
Post NE
7 days after NE
B
4kHz
ABR Threshold (dB SPL)
Baseline
Post NE
7 days after NE
C
16kHz
ns
ABR Threshold (dB SPL)
Baseline
Post NE
7 days after NE
D
24kHz
***
ABR Threshold (dB SPL)
Baseline
Post NE
7 days after NE

Figure S 3.1. qMRI of WT and dKO mice show no significant differences in normalized fat or lean mass.

Young adult (10-11 weeks) WT and dKO mice were fed normal chow ad libitum and analyzed using echo-MRI (qMRI) to determine raw lean mass (A) and raw fat mass (B). Overall lean mass (C) and overall fat mass (D) were normalized to body weight. N=4 for both WT and dKO mice. *$P < 0.05$. Bars represent mean ± SEM. N = number of biological replicates.

Figure S 3.1.

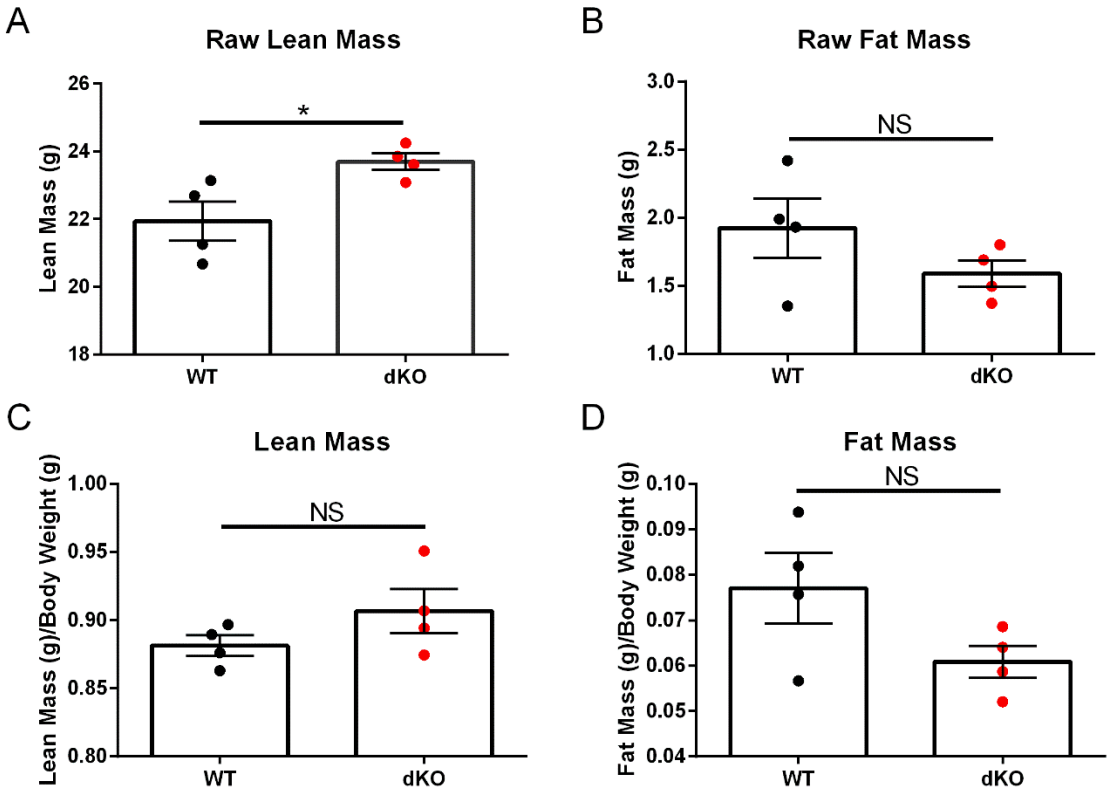
A
Raw Lean Mass
Lean Mass (g)
26
24
22
20
18
*
WT
dKO
B
Raw Fat Mass
Fat Mass (g)
3.0
2.5
2.0
1.5
1.0
NS
WT
dKO
C
Lean Mass
Lean Mass (g)/Body Weight (g)
1.00
0.95
0.90
0.85
0.80
NS
WT
dKO
D
Fat Mass
Fat Mass (g)/Body Weight (g)
0.10
0.09
0.08
0.07
0.06
0.05
0.04
NS
WT
dKO

Figure S 3.2. In dorsal skin, dKO mice show no differences in Panx2, Cx26, Cx30, or Cx43 expression compared to WT mice.

Panx2 full length and Panx2 isoform 202 (ENSMUST00000161372.1) qPCR and Western blot for P4-P5 skin. Panx2 transfected HEK cells were used as a positive control and represent full length Panx2. GAPDH was used as a positive control. Protein markers in kDa. (B) mRNA expression for Cx26, Cx30 and Cx43 in P5 skin. 18SrRNA or GAPDH was used to calculate normalized mRNA expression using the delta delta CT method. Bars represent mean ± SEM. N=4 for both WT and dKO in skin western blot, N=3 for both WT and dKO skin in Panx2 full length transcript in qPCR, and N=7 for both WT and dKO skin in Panx2 202 isoform, Cx26, Cx30 and Cx43 qPCR. N = number of biological replicates.

Figure S 3.2.

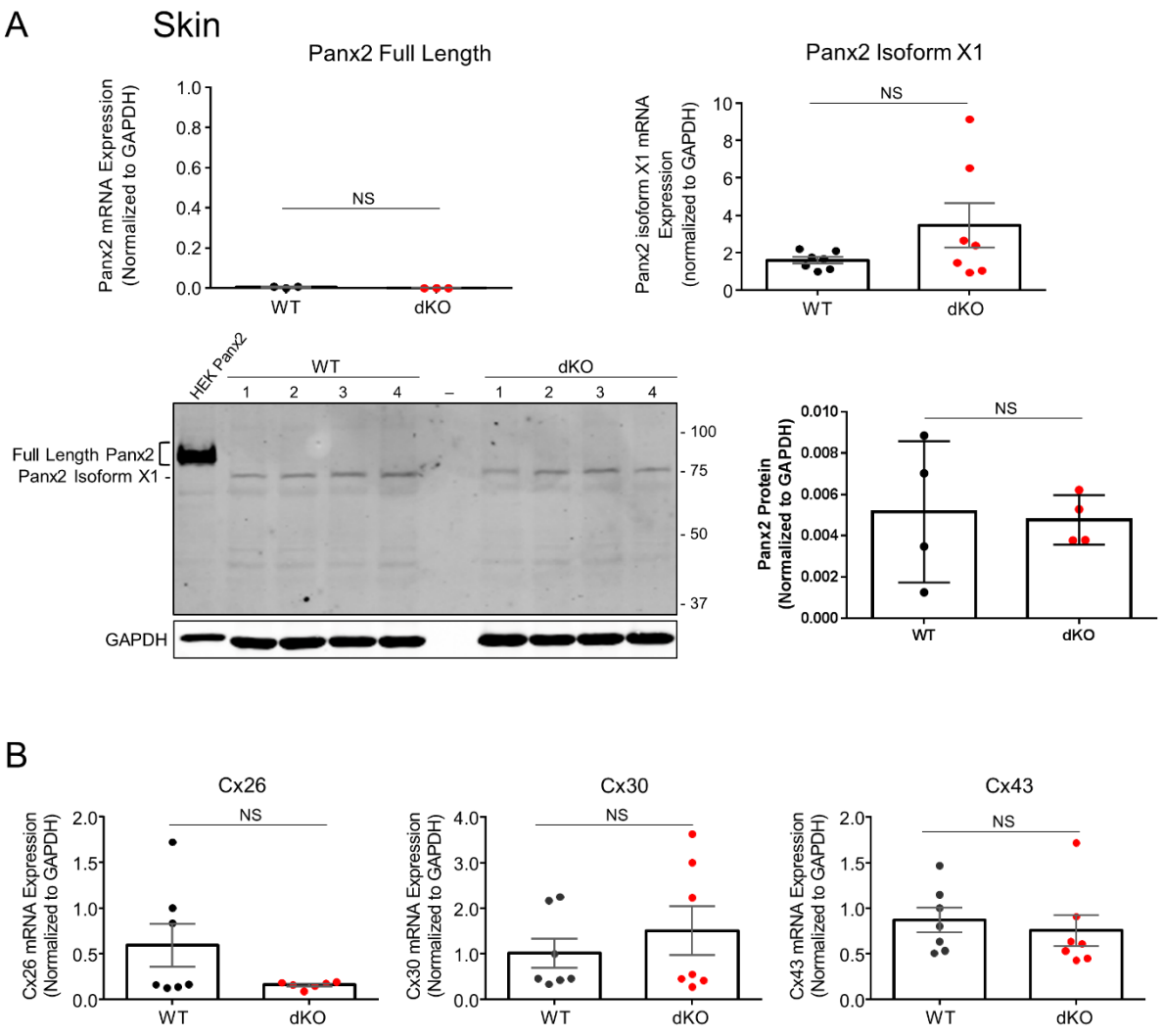
A
Skin
Panx2 Full Length
Panx2 mRNA Expression (Normalized to GAPDH)
1.0
0.8
0.6
0.4
0.2
0.0
NS
WT
dKO
Panx2 Isoform X1
Panx2 isoform X1 mRNA Expression (normalized to GAPDH)
10
8
6
4
2
0
NS
WT
dKO
HEK Panx2
WT
dKO
1 2 3 4 – 1 2 3 4
Full Length Panx2
Panx2 Isoform X1
GAPDH
100
75
50
37
Panx2 Protein (Normalized to GAPDH)
0.010
0.008
0.006
0.004
0.002
0.000
NS
WT
dKO
B
Cx26
Cx26 mRNA Expression (Normalized to GAPDH)
2.0
1.5
1.0
0.5
0.0
NS
WT
dKO
Cx30
Cx30 mRNA Expression (Normalized to GAPDH)
4.0
3.0
2.0
1.0
0.0
NS
WT
dKO
Cx43
Cx43 mRNA Expression (Normalized to GAPDH)
2.0
1.5
1.0
0.5
0.0
NS
WT
dKO

Figure S 3.3. In both hindlimb and cochlea there are no differences in Panx2, Cx26, Cx30, or Cx43 between WT and dKO mice.

(A) Panx2 Western blot and Panx2, Cx26, Cx30 and Cx43 mRNA expression via qPCR for P4-P5 hindlimb. Panx2 transfected HEK cells were used as a positive control and represent full length Panx2. GAPDH was used as the loading control. Protein measured in kDa. (B) mRNA expression for Cx26, Cx30 and Cx43 in P4-P5 cochleae. GAPDH was used to calculate normalized mRNA expression using the delta delta CT method. Protein markers in kDa. Bars represent mean ± SEM. N=3 for both WT and dKO in limbs and N=7 for both WT and dKO in cochleae. N = number of biological replicates.

Figure S 3.3.

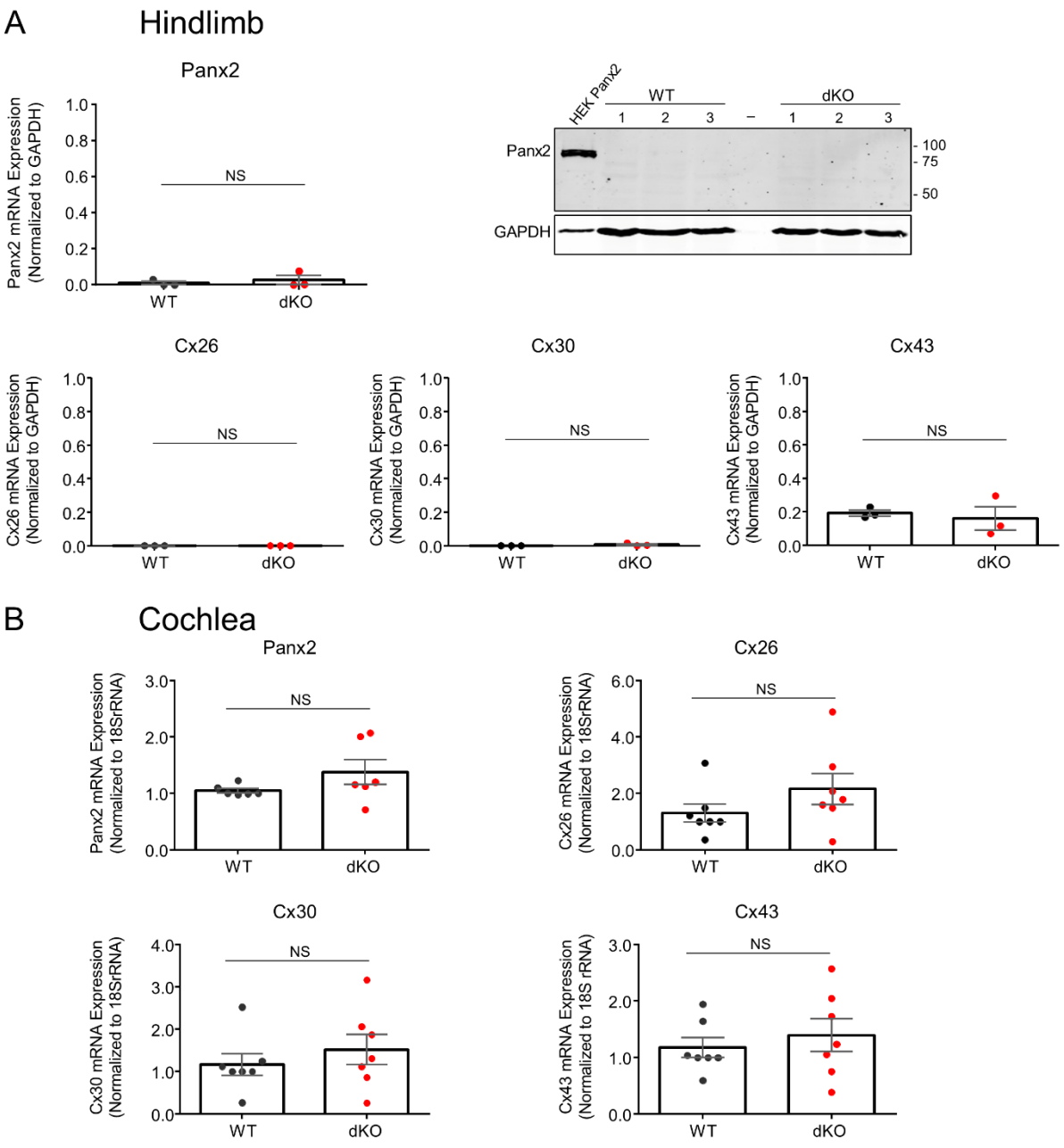
A
Hindlimb
Panx2
Panx2 mRNA Expression (Normalized to GAPDH)
NS
WT
dKO
HEK Panx2
WT
dKO
1 2 3 – 1 2 3
Panx2
GAPDH
100
75
50
Cx26
Cx26 mRNA Expression (Normalized to GAPDH)
Cx30
Cx30 mRNA Expression (Normalized to GAPDH)
Cx43
Cx43 mRNA Expression (Normalized to GAPDH)
B
Cochlea
Panx2
Panx2 mRNA Expression (Normalized to 18SrRNA)
Cx26
Cx26 mRNA Expression (Normalized to 18SrRNA)
Cx30
Cx30 mRNA Expression (Normalized to 18SrRNA)
Cx43
Cx43 mRNA Expression (Normalized to 18S rRNA)

3.4. Discussion

Single pannexin knockout mice have been used to assess the impacts of Panx channels in various organs [3]. However, recent findings suggest potential compensatory mechanisms between Panx family members, reinforcing that dKO mice are necessary to examine their true functions within different organ systems. We created the first Panx1 and Panx3 double knock-out mouse model (dKO) which was not trivial, since both *Panx1* and *Panx3* genes are closely located in chromosome 9 within 22 Mb of each other in the mouse genome (NCBI), thus making the recombination efficiency of this event very low.

dKO mice showed decreased body weight, and this change was not previously observed in either of the two single KO models of Panx1 and Panx3 [22, 30]. However, qMRI of adult dKO mice did not show any differences in fat mass or lean mass, when normalized to body weight. In addition, dKO mice had significantly decreased litter sizes (fewer pups per litter) compared to controls; a finding that was also shown for $Panx3^{-/-}$ mice [22] and that may be due to higher intra-uterine death but remains to be studied.

At P0, dKO mice had reduced dorsal skin thickness which was similarly found in our previous study for $Panx1^{-/-}$ mice [17]. At P4, however, this finding was no longer evident and instead dKO mice exhibited increased hypodermal area where subcutaneous fat is found. The $Panx1^{-/-}$ mice also had a significant increase in hypodermal area and an increase in overall fat content due to the enhanced differentiation capacity of adipose stromal cells from the $Panx1^{-/-}$ to form adipocytes with higher fat content [38].

While an overt skeletal phenotype has not been associated with Panx1 KO mice, Panx3 KO mice have been reported to have shortened long bones, and hypo- mineralization of the skull and long bones [23, 39, 40]. Thus, the relatively mild skeletal phenotype observed in our dKO mice is unexpected, but similar to our previous report on the bone morphology of the global Panx3 KO mouse [23]. While we found significant skull shape differences between dKO and WT mice at P0, by three months dKO mouse skull morphology appeared to “recover”. This could be due to a combination of the minor phenotypic effects observed at P0 coupled with the rapid growth and remodeling of the mouse skull within the first two months of post-natal development [23]. The main skull shape changes we observed in dKO mice at P0 were

localized to the cranial base and cranial vault. Early postnatal growth of these regions is quite rapid, plateauing by P14-P21 in mice [41].

Tibial and femoral lengths were shorter in dKO than WT mice at P0. However, no differences in tibial growth plates were observed at P0 between genotypes suggesting that subsequent tibial growth would be similar to WT, potentially enabling recovery of the phenotype through post-natal development. For the humerus, cortical area (CA) and polar second moment of area (J) are significantly larger in dKO mice than WT at P0, suggesting that dKO humeri have an increased resistance to compressive and torsional forces respectively. By three months, CA and J of the humerus are similar between genotypes but the proportion of cortical area to total subperiosteal area (%CA) is significantly greater in dKO mice, indicating thicker cortical bone. At three months, dKO mice have significantly larger Imax/Imin ratios for the femur which indicates that the distribution of cortical bone within the cross-section is altered. Previously, we reported that humeri and femora of adult Panx3 KO mice have increased J and CA compared to WT mice [23]. While we expected similar results in our dKO model, it appears that knocking out both genes results in a phenotype separate from the single Panx3 KO.

Previous studies showed that a conditional ablation of Panx1 in the cochlea resulted in severe hearing loss [25]. Additionally, a human patient harbouring a Panx1 mutation was found to exhibit many clinical symptoms including hearing loss [42]. In contrast, another $Panx1^{-/-}$ mouse had normal hearing and did not exhibit any auditory brainstem morphology deformities [24]. Recently, that same $Panx1^{-/-}$ model was found to have mild hearing loss at low frequencies which was more pronounced at higher frequencies (i.e. 32 and 40 kHz) [43]. Zorzi and colleagues re-examined the auditory phenotype of the first-generated $Panx1^{-/-}$ mice, and found that they did not have hearing loss [44]. To rule out the possibility that in the global Panx1 KO, Panx3 could be compensating for its function, we tested the dKO hearing and found that both pannexins are dispensable for hearing function. In fact, dKO mice had increased ABR wave amplitudes representing enhancement of the neural synchrony within these auditory brainstem regions.

The double deletion of Panx1/Panx3 did not show more overt phenotypes than the single KO models and in some cases, reduced the severity of the phenotypes observed. As with Panx1 and Panx3 single KOs, we might see more pronounced phenotypes once they are challenged

with different insults. In the dKO, there was no upregulation of Panx2 and connexins known to be expressed in some of these tissues [11, 45-47], plus in hindlimb we could not detect any expression of Panx2, Cx26 or Cx30. However, it is possible that these and other large pore channels can still functionally compensate for the missing Panxs deleted from germline throughout development. Therefore, in some instances, the use of conditional KOs may be necessary to avoid this potential issue with compensation that could mask some phenotypes.

3.5. Conclusions

In conclusion, we have shown that dKO mice have alterations in skin and bone at early stages but do not exhibit hearing loss, and show better recovery upon noise damage. Our findings suggest that Panx1 and Panx3 may be important in early development of musculoskeletal tissues but are not required for hearing.

3.6. Acknowledgements

We thank Genentech Inc. (San Francisco, CA) for the gift of the Panx1 knockout mouse. JMA was funded by a Natural Sciences and Engineering Research Council (NSERC) Scholarship. BO and CBW were funded by an Ontario Graduate Scholarship (OGS). EJ and CBW received the Collaborative Specialization in Musculoskeletal Health Research (CMHR) award. NSERC Discovery Grant to KW. CIHR Project grant to BLA. NSERC Discovery Grant to SP.

3.7. References

1. Panchin Y, Kelmanson I, Matz M, Lukyanov K, Usman N, Lukyanov S (2000) A ubiquitous family of putative gap junction molecules. Curr Biol **10**, R473-474.

2. Baranova A, Ivanov D, Petrash N, Pestova A, Skoblov M, Kelmanson I, Shagin D, Nazarenko S, Geraymovych E, Litvin O, et al. (2004) The mammalian pannexin family is homologous to the invertebrate innexin gap junction proteins. Genomics **83**, 706-716.

3. Penuela S, Gehi R, Laird DW (2013) The biochemistry and function of pannexin channels. Biochim Biophys Acta 1828: 15-22.

4. Sosinsky GE, Boassa D, Dermietzel R, Duffy HS, Laird DW, MacVicar B, Naus CC, Penuela S, Scemes E, Spray DC, et al. (2011) Pannexin channels are not gap junction hemichannels. Channels (Austin) 5: 193-197.

5. Scemes E, Spray DC, Meda P (2009) Connexins, pannexins, innexins: novel roles of "hemi-channels". Pflugers Arch 457: 1207-1226.

6. Bruzzone R, Hormuzdi SG, Barbe MT, Herb A, Monyer H (2003) Pannexins, a family of gap junction proteins expressed in brain. Proc Natl Acad Sci U S A 100: 13644-13649.

7. Penuela S, Bhalla R, Nag K, Laird DW (2009) Glycosylation regulates pannexin intermixing and cellular localization. Mol Biol Cell 20: 4313-4323.

8. Ray A, Zoidl G, Weickert S, Wahle P, Dermietzel R (2005) Site-specific and developmental expression of pannexin1 in the mouse nervous system. Eur J Neurosci 21: 3277-3290.

9. Wang XH, Streeter M, Liu YP, Zhao HB (2009) Identification and characterization of pannexin expression in the mammalian cochlea. J Comp Neurol 512: 336-346.

10. Tang W, Ahmad S, Shestopalov VI, Lin X (2008) Pannexins are new molecular candidates for assembling gap junctions in the cochlea. Neuroreport 19: 1253-1257.

11. Le Vasseur M, Lelowski J, Bechberger JF, Sin WC, Naus CC (2014) Pannexin 2 protein expression is not restricted to the CNS. Front Cell Neurosci 8: 392.

12. Turmel P, Dufresne J, Hermo L, Smith CE, Penuela S, Laird DW, Cyr DG (2011) Characterization of pannexin1 and pannexin3 and their regulation by androgens in the male reproductive tract of the adult rat. Mol Reprod Dev 78: 124-138.

13. Bao L, Locovei S, Dahl G (2004) Pannexin membrane channels are mechanosensitive conduits for ATP. FEBS Lett 572: 65-68.

14. Locovei S, Wang J, Dahl G (2006) Activation of pannexin 1 channels by ATP through P2Y receptors and by cytoplasmic calcium. FEBS Lett 580: 239-244.

15. Chekeni FB, Elliott MR, Sandilos JK, Walk SF, Kinchen JM, Lazarowski ER, Armstrong AJ, Penuela S, Laird DW, Salvesen GS, et al. (2010) Pannexin 1 channels mediate 'find-me' signal release and membrane permeability during apoptosis. Nature 467: 863-867.

16. Penuela S, Bhalla R, Gong XQ, Cowan KN, Celetti SJ, Cowan BJ, Bai D, Shao Q, Laird DW (2007) Pannexin 1 and pannexin 3 are glycoproteins that exhibit many distinct characteristics from the connexin family of gap junction proteins. J Cell Sci 120: 3772-3783.

17. Penuela S, Kelly JJ, Churko JM, Barr KJ, Berger AC, Laird DW (2014) Panx1 regulates cellular properties of keratinocytes and dermal fibroblasts in skin development and wound healing. J Invest Dermatol 134: 2026-2035.

18. Celetti SJ, Cowan KN, Penuela S, Shao Q, Churko J, Laird DW (2010) Implications of pannexin 1 and pannexin 3 for keratinocyte differentiation. J Cell Sci 123: 1363-1372.

19. Bond SR, Lau A, Penuela S, Sampaio AV, Underhill TM, Laird DW, Naus CC (2011) Pannexin 3 is a novel target for Runx2, expressed by osteoblasts and mature growth plate chondrocytes. J Bone Miner Res 26: 2911-2922.

20. Ishikawa M, Yamada Y (2017) The Role of Pannexin 3 in Bone Biology. J Dent Res 96: 372-379.

21. Ishikawa M, Iwamoto T, Nakamura T, Doyle A, Fukumoto S, Yamada Y (2011) Pannexin 3 functions as an ER Ca(2+) channel, hemichannel, and gap junction to promote osteoblast differentiation. J Cell Biol 193: 1257-1274.

22. Moon PM, Penuela S, Barr K, Khan S, Pin CL, Welch I, Attur M, Abramson SB, Laird DW, Beier F (2015) Deletion of Panx3 Prevents the Development of Surgically Induced Osteoarthritis. J Mol Med (Berl) 93: 845-856.

23. Caskenette D, Penuela S, Lee V, Barr K, Beier F, Laird DW, Willmore KE (2016) Global deletion of Panx3 produces multiple phenotypic effects in mouse humeri and femora. J Anat 228: 746-756.

24. Abitbol JM, Kelly JJ, Barr K, Schormans AL, Laird DW, Allman BL (2016) Differential effects of pannexins on noise-induced hearing loss. Biochem J 473: 4665-4680.

25. Chen J, Zhu Y, Liang C, Zhao HB (2015) Pannexin1 channels dominate ATP release in the cochlea ensuring endocochlear potential and auditory receptor potential generation and hearing. Sci Rep 5: 10762.

26. Zhao HB, Zhu Y, Liang C, Chen J (2015) Pannexin 1 deficiency can induce hearing loss. Biochem Biophys Res Commun 463: 143-147.

27. Bargiotas P, Krenz A, Hormuzdi SG, Ridder DA, Herb A, Barakat W, Penuela S, von Engelhardt J, Monyer H, Schwaninger M (2011) Pannexins in ischemia-induced neurodegeneration. Proc Natl Acad Sci U S A 108: 20772-20777.

28. Lohman AW, Billaud M, Straub AC, Johnstone SR, Best AK, Lee M, Barr K, Penuela S, Laird DW, Isakson BE (2012) Expression of pannexin isoforms in the systemic murine arterial network. J Vasc Res 49: 405-416.

29. Whyte-Fagundes P, Kurtenbach S, Zoidl C, Shestopalov VI, Carlen PL, Zoidl G (2018) A Potential Compensatory Role of Panx3 in the VNO of a Panx1 Knock Out Mouse Model. Front Mol Neurosci 11: 135.

30. Qu Y, Misaghi S, Newton K, Gilmour LL, Louie S, Cupp JE, Dubyak GR, Hackos D, Dixit VM (2011) Pannexin-1 is required for ATP release during apoptosis but not for inflammasome activation. J Immunol 186: 6553-6561.

31. Beaucage KL, Xiao A, Pollmann SI, Grol MW, Beach RJ, Holdsworth DW, Sims SM, Darling MR, Dixon SJ (2014) Loss of P2X7 nucleotide receptor function leads to abnormal fat distribution in mice. Purinergic Signal 10: 291-304.

32. Hill CA, Sussan TE, Reeves RH, Richtsmeier JT (2009) Complex contributions of Ets2 to craniofacial and thymus phenotypes of trisomic "Down syndrome" mice. Am J Med Genet A 149A: 2158-2165.

33. Motch Perrine SM, Cole TM, 3rd, Martinez-Abadias N, Aldridge K, Jabs EW, Richtsmeier JT (2014) Craniofacial divergence by distinct prenatal growth patterns in Fgfr2 mutant mice. BMC Dev Biol 14: 8.

34. Martinez-Abadias N, Holmes G, Pankratz T, Wang Y, Zhou X, Jabs EW, Richtsmeier JT (2013) From shape to cells: mouse models reveal mechanisms altering palate development in Apert syndrome. Dis Model Mech 6: 768-779.

35. Adams DC, Otarola-Castillo E (2013) geomorph: an r package for the collection and analysis of geometric morphometric shape data. Methods Ecol Evol 4: 393-399.

36. Collyer ML, Sekora DJ, Adams DC (2015) A method for analysis of phenotypic change for phenotypes described by high-dimensional data. Heredity (Edinb) 115: 357-365.

37. McLeod MJ (1980) Differential staining of cartilage and bone in whole mouse fetuses by alcian blue and alizarin red S. Teratology 22: 299-301.

38. Lee VR, Barr KJ, Kelly JJ, Johnston D, Brown CFC, Robb KP, Sayedyahossein S, Huang K, Gros R, Flynn LE, et al. (2018) Pannexin 1 regulates adipose stromal cell differentiation and fat accumulation. Sci Rep 8: 16166.

39. Oh SK, Shin JO, Baek JI, Lee J, Bae JW, Ankamerddy H, Kim MJ, Huh TL, Ryoo ZY, Kim UK, et al. (2015) Pannexin 3 is required for normal progression of skeletal development in vertebrates. FASEB J 29: 4473-4484.

40. Ishikawa M, Williams GL, Ikeuchi T, Sakai K, Fukumoto S, Yamada Y (2016) Pannexin 3 and connexin 43 modulate skeletal development through their distinct functions and expression patterns. J Cell Sci 129: 1018-1030. DOI 10.1242/jcs.176883 jcs.176883 [pii]

41. Vora SR, Camci ED, Cox TC (2015) Postnatal Ontogeny of the Cranial Base and Craniofacial Skeleton in Male C57BL/6J Mice: A Reference Standard for Quantitative Analysis. Front Physiol 6: 417.

42. Shao Q, Lindstrom K, Shi R, Kelly J, Schroeder A, Juusola J, Levine KL, Esseltine JL, Penuela S, Jackson MF, et al. (2016) A Germline Variant in the PANX1 Gene Has Reduced Channel Function and Is Associated with Multisystem Dysfunction. J Biol Chem 291: 12432-12443.

43. Chen J, Liang C, Zong L, Zhu Y, Zhao HB (2018) Knockout of Pannexin-1 Induces Hearing Loss. Int J Mol Sci 19.

44. Zorzi V, Paciello F, Ziraldo G, Peres C, Mazzarda F, Nardin C, Pasquini M, Chiani F, Raspa M, Scavizzi F, et al. (2017) Mouse Panx1 Is Dispensable for Hearing Acquisition and Auditory Function. Front Mol Neurosci 10: 379.

45. Forge A, Becker D, Casalotti S, Edwards J, Marziano N, Nevill G (2003) Gap junctions in the inner ear: comparison of distribution patterns in different vertebrates and assessement of connexin composition in mammals. J Comp Neurol 467: 207-231.

46. Plotkin LI, Bellido T (2013) Beyond gap junctions: Connexin43 and bone cell signaling. Bone 52: 157-166.

47. Xu J, Nicholson BJ (2013) The role of connexins in ear and skin physiology - functional insights from disease-associated mutations. Biochim Biophys Acta 1828: 167-178.

Chapter 4：Mice harbouring an oculodentodigital dysplasia-linked Cx43 G60S mutation have severe hearing loss

The purpose of this study was to characterize the localization profile and functional role of Cx43 within the mammalian cochlea in two different mouse models harbouring Cx43 mutations. This study also aimed to examine the relationship between the functional status of Cx43 and auditory function.

A version of this paper is published:

Abitbol JM, Kelly JJ, Barr KJ, Allman BL, Laird DW. Mice harbouring an oculodentodigital dysplasia-linked Cx43 G60S mutation have severe hearing loss. *J. Cell Science.* 131(9):214635, 2018.

4.1. Introduction

Connexin (Cx), gap junction proteins form channels that allow for direct intercellular communication via the passage of small molecules and ions between contacting cells [1-3]. Although less understood *in vivo*, connexins may occasionally act as hemichannels at the cell surface to allow for transient exchange of small molecules between the cell cytosol and the extracellular environment [4]. Gap junctional intercellular communication (GJIC) is essential for the maintenance of key cellular processes such as apoptosis, proliferation, and differentiation in many tissues in the body including the inner ear [5, 6]. Gap junctions are critical in hearing as they form two specific networks in the cochlea; the epithelial and connective tissue gap junction networks [7, 8]. These networks allow passage of small molecules and ions throughout the syncytium and are thought to play roles in potassium buffering and metabolite transport [9, 10]. Gap junction channels are also thought to maintain ionic homeostasis through recycling of small molecules and secondary messengers within the cochlear duct [11-13]. In addition, connexin hemichannels may play a role in hair cell maturation and development, through release of calcium and ATP which are both required in early stages of hair cell development [14-17].

The auditory system is broadly divided into two sub-categories; the peripheral auditory system which is made up of the outer (ear canal and eardrum), middle (middle ear bones) and inner (cochlea) ear, and the central auditory system which consists of the neurons that ultimately connect the mechanosensory hair cells in the cochlea to the brain. The auditory system is known to express multiple connexin family members including; Cx26, Cx30, Cx31, Cx29, Cx32 and Cx43, which are all expressed in various locations along the auditory tract [8, 10]. Importantly, the two types of mechanosensory hair cells, which either amplify sound coming into the cochlea (“outer” hair cells) or transform sound waves into electrical signals (“inner” hair cells) within an area of the cochlea called the organ of Corti, are devoid of any known connexins [6, 18]. Cx26 and Cx30, which are the most abundant connexins in the inner ear, form the two gap junction networks in the cochlea and have thus been the most studied connexins within the auditory system. Mutations in the genes encoding Cx26 are prevalent in patients with inherited hearing loss. Over 100 different gain or loss-of-function *GJB2* (Cx26) gene mutations have been identified. In addition, mice harbouring both ablations and/or mutations in *GJB2* (Cx26) and *GJB6* (Cx30) have hearing deficits as well as altered cochlear

morphology in some cases [19-24]. Thus, due to the prevalence of *GJB2* and *GJB6* mutations in hearing loss, there is a strong need to identify molecules that can regulate connexin expression or function as a possible means to compensate for genetic deficiencies caused by connexin gene mutations.

Cx43 is the most ubiquitously expressed connexin family member in the body and has been documented in various regions of the auditory tract including the stria vascularis, supporting cells [25], spiral ligament [26], and Schwann and satellite cells of the spiral ganglion neurons [27-29], all of which reside within the inner ear. In addition, Cx43 has been found in the cochlear bone that encapsulates the cochlea [30] as well as in resident cells of the auditory brainstem and midbrain relays (eighth cranial nerve, cochlear nucleus, olivary complex, lateral lemniscus, and the inferior colliculus) that are responsible for propagation of electrical signals throughout the brain [31, 32]. Although studies have identified Cx43 in these different regions along the auditory tract, its functional role and link to hearing remains unclear. Few studies have examined the prevalence of Cx43 mutations in patients harbouring hearing loss, with variable findings. In a group of Taiwanese patients with hearing loss, *GJA1* (Cx43) gene mutations were found to be the second most common after *GJB2* (Cx26) mutations [33]. However, other studies have found no evidence of Cx43 mutations in Turkish and African patients with hearing loss [34-36]. Interestingly, two recessive gene mutations in *GJA1* (Cx43) leading to L11F and V24A amino acid substitutions in the cytoplasmically-exposed N terminal domain and the first transmembrane domain of Cx43, respectively, have been discovered in human patients and linked to non-syndromic hearing loss [37].

In addition to genetic forms of hearing loss, environmental factors such as exposure to loud sound can lead to hearing impairments. Both Cx26 and Cx30, connexin family members that are critical for hearing, are thought to play a role in the active transport of sodium and potassium within the cochlea to maintain its proper function and homeostasis [7]. Recently, a study found that both Cx26 and Cx30 protein levels were significantly decreased after noise exposure [38]. Since then, another study has shown that when Cx26 was conditionally knocked down at postnatal day 18, these mice exhibited more pronounced noise-induced hearing loss than their wildtype counterparts [39]. At present, it is unknown if patients harbouring *GJA1* (Cx43) mutations are more susceptible to auditory damage after a loud noise exposure.

The limitations of examining the functional roles of Cx43 in the auditory system have been hindered by the fact that global Cx43 knock-out mice are lethal at birth [40]. To overcome this limitation, it is now possible to use genetically-modified mice to model human-linked Cx43 diseases that typically manifest as the developmental abnormality known as oculodentodigital dysplasia (ODDD) [41-43]. ODDD is a human-linked disease that is inherited in mostly an autosomal dominant manner, where patients typically exhibit craniofacial abnormalities, fusion of soft tissue digits, small eyes, enamel defects, and in some rare cases neurological defects and/or hearing loss [41]. Previously, to assess the role of Cx43 in a wide variety of tissues and organs such as the skin, heart, mammary glands, bone, and brain, $Cx43^{I130T/+}$ and $Cx43^{G60S/+}$ mice have been used, which reduce Cx43 function to ~50% and ~20% of controls, respectively [44-48]. Given the differential levels of Cx43 function in these mutant mice, they become excellent surrogates to assess the role of Cx43 in hearing as we postulated that hearing loss might be found in both mutant mice or only mice that have little remaining Cx43 function (i.e. the $Cx43^{G60S/+}$ mice).

The aim of this study was to use mouse models of ODDD to investigate the impact of Cx43 in auditory function through various physiological assessments. First, to examine if fully functional Cx43 is crucial for proper development of the auditory tract. Secondly, to examine if the level of functional Cx43-based GJIC impacts auditory function and finally, to determine if the auditory system of Cx43 mutant mice is more susceptible to insult upon exposure to loud noise. We discovered that although $Cx43^{I130T/+}$ mutant mice had normal hearing which persisted in mature adult mice and after a loud noise auditory insult, $Cx43^{G60S/+}$ mutant mice had severe hearing loss suggesting that hearing impairment is a result of severe loss of Cx43 function.

4.2. Materials and methods

4.2.1. Animals

Heterozygous mice harbouring the Cx43 I130T mutation (generously obtained from Glenn Fishman) were created as previously described [44] and were bred on a C57BL/6 background and backcrossed in house for over 6 generations. Both male $Cx43^{I130T/+}$ mutant and WT littermate controls were used for our studies. Mutant mice were phenotyped by evident syndactyly of the digits, and all mice were genotyped. In addition, heterozygote mice carrying

the Cx43 G60S mutation (generously obtained from Janet Rossant) were created as previously described [46]. These mice were on a mixed C3H/HeJ and C57BL/6 background, and $Cx43^{G60S/+}$ mutant mice used in these studies were compared to their WT littermate controls. All mice tested were male and 2-3 months of age unless otherwise stated. Mice were housed in the animal care facilities at the University of Western Ontario, and maintained on a 12/12-hour light/dark cycle and fed ad libitum. All experiments were approved by the Animal Care Committee at the University of Western Ontario.

4.2.2. Ribonucleic acid extraction and reverse-transcription polymerase chain reaction

Following euthanasia by CO_2, cochleae were dissected from mice and flash-frozen in liquid nitrogen. Ribonucleic acid (RNA) was extracted from tissues using a combination of Trizol and a Qiagen RNeasy mini kit as was previously described [49]. A NanoDrop spectrophotometer was used to measure the absorbance of RNA and a one-step reverse transcription-polymerase chain reaction (RT-PCR) was performed using an RT-PCR Qiagen kit. The PCR profile was as follows: 50°C for 30min, 95°C for 15min, 94°C for 30s, 64°C for 30s, and 72°C for 1 min for 30 cycles. Primers used were as follows: Cx43 specific primers (forward: 5' -ACAACAAGCAAGCCAGCGAG-3' and reverse: 5' -TCGTCAGGGAAATCAAACGG-3'), Cx26 specific primers (forward: 5' -CCGTCTTCATGTACGTCTTTTACAT-3' and reverse: 5' -ATACCTAACGAACAAATAGCACAGC-3') and Cx30 specific primers (forward: 5' -GGCCGAGTTGTGTTACCTGCT-3' and reverse: 5' -TCTCTTTCAGGGCATGGTTGG-3'). 18S ribosomal ribonucleic acid (rRNA) was used as a housekeeping gene (forward: 5' -GTA ACCCGTTGAACCCCATT-3' and reverse: 5' -CCATCCAATCGGTAGTAGCG-3'). The amplified products were run on a 2% agarose gel with ethidium bromide for visualization.

4.2.3. Quantitative RT-PCR

Following euthanasia by CO_2, cochleae were dissected from mice and flash-frozen in liquid nitrogen. RNA was extracted and converted to cDNA as previously described [49]. Two-step quantitative PCRs (qPCRs) were performed using a SYBR green PCR master mix by Life Technologies in order to quantify Cx43, Cx26, and Cx30 expression. The PCR protocol for all primers were as follows: 50°C for 2 min, 95°C for 2 min, 95°C for 5s, 60°C for 15s, followed by a melt curve. The same primers as mentioned above were used for qPCR and transcripts

were normalized to 18S rRNA. Normalized mRNA expression levels were analyzed using the delta delta CT method which was calculated using BioRad Software. A WT sample was set as the control for all calculations.

4.2.4. Immunoblotting

Following euthanasia by CO_2, a litter of mice (approximately 6-10 cochleae) were dissected and pooled together (due to small tissue sizes) for one lysate sample and stored at -80°C. Cochleae were crushed with a mortar and pestle with liquid nitrogen as previously described [49]. Tissues were solubilized in RIPA buffer (50mM Tris-HCL, 150mM NaCl, 1% TritonX-100, 13mM deoxycholic acid, 0.1% SDS) and 30 μg of lysate were run on 10% polyacrylamide gels using SDS-PAGE and transferred to nitrocellulose membranes using an iBlot transfer apparatus (Invitrogen). Membranes were blocked with 3% bovine serum albumin (BSA) in PBS-Tween (1X phosphate buffered saline, 0.05% Tween 20) for 1 hr. Blots were probed overnight with anti-rabbit Cx43 (1:750, Sigma, catalog#C6219) and anti-mouse GAPDH (1:10000 dilution, Chemicon, catalog#MAB374) antibodies. Blots were then washed and stained with mouse AlexaFluor 680 secondary antibody (1:5000 dilution, Life Technologies) for Cx43 and rabbit IRdye800 (1:5000, Rockland) for GAPDH for 2 hours. Membranes were visualized with an Odyssey infrared imaging system (LiCor). Quantitative analysis was performed using Odyssey software to assess the amount of Cx43 total protein expression in 2-3-month-old mice. GAPDH was used as a loading control and a reference protein for quantitative analysis.

4.2.5. Immunofluorescent labelling

Following dissections of cochleae, a small incision was made in the cochlear bone near the apical turn and 4% paraformaldehyde (PFA) was perfused through both the round and oval windows of the cochlea. Cochleae were fixed in 4% PFA overnight at 4°C, then subsequently washed with PBS. Cochleae were then decalcified in 4% EDTA for 3 days and upon full decalcification were immersed in 30% sucrose overnight for cryopreservation of the tissue. Each pair of cochleae was embedded in an agarose solution, flash frozen, and allowed to acclimate in the cryostat at -25°C. Sections were cut at 18 μm thickness and stored at -20°C until use. Slides were blocked and permeabilized for 1 hr in 3% BSA+ 0.02% Triton-X 100 solution. Subsequently, slides were incubated with primary antibodies in 4°C overnight. These

antibodies included; anti-rabbit Cx43 (1:750, Sigma, catalog#C6219), anti-mouse CNPase (1:200, Millipore, catalog#MAB326), anti-mouse GFAP (1:200, Sigma, catalog#63893), anti-rabbit myosin VI (1:200, Proteus Biosciences, catalog#25-6791), anti-mouse CtBP2 (1:200, BD Transduction laboratories, catalog#612044), anti-mouse myelin basic protein (1:200, Abcam, catalog#62631), and anti-rabbit beta III tubulin (1:400, Abcam, catalog#18207). Slides were then washed and incubated with a fluorescent conjugated secondary antibody as well as phalloidin (1:400, Invitrogen, catalog#A12379) for 1 hr following a nuclear Hoechst stain. Slides were then mounted and confocal immunofluorescent images were acquired using an LSM800 Zeiss confocal microscope.

4.2.6. Hearing assessment with the auditory brainstem response (ABR)

Hearing levels were determined using the ABR technique, which measures the electrical activity in the brainstem evoked by the repeated presentation of a given acoustic stimulus to ultimately assess hearing sensitivity. Five individual acoustic stimuli were used in our studies which allowed us to test auditory function at various regions along the cochlea which code for different sound frequencies. These stimuli included a broadband click stimulus which comprises the 1-10 kHz frequency region of the cochlea, and four tonal specific stimuli of 4-, 8-, 16-, and 24 kHz in order to assess both broadband as well as tonal specific frequencies. In this manner, the low to mid-frequency ranges spanning the apical and middle turns of the cochlea would be tested. A detailed description of the experimental procedures for ABR recordings was previously described [49]. Briefly, mice were deeply anaesthetized with ketamine (100 mg/kg) and xylazine (10 mg/kg) administered via intraperitoneal injections, and electrical activity was recorded through subdermal electrodes placed at the vertex (active electrode), mastoid of the stimulated ear (reference electrode) and on the mid-back (ground electrode). Mice were maintained at ~37°C on a digital homeothermic heating pad throughout the duration of the experiment. For ABR waveform analysis, BioSig software program was used to measure the amplitudes and latencies of 90 dB sound pressure level (SPL) click stimuli for each wave and each mouse group tested.

4.2.7. Noise Exposures

For a separate cohort of mice at one month of age, an initial ABR was followed immediately by a loud 12 kHz tonal stimulus at 115 dB SPL bilaterally for exposure in both ears for a one

hour time period as has been previously described [49]. During the procedure, mice were deeply anaesthetized with ketamine (100 mg/kg) and xylazine (10 mg/kg), while noise exposures were performed in a sound attenuated chamber. Immediately following noise exposure, mice were reassessed with a second ABR to confirm elevation of thresholds at high frequencies following noise exposure. Mice were then administered antipamezole (1 mg/kg) to reverse the effects of anaesthesia and allowed to recover in their home cages. One week after the noise exposure, a third and final ABR was performed to determine the extent of permanent hearing damage incurred by the loud noise exposure.

4.2.8. Organotypic cochlear cultures

Organotypic cochlear explant cultures were prepared from the cochleae of postnatal day 1 to 3 pups and grown in MatTek dishes with glass coverslip as has been described [50]. Mouse pups were sacrificed by cervical dislocation and were surface sterilized by immersion in 80% ethanol for 10 mins. The heads were removed and placed in Leibovitz L-15 medium (Invitrogen) where they were bisected midsagitally. The cochlear capsule was removed followed by the stria vascularis leaving the organ of Corti and the epithelium. The explants were then plated in a MatTek dish onto a 14 mm diameter round glass coverslip that was coated with Cell Taq (Corning) for adhesion. Coverslips were immersed in 150 μL DMEM/F12 medium supplemented with 5% FBS (Invitrogen). Cultures were incubated at 37°C and 5% CO_2 for approximately 24 hrs. Cochlear cultures were fixed with 4% PFA, blocked for one hour with 3% BSA+ 0.2% Triton-X 100 and subsequently incubated with a myosin VI antibody (1:200, Proteus Biosciences) overnight at 4°C. Alexa Fluor secondary antibody (1:1000, Invitrogen) was added to reveal labelling in addition to an Alexa Fluor-conjugated phalloidin stain to visualize hair cell stereocilia. In addition, cultures were subjected to a fluorescently labelled dye, FM1-43, that is readily taken up by hair cells through the mechanoelectrical transduction channel. Cultures were loaded with FM1-43 dye for 30 seconds and were subsequently fixed with 4% PFA then washed and mounted. Cultures were imaged using a Zeiss LSM800 high-resolution confocal microscopy. Images were acquired using a 25X objective lens, averaged 4 times, where 20 individual slices were taken and merged together for a an averaged image.

4.2.9. Statistical Analysis

Two-tailed independent unpaired student's t-test were used for comparisons of connexin expression in qPCR as well as in Western blots for Cx43 between WT and $Cx43^{I130T/+}$ and WT and $Cx43^{G60S/+}$ mice. Two-way analysis of variance (ANOVA) with Sidak's post hoc tests were used to compare different cohorts in ABR threshold analysis, amplitudes and latencies of ABR waveform analysis, hair cells counts and ABR thresholds for noise exposure analysis at each individual stimuli.

4.3. Results

4.3.1. Cx43 mRNA transcript is expressed in the cochlea with no evidence of Cx26 or Cx30 compensation in Cx43 mutant mice

To confirm that Cx43 is expressed specifically in the cochlea, we used reverse transcriptase quantitative real-time polymerase chain reaction (qRT-PCR) to determine the level of Cx43 in the cochlea of 2-3-month-old $Cx43^{I130T/+}$, $Cx43^{G60S/+}$ mutant mice and their respective age and sex matched littermate controls. We found that Cx43 mRNA transcripts were similarly expressed in cochleae of $Cx43^{I130T/+}$, $Cx43^{G60S/+}$ mutant mice and their WT littermate controls when normalized to 18S rRNA (Figure 4.S1A,B). Interestingly, both Cx26 and Cx30 mRNA transcripts were similarly expressed in cochleae of WT and Cx43 mutant mice suggesting no evidence of Cx26 or Cx30 compensation in $Cx43^{I130T/+}$ or $Cx43^{G60S/+}$ mutant mice at the mRNA level (Figure 4.S1C-F).

4.3.2. Total Cx43 protein levels is lower in the cochleae of $Cx43^{G60S/+}$ mutant mice

Total Cx43 protein levels were analyzed in cochlear lysates obtained from dissected whole cochleae at various postnatal time points (postnatal day 4 (P4), P8, P14, and P30, and P60-P90). Both strains of WT mice had a high abundance of total Cx43 protein expression at all developmental time points with both phosphorylated (P1/P2) and non-phosphorylated Cx43 species (NP) present (Figure 4.1A, B).

Figure 4.1. Cx43 protein levels are reduced in $Cx43^{G60S/+}$ mice.

Western blots revealed that Cx43 is prevalent in the cochlea of all mice with mutant mice exhibiting variable amounts of the P1/P2 phosphorylated species (A, B). Total Cx43 levels in the cochleae were quantified at 2-3 months of age and there were no differences in $Cx43^{I130T/+}$ mice compared to controls (C), but there was a significant decrease in $Cx43^{G60S/+}$ mutant mice compared to their WT littermates (D). N=5 pooled cochlear samples for each genotype. GAPDH was used as a loading control for western blots. Independent student T-tests were performed, $^{****}P<0.0001$. P= postnatal. NP = not phosphorylated; P1/P2 = phosphorylated species of Cx43.

Figure 4.1.

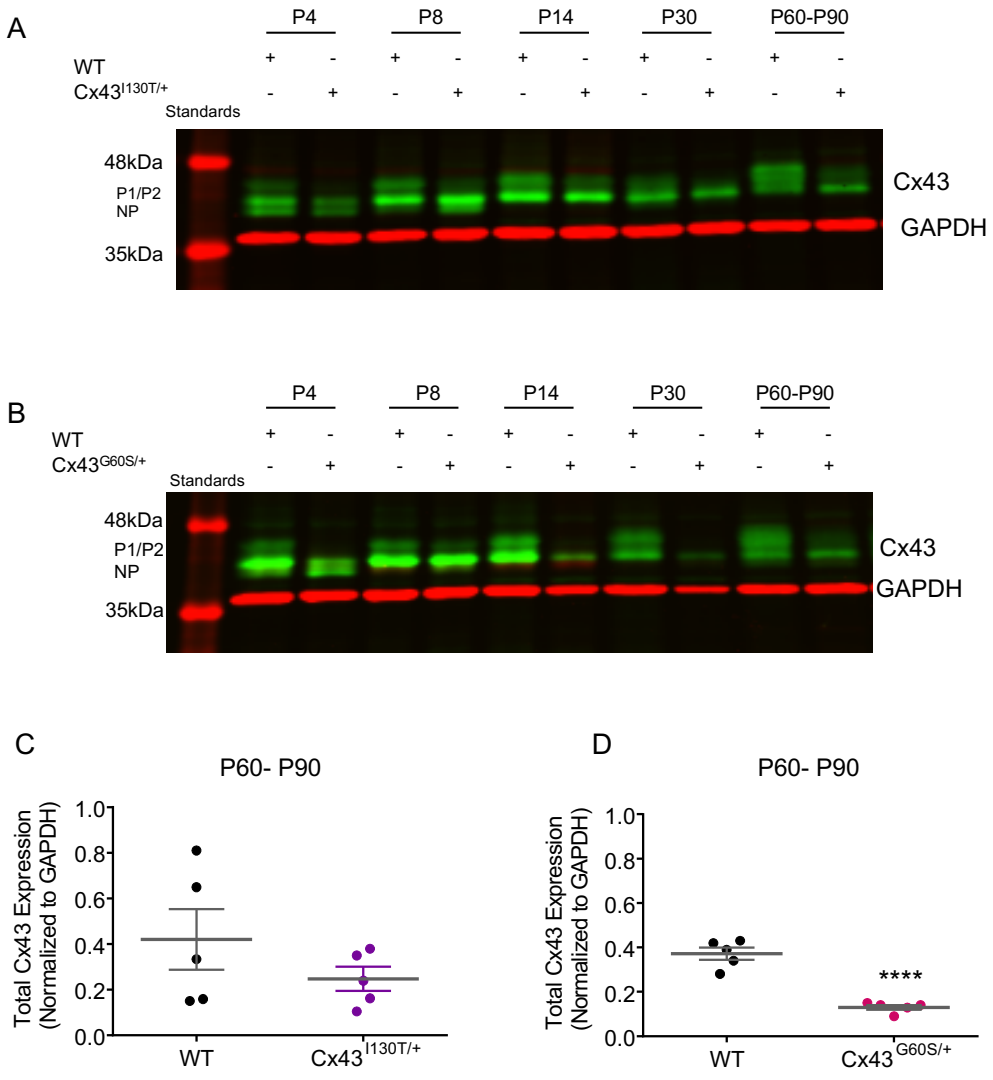
A
P4
P8
P14
P30
P60-P90
WT
Cx43I130T/+
Standards
48kDa
P1/P2
NP
35kDa
Cx43
GAPDH
B
P4
P8
P14
P30
P60-P90
WT
Cx43G60S/+
Standards
48kDa
P1/P2
NP
35kDa
Cx43
GAPDH
C
P60- P90
Total Cx43 Expression (Normalized to GAPDH)
1.0
0.8
0.6
0.4
0.2
0.0
WT
Cx43I130T/+
D
P60- P90
Total Cx43 Expression (Normalized to GAPDH)
1.0
0.8
0.6
0.4
0.2
0.0
****
WT
Cx43G60S/+

$Cx43^{I130T/+}$ mutant mice appeared to have decreased Cx43 compared to their WT counterparts at all developmental time points; however, this difference was not significant when quantified for P60-P90 mice (Figure 4.1C). $Cx43^{G60S/+}$ mutant mice had an apparent reduction in Cx43 in the cochleae at every developmental time point and a significantly lower level of total Cx43 compared to wildtype littermates at the P60-P90 time point (Figure 4.1B,D).

4.3.3. Cx43 is localized to cells of the cochlear nerve region

A clear understanding of the localization profile of Cx43 along the auditory tract remains controversial. In an attempt to resolve this issue, cochlear cross sections from wildtype and mutant mice were immunostained for Cx43. As might be expected, there was no detectable Cx43 (absence of red staining) in inner ear hair cells which were demarcated by phalloidin staining of actin-rich stereocilia (green, Figure 4.2A,B). Little Cx43 (denoted by red) was detected in the spiral ganglion neurons or in satellite cells surrounding the neurons, labelled by CNPase (green) (Figure 4.2C). Farther along the auditory pathway, Cx43 was highly expressed in resident cells of the cochlear nerve region within the central modiolus, where all the spiral ganglion neurons are bundled together (Figure 4.2D). Upon higher level imaging, Cx43 was found in distinct gap junction plaques in areas surrounding GFAP-positive cells, an astrocytic glial cell marker (green) (Figure 4.2E, F, arrows). Cx43 gap junctions were also found between the cell processes which formed a "glial- like" syncytium in the cochlear nerve region (Figure 4.2F). There was a noticeable reduction of Cx43 gap junctions in the cochlear nerve region of both mutant mice (Figure 4.2E,F).

4.3.4. $Cx43^{G60S/+}$ mutant mice have severe hearing loss and auditory brainstem deficits

To assess whether hearing in the mutant mice is directly influenced by the extent of Cx43 function, we utilized the auditory brainstem response (ABR) technique to measure hearing thresholds (i.e., hearing sensitivity) in response to various acoustic stimuli. Firstly, we administered a broadband click stimulus to the animals, which activates several regions of the cochlear sensory epithelium and thus provides an overall measurement of hearing sensitivity. Secondly, we played specific tonal frequencies (4, 8, 16 and 24 kHz), that activate hair cells in specific regions of the cochlea, to give an indication of where along the sensory epithelium any dysfunction is present.

Figure 4.2. Cx43 is highly expressed in select cells found in the cochlear nerve.

Immunofluorescent images revealed that Cx43 is not expressed in the cochlear duct region (red=Cx43, green= phalloidin staining actin-rich stereocilia) (A) or in areas surrounding hair cells of the organ of Corti (B). There was little to no detection of Cx43 in the spiral ganglion neurons, red=Cx43, green=Schwann cells (C). Scale bars = 20μm. Cx43 was found in the modiolus region of the cochlea (red=Cx43, blue=nuclei) (D) and was localized amongst GFAP-positive cells (green=GFAP, red=Cx43, blue=nuclei) (E, F). OC= organ of Corti, SGN= spiral ganglion neurons, CN= cochlear nerve. Dashed line in (D) delineates the glial juncture of the cochlear nerve. Dashed box in (E) delineated area zoomed in (F). Arrows in (F) represent examples of Cx43 gap junction plaques in the cochlear nerve region. Scale bars = (A-C) 20μm (D) 100μm, (E, F) 20μm.

Figure 4.2.

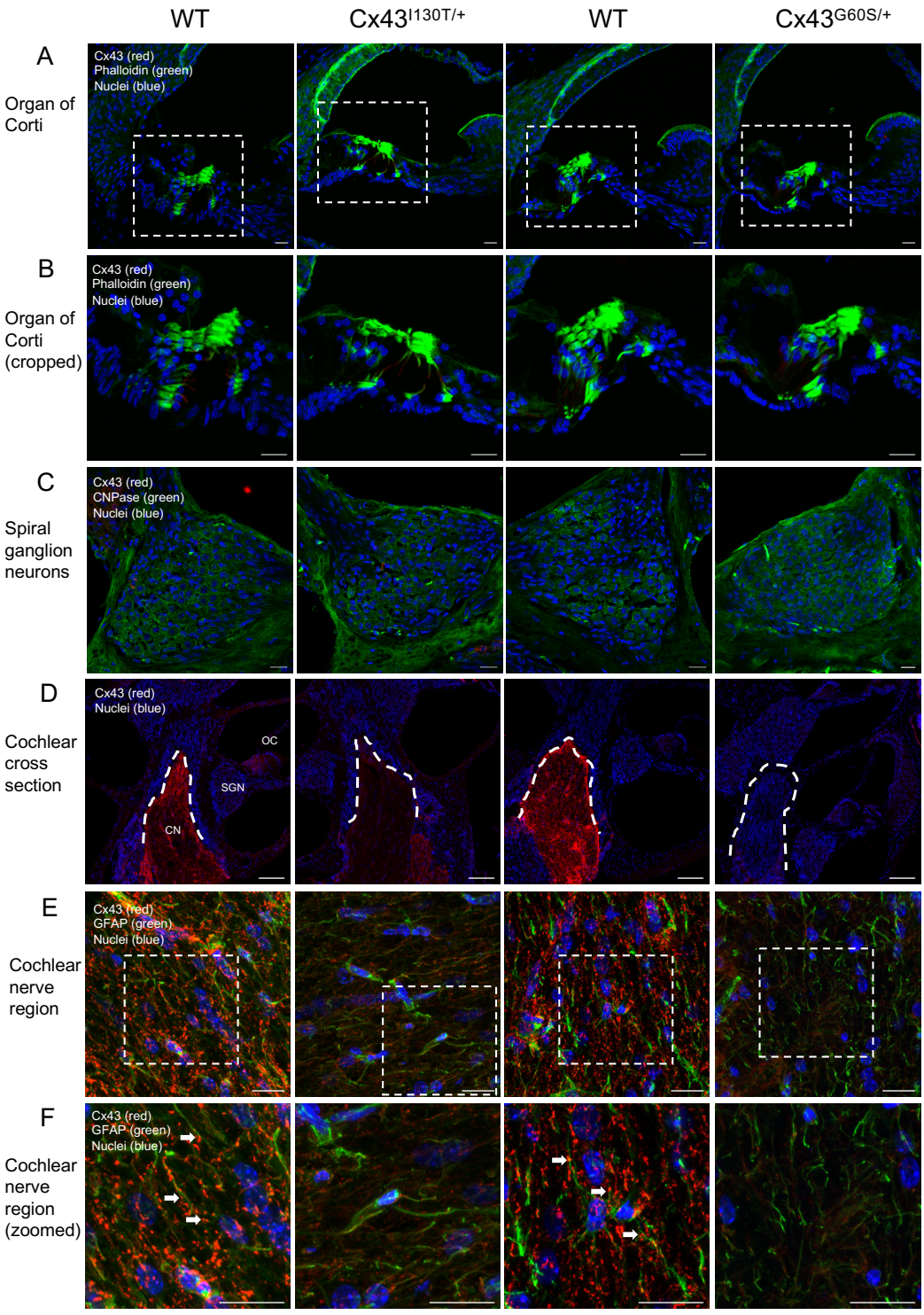
WT
Cx43I130T/+
WT
Cx43G60S/+
A
Organ of Corti
Cx43 (red)
Phalloidin (green)
Nuclei (blue)
B
Organ of Corti (cropped)
Cx43 (red)
Phalloidin (green)
Nuclei (blue)
C
Spiral ganglion neurons
Cx43 (red)
CNPase (green)
Nuclei (blue)
D
Cochlear cross section
Cx43 (red)
Nuclei (blue)
OC
SGN
CN
E
Cochlear nerve region
Cx43 (red)
GFAP (green)
Nuclei (blue)
F
Cochlear nerve region (zoomed)
Cx43 (red)
GFAP (green)
Nuclei (blue)

Representative examples of an ABR trace recording from WT and $Cx43^{I130T/+}$ mutant mice showed similar waveform characteristics and thresholds in response to a click stimulus at decreasing sound intensity levels (90 to 30 dB sound pressure level, SPL; Figure 4.3A). However, $Cx43^{G60S/+}$ mutant mice had different waveform profiles including decreased ABR amplitudes (indicating less synchronized neural firing in the auditory brainstem relays), and increased thresholds (i.e. worse hearing) compared to their WT littermate controls (Figure 4.3B). Averaged ABR thresholds were similar for all stimuli tested in WT and $Cx43^{I130T/+}$ mutant mice at 2-3 months of age (Figure 4.3C). Normal hearing in $Cx43^{I130T/+}$ mutant mice persisted in older mice at 6 months of age, albeit with an increase in ABR thresholds at higher frequencies, consistent with expected age-dependent high-frequency hearing loss due to their C57BL/6 background [51-53] (Figure 4.3E). Although hearing remained intact in $Cx43^{I130T/+}$ mutant mice, averaged ABR thresholds for all stimuli tested were significantly increased in $Cx43^{G60S/+}$ mutant mice compared to their WT littermate controls at both 1 and 2-3 months of age (Figure 4.3D,F) indicating that these mutant mice had severe hearing loss. ABR thresholds for $Cx43^{G60S/+}$ mutant mice ranged from approximately 60-80dB SPL compared to 20-40dB SPL for WT littermate controls across all stimuli tested, showing a 40dB elevation in hearing thresholds (i.e., worsened hearing) of $Cx43^{G60S/+}$ mutant mice compared to their WT controls. Collectively, these data show that although $Cx43^{I130T/+}$ mutant mice have normal hearing, $Cx43^{G60S/+}$ mutant mice have severe hearing loss.

In addition to measuring hearing sensitivity, ABR waveform morphologies provide an indication of the integrity of the ascending auditory pathway, where waves I-V correspond with the successive relay centers (i.e., cochlear nerve, cochlear nucleus, superior olivary complex, lateral lemniscus, and interior colliculus, respectively). In order to examine whether Cx43 mutant mice had any defects in specific auditory brainstem regions, we analyzed the amplitudes and latencies of the loudest (90dB SPL) click ABR waveforms to assess neural synchrony, where larger amplitude represents more synchronous neural firing, and latency represents the speed of neurons firing, respectively.

Figure 4.3. $Cx43^{G60S/+}$ mutant mice exhibit severe hearing loss.

Representative examples of a click stimulus for $Cx43^{I130T/+}$, $Cx43^{G60S/+}$, and their respective WT littermate controls overlaid together (A, B). Mean ABR thresholds of all stimuli of $Cx43^{I130T/+}$ and $Cx43^{G60S/+}$ mutant mice and their WT littermate controls (C-F). $Cx43^{G60S/+}$ mutant mice had significantly elevated ABR thresholds (i.e. worse hearing) at both 1 and 2-3 months of age compared to their WT littermate controls, two-way repeated measures ANOVA, ***P<0.001, ****P<0.0001 (D, F). WT and $Cx43^{I130T/+}$ mutant mice: N= 8 mice for 2-3 months and N=6 mice for 6 months in each genotype. WT and $Cx43^{G60S/+}$ mutant mice: N=6 for 1 month and N=8 for 2-3- months in each genotype. Bars represent mean ± SE.

Figure 4.3.

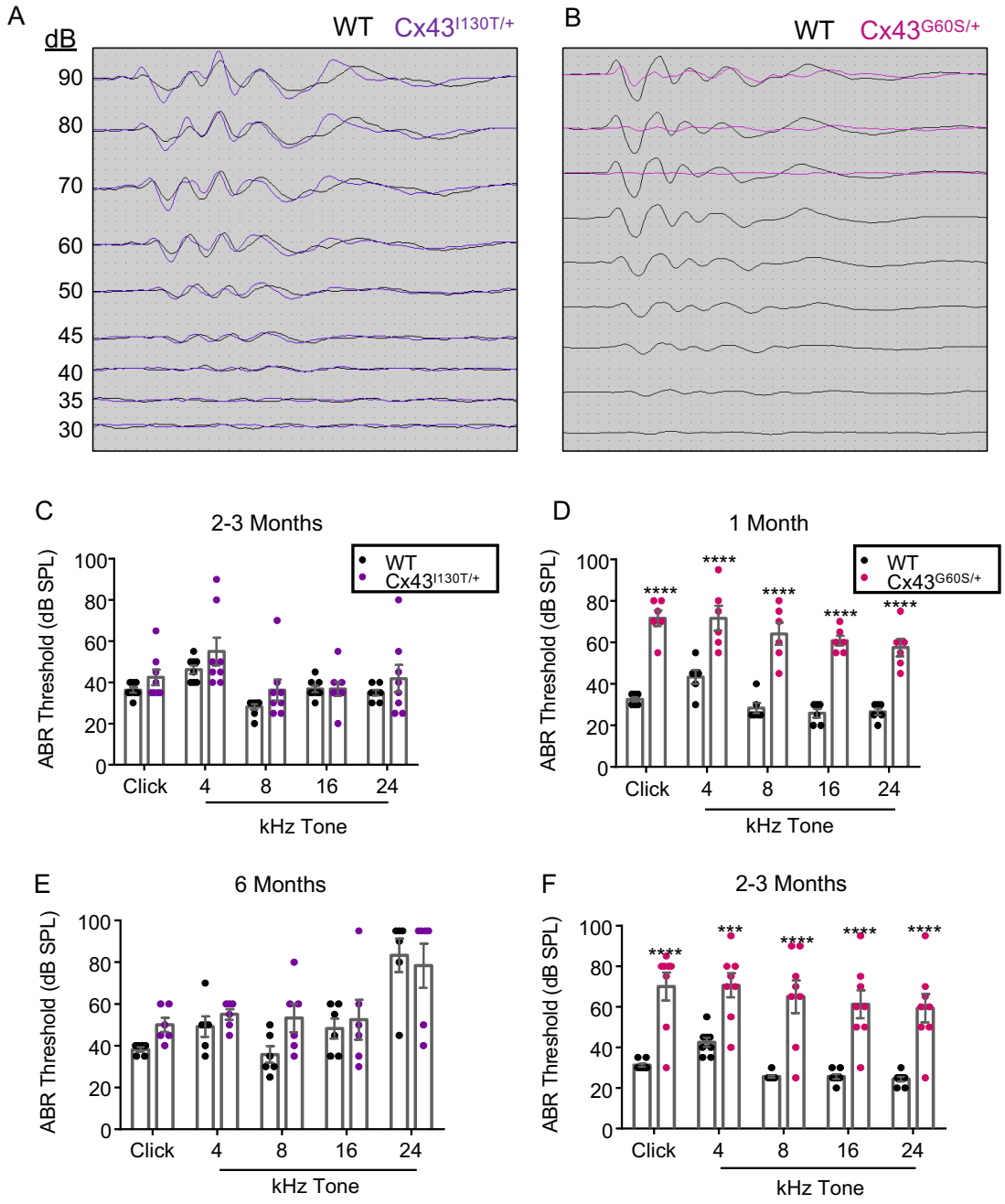
A
dB
WT
Cx43I130T/+
90
80
70
60
50
45
40
35
30
B
WT
Cx43G60S/+
C
2-3 Months
WT
Cx43I130T/+
ABR Threshold (dB SPL)
Click
4
8
16
24
kHz Tone
D
1 Month
WT
Cx43G60S/+
****
E
6 Months
F
2-3 Months
***

$Cx43^{I130T/+}$ mutant mice had similar ABR amplitudes and latencies as WT controls (Figure 4.4A,C). Interestingly, $Cx43^{G60S/+}$ mutant mice had significantly decreased ABR wave amplitudes but no difference in latencies, suggesting Cx43-linked defects in neural synchrony and/or firing at those auditory brainstem regions but not conduction speeds (Figure 4.4B,D). Taken together, these results suggest that although $Cx43^{I130T/+}$ mutant mice do not have auditory brainstem region deficits, $Cx43^{G60S/+}$ mutant mice exhibit sensorineural hearing loss.

4.3.5. Hearing loss in $Cx43^{G60S/+}$ mice is not due to reduced hair cell number or functional loss

Given that loss of hair cell number is a common cause of hearing impairment, we next assessed whether hearing loss in $Cx43^{G60S/+}$ mice was due to inefficient development of the sensory epithelium. To this end, we cultured the organ of Corti from WT and Cx43 mutant pups (P0-P3) to visualize and count the number of hair cells. Representative images of organotypic cochlear cultures from WT and Cx43 mutant mice in each turn of the cochlea (apical, mid-apical, basal and mid-basal) showed that hair cells were intact in all mice as visualized with the hair cell marker, myosin VI (green), and the stereocilia marker, phalloidin (red) (Figure 4.5A). When the number of outer and inner hair cells were quantified from cochlear cultures there was no hair cell loss evident in $Cx43^{I130T/+}$ or $Cx43^{G60S/+}$ mutant mice in any of the cochlear regions (Figure 4.5B).

Hair cell activation occurs via the deflection of hair-like stereocilia on the apical surface of hair cells in response to sound-induced vibration of the sensory epithelium (organ-of-Corti). The deflection causes the opening of mechanotransducer (MET) channels that allows the influx of cations including K^+, of which the concentration in endolymph is extremely high (150 mM). This leads to depolarization of hair cells and consequent calcium uptake and neurotransmitter release. Taking advantage of this mechanism, we investigated whether hair cells in $Cx43^{G60S/+}$ mice were functional by exposing cochlear cultures to a MET channel-permeable, fluorescent FM1-43 dye. If MET channels are functional, the dye would enter hair cells and fluoresce green. Representative low (Figure 4.S2A) and high (Figure 4.S2B) resolution images revealed that the rows of inner and outer hair cells of both Cx43 mutant and WT mice were able to take up the FM1-43 dye. Taken together, organotypic cochlear cultures revealed that hearing loss in $Cx43^{G60S/+}$ mutant mice is not due to hair cell damage in early postnatal development.

Figure 4.4. Amplitudes and latencies of all five ABR waveforms were analyzed for a 90dB SPL click stimulus.

$Cx43^{I130T/+}$ mutant mice had similar ABR wave amplitudes (neural firing/synchrony) and latencies (neural conduction speeds) for all five ABR waves compared to WTs (A, C). However, $Cx43^{G60S/+}$ mutant mice had significantly decreased ABR wave amplitudes compared to WTs (B), two-way ANOVA, *P<0.05, **P<0.01, ***P<0.001, ****P<0.0001), although the ABR wave latencies remained the same (D). N=8 mice per each cohort of each genotype. Bars represent mean ± SE.

Figure 4.4.

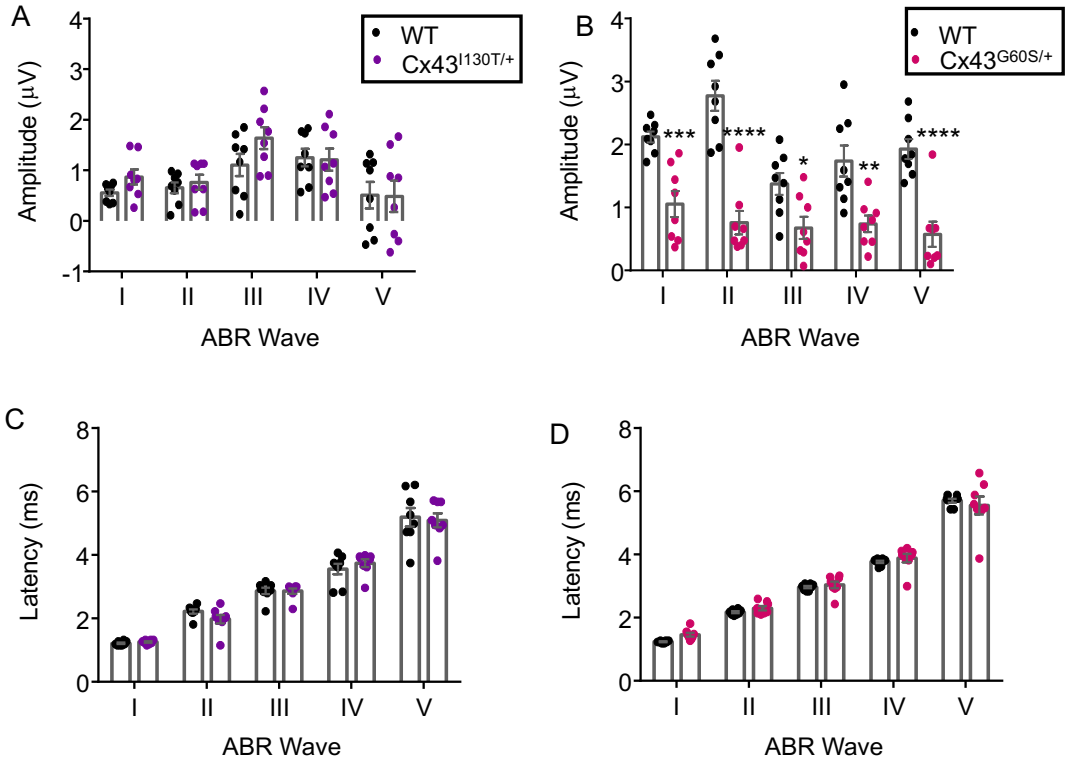
A
Amplitude (μV)
WT
Cx43I130T/+
ABR Wave
B
Amplitude (μV)
WT
Cx43G60S/+
***
****
*
**
****
ABR Wave
C
Latency (ms)
ABR Wave
D
Latency (ms)
ABR Wave

Figure 4.5. Cx43$^{G60S/+}$ mutant mice do not exhibit postnatal hair cell loss in cochlear cultures.

Representative confocal images of hair cell staining in each genotype of mice in four different regions of the cochlea representing different frequency ranges; Basal- high frequency, Mid-Basal- Mid-high frequencies, Mid-Apical- Mid-low frequencies, and Apical- Low frequencies (A). Hair cell bodies were stained with myosin VI (green) and stereocilia of hair cells were stained with phalloidin (red). When the number of outer and inner hair cells were quantified for each cochlear region, there were no differences found in either Cx43 mutant mice compared to their WT littermate controls (B). Images were acquired on a 25x lens from 20 individual stacked slices (from the top to bottom span of the culture) and compiled to generate one merged image. OHC= outer hair cells, IHC= inner hair cells. Blue= nuclei. Scale bars = 50μm.

Figure 4.5.

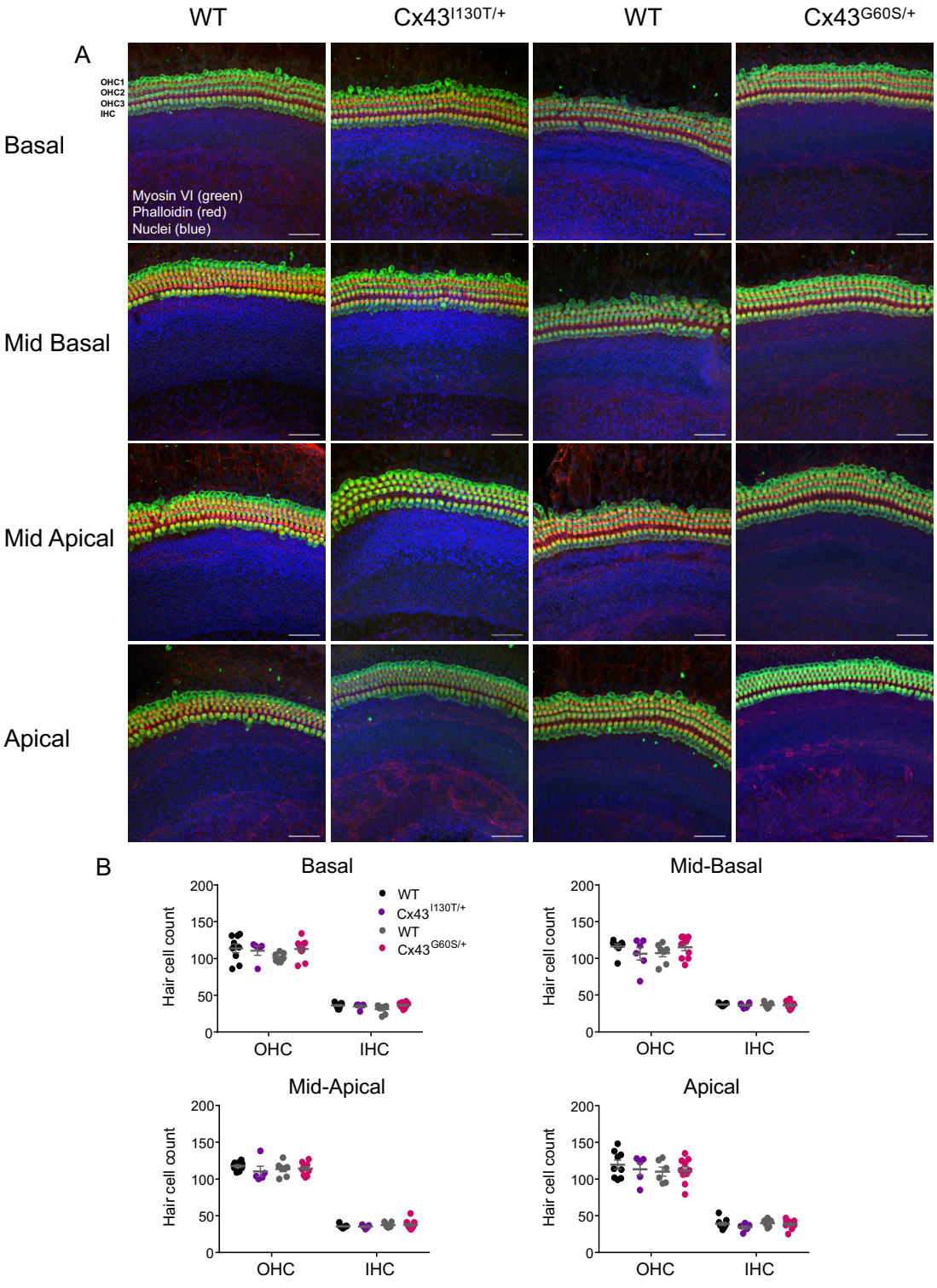
WT
Cx43I130T/+
WT
Cx43G60S/+
A
OHC1
OHC2
OHC3
IHC
Basal
Mid Basal
Mid Apical
Apical
Myosin VI (green)
Phalloidin (red)
Nuclei (blue)
B
Basal
Mid-Basal
Mid-Apical
Apical
WT
Cx43I130T/+
WT
Cx43G60S/+
Hair cell count
0
50
100
150
200
OHC
IHC

Although cochlear cultures from P0-P3 pups revealed that $Cx43^{G60S/+}$ mutant mice did not have hair cell loss, hair cells at this stage are still immature and are not fully developed until ~P14. Since $Cx43^{G60S/+}$ mutant mice exhibited hearing loss at both 1 and 2-3 months of age, we assessed whether there was hair cell loss in adult (2-3 month-old) mutant mice. Staining for hair cell markers, myosin VI and actin, in whole mount cochlear epithelium preparations of adult cochleae from the apical turns showed no evidence of hair cell loss, and the hair cells retained normal morphological appearances in $Cx43^{G60S/+}$ mutant mice (Figure 4.6A). Further, to examine the structural integrity of the synaptic interface between the inner hair cells and the spiral ganglion neurons, we stained adult whole mount sections with myosin VI to visualize hair cells, and CtBP2, a molecular marker expressed in ribbon synapses of hair cells that promotes rapid release of neurotransmitters to the spiral ganglion neurons. These dense ribbon synapses are essential for propagation of electrical signals to the brainstem, and loss of such markers as CtBP2 can lead to hearing loss. Inner hair cells of $Cx43^{G60S/+}$ mutant mice appeared to have a similar number of CtBP2-positive synapses as controls suggesting no shortages in the innervation of inner hair cells (Figure 4.6B).

4.3.6. Hearing loss in $Cx43^{G60S/+}$ mice is not due to any evident spiral ganglion neuron degeneration or demyelination in the cochlear nerve region

Since there was no evidence of hair cell loss in the mutant mice, we next looked at spiral ganglion neuron morphology. There was no evidence of neuronal loss in $Cx43^{G60S/+}$ mutant mice as evidenced by immunofluorescent labeling of beta III tubulin, a neuronal marker, showing similar staining patterns in both WT and mutant mice (Figure 4.7A). Further, we examined if $Cx43^{G60S/+}$ mutant mice presented any evidence of differential expression of myelin in the modiolus region using a marker of myelin, myelin basic protein. The cochlear nerve regions in both WT and $Cx43^{G60S/+}$ mutant mice had abundant expression of myelin basic protein (Figure 4.7B,C), however, whether there is more intricate disarrangement of myelin within the cochlear nerve region of $Cx43^{G60S/+}$ mutant mice remains unknown.

Figure 4.6. Hair cells of Cx43$^{G60S/+}$ mutant mice remain intact in adult mice.

Hair cells dissected from the apical region of adult (2-3 month-old mice) cochleae labeled with myosin VI (green) and phalloidin (red) revealed that hair cells were intact (A). Similarly, adult Cx43$^{G60S/+}$ mutant mice did not exhibit hair cell loss (A). Adult whole mounts were also stained for hair cell-specific ribbon synapses using antibodies that target CtBP2 (red) (B). Arrows indicate individual synapses that can be visualized. OHC= outer hair cells, IHC= inner hair cells. Scale bars = 10μm.

Figure 4.6.

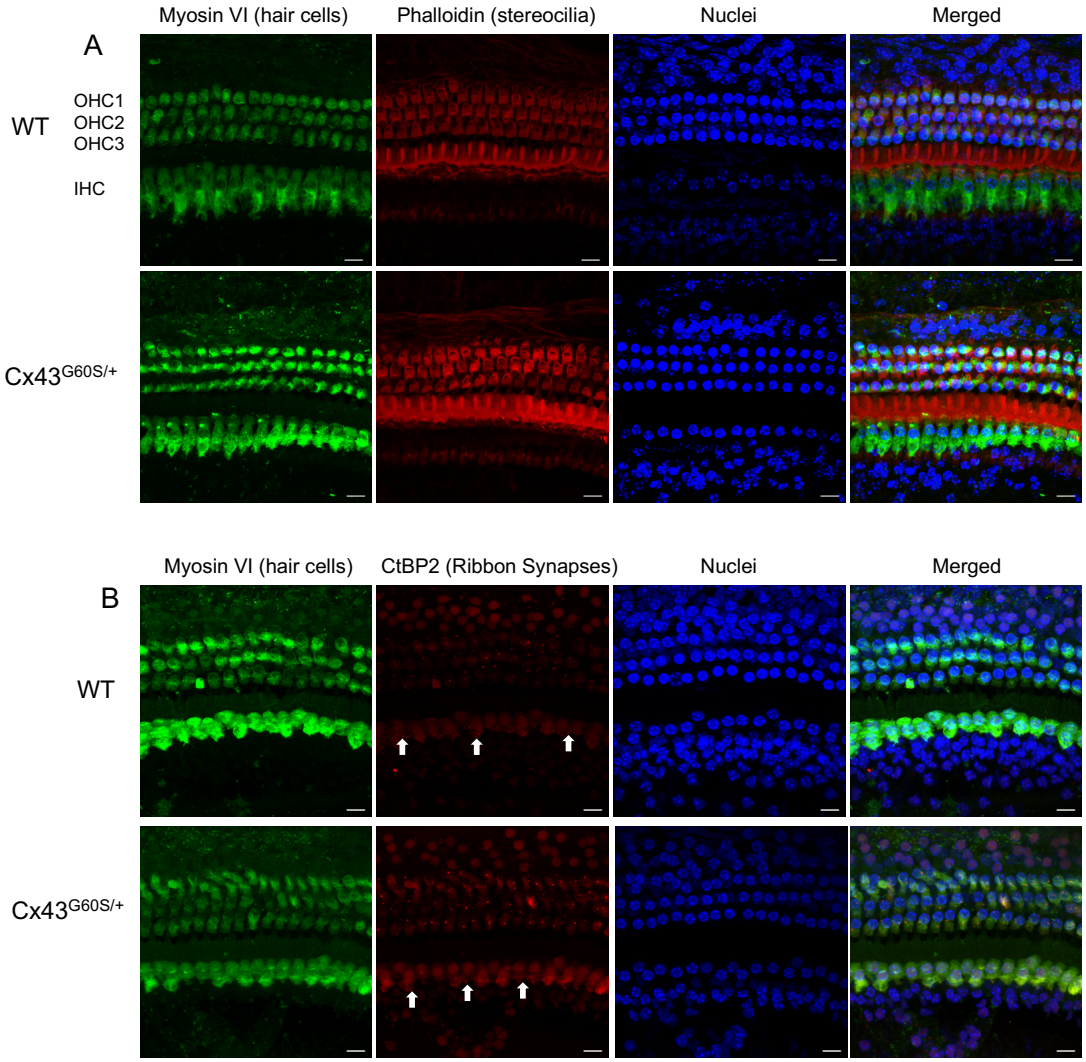
Myosin VI (hair cells)
Phalloidin (stereocilia)
Nuclei
Merged
A
WT
OHC1
OHC2
OHC3
IHC
Cx43G60S/+
Myosin VI (hair cells)
CtBP2 (Ribbon Synapses)
Nuclei
Merged
B
WT
Cx43G60S/+

Figure 4.7. Spiral ganglion neurons remain intact with no evidence of spiral ganglion neuron degeneration or demyelination of the cochlear nerve in Cx43$^{G60S/+}$ mutant mice.

Immunofluorescent confocal images of spiral ganglion neurons of WT and Cx43$^{G60S/+}$ mutant mice labeled for beta-tubulin (neurons = green) and CNPase (Schwann cells = red) (A). Representative images of cochlear cross sections in WT and Cx43$^{G60S/+}$ mutant mice (B). Higher magnification images revealed abundant myelin, stained with myelin basic protein (green) in the cochlear nerve region (C). Note that Cx43 (red) is far less abundant in the cochlear nerve region of mutant mice compared to littermate controls (B, C). OC= organ of Corti, SGN= spiral ganglion neurons, CN= cochlear nerve. Scale bars = (A) 20μm, (B) 100μm, and (C) 20μm.

Figure 4.7.

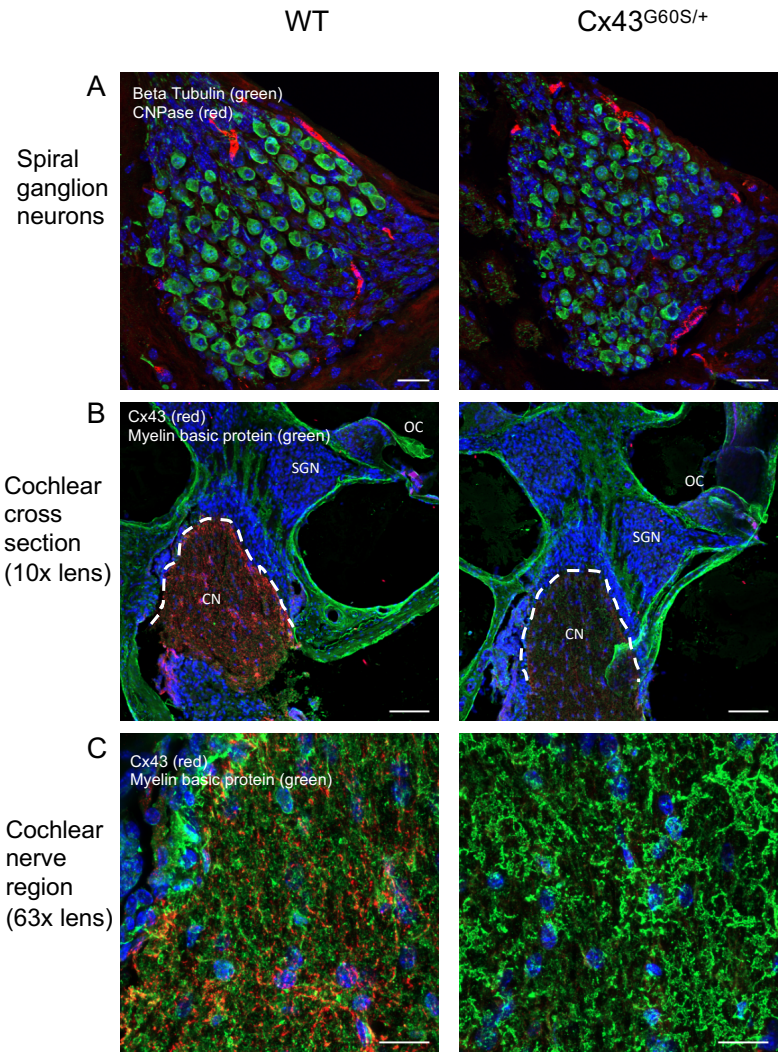
WT
Cx43G60S/+
A
Spiral ganglion neurons
Beta Tubulin (green)
CNPase (red)
B
Cochlear cross section (10x lens)
Cx43 (red)
Myelin basic protein (green)
OC
SGN
CN
C
Cochlear nerve region (63x lens)

4.3.7. WT and Cx43$^{I130T/+}$ mutant mice have similar susceptibility to noise-induced hearing loss

To examine whether Cx43 plays a role in noise-induced hearing loss, we delivered a 12 kHz tonal stimulus at 115 dB SPL for 1 h to Cx43$^{I130T/+}$ mutant mice and their WT littermate controls. Since reduced expression of Cx26, a known connexin family member that is required for hearing, has been shown to sensitize mice to noise-induced hearing loss, we postulated that mutant mice with reduced Cx43 function would be more susceptible to loud noise-induced hearing loss if Cx43 played a central role in this process. Hearing testing was measured using the ABRs at three separate time points; (1) baseline; (2) immediately after loud noise exposure; and (3) one week after noise exposure. While ABR thresholds remained similar in the low frequencies (Figure 4.8A-C), as expected, thresholds were elevated immediately after noise-exposure in both WT and Cx43$^{I130T/+}$ mice at the high (16- and 24 kHz) frequencies (Figure 4.8D,E). With the exception of the broadband click stimulus which changed only by ~10%, there were no differences in ABR thresholds between WT and Cx43$^{I130T/+}$ mutant mice one week after noise-exposure (Figure 4.8A-E). Importantly, WT and Cx43$^{I130T/+}$ mutant mice recovered to the same degree 7 days after noise-exposure at the high frequency stimuli, where the chosen noise-exposure preferentially damaged the peripheral auditory system (i.e., thresholds were greater at the high versus the low frequency stimuli). Thus, upon challenging the auditory system with a loud noise exposure, both WT and Cx43$^{I130T/+}$ mutant mice have similar susceptibility to noise-induced hearing loss.

Figure 4.8. WT and Cx43$^{I130T/+}$ mutant mice have similar susceptibility to noise-induced hearing loss.

Noise exposure (NE) increased ABR thresholds immediately after NE (Post NE) for all stimuli tested, confirming auditory damage in both WT and Cx43$^{I130T/+}$ mutant mice (A-E). The highest ABR thresholds post NE were found at the higher frequency stimuli (D) 16kHz and (E) 24kHz tones. There were no differences between the two groups at the higher frequency stimuli 7 days after NE (D, E). Two-way repeated-measures ANOVAs with a post hoc Sidak's test were performed for each individual stimulus, *$P<0.05$. N=6 for both WT and Cx43$^{I130T/+}$ mice. Bars represent mean ABR threshold ± SE.

Figure 4.8.

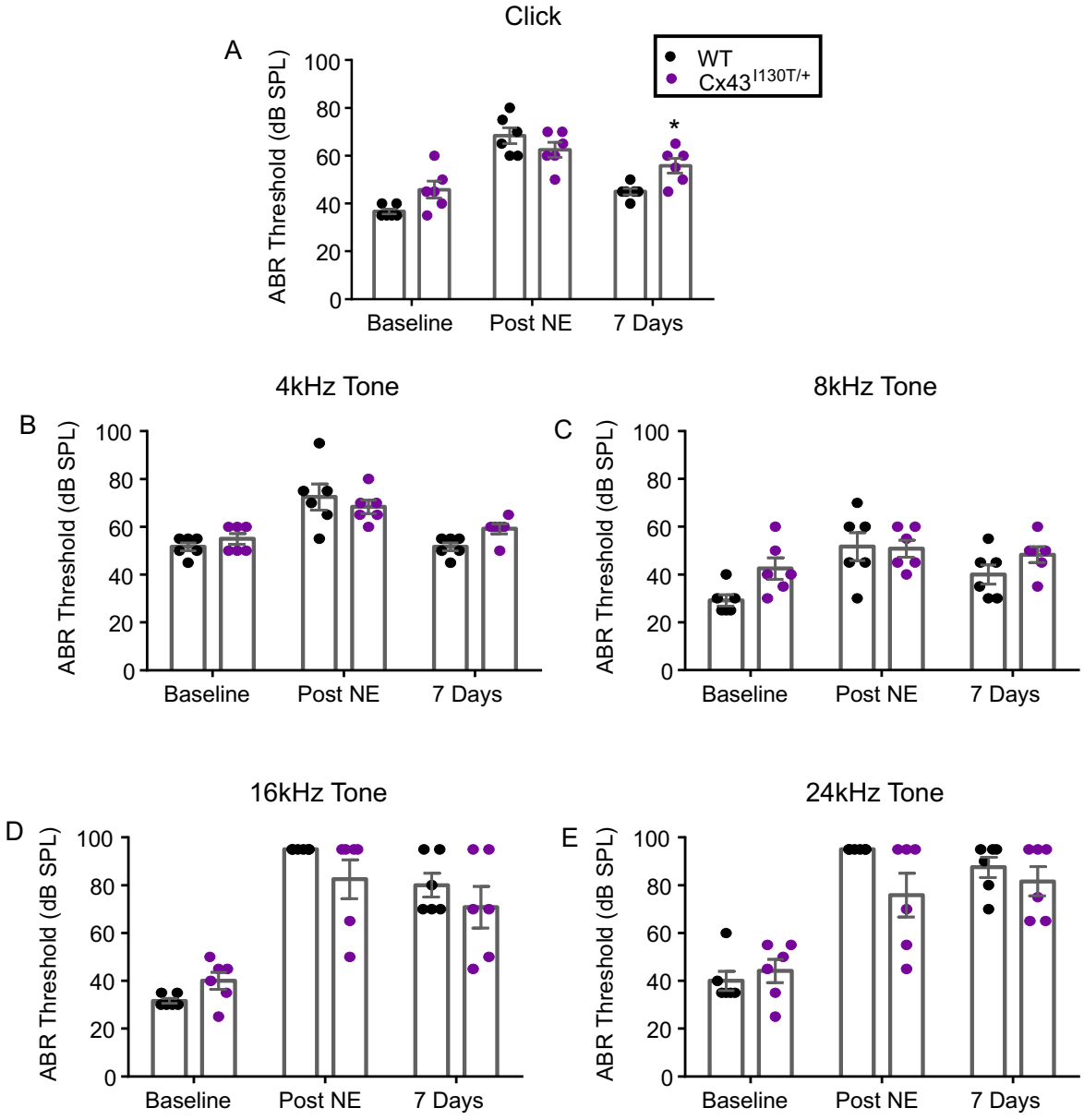
A
Click
WT
Cx43I130T/+
ABR Threshold (dB SPL)
100
80
60
40
20
0
*
Baseline
Post NE
7 Days
B
4kHz Tone
C
8kHz Tone
D
16kHz Tone
E
24kHz Tone

Figure S 4.1. Connexin mRNA transcripts are expressed in the cochlea at similar levels in WT and mutant mice.

Cx43 is expressed in the cochlea of both Cx43 mutant mice as well as their wildtype (WT) littermate controls (A, B). There was no evidence of compensation by Cx26 or Cx30 mRNA transcripts in Cx43 mutant mice (C-F). Gels presented reflect RT-PCR and graphs represent qPCR where mRNA transcript expression were quantified. 18S rRNA was used as a reference gene. Independent student T-tests were used for each group, N=4, n=12 for $Cx43^{I130T/+}$ and N=7, n=21 for $Cx43^{G60S/+}$ cochleae for each genotype in each qPCR experiment. Points on graph represent mean of triplicates for each biological sample (i.e., mean of 4 and 7 for $Cx43^{I130T/+}$ and $Cx43^{G60S/+}$, respectively. Bars represent ±SEM of biological samples (i.e., 4 and 7).

Figure S 4.1.

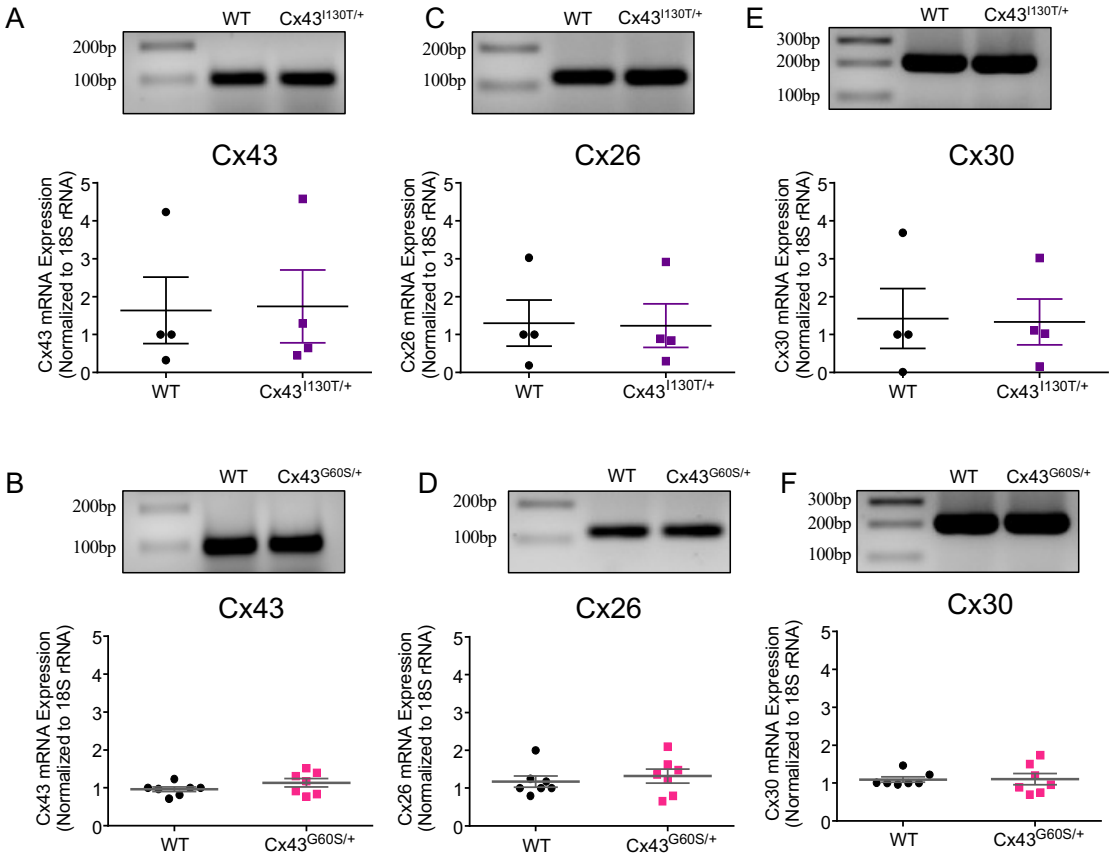
A
WT
Cx43I130T/+
200bp
100bp
Cx43
Cx43 mRNA Expression (Normalized to 18S rRNA)
WT
Cx43I130T/+
C
WT
Cx43I130T/+
200bp
100bp
Cx26
Cx26 mRNA Expression (Normalized to 18S rRNA)
WT
Cx43I130T/+
E
WT
Cx43I130T/+
300bp
200bp
100bp
Cx30
Cx30 mRNA Expression (Normalized to 18S rRNA)
WT
Cx43I130T/+
B
WT
Cx43G60S/+
200bp
100bp
Cx43
Cx43 mRNA Expression (Normalized to 18S rRNA)
WT
Cx43G60S/+
D
WT
Cx43G60S/+
200bp
100bp
Cx26
Cx26 mRNA Expression (Normalized to 18S rRNA)
WT
Cx43G60S/+
F
WT
Cx43G60S/+
300bp
200bp
100bp
Cx30
Cx30 mRNA Expression (Normalized to 18S rRNA)
WT
Cx43G60S/+

Figure S 4.2. Hair cells in control and mutant mice have functional mechanoelectrical transducer channels.

Representative examples of FM1-43 dye uptake into hair cells in $Cx43^{I130T/+}$, $Cx43^{G60S/+}$ mutant mice and their WT littermate controls (A). Arrow indicates location of hair cells, which have taken up fluorescently labelled dye that is shown in green. Higher magnifications of FM1-43 dye-labeled hair cells revealed fluorescent dye within the cytoplasm of the hair cell. (B). Images were acquired using a confocal microscope equipped with a 10X objective lens. Six individual tiled images were seamlessly compiled together into a montage. OHC= outer hair cells, IHC= inner hair cells. Scale bars=200μm in (A) and 20μm in (B).

Figure S 4.2.

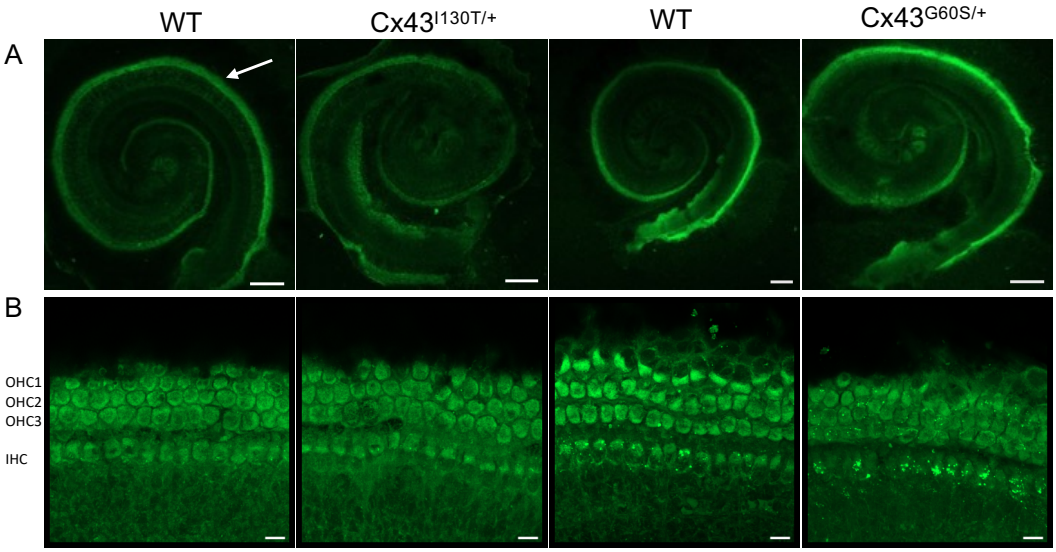

4.4. Discussion

It has been known for some time that Cx26 and Cx30 are essential for auditory function as mutations in the genes encoding both of these connexins are causal of hearing loss. The role of Cx43 in hearing is far less clear although this connexin has been reported to be expressed at defined locations along both the peripheral and central auditory regions [25, 28, 30, 31, 54]. Furthermore, two mutations in the gene encoding Cx43 (*GJA1*), L11F and V24A, have been identified in a cohort of patients with non-syndromic hearing loss providing a putative link between Cx43 and hearing loss [37]. To ascertain whether Cx43 contributes to hearing, we used two genetically-modified mouse lines that have been classically used to investigate the role of Cx43 in the developmental disorder known as oculodentodigital dysplasia (ODDD). We found that $Cx43^{I130T/+}$ mutant mice, which have been shown in other cell lines and tissue to retain ~50% of total Cx43 gap junction function [44], have normal hearing which persisted in middle aged mature mice. However, $Cx43^{G60S/+}$ mutant mice, which have been shown to have ~20% Cx43 function in other cell types and tissues [46], exhibit severe hearing loss and auditory brainstem (where Cx43 is expressed) neural firing deficits. Intriguingly, hearing loss was not attributed to loss of hair cell number or function suggesting the defect lies downstream of the organ of Corti, i.e., within the central neural pathway. In challenging the auditory system with exposure to a loud noise, $Cx43^{I130T/+}$ mutant mice exhibited similar susceptibility to hearing impairment as their wildtype littermate controls, thereby minimizing a possible role of Cx43 in noise-induced hearing loss. Taken together, this study suggests that Cx43 is involved in the normal function of the auditory system.

Cx43 is the most ubiquitously expressed connexin family member and it has been linked to ODDD, a human disease that is inherited in mostly an autosomal dominant manner [41]. Patients with ODDD exhibit many different symptoms including; craniofacial bone abnormalities, small eyes, enamel loss, and fusion of soft tissue digits [41, 42]. In rare cases, patients can also exhibit neurological deficits and hearing loss, which has been found in ~7% of reported ODDD cases [42]. Hearing loss in ODDD patients has been mostly attributed to conductive hearing loss, which is caused by abnormalities in either the outer or middle ear, where sound cannot adequately reach the cochlea, while others were reported to be due to central auditory deficits and a few remain idiopathic [42]. However, it is currently unknown why some patients with ODDD exhibit hearing loss while others do not and whether this is

regulated by the functional status of Cx43. Thus, to examine Cx43 in the auditory system we repurposed two different human disease-linked mutant mouse models of ODDD, $Cx43^{I130T/+}$ and $Cx43^{G60S/+}$, that were previously used to study ODDD in a variety of tissues and organs [44-48]. These two Cx43 mutants have distinct effects on Cx43 function. For example, when expressed alone in gap junction-deficient N2A or HeLa cells, the I130T mutant maintains residual gap junction channel function [43, 45] while the G60S mutant is functionally dead [45, 46, 55]. However, when the same mutants are expressed in cells that co-express wild-type or endogenous Cx43, the functional levels of total Cx43 channels are consistently reduced to ~50% normal (I130T) or ~20% normal (G60S) reflecting their dominant behavior on Cx43 [44-48, 56, 57]. Thus, although Cx43-based GJIC function has not been examined specifically in the auditory system (due to inaccessibility of the auditory tract for GJIC studies), we can extrapolate that the loss of Cx43 function in both mutant mice within Cx43 expressing cells of the auditory system should be similar to what has been previously reported. Therefore, using these two different mutant mice with both mild and severe loss of Cx43-based GJIC, we were able to assess how the level of functional Cx43 impacts hearing.

To our knowledge, only one study in mice has attempted to assess the role of Cx43 in hearing and they found that 3-4 month-old $Cx43^{+/-}$ mice had comparable hearing competence to controls with a modest decrease in hearing capability in 10 month old $Cx43^{+/-}$ mice [31]. These findings are consistent with adult $Cx43^{I130T/+}$ mice that did not have any significant hearing impairments probably due to the fact that they also retained at least 50% normal Cx43 function. However, $Cx43^{G60S/+}$ mutant mice harbouring only ~20% Cx43-based GJIC had severe hearing loss which was found to be ~60dB across all sound frequencies. Hearing loss in $Cx43^{G60S/+}$ mutant mice was accompanied by decreases in all ABR waveform amplitudes which indicate decreased neural synchrony and/or firing of downstream auditory brainstem regions, where wave I represents the cochlear nerve activity and the subsequent waves (II-V) represent electrical activity in the subsequent relay nuclei of the central auditory pathway [58]. In this manner, reductions of neural synchrony and/or firing could lead to inadequate transmission of auditory signals to the central auditory system. This finding suggests that Cx43 is involved in proper firing of neurons within the auditory brainstem nuclei as mice with severe loss of Cx43 function exhibited significantly decreased amplitudes. A previous study reported a similar phenotype in $Cx29^{-/-}$ mice, where they had severe hearing loss and distorted ABR wave I

amplitudes [59]. Interestingly, Cx29 is expressed in the myelinating Schwann cells of the spiral ganglion neurons, whose axons are bundled together to form the cochlear nerve (i.e. represented by the ABR wave I). Upon further analysis, it was found that hearing loss and cochlear nerve defects in $Cx29^{-/-}$ mice was due to demyelinated auditory nerve fibers in the spiral ganglion neurons [59]. Thus, the authors speculated that hearing loss in $Cx29^{-/-}$ mice was due to auditory neuropathy spectrum disorder, which is hearing loss in the presence of intact hair cells within the peripheral auditory system, but where there is abnormal transmission of sound conduction through the auditory nerve and to the brain within the central auditory system. Another gene linked to auditory neuropathy is Cx32, where mutations in the gene encoding Cx32 cause X-linked Charcot-Marie-tooth disease (CMTX). In the auditory system, Cx32 is expressed in the stria vascularis [60] and in the cochlear nerve region near the glial juncture [59], where we have also found Cx43 to be expressed. Patients with CMTX also exhibit hearing loss in some cases, which has been attributed to both cochlear and neural auditory pathologies [61, 62]. Thus, Cx29, Cx32, and Cx43-induced hearing loss appear to manifest from abnormal transmission of sound to the higher-order centers of the auditory pathway, consistent with auditory neuropathy spectrum disorder.

To further elucidate the mechanism of hearing loss in $Cx43^{G60S/+}$ mutant mice, we examined Cx43 expression and cell/tissue integrity using a top-bottom approach of the auditory tract from the peripheral auditory system including the morphology of the cochlea, to the status of hair cells and spiral ganglion neurons, to the cochlear nerve region, and finally to the first part of the central auditory system. First, at the level of the cochlea, we found that $Cx43^{G60S/+}$ mutant mice did not exhibit hair cell loss, and these cells remained functional as assessed via FM1-43 dye uptake through MET channels that are essential for proper depolarization of hair cells. Upon examination of hair cells in 2-3 month-old adult mice, it was evident that the mechanism of hearing loss in $Cx43^{G60S/+}$ mice was not due to mature hair cell loss in animals. Likewise, farther along the auditory tract, there was no evidence of spiral ganglion neuron degeneration in $Cx43^{G60S/+}$ mutant mice compared to WTs. Finally, we found that $Cx43^{G60S/+}$ mutant mice had significantly decreased ABR wave amplitudes in all five waves suggesting that neural synchrony is altered in the auditory brainstem regions where we and others [31] have shown Cx43 to be expressed. Decreases in the first ABR wave have been previously associated with auditory nerve fibre reductions which can lead to hearing loss [63]. However, $Cx43^{G60S/+}$

mutant mice did not exhibit any differences in inner hair cell synapses as was revealed by CtBP2 staining of ribbon synapses. Due to the presence of an intact organ of Corti, the lack of hair cell loss, and the high abundance of Cx43 in the cochlear nerve, it is likely that the mechanism of hearing loss in $Cx43^{G60S/+}$ mice is due to auditory brainstem neural deficits and is occurring downstream of the organ of Corti. Due to the abundant expression of Cx43 gap junction plaques in the cochlear nerve region and the decreased ABR wave amplitudes, the most probable mechanistic site of hearing loss in $Cx43^{G60S/+}$ mutant mice is in the cochlear nerve region.

In the auditory tract of young guinea pigs, rats and humans, Cx43 has been found in the satellite glial cells of the spiral ganglion neurons [27, 28, 54]. In mice, a study showed that Cx43 was weakly expressed in the immature sensory epithelium until postnatal day 8 when Cx43 became exclusively localized to the cochlear bone [30]. Recently, Cx43 has also been described in mice in the modiolus region of the cochlea as well as the higher auditory brainstem relays [31]. The current study showed that Cx43 is found in gap junctions within the cochlear nerve region and surrounding astrocytic processes. This Cx43 localization pattern has also been shown in the brain where it is expressed amongst astrocytic processes that produce a glial syncytium network enabling a conduit for glial cell communication [64, 65]. The proposed role of Cx43 in these networks is to clear out waste materials such as excess neurotransmitter and potassium ions, allow the passage of metabolites and ions from capillaries to neurons, as well as to recycle metabolites and ions that are important in normal neuronal homeostasis within the brain [32, 66, 67]. For example, one of the most prevalent roles of Cx43 in astrocytes of the brain is potassium buffering and clearance where it is proposed to shuttle potassium ions from areas of high concentration to areas of low concentration in the brain to redistribute these excess ions arising from neural activity [68, 69]. In this manner, Cx43 maintains homeostasis and alleviates toxicity as well as the buildup of unwanted ions in the brain. Therefore, due to the prevalence of Cx43 around glial cells in the cochlear nerve regions and the decreased neural output of the auditory brainstem regions, we propose that Cx43 may be playing a similar role in the cochlear nerve region. More specifically, Cx43 gap junctions in this region can assist in maintaining ion homeostasis and dissipation of potentially harmful molecules such as overexposure to potassium ions or glutamate neurotransmitters, which have both been shown to cause hearing damage [70]. These Cx43 based gap junction channels would provide communication in glial

cells of the cochlear nerve region and in turn could shuttle K^+, glutamate, and other ions and neurotransmitters from areas of high to low concentrations to maintain proper cellular homeostasis within this auditory region, similar to the role of Cx43 in astrocytes of the brain. In turn, lack of efficient Cx43-based GJIC in astrocytes in the cochlear nerve could impede further conduction of auditory signals throughout subsequent brainstem relays.

Although studies have suggested a link between Cx43 and hearing its involvement in noise-induced hearing loss is unknown. Both Cx26 and Cx30 are thought to play a role in the active transport of sodium and potassium within the cochlea and [7] both Cx26 and Cx30 protein levels were significantly decreased after noise exposure [38]. In addition, when Cx26 was conditionally knocked down at postnatal day 18, mice exhibited more pronounced noise-induced hearing loss than their wild type counterparts [39]. In the present study we sought to investigate the potential contributions of Cx43 to noise-induced hearing loss. When we challenged the auditory system of Cx43-compromised (~50% normal Cx43 function) $Cx43^{I130T/+}$ mutant mice with an acute loud noise, we found that there was no increase in susceptibility to noise trauma, or recovery, when compared to littermate controls, unlike what has been shown for Cx26. The relative differences in the impact of noise-exposure of these two different connexins may give us novel insights into their relative roles within the auditory tract. This suggests that Cx43 is not likely linked to noise-induced hearing loss as might be the case for Cx26.

4.5. Conclusions

In summary, it is well known that mutations in genes encoding connexin family members (such as Cx26 and Cx30) lead to mild, moderate, and severe hearing loss [19-24]. Here, we have identified that $Cx43^{G60S/+}$ mutant mice that retain only ~20% normal Cx43 function exhibit severe hearing loss and central auditory deficits, thereby expanding the list of connexin family members linked to hearing loss. We propose that Cx43 is essential in the propagation of sound from the cochlear nerve to the higher-order auditory regions, and thus, a loss of Cx43-based GJIC results in abnormal transmission of sound conduction, similar to what is seen in auditory neuropathy spectrum disorders. Furthermore, we have found that a 50% reduction of Cx43 does not appear to play a role in noise-induced hearing loss in mice. Taken together, we have

identified Cx43 function as being critically important in hearing, which may explain why some ODDD patients harbouring Cx43 mutants have the additional morbidity of hearing loss.

4.6. Acknowledgements

The authours would like to thank Dr. Glenn Fishman and Dr. Janet Rossant for providing the mutant mice. This work was supported by operating grants from the Canadian Institutes of Health Research to D.W.L and B.L.A. (148584) and grant (137098) to B.L.A. J.M.A. was supported by a Natural Sciences and Engineering Research Council of Canada studentship.

4.7. References

1. Bruzzone R, White TW, Paul DL (1996) Connections with connexins: the molecular basis of direct intercellular signaling. Eur J Biochem 238: 1-27

2. Laird DW (1996) The life cycle of a connexin: gap junction formation, removal, and degradation. J Bioenerg Biomembr 28: 311-318

3. Laird DW (2006) Life cycle of connexins in health and disease. Biochem J 394: 527-543.

4. Goodenough DA, Goliger JA, Paul DL (1996) Connexins, connexons, and intercellular communication. Annu Rev Biochem 65: 475-502.

5. Kikuchi T, Adams JC, Paul DL, Kimura RS (1994) Gap junction systems in the rat vestibular labyrinth: immunohistochemical and ultrastructural analysis. Acta Otolaryngol 114: 520-528

6. Kikuchi T, Kimura RS, Paul DL, Adams JC (1995) Gap junctions in the rat cochlea: immunohistochemical and ultrastructural analysis. Anat Embryol (Berl) 191: 101-118

7. Kikuchi T, Kimura RS, Paul DL, Takasaka T, Adams JC (2000) Gap junction systems in the mammalian cochlea. Brain Res Brain Res Rev 32: 163-166.

8. Forge A, Becker D, Casalotti S, Edwards J, Evans WH, Lench N, Souter M (1999) Gap junctions and connexin expression in the inner ear. Novartis Found Symp 219: 134-150; discussion 151-136

9. Chang Q, Tang W, Ahmad S, Zhou B, Lin X (2008) Gap junction mediated intercellular metabolite transfer in the cochlea is compromised in connexin30 null mice. PLoS One 3: e4088.

10. Kikuchi T, Adams JC, Miyabe Y, So E, Kobayashi T (2000) Potassium ion recycling pathway via gap junction systems in the mammalian cochlea and its interruption in hereditary nonsyndromic deafness. Med Electron Microsc 33: 51-56.

11. Jagger DJ, Forge A (2006) Compartmentalized and signal-selective gap junctional coupling in the hearing cochlea. J Neurosci 26: 1260-1268.

12. Nickel R, Forge A (2008) Gap junctions and connexins in the inner ear: their roles in homeostasis and deafness. Curr Opin Otolaryngol Head Neck Surg 16: 452-457.

13. Jagger DJ, Forge A (2015) Connexins and gap junctions in the inner ear--it's not just about K(+) recycling. Cell Tissue Res 360: 633-644.

14. Anselmi F, Hernandez VH, Crispino G, Seydel A, Ortolano S, Roper SD, Kessaris N, Richardson W, Rickheit G, Filippov MA, et al. (2008) ATP release through connexin hemichannels and gap junction transfer of second messengers propagate Ca2+ signals across the inner ear. Proc Natl Acad Sci U S A 105: 18770-18775.

15. Piazza V, Ciubotaru CD, Gale JE, Mammano F (2007) Purinergic signalling and intercellular Ca2+ wave propagation in the organ of Corti. Cell Calcium 41: 77-86.

16. Verselis VK (2019) Connexin hemichannels and cochlear function. Neurosci Lett 695: 40-45.

17. Johnson SL, Ceriani F, Houston O, Polishchuk R, Polishchuk E, Crispino G, Zorzi V, Mammano F, Marcotti W (2017) Connexin-Mediated Signaling in Nonsensory Cells Is Crucial for the Development of Sensory Inner Hair Cells in the Mouse Cochlea. J Neurosci 37: 258-268.

18. Zhao HB, Santos-Sacchi J (1999) Auditory collusion and a coupled couple of outer hair cells. Nature 399: 359-362.

19. Cohen-Salmon M, Ott T, Michel V, Hardelin JP, Perfettini I, Eybalin M, Wu T, Marcus DC, Wangemann P, Willecke K, et al. (2002) Targeted ablation of connexin26 in the inner ear epithelial gap junction network causes hearing impairment and cell death. Curr Biol 12: 1106-1111.

20. Kudo T, Kure S, Ikeda K, Xia AP, Katori Y, Suzuki M, Kojima K, Ichinohe A, Suzuki Y, Aoki Y, et al. (2003) Transgenic expression of a dominant-negative connexin26 causes degeneration of the organ of Corti and non-syndromic deafness. Hum Mol Genet 12: 995-1004.

21. Sun Y, Tang W, Chang Q, Wang Y, Kong W, Lin X (2009) Connexin30 null and conditional connexin26 null mice display distinct pattern and time course of cellular degeneration in the cochlea. J Comp Neurol 516: 569-579.

22. Wang Y, Chang Q, Tang W, Sun Y, Zhou B, Li H, Lin X (2009) Targeted connexin26 ablation arrests postnatal development of the organ of Corti. Biochem Biophys Res Commun 385: 33-37.

23. Crispino G, Di Pasquale G, Scimemi P, Rodriguez L, Galindo Ramirez F, De Siati RD, Santarelli RM, Arslan E, Bortolozzi M, Chiorini JA, et al. (2011) BAAV mediated GJB2 gene transfer restores gap junction coupling in cochlear organotypic cultures from deaf Cx26Sox10Cre mice. PLoS One 6: e23279.

24. Teubner B, Michel V, Pesch J, Lautermann J, Cohen-Salmon M, Sohl G, Jahnke K, Winterhager E, Herberhold C, Hardelin JP, et al. (2003) Connexin30 (Gjb6)-deficiency causes severe hearing impairment and lack of endocochlear potential. Hum Mol Genet 12: 13-21.

25. Lautermann J, ten Cate WJ, Altenhoff P, Grummer R, Traub O, Frank H, Jahnke K, Winterhager E (1998) Expression of the gap-junction connexins 26 and 30 in the rat cochlea. Cell Tissue Res 294: 415-420

26. Locher H, de Groot JC, van Iperen L, Huisman MA, Frijns JH, Chuva de Sousa Lopes SM (2015) Development of the stria vascularis and potassium regulation in the human fetal cochlea: Insights into hereditary sensorineural hearing loss. Dev Neurobiol 75: 1219-1240.

27. Liu W, Bostrom M, Kinnefors A, Rask-Andersen H (2009) Unique expression of connexins in the human cochlea. Hear Res 250: 55-62.

28. Liu W, Glueckert R, Linthicum FH, Rieger G, Blumer M, Bitsche M, Pechriggl E, Rask-Andersen H, Schrott-Fischer A (2014) Possible role of gap junction intercellular channels and connexin 43 in satellite glial cells (SGCs) for preservation of human spiral ganglion neurons : A comparative study with clinical implications. Cell Tissue Res 355: 267-278.

29. Liu WJ, Yang J (2015) Developmental expression of inositol 1, 4, 5-trisphosphate receptor in the post-natal rat cochlea. Eur J Histochem 59: 2486.

30. Cohen-Salmon M, Maxeiner S, Kruger O, Theis M, Willecke K, Petit C (2004) Expression of the connexin43- and connexin45-encoding genes in the developing and mature mouse inner ear. Cell Tissue Res 316: 15-22.

31. Kim AH, Nahm E, Sollas A, Mattiace L, Rozental R (2013) Connexin 43 and hearing: possible implications for retrocochlear auditory processing. Laryngoscope 123: 3185-3193.

32. Ball KK, Gandhi GK, Thrash J, Cruz NF, Dienel GA (2007) Astrocytic connexin distributions and rapid, extensive dye transfer via gap junctions in the inferior colliculus: implications for [(14)C]glucose metabolite trafficking. J Neurosci Res 85: 3267-3283.

33. Yang JJ, Huang SH, Chou KH, Liao PJ, Su CC, Li SY (2007) Identification of mutations in members of the connexin gene family as a cause of nonsyndromic deafness in Taiwan. Audiol Neurootol 12: 198-208.

34. Wonkam A, Bosch J, Noubiap JJ, Lebeko K, Makubalo N, Dandara C (2015) No evidence for clinical utility in investigating the connexin genes GJB2, GJB6 and GJA1 in non-syndromic hearing loss in black Africans. S Afr Med J 105: 23-26

35. Uyguner O, Emiroglu M, Uzumcu A, Hafiz G, Ghanbari A, Baserer N, Yuksel-Apak M, Wollnik B (2003) Frequencies of gap- and tight-junction mutations in Turkish families with autosomal-recessive non-syndromic hearing loss. Clin Genet 64: 65-69.

36. Bosch J, Lebeko K, Nziale JJ, Dandara C, Makubalo N, Wonkam A (2014) In search of genetic markers for nonsyndromic deafness in Africa: a study in Cameroonians and Black South Africans with the GJB6 and GJA1 candidate genes. OMICS 18: 481-485.

37. Liu XZ, Xia XJ, Adams J, Chen ZY, Welch KO, Tekin M, Ouyang XM, Kristiansen A, Pandya A, Balkany T, et al. (2001) Mutations in GJA1 (connexin 43) are associated with non-syndromic autosomal recessive deafness. Hum Mol Genet 10: 2945-2951.

38. Yamaguchi T, Nagashima R, Yoneyama M, Shiba T, Ogita K (2014) Disruption of ion-trafficking system in the cochlear spiral ligament prior to permanent hearing loss induced by exposure to intense noise: possible involvement of 4-hydroxy-2-nonenal as a mediator of oxidative stress. PLoS One 9: e102133.

39. Zhou XX, Chen S, Xie L, Ji YZ, Wu X, Wang WW, Yang Q, Yu JT, Sun Y, Lin X, et al. (2016) Reduced Connexin26 in the Mature Cochlea Increases Susceptibility to Noise-Induced Hearing Lossin Mice. Int J Mol Sci 17: 301.

40. Reaume AG, de Sousa PA, Kulkarni S, Langille BL, Zhu D, Davies TC, Juneja SC, Kidder GM, Rossant J (1995) Cardiac malformation in neonatal mice lacking connexin43. Science 267: 1831-1834

41. Paznekas WA, Boyadjiev SA, Shapiro RE, Daniels O, Wollnik B, Keegan CE, Innis JW, Dinulos MB, Christian C, Hannibal MC, et al. (2003) Connexin 43 (GJA1) mutations cause the pleiotropic phenotype of oculodentodigital dysplasia. Am J Hum Genet 72: 408-418.

42. Paznekas WA, Karczeski B, Vermeer S, Lowry RB, Delatycki M, Laurence F, Koivisto PA, Van Maldergem L, Boyadjiev SA, Bodurtha JN, et al. (2009) GJA1 mutations,

variants, and connexin 43 dysfunction as it relates to the oculodentodigital dysplasia phenotype. Hum Mutat 30: 724-733.

43. Shibayama J, Paznekas W, Seki A, Taffet S, Jabs EW, Delmar M, Musa H (2005) Functional characterization of connexin43 mutations found in patients with oculodentodigital dysplasia. Circ Res 96: e83-91.

44. Kalcheva N, Qu J, Sandeep N, Garcia L, Zhang J, Wang Z, Lampe PD, Suadicani SO, Spray DC, Fishman GI (2007) Gap junction remodeling and cardiac arrhythmogenesis in a murine model of oculodentodigital dysplasia. Proc Natl Acad Sci U S A 104: 20512-20516.

45. Stewart MK, Gong XQ, Barr KJ, Bai D, Fishman GI, Laird DW (2013) The severity of mammary gland developmental defects is linked to the overall functional status of Cx43 as revealed by genetically modified mice. Biochem J 449: 401-413.

46. Flenniken AM, Osborne LR, Anderson N, Ciliberti N, Fleming C, Gittens JE, Gong XQ, Kelsey LB, Lounsbury C, Moreno L, et al. (2005) A Gja1 missense mutation in a mouse model of oculodentodigital dysplasia. Development 132: 4375-4386.

47. Manias JL, Plante I, Gong XQ, Shao Q, Churko J, Bai D, Laird DW (2008) Fate of connexin43 in cardiac tissue harbouring a disease-linked connexin43 mutant. Cardiovasc Res 80: 385-395.

48. Plante I, Laird DW (2008) Decreased levels of connexin43 result in impaired development of the mammary gland in a mouse model of oculodentodigital dysplasia. Dev Biol 318: 312-322.

49. Abitbol JM, Kelly JJ, Barr K, Schormans AL, Laird DW, Allman BL (2016) Differential effects of pannexins on noise-induced hearing loss. Biochem J 473: 4665-4680.

50. Russell IJ, Richardson GP (1987) The morphology and physiology of hair cells in organotypic cultures of the mouse cochlea. Hear Res 31: 9-24.

51. Mikaelian DO (1979) Development and degeneration of hearing in the C57/b16 mouse: relation of electrophysiologic responses from the round window and cochlear nucleus to cochlear anatomy and behavioral responses. Laryngoscope 89: 1-15.

52. Henry KR, Chole RA (1980) Genotypic differences in behavioral, physiological and anatomical expressions of age-related hearing loss in the laboratory mouse. Audiology 19: 369-383

53. Keithley EM, Canto C, Zheng QY, Fischel-Ghodsian N, Johnson KR (2004) Age-related hearing loss and the ahl locus in mice. Hear Res 188: 21-28.

54. Liu WJ, Yang J (2015) Preferentially regulated expression of connexin 43 in the developing spiral ganglion neurons and afferent terminals in post-natal rat cochlea. Eur J Histochem 59: 2464.

55. McLachlan E, Shao Q, Wang HL, Langlois S, Laird DW (2006) Connexins act as tumor suppressors in three-dimensional mammary cell organoids by regulating differentiation and angiogenesis. Cancer Res 66: 9886-9894.

56. Tong D, Lu X, Wang HX, Plante I, Lui E, Laird DW, Bai D, Kidder GM (2009) A dominant loss-of-function GJA1 (Cx43) mutant impairs parturition in the mouse. Biol Reprod 80: 1099-1106.

57. Kozoriz MG, Lai S, Vega JL, Saez JC, Sin WC, Bechberger JF, Naus CC (2013) Cerebral ischemic injury is enhanced in a model of oculodentodigital dysplasia. Neuropharmacology 75: 549-556.

58. Markand ON (1994) Brainstem auditory evoked potentials. J Clin Neurophysiol 11: 319-342

59. Tang W, Zhang Y, Chang Q, Ahmad S, Dahlke I, Yi H, Chen P, Paul DL, Lin X (2006) Connexin29 is highly expressed in cochlear Schwann cells, and it is required for the normal development and function of the auditory nerve of mice. J Neurosci 26: 1991-1999.

60. Degen J, Schutz M, Dicke N, Strenzke N, Jokwitz M, Moser T, Willecke K (2011) Connexin32 can restore hearing in connexin26 deficient mice. Eur J Cell Biol 90: 817-824.

61. Papadakis CE, Hajiioannou JK, Kyrmizakis DE, Bizakis JG (2003) Bilateral sudden sensorineural hearing loss caused by Charcot-Marie-Tooth disease. J Laryngol Otol 117: 399-401.

62. Rance G, Ryan MM, Bayliss K, Gill K, O'Sullivan C, Whitechurch M (2012) Auditory function in children with Charcot-Marie-Tooth disease. Brain 135: 1412-1422.

63. Verhulst S, Jagadeesh A, Mauermann M, Ernst F (2016) Individual Differences in Auditory Brainstem Response Wave Characteristics: Relations to Different Aspects of Peripheral Hearing Loss. Trends Hear 20. DOI 2331216516672186 [pii]20/0/2331216516672186 [pii]10.1177/2331216516672186

64. Dermietzel R, Hertberg EL, Kessler JA, Spray DC (1991) Gap junctions between cultured astrocytes: immunocytochemical, molecular, and electrophysiological analysis. J Neurosci 11: 1421-1432

65. Giaume C, Tabernero A, Medina JM (1997) Metabolic trafficking through astrocytic gap junctions. Glia 21: 114-123.

66. Nagy JI, Rash JE (2000) Connexins and gap junctions of astrocytes and oligodendrocytes in the CNS. Brain Res Brain Res Rev 32: 29-44.

67. Saez JC, Contreras JE, Bukauskas FF, Retamal MA, Bennett MV (2003) Gap junction hemichannels in astrocytes of the CNS. Acta Physiol Scand 179: 9-22.

68. Walz W, Hertz L (1983) Functional interactions between neurons and astrocytes. II. Potassium homeostasis at the cellular level. Prog Neurobiol 20: 133-183.

69. Wallraff A, Kohling R, Heinemann U, Theis M, Willecke K, Steinhauser C (2006) The impact of astrocytic gap junctional coupling on potassium buffering in the hippocampus. J Neurosci 26: 5438-5447.

70. Wong AC, Ryan AF (2015) Mechanisms of sensorineural cell damage, death and survival in the cochlea. Front Aging Neurosci 7: 58.

Chapter 5 : Cisplatin-induced ototoxicity in organotypic cochlear cultures occurs independent of gap junctional intercellular communication

Cisplatin is a very effective chemotherapeutic agent used to treat cancers, however, it causes hearing loss in the majority of patients. In this chapter, we use two different models to ablate Cx43 function in inner ear derived cultures and assessed whether decreasing GJIC impacts cisplatin-induced ototoxicity.

A version of this manuscript is submitted:

Abitbol, J.M., Beach, R., Esseltine, J., Barr, K., Allman, B.L., and Laird, D.W. Cisplatin-induced ototoxicity occurs independent of gap junctional intercellular communication.

5.1. Introduction

Connexins, the protein subunits that form gap junction channels, allow for the passage of members of the metabolome up to 1kDa in size, establishing a form of cellular signaling called gap junctional intercellular communication (GJIC) [1,2]. Mounting evidence suggests that connexin hemichannels where cochlear cells communicate with the extracellular milieu also serve important functions [3]. Gap junctions are essential to maintain proper tissue homeostasis as evidenced by nearly 30 distinct diseases that are associated with connexin gene mutations, with hearing loss being the most frequently occurring impairment [4]. Clinically, mutations and/or deletions in *GJB2* (encoding Cx26) and/or *GJB6* (encoding Cx30) are responsible for nearly 50% of congenitally acquired hearing loss with approximately 135 different mutations in *GJB2* causing hearing loss [4,5].

Spontaneous activity in the cochlea depends upon ATP and calcium release, suggesting a critical role for connexins in cochlear development [3,6]. The necessity of connexins in the development of the organ of Corti (i.e. the sensory epithelium in the cochlea) is revealed from the use of Cx26 conditional knock-out mice where hair cell loss and underdevelopment of the organ of Corti leads to hearing loss [7–9]. Complementary studies using tamoxifen-induced Cx26 knock-down mice revealed that Cx26 was a key regulator in early cochlear development. Indeed, knocking down Cx26 in early postnatal stages resulted in severe hearing loss, malformation of the cochlea, and defects in supporting cells [10–13].

The localization and expression pattern of Cx43 in the cochlea remains controversial but Cx43 has been reported to be expressed at distinct developmental time points in the organ of Corti [14–16], spiral limbus [17], spiral ganglion neurons [18–20], cochlear lateral wall [21], cochlear nerve, and auditory brainstem tract [22]. In keeping with a key role for Cx43 in hearing, we previously showed that the severe loss of Cx43 function led to hearing loss [23], suggesting that Cx43 plays an important role in the development and/or function of the auditory pathway. That said, it remains unclear if dysregulated Cx43 status during development influences the susceptibility of cochlear cells to drug-induced cell death and hearing loss.

One of the most effective and commonly used chemotherapy drugs to treat solid malignant tumours in both children and adults is cisplatin (*cis*-diamminedichloroplatinumII) [24]. Although commonly used, it causes hearing loss in approximately 75-100% of patients [25].

In most cases, cisplatin-induced hearing loss is permanent, and often progressive. Notably, approximately 60-80% of children who are treated with cisplatin will develop significant hearing loss [26], which can hinder their cognitive and speech skills throughout development [27]. Within the cochlea specifically, animal models have shown that cisplatin causes damage to the stria vascularis, spiral ganglion neurons, and hair cells [28]. Given that supporting cells of the organ of Corti have some of the largest and most active gap junctions found in the human body [29], it has been proposed that these channels may facilitate the spread of toxic death signals to adjoining cells amplifying cell death in a process called the bystander effect [30]. Others have argued that the bystander effect acts as a "Good Samaritan" by diluting the effect of toxins which protects the organ of Corti from increased damage [30]. To address the cellular mechanisms of cisplatin-induced ototoxicity, we utilized organ of Corti cultures that retain the three-dimensional aspects and architecture of this sensory organ in addition to a well-known immortalized cochlear cell line, HEI-OC1, which resembles cochlear progenitor cells [31].

The aims of this study were threefold. We first used organotypic cochlear cultures from two Cx43 mutant mice which harbor either a moderate ($Cx43^{I130T/+}$) or severe ($Cx43^{G60S/+}$) loss of Cx43 function to determine the impact of reduced GJIC on cisplatin-induced ototoxicity. Secondly, we co-administered a gap junction blocker with cisplatin to determine whether blocking all cochlear gap junctions alters susceptibility to cisplatin-induced ototoxicity. Thirdly, we used control and Cx43 knockout HEI-OC1 cochlear-derived cells to evaluate the cellular mechanisms underpinning cisplatin-induced ototoxicity.

5.2. Materials and methods

5.2.1. Mice

Heterozygous mice harboring the Cx43 I130T mutation (generously obtained from Glenn Fishman, New York University School of Medicine, New York, NT, USA) were created as previously described [32] and were bred on a C57BL/6 background and backcrossed in house for over six generations. Heterozygous mice harboring a Cx43 G60S mutation (generously obtained from Janet Rossant, The Hospital for Sick Children, Toronto, ON, Canada), were created as previously described and [33] were bred on a C3H/HeJ and C57BL/6 mixed background and backcrossed in house on a C3H background for over six generations. Both mutant mice were compared to their wild type (WT) littermates for all experiments and both

male and female neonatal pups were used. WT C3H mice were used for all experiments where carbenoxolone was employed as a gap junction blocker. Mice were housed in the animal care facilities at the University of Western Ontario and maintained on a 12-h-light-12-h-dark cycle and fed *ad libitum*. All experiments were approved by the Animal Care Committee at the University of Western Ontario.

5.2.2. Organotypic cochlear cultures

Organotypic cochlear cultures were prepared from the cochleae of postnatal day 0-3 (P0-P3) pups of both sexes, combined, and maintained in glass bottom dishes as was previously described [23]. Briefly, mouse pups were sacrificed by decapitation and sterilized in 80% ethanol for 10 minutes and dissected in ice-cold Leibovitz-L15 media (Invitrogen, catalog#11415-064). The epithelium of the organ of Corti was removed and the explants were plated in a glass bottom dish coated with Cell Tak (Corning; catalog#CB40240) to enhance adhesion to the substrate. Cultures were immersed in 200μL Dulbecco's Modified Eagle's Medium (DMEM)/F12 medium supplemented with 5% fetal bovine serum (FBS) (Invitrogen), and 100μg/mL ampicillin. Cultures were incubated at 37ºC and 5% CO_2 overnight after dissection to ensure proper adhesion. Subsequently, cultures were treated with either regular media or 20μM cisplatin, 100μM carbenoxolone (CBX), or a combination of 20μM cisplatin + 100μM CBX for a total of 48 hours prior to fixing with 4% paraformaldehyde (PFA). Media was replaced every 24 hours for all respective treatments.

5.2.3. Immunofluorescence labelling

Fixed cell cultures were blocked and permeabilized in either a 3% bovine serum albumin (BSA) + 0.1% TritonX-100 (HEI-OC1 cells) or 3% BSA+ 0.2% Triton X-100 (organotypic cochlear cultures) solution for one hour. Subsequently, cell cultures were incubated at 4ºC overnight with primary antibodies, with the exception of antibodies to cleaved caspase-3 which was incubated for two hours at room temperature. These antibodies included; rabbit anti-Cx30 (1:400, Thermo-Fisher, catalog#71-2200), mouse anti-Cx26 (1:400, Thermo-Fisher, catalog#33-5800), rabbit anti-Cx43 (1:500, Sigma, catalog#C6219), rabbit anti-MyosinVI (1:200, Proteus Biosciences, catalog#25-6791), rabbit anti-cleaved caspase-3 (1:1000, Sigma, catalog#C9598), mouse anti-protein disulfide isomerase (PDI) (1:500, Assay Designs, catalog#SPA-891), and anti-BiP (1:1000, Sigma Aldrich, catalog# G8918). Cell cultures were

washed and incubated with fluorescent-conjugated secondary antibodies for one hour followed by a nuclear Hoechst 33342 stain. Cultures were additionally stained with phalloidin (1:400, Invitrogen, catalog#A12379). HEI-OC1 cells were mounted on a glass slide with airvol. A Zeiss LSM800 confocal microscope was used to acquire Z-stacks and high resolution Airyscan images. For all quantifications performed on organotypic cochlear cultures (i.e. hair cell counts and cleaved caspase 3 positive hair cell counts), the experimenter was blinded to treatment group, genotype, and cochlear region when counting. N values for each are described in figure legends.

5.2.4. Co-localization and particle analysis

Fixed cell cultures were blocked and permeabilized in either a 3% bovine serum albumin (BSA) + 0.1% TritonX-100 (HEI-OC1 cells) or 3% BSA+ 0.2% Triton X-100 (organotypic cochlear cultures) solution for one hour. Subsequently, cell cultures were incubated at 4ºC overnight with primary antibodies, with the exception of antibodies to cleaved caspase-3 which was incubated for two hours at room temperature. These antibodies included; rabbit anti-Cx30 (1:400, Thermo-Fisher, catalog#71-2200), mouse anti-Cx26 (1:400, Thermo-Fisher, catalog#33-5800), rabbit anti-Cx43 (1:500, Sigma, catalog#C6219), rabbit anti-myosinVI (1:200, Proteus Biosciences, catalog#25-6791), rabbit anti-cleaved caspase-3 (1:1000, Sigma, catalog#C9598), mouse anti-protein disulfide isomerase (PDI) (1:500, Assay Designs, catalog#SPA-891), and anti-BiP (1:1000, Sigma Aldrich, catalog# G8918). Cell cultures were washed and incubated with fluorescent-conjugated secondary antibodies for one hour followed by a nuclear Hoechst 33342 stain. Cultures were additionally stained with phalloidin (1:400, Invitrogen, catalog#A12379). HEI-OC1 cells were mounted on a glass slide with airvol. A Zeiss LSM800 confocal microscope was used to acquire Z-stacks and high resolution Airyscan images. For all quantifications performed on organotypic cochlear cultures (i.e. hair cell counts and cleaved caspase 3 positive hair cell counts), the experimenter was blinded to treatment group, genotype, and cochlear region when counting. N values for each are described in figure legends.

5.2.5. Fluorescence recovery after photobleaching (FRAP)

Control and drug-treated organotypic cochlear cultures were incubated for 48 hours. Cultures were then washed with phosphate-buffered saline (PBS) and incubated for five minutes at room temperature in 2μM calcein-AM dye (Invitrogen, catalog#3100-MP) in DMEM/F12 medium. Cultures were next washed twice with PBS and fresh DMEM/F12 medium was added. Dye loaded cultures were placed in a live cell incubation chamber (37°C, 5% CO_2) under a Zeiss LSM 800 confocal microscope. To assess the level of gap junction function, both the outer sulcus and inner sulcus regions of organotypic cultures were selected for FRAP analysis. One outer sulcus cell that was adjacent to at least three other cells was photobleached and the recovery of fluorescence into the photobleached cell was examined every 10 seconds for eight minutes. Defined regions (288.5μm^2 in diameter) of the tightly packed cells of the inner sulcus region were photobleached and fluorescence recovery to the photobleached region was determined as described above. The intensities of fluorescence were measured in ImageJ and the percent recovery was calculated as; $(F_x\text{-}F_P/F_I) \times 100$, F_x= fluorescence at each time point, F_P= fluorescence after photobleaching, and F_I= initial fluorescence before photobleaching. Area under the curve of a linear regression analysis was calculated using GraphPad Prism 6.

5.2.6. Cell culture and reagents

House Ear Institute-Organ of Corti 1 (HEI-OC1) cells were kindly provided by Dr. Kalinec (House Ear Institute, Los Angeles, CA). HEI-OC1 cells were grown in high glucose DMEM supplemented with 10% FBS and 2mM L glutamine and incubated in permissive conditions (33°C, 10% CO_2). Once HEI-OC1 cells reached 80% confluency they were treated with various doses of cisplatin (Sigma-Aldrich, catalog#PHR1624) or saline as a vehicle control (referred to as untreated) for 24 or 48 hours. Positive controls for the induction of apoptosis in HEI-OC1 cells were treated with 1uM staurosporine (Sigma, catalog#S6942) for two hours. Positive controls for the induction of ER stress in HEI-OC1 cells were treated with 2uM Thapsigargin (Sigma, catalog#T9033) for four hours.

5.2.7. CRISPR-Cas-9 gene ablation

HEI-OC1 cells were transiently transfected using the MIRUS-LT1 transfection reagent with the pSpCas9(BB)-2A-GFP plasmid (PX458, Addgene, Cambridge, MA, USA) which encodes

for the Cas9 protein along with a cloning backbone for a single guide RNA (sgRNA). sgRNAs were designed targeting the sole exon of the *GJA1* gene (encoding Cx43) to induce in/del mutations in *GJA1,* rendering the gene functionally ablated. Two gRNAs were designed using the Sanger Institute CRISPR finder (**http://www.sanger.ac.uk/htgt/wge/**) and are predicted to exhibit extremely low to zero exonic off-targets (mouse *GJA1*: Sanger sgRNA ID: 324658622 (5'- CGCTGTAACACTCAACAACC-3') and Sanger sgRNA ID: 324658605 (5'-AAGCCTACTCCACGGCCGGA-3')). After transfection, GFP-expressing HEI-OC1 cells were sorted using fluorescence-activated cell sorting (FACS) and individual clones were examined for Cx43 ablation. Cx43 protein levels were assessed via Western blotting and immunofluorescence. A minimum of two different CRISPR clones were used in all subsequent experiments. Cx43-ablated HEI-OC1 cells will be hereafter referred to as Cx43 KO cells.

5.2.8. WST-1 assay

Cell viability was analyzed using the WST-1 assay (Sigma, catalog# 5015944001). HEI-OC1 cells were plated at a density of $1x10^4$ cells (low density) or $3x10^4$ cells (high density) in each well of a 96 well dish and incubated overnight. HEI-OC1 cells were treated with the intended concentration of cisplatin in triplicate for 24 or 48 hours. HEI-OC1 cells were then treated with 1:10 dilution of WST-1 in fresh media for two hours. Wells with no cells or media only were used as a negative control. The optical density of each sample was measured using a spectrophotometer reader at 450nm and a reference wavelength at 630nm. Cell viability was determined by subtracting the reference absorbance, and the optical density of the negative control from each sample. Cell viability was then measured as a percentage of the cell viability of cells treated with saline, denoted as 100%.

5.2.9. Immunoblotting

Control or drug-treated HEI-OC1 cells were washed with PBS and lysed using 1x IP lysis buffer ((2x IP lysis buffer (2 % Triton X-100, 330mM NaCl, 20mM Tris, 2mM EDTA, 2mM EGTA, 1 % NP-40, pH 7.4), containing 1 tablet complete mini protease inhibitor cocktail (Sigma-Aldrich), 1:100 sodium fluoride (Millipore Sigma, catalog# SX0550-1) and 1:100 sodium orthovanadate (Sigma, catalog# S6508) phosphatase inhibitors in PBS. Once protein concentrations were measured, equal amounts of protein were resolved using SDS-PAGE (10% or 12% polyacrylamide gel) and were transferred to a nitrocellulose membrane using an

iBlot transfer system. Membranes were probed overnight with primary antibodies in 3% BSA dissolved in PBS Tween (0.05% Tween 20) unless indicated otherwise. Primary antibodies included: mouse anti-GAPDH (1:5000, EMD Millipore, catalog# MAB374), rabbit anti-Bax (dissolved in Tris-buffered saline (TBS) Tween, 1:1000, Cell Signaling, catalog#2772), and rabbit anti-BiP (1:1000, Sigma Aldrich, catalog# G8918). Membranes were then washed with PBS or TBS Tween and incubated with Alexa Fluor 680-conjugated anti-rabbit-IgG secondary antibody (1:5000, Life Technologies, catalog#A21057) or IRdye800-conjugated anti-mouse-IgG antibody (1:5000, Rockland, catalog#611-132-002) for one hour. Protein signals were then visualized using an Odyssey infrared imaging system (LiCor) and the intensity of the bands were quantified using Odyssey software. Protein expression was normalized to the loading control GAPDH.

5.2.10. Quantitative reverse transcriptase polymerase chain reaction (RT-PCR)

Total RNA was extracted from samples using RNeasy Mini Protocol for Isolation of Total RNA from Animal Cells (Qiagen, catalog# 74106) and converted to cDNA using the High Capacity cDNA Reverse Transcription Kit (ThermoFisher, catalog#4368814). Quantitative real-time polymerase chain reaction (qRT-PCR) was performed using PowerUp SYBR Green Master Mix (Life Technologies, Cat# A25742) and the cycle conditions for each primer consisted of: 50°C for 2 min, 95°C for 2 min, 95°C for 5 s, 60°C for 15 s for 40 cycles, followed by a melt curve. The following primers were used: 18s rRNA, the house keeping gene (forward, 5'- GTAACCCGTTGAACCCCATT; reverse, 5'-CCATCCAATCGGTAGTAGCG), manganese superoxide dismutase (MnSOD) (forward, 5'- GGCCAAGGGAGATGTTACAA; reverse, 5'- CCTTGGACTCCCACAGACAT), glutathione peroxidase (GPx1) (forward, 5' -GTCCACCGTGTATGCCTTCT; reverse 5' -CCTCAGAGAGACGCGACATT), catalase (forward, 5'- GGAGGCGGGAACCCAATAG; reverse, 5'-GTGTGCCATCTCGTCAGTGAA, Bcl-2 (forward, 5' –CCTGTGGATGACTGAGTACC; reverse, 5'-GAGACAGCCAGGAGAAATCA), Bax (forward, 5' –GTTTCATCCAGGATCGAGCA; reverse, 5'-CATCTTCTTCCAGATGGTGA). WT was set as a control and mRNA levels were normalized to 18s rRNA and measured using the ΔΔCT method.

5.2.11. Statistical analysis

Two-way analysis of variance (ANOVA) followed by Tukey's post hoc tests were used for hair cell counts, cell viability, cleaved caspase 3 staining, mRNA and protein analysis, and gap junction particle analysis at each individual cochlear region (i.e. apical, middle, and basal). A one-way ANOVA followed by Tukey's post hoc tests were performed for analyzing cleaved caspase 3 staining of organotypic cochlear cultures, and Pearson's correlation co-efficient of each cochlear region. A regression line analysis was performed for percent of dye recovery which was used to generate the area under the curve. Additional one-way ANOVAs followed by Tukey's post hoc tests were performed for HEI-OC1 cell experiments and are denoted in figure legends. All statistical analysis was performed using GraphPad Prism 6.

5.3. Results

5.3.1. Cx26 and Cx30 are abundantly expressed in the inner ear while Cx43 is detected at low levels

To assess the connexin content of organotypic cochlear cultures from Cx43 mutant and WT littermate mice, cultures were immunolabeled for Cx26 and Cx30. High levels of Cx26 and Cx30 protein were found in Kolliker's organ supporting cells of the cochlea (Figure 5.1A,B). Of note, there were no detectable changes in the distribution or levels of Cx26 or Cx30 in either Cx43 mutant mice compared to their respective WT littermates (Figure 5.1A,B). In all cases, both Cx26 and Cx30 appeared to be more predominantly found in the apical (low-frequency) regions compared to the basal (high-frequency) regions (Figure 5.1).

To examine the localization of Cx43 in the cochlea, Cx43 immunofluorescence labelling was performed on cross sections from young WT and mutant mice (P0 and P4) as well as organotypic cochlear cultures from WT mice. Low magnification confocal images of P0 and P4 cochleae revealed no Cx43 gap junctions in the organ of Corti (Figure 5.2A). Higher magnification confocal images also revealed no evidence for Cx43 in the organ of Corti, inner sulcus, or spiral limbus regions (Figure 5B).

Figure 5.1. Cx26 and Cx30 are highly expressed in supporting cells of organotypic cochlear cultures.

(A) Representative confocal images of Cx26 and Cx30 distribution in organotypic cochlear cultures from WT and $Cx43^{I130T/+}$ mutant mice denoting the apical (low-), middle (mid-), and, basal (high frequency) regions. (B) Representative confocal images of Cx26 and Cx30 distribution in organotypic cochlear cultures of WT and $Cx43^{G60S/+}$ mutant mice. OHC= outer hair cell, IHC= inner hair cell. Cx30 is denoted in green, Cx26 is in red, phalloidin labelling hair cell stereocilia is in white, and Hoechst nuclear stain is in blue. Scale bars =20μm.

Figure 5.1

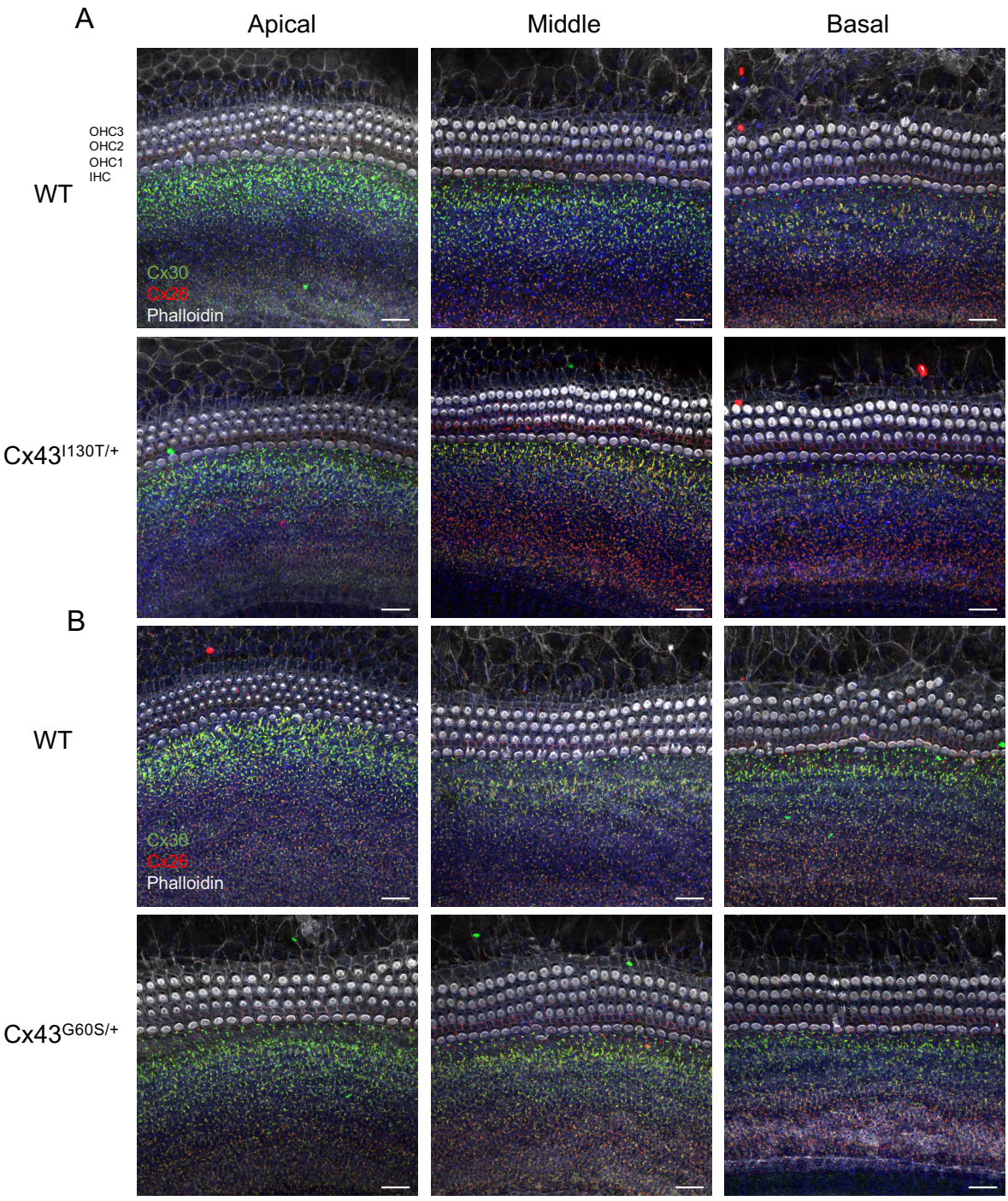
A
Apical
Middle
Basal
OHC3
OHC2
OHC1
IHC
WT
Cx30
Cx26
Phalloidin
Cx43I130T/+
B
WT
Cx30
Cx26
Phalloidin
Cx43G60S/+

Figure 5.2. Low but detectable amount of Cx43 are expressed in organotypic cochlear cultures.

(A) 3D reconstruction of consecutively stacked confocal images of cochleae obtained from $Cx43^{I130T/+}$ mutant mice and their WT littermates (P0 and P4). (B) Higher magnification images of specific cochlear regions of WT P4 cochleae. (C) Stacked confocal images of organotypic cochlear cultures from WT mice. (D) Schematic diagram representing the localization and relative expression levels of cochlear connexins in organotypic cochlear cultures. Cx43 is denoted in green, Cx26 is in red, phalloidin is in white, and Hoechst nuclear stain is in blue. Orange arrowheads indicate areas of gap junction plaques. Scale bars =10μm.

Figure 5.2.

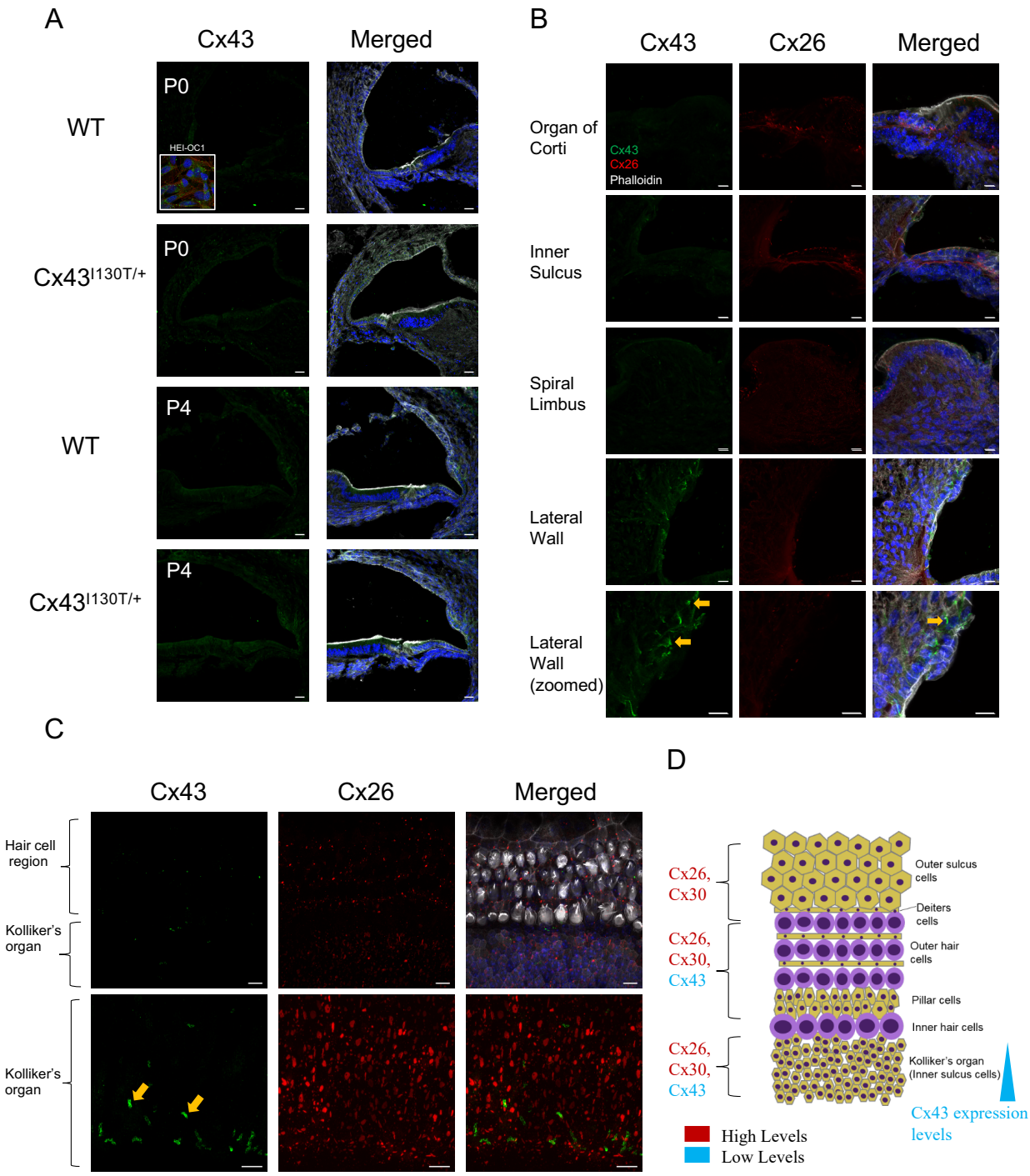
A
Cx43
Merged
WT
P0
HEI-OC1
Cx43I130T/+
P0
WT
P4
Cx43I130T/+
P4
B
Cx43
Cx26
Merged
Organ of Corti
Cx43
Cx26
Phalloidin
Inner Sulcus
Spiral Limbus
Lateral Wall
Lateral Wall (zoomed)
C
Cx43
Cx26
Merged
Hair cell region
Kolliker's organ
Kolliker's organ
D
Cx26, Cx30
Cx26, Cx30, Cx43
Cx26, Cx30, Cx43
Outer sulcus cells
Deiters cells
Outer hair cells
Pillar cells
Inner hair cells
Kolliker's organ (Inner sulcus cells)
Cx43 expression levels
High Levels
Low Levels

However, detectable Cx43 expression was found in the cochlear lateral wall region and in supporting cells of Kolliker's organ within organotypic cochlear cultures with higher expression in the inferior region of Kolliker's organ (Figure 5.2B,C). A diagrammatic representation of the relative distribution patterns of Cx26, Cx30, and Cx43 in organotypic cochlear cultures is outlined (Figure 5.2D).

5.3.2. Cisplatin causes hair cell death in Cx43 mutant mice and their WT littermates

Since we know that low levels of Cx43 are present in distinct regions of the organ of Corti, specifically the cochlear lateral wall, and we hypothesize that Cx43 is important in the development of the organ of Corti, we wanted to determine if organotypic cultures from Cx43 mutant mice have differential susceptibility to cisplatin-induced hair cell loss. First, organotypic cochlear cultures from control and $Cx43^{I130T/+}$ mutant mice were treated with 20 μM cisplatin for 48 hours and hair cells were immunolabeled for the hair cell body marker, MyosinVI, and phalloidin to visualize the hair cell stereocilia. There was no evidence of hair cell loss in untreated organotypic cochlear cultures from $Cx43^{I130T/+}$ mutant mice (Figure 5.3A). However, there was a significant decrease in the number of outer hair cells in all cochlear regions in cisplatin-treated cultures (Figure 5.3B). Notably, there were no differences between WT and $Cx43^{I130T/+}$ mutant hair cell loss after cisplatin treatment (Figure 5.3B). To further examine whether a severe loss of Cx43 function led to differential hair cell death, organotypic cultures from control and $Cx43^{G60S/+}$ mutant mice were treated with cisplatin. Cisplatin treatment caused a significant loss of outer hair cells, however, there were again no differences between WT and mutant cisplatin-treated organotypic cultures (Figure 5.3C).

5.3.3. Cisplatin induces regional changes in apoptosis in organotypic cochlear cultures from $Cx43^{G60S/+}$ mutant mice

One of the most common mechanisms by which cisplatin causes damage to the inner ear is through apoptosis. To examine whether reduced Cx43 function regulates the level of apoptosis, immunofluorescent staining of cleaved caspase 3 (CC3), a marker of late apoptosis, was examined. In untreated cultures, no CC3-positive hair cells were found, however, after cisplatin treatment CC3-positive hair cells were readily identified indicative of apoptosis (Figure 5.S1A,B).

Figure 5.3. Cisplatin causes hair cell loss in organotypic cochlear cultures from WT and $Cx43^{I130T/+}$ mutant mice.

(A) Representative confocal images of organotypic cochlear cultures from WT and $Cx43^{I130T/+}$ mutant littermate mice either untreated or treated with 20μM cisplatin for 48 hours. MyosinVI was immunolabeled to denote the hair cell body (green), phalloidin staining was used to demarcate actin (red), and Hoechst staining was used to locate the position of the nuclei (blue). (B) Quantitative analysis of hair cell counts in apical, middle, and basal regions of $Cx43^{I130T/+}$ and WT littermate mouse cultures, either untreated or treated with 20μM cisplatin. N values; WT untreated= 4, WT cisplatin= 5-6, $Cx43^{G60S/+}$ untreated= 5, $Cx43^{G60S/+}$ cisplatin= 4-5. (C) Quantitative analysis of hair cell counts in apical, middle, and basal regions of cultures for $Cx43^{G60S/+}$ mutant mice and WT littermates. N values; WT untreated= 4-6, WT cisplatin= 3-4, $Cx43^{G60S/+}$ untreated= 3-5, $Cx43^{G60S/+}$ cisplatin= 3-6. OHC= outer hair cell, IHC= inner hair cell. Means represent mean ± standard error. Scale bars= 20μm. Two-way ANOVAs were performed for each cochlear region with a subsequent Tukey's post hoc test. *$p<0.05$, **$p<0.01$, ***$p<0.001$.

Figure 5.3.

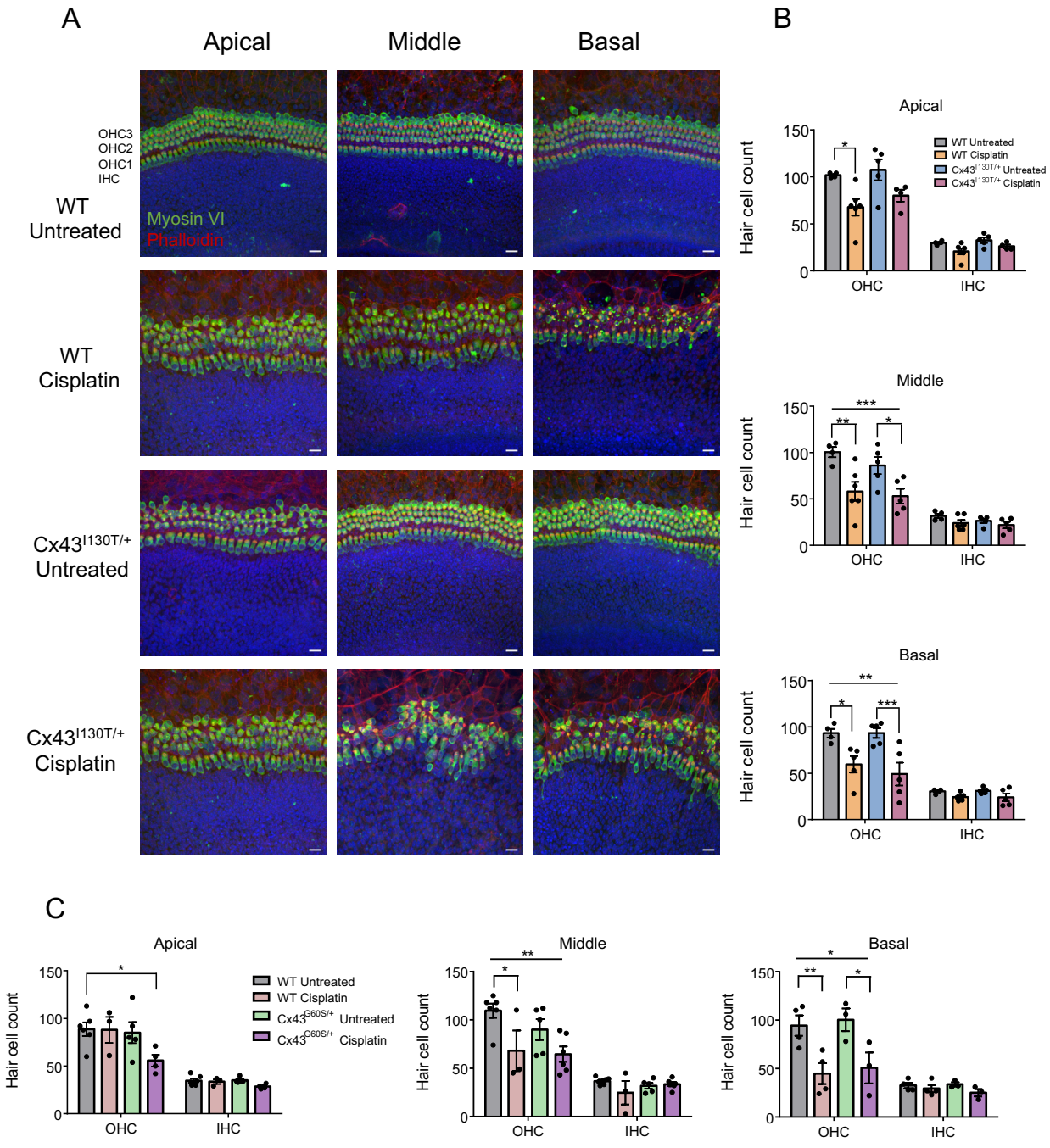
A
Apical
Middle
Basal
OHC3
OHC2
OHC1
IHC
WT Untreated
WT Cisplatin
Cx43I130T/+ Untreated
Cx43I130T/+ Cisplatin
Myosin VI
Phalloidin
B
Apical
Middle
Basal
Hair cell count
WT Untreated
WT Cisplatin
Cx43I130T/+ Untreated
Cx43I130T/+ Cisplatin
OHC
IHC
C
Apical
Middle
Basal
Hair cell count
WT Untreated
WT Cisplatin
Cx43G60S/+ Untreated
Cx43G60S/+ Cisplatin
OHC
IHC

In all regions there was a significant increase in the number of CC3 positive hair cells in cisplatin-treated WT cultures (Figure 5.S1A,B), however, there were no differences in the number of CC3-positive hair cells between WT and $Cx43^{I130T/+}$ mutant mice (Figure 5.S1A B). Similarly, the number of CC3-positive hair cells were significantly increased after cisplatin treatment in WT and $Cx43^{G60S/+}$ mutant mice (Figure 5.4A,B). Intriguingly, cisplatin-treated cultures from $Cx43^{G60S/+}$ mutant mice had a significant increase in CC3-positive hair cells in the middle turn compared to cisplatin treated WT littermates (Figure 5.4A,B).

5.3.4. Cx43 KO HEI-OC1 cells have similar sensitivity to cisplatin as WT cells

Dose controlled cisplatin treatments for 24 hours and 48 hours revealed that both WT and Cx43 KO cells had greatly reduced cell viability (Figure 5.5A). After 24 hours of low dose (10 μM) cisplatin treatment, Cx43 KO cells were unaffected as compared to WT cells, however, this difference did not persist at higher cisplatin doses or at the 48 hour time point (Figure 5.5A). To assess whether the extent of gap junction formation may play a role in cisplatin-induced cell death, cells were plated at low density to minimize gap junction assembly. While the IC50 was reduced by 50% when cells were plated at low density, there was no difference between WT and Cx43 KO cells (Figure 5.5A). The number of CC3-positive cells was significantly increased at both 15 μM and 30 μM cisplatin compared to untreated cells (Figure 5.5B,C). However, no differences in the number of CC3-positive cells were observed between WT and Cx43 KO cells (Figure 5.5C).

5.3.5. Reduced Cx26 and Cx30 colocalization after cisplatin treatment of organotypic cochlear cultures

To assess whether cisplatin alters cochlear connexin distribution, double-immunolabeling for Cx26 and Cx30 was performed on control and cisplatin-treated cochlear cultures from WT and $Cx43^{G60S/+}$ mutant mice. Representative confocal images of the basal region revealed altered hair cell morphology, hair cell loss, and supporting cell expansion, particularly in the pillar supporting cells (arrowheads), after cisplatin treatment (Figure 5.6A). High resolution Airyscan confocal images from the Kolliker's organ were acquired and Pearson's correlation coefficient was performed to assess the spatial localization of both Cx26 and Cx30.

Figure 5.4. CC3 is preferentially upregulated in cochlear cultures obtained from Cx43$^{G60S/+}$ mutant mice.

(A) Representative confocal images of the apical, middle, and basal regions of organotypic cochlear cultures from WT and Cx43$^{G60S/+}$ mice labelled for CC3 after being untreated or treated with 20μM cisplatin. CC3 is denoted in red, phalloidin in green, and nuclei in blue. (B) CC3- positive hair cells were quantified as hair cells labelled positive for CC3 and phalloidin. N values; WT untreated= 5, WT cisplatin= 5-6, Cx43$^{G60S/+}$ untreated= 4, Cx43$^{G60S/+}$ cisplatin= 3. Means represent mean ± standard error. Scale bars= 20μm. One-way ANOVA's were performed for each cochlear region and subsequently a post hoc Tukey's test was performed. *p<0.05, **p<0.01, ***p<0.001, ****p<0.0001.

Figure 5.4.

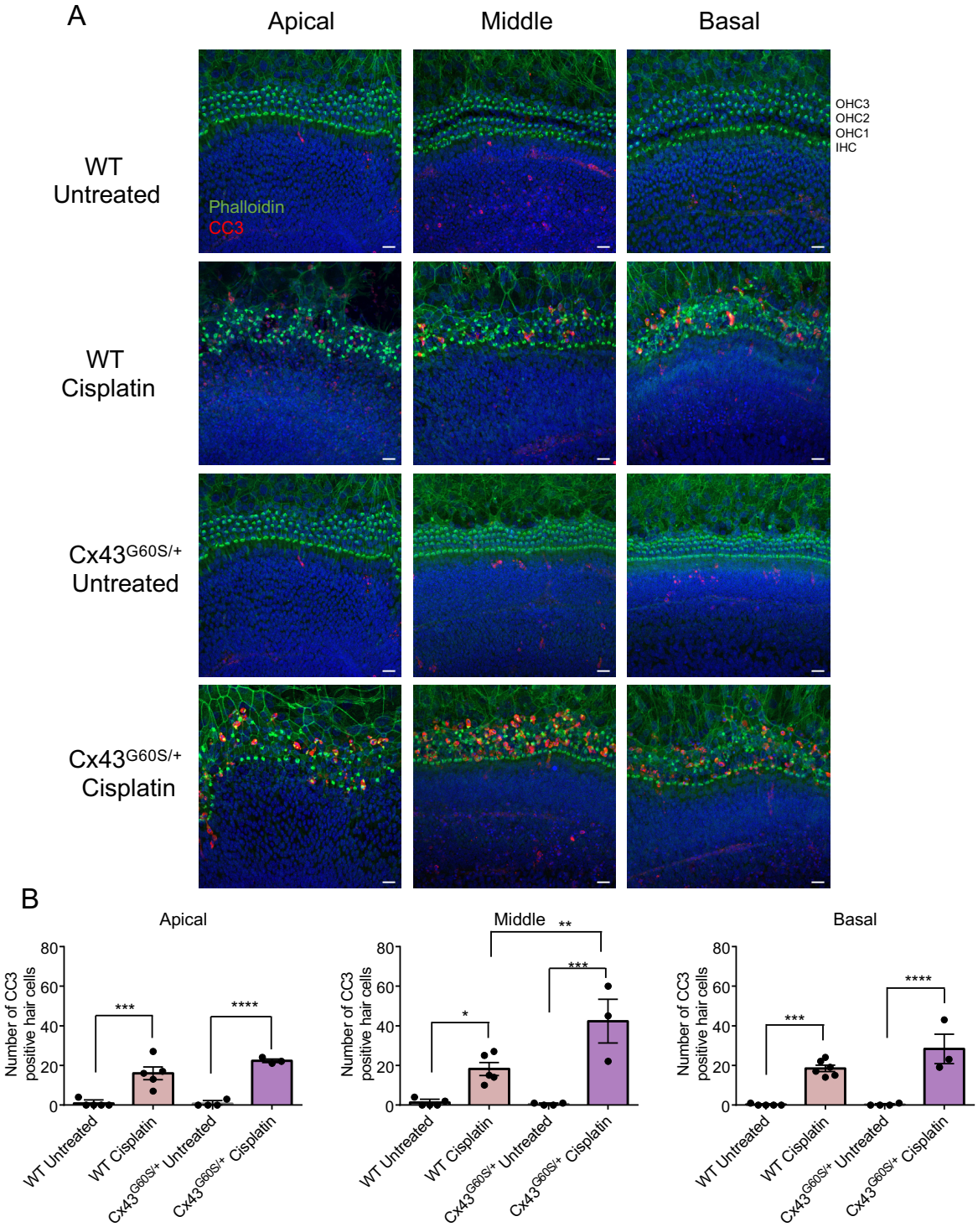
A
Apical
Middle
Basal
WT
Untreated
WT
Cisplatin
Cx43G60S/+
Untreated
Cx43G60S/+
Cisplatin
Phalloidin
CC3
OHC3
OHC2
OHC1
IHC
B
Apical
Middle
Basal
Number of CC3 positive hair cells
0
20
40
60
80
***
****
*
**
WT Untreated
WT Cisplatin
Cx43G60S/+ Untreated
Cx43G60S/+ Cisplatin

Figure 5.5. WT and Cx43-ablated HEI-OC1 cells both have reduced cell viability after cisplatin treatment.

(A) Cell viability of HEI-OC1 cells at 24 and 48 hours after cisplatin treatment. IC50s were calculated as the dose required to kill 50% of cells (B) Representative confocal images of CC3 staining in control and cisplatin-treated cells. CC3 is denoted in red, and nuclei are in blue. Staurosporine-treated cells were used as a positive control. (C) Quantification of the percentage of CC3-positive cells showed a significant increase in the percentage of CC3-positive cells after cisplatin treatment. Bars represent mean ± standard error from four independent experiments comprised of two different Cx43 KO HEI-OC1 clones. N values; WT: N=4, Cx43KO: N=7. Scale bars= 10μm. Two-way ANOVA with Tukey's post hoc test, *$p<0.05$, **$p<0.01$, ****$p<0.0001$.

Figure 5.5.

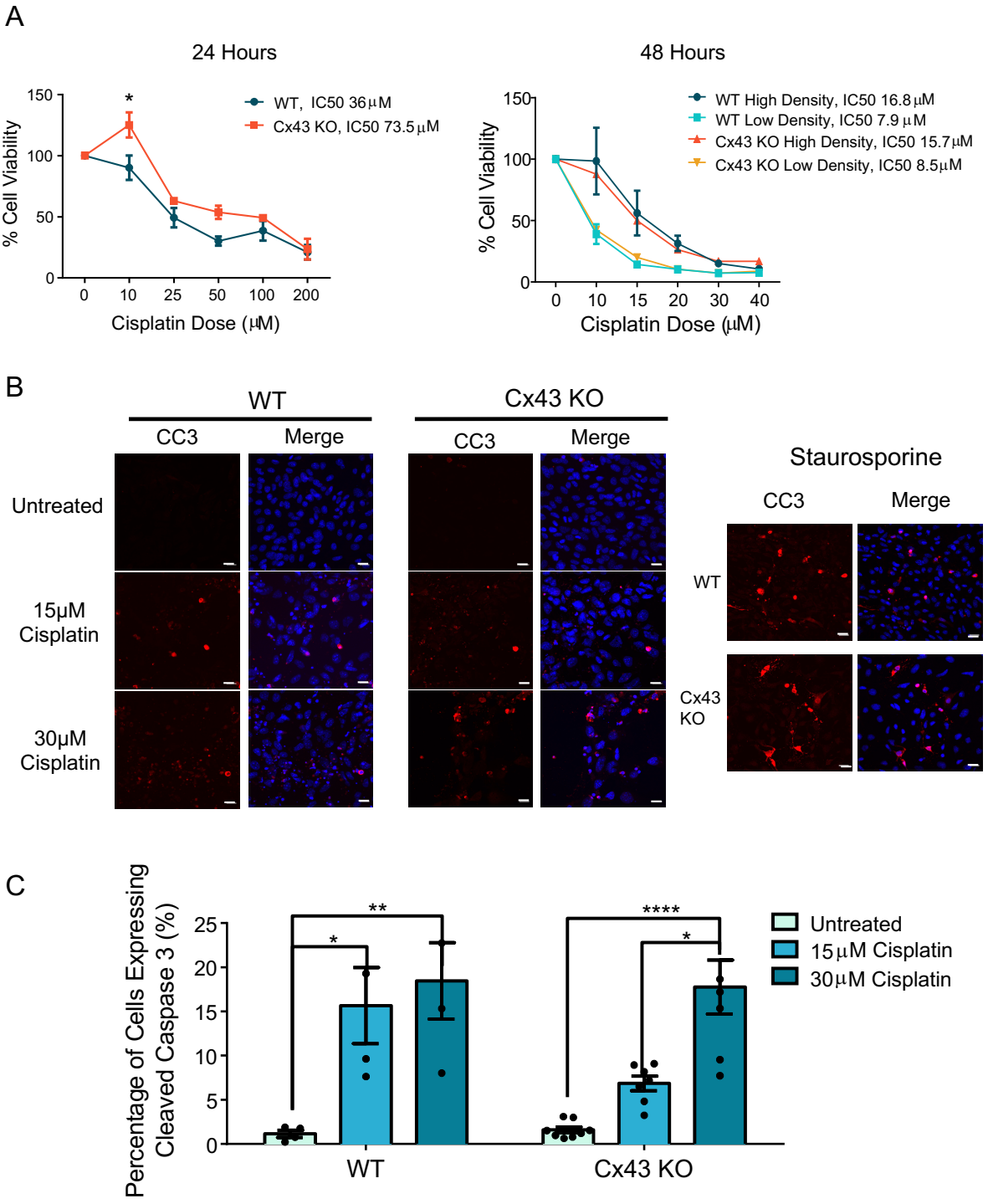
A
24 Hours
48 Hours
% Cell Viability
Cisplatin Dose (μM)
WT, IC50 36μM
Cx43 KO, IC50 73.5μM
WT High Density, IC50 16.8μM
WT Low Density, IC50 7.9μM
Cx43 KO High Density, IC50 15.7μM
Cx43 KO Low Density, IC50 8.5μM
B
WT
Cx43 KO
CC3
Merge
Staurosporine
Untreated
15μM Cisplatin
30μM Cisplatin
Cx43 KO
C
Percentage of Cells Expressing Cleaved Caspase 3 (%)
Untreated
15μM Cisplatin
30μM Cisplatin

Figure 5.6. Cisplatin treatment alters the spatial location of hair cells, causes supporting cell expansion, and induces the reorganization of Cx26 and Cx30 gap junctions.

(A) Representative confocal images of the basal region of organotypic cochlear cultures obtained from untreated and cisplatin-treated $Cx43^{G60S/+}$ mutant mice and WT littermates. Orange arrows denote areas of Pillar cell expansion. (B) High magnification Airyscan images were acquired of the basal area from the inner sulcus region. Cx26 is denoted in red and Cx30 is in green. (C) Pearson's correlation coefficient was quantified in apical, middle, and basal regions of organotypic cultures to measure Cx26 and Cx30 co-localization. N values; WT untreated= 5-6, WT cisplatin= 3-5, $Cx43^{G60S/+}$ untreated= 6-7, $Cx43^{G60S/+}$ cisplatin= 4-6. Means represent mean ± standard error. Scale bars= 10μm. One-way ANOVA's were performed for each cochlear region and subsequently a post hoc Tukey's test was performed. *$p<0.05$.

Figure 5.6.

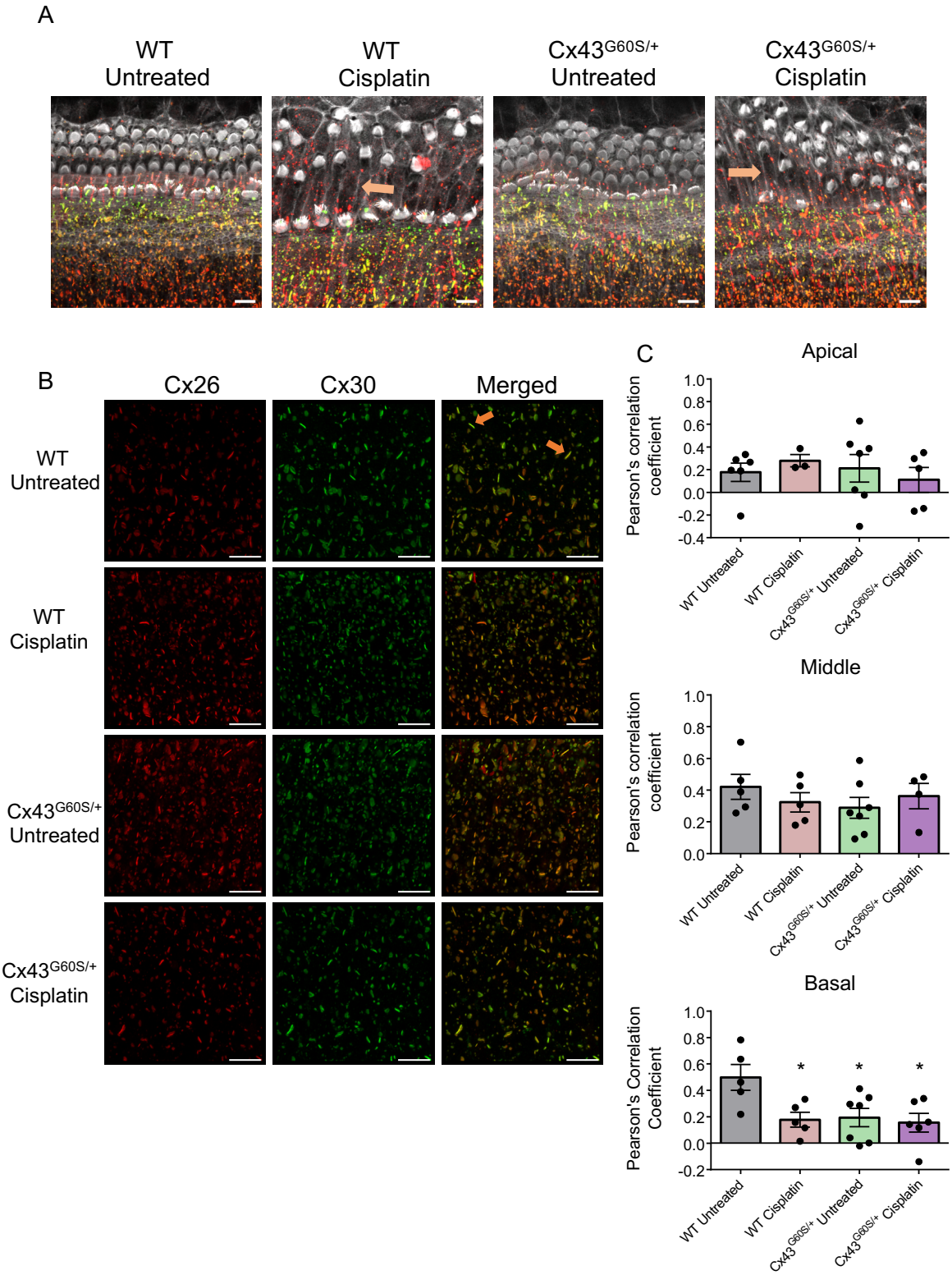
A
WT Untreated
WT Cisplatin
Cx43G60S/+ Untreated
Cx43G60S/+ Cisplatin
B
Cx26
Cx30
Merged
WT Untreated
WT Cisplatin
Cx43G60S/+ Untreated
Cx43G60S/+ Cisplatin
C
Apical
Middle
Basal
Pearson's correlation coefficient
Pearson's Correlation Coefficient
1.0
0.8
0.6
0.4
0.2
0.0
-0.2
-0.4
WT Untreated
WT Cisplatin
Cx43G60S/+ Untreated
Cx43G60S/+ Cisplatin
*

Cx26 and Cx30 were colocalized in untreated cultures within the basal region with a correlation coefficient of approximately 0.5, suggesting that 50% of Cx26 and Cx30 were co-localized (Figure 5.6B,C).

After cisplatin treatment, Cx26 and Cx30 were predominantly found separated into their own distinct gap junction plaques as colocalization was significantly decreased (Figure 5.6B,C). Interestingly, both untreated and cisplatin-treated cultures from $Cx43^{G60S/+}$ mutant mice had significantly decreased Cx26 and Cx30 colocalization compared to WT untreated cultures (Figure 5.6B,C). Particle analysis was performed to determine the average intensity, number of gap junction plaques, and the size of gap junction plaques in untreated and cisplatin-treated cultures. No differences were found in any of the parameters tested in untreated and cisplatin-treated cultures (Figure 5.S2A-C).

5.3.6. Carbenoxolone decreases Cx26 and Cx30 levels and GJIC in organotypic cochlear cultures

We next took a pharmacological approach to determine if blocking all cochlear gap junction function would attenuate the effect of cisplatin-induced cell death. To confirm that carbenoxolone (CBX) blocked GJIC in WT organotypic cochlear cultures, fluorescence recovery after photobleaching (FRAP) was performed. As expected, supporting cells in the Kolliker's organ region were well coupled via gap junctions as WT cultures recovered approximately 60% of their initial fluorescence intensity after photobleaching (Figure 5.7A,B). However, CBX treated cultures exhibited a greatly reduced fluorescence recovery (Figure 5.7A,B). Cells from untreated cultures in the outer sulcus region of cochlear cultures were also well coupled, but to a lesser degree than cells of Kolliker's organ region, as they recovered approximately 30% of their original fluorescence intensity (Figure 5.7A,B). A linear regression analysis of the slopes of the lines and assessment of the area under the curve of the linear regression all confirmed that CBX treatment significantly inhibited GJIC in both inner and outer sulcus regions (Figure 5.7A-C). To assess whether CBX treatment altered Cx26 and Cx30 levels, organotypic cultures were treated with 100 μM CBX, 20 μM cisplatin, or a combination of 100 μM CBX + 20 μM cisplatin.

Figure 5.7. Carbenoxolone blocks calcein dye transfer in cochlear supporting cells.

(A) Representative images of prebleach, bleached, and dye recovery after photobleach of calcein fluorescence in untreated or CBX-treated cochlear culture regions. Dashed areas represent photobleached regions. The photobleached region of inner sulcus cells was 288.5μm^2. (B) Percentage of fluorescence recovery compared to baseline in the inner and outer sulcus regions of untreated or 100μM CBX-treated cochlear cultures. (C) Area under the curve for both inner and outer sulcus regions revealed that CBX was an effective inhibitor of dye transfer. N=3, n=6 in each group and for each region. CBX= carbenoxolone treated. Scale bars= 10μm. Linear regression analysis of slopes performed for each region and area, ****$p<0.0001$.

Figure 5.7.

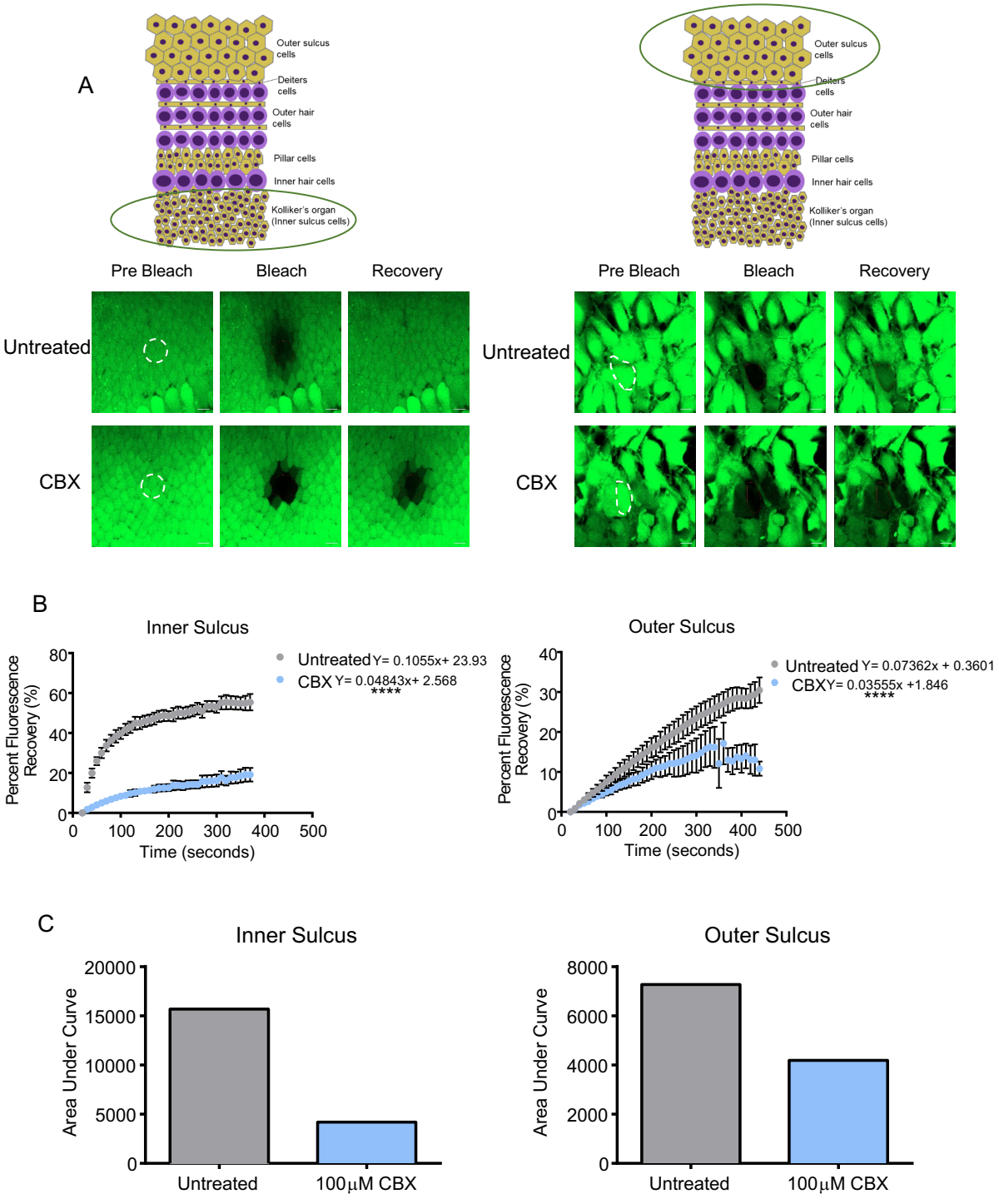
A
Outer sulcus cells
Deiters cells
Outer hair cells
Pillar cells
Inner hair cells
Kolliker's organ (Inner sulcus cells)
Pre Bleach
Bleach
Recovery
Untreated
CBX
B
Inner Sulcus
Untreated Y= 0.1055x+ 23.93
CBX Y= 0.04843x+ 2.568
****
Percent Fluorescence Recovery (%)
Time (seconds)
Outer Sulcus
Untreated Y= 0.07362x + 0.3601
CBX Y= 0.03555x +1.846
****
C
Inner Sulcus
Area Under Curve
Untreated
100μM CBX
Outer Sulcus

At low magnification of cultures treated with CBX, little immunolabeled Cx26 or Cx30 was detected as compared to the abundant signal found in untreated and cisplatin-treated cultures (Figure 5.S3A). Similarly, at higher magnification, supporting cells of the inner sulcus and outer sulcus regions expressed abundant amounts of Cx26 and Cx30 in both the untreated and cisplatin-treated groups, but both isoforms were undetectable after CBX treatment (Figure 5.S3B).

5.3.7. Blocking gap junctions does not alter cisplatin-induced hair cell death

Since CBX was a found to be an excellent blocker of cochlear connexins we assessed if this caused a change in hair cell susceptibility to cisplatin-induced cell death. Representative images of hair cells revealed that CBX treatment did not induce cell death, but cisplatin alone or in combination with CBX was a potent inducer of hair cell death (Figure 5.8A). Specifically, hair cell counts revealed that when 20 μM cisplatin and 100 μM CBX were co-administered, there were no significant differences in hair cell number compared to cisplatin treatment alone (Figure 5.8B). Thus, blocking gap junctions in cochlear organotypic cultures does not affect cisplatin-induced hair cell loss.

5.3.8. WT and Cx43 KO HEI-OC1 cells undergo different mechanistic routes leading to cisplatin-induced cell death

To examine the mechanisms of action of cisplatin-induced cell death in gap junction competent and deficient HEI-OC1 cells, markers of reporter proteins for intrinsic mitochondrial cell death and endoplasmic reticulum (ER) stress were assessed. First, to assess whether WT or Cx43 KO cells have differential susceptibility to reactive oxygen species (ROS) accumulation, mRNA expression of antioxidant enzymes were examined. A series of antioxidants including: manganese superoxide (MnSOD), catalase, and glutathione peroxidase (GPx1) were significantly increased after 15 μM and/or 30 μM cisplatin treatment for 48 hours in Cx43 KO but not in WT cells (Figure 5.S4A). To implicate a role for the mitochondrial pathway, the Bax (pro-apoptotic) and Bcl-2 (anti-apoptotic) mRNA ratio was elevated in both cell lines with more profound upregulation in WT HEI-OC1 cells, suggesting enhanced mitochondrial dysfunction. In addition, western blots showed that Bax protein expression in WT HEI-OC1 cells was significantly increased after treatment with 15 μM cisplatin, however no differences were found in Cx43 KO cells (Figure 5.S4B,C).

Figure 5.8. Blocking gap junctions does not impact cisplatin-induced hair cell loss.

(A) Representative confocal images of hair cells in WT cultures that were untreated or treated with 100μM carbenoxolone (CBX), 20μM cisplatin, or 100μM CBX and 20μM cisplatin (Cisplatin + CBX) for 48 hours. MyosinVI is denoted in green, phalloidin is in red, and nuclei are in blue. (B) Quantification of hair cell counts from all four treatment groups at the apical, middle, and basal regions. N values; untreated=4-7, CBX= 4-6, Cis= 4, Cis+ CBX= 3-5. OHC= outer hair cell, IHC= inner hair cell. Bars represent mean ± standard error. Scale bars= 20μm. Two way ANOVA's and subsequent Tukey's post hoc tests were performed for each region. *p<0.05, **p<0.01, ***p<0.001, ****p<0.0001.

Figure 5.8.

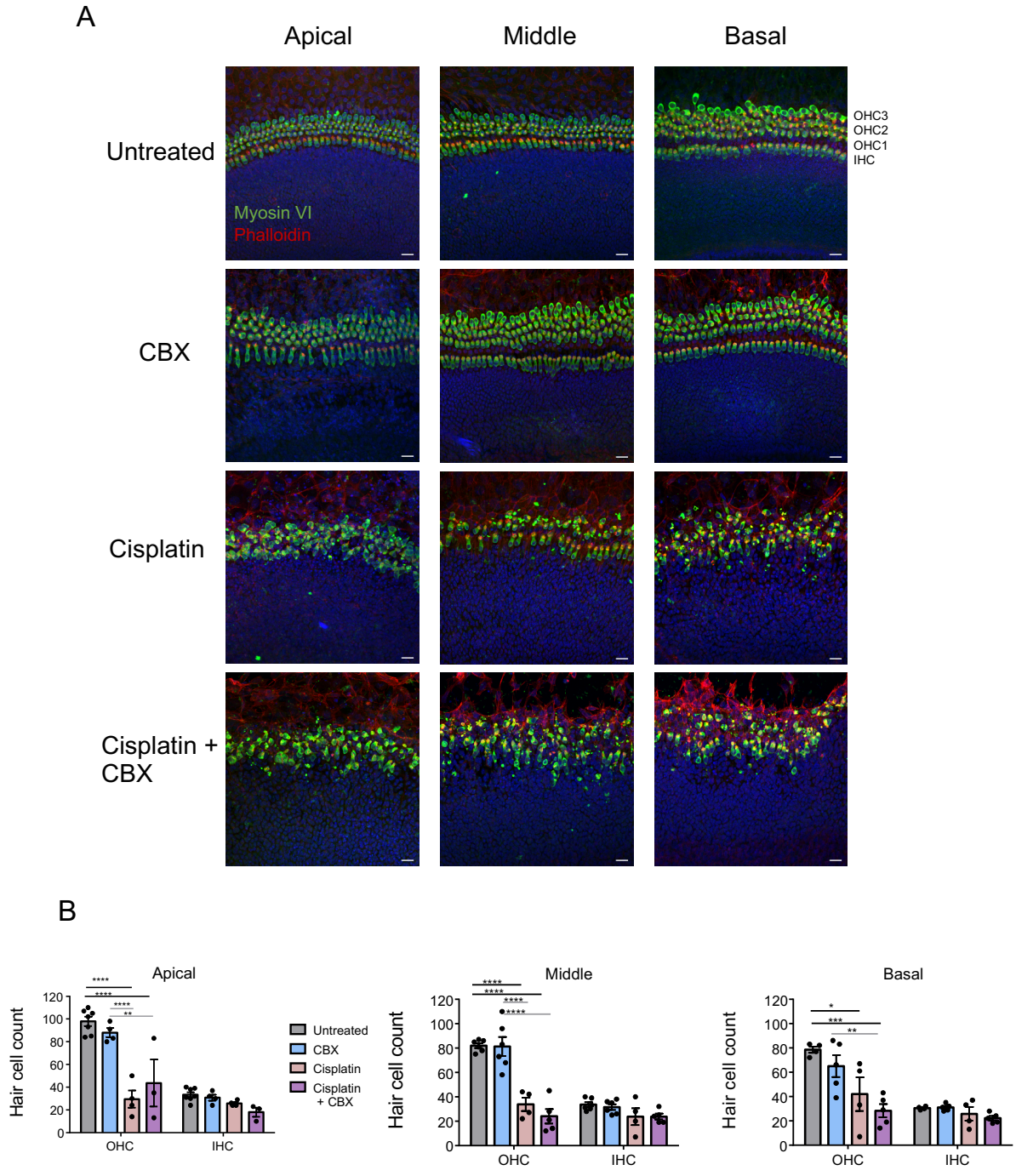
A
Apical
Middle
Basal
Untreated
CBX
Cisplatin
Cisplatin +
CBX
Myosin VI
Phalloidin
OHC3
OHC2
OHC1
IHC
B
Apical
Middle
Basal
Hair cell count
OHC
IHC
Untreated
CBX
Cisplatin
Cisplatin
+ CBX

To evaluate if ER stress is at the root of cisplatin-induced cell death, the expression of immunoglobulin protein (BiP), an ER chaperone protein upregulated during ER stress, was examined. Immunofluorescence revealed that BiP was readily detected after cisplatin treatment in both WT and Cx43 KO HEI-OC1 cells and was localized to the ER compartment as evident by colocalization with protein disulfide isomerase (PDI) (Figure 5.S5A). Western blots revealed that BiP was found in higher abundance in Cx43 KO but not WT cells after cisplatin treatment compared to untreated cells (Figure 5.S5B,C).

Figure S 5.1. Cleaved caspase 3 is upregulated after cisplatin treatment.

(A) Representative confocal images of organotypic cochlear cultures labelled for cleaved caspase 3 (CC3) both in untreated and in 20 μM cisplatin treated cultures from $Cx43^{I130T/+}$ mutant mice and WT littermates. CC3 is denoted in red, phalloidin is in green, and nuclei are in blue. (B) CC3-positive hair cells were quantified as hair cells labelled positive for CC3 and phalloidin. N values; WT untreated= 4-5, WT cisplatin= 5-7, $Cx43^{I130T/+}$ untreated= 4, $Cx43^{I130T/+}$ cisplatin= 4. Bars represent means ± SEM. Scale bars= 20 μm. One-way ANOVAs were performed for each cochlear region and subsequently a post hoc Tukey's test was performed. *$p<0.5$, **$p<0.01$, ***$p<0.001$.

Figure S 5.1.

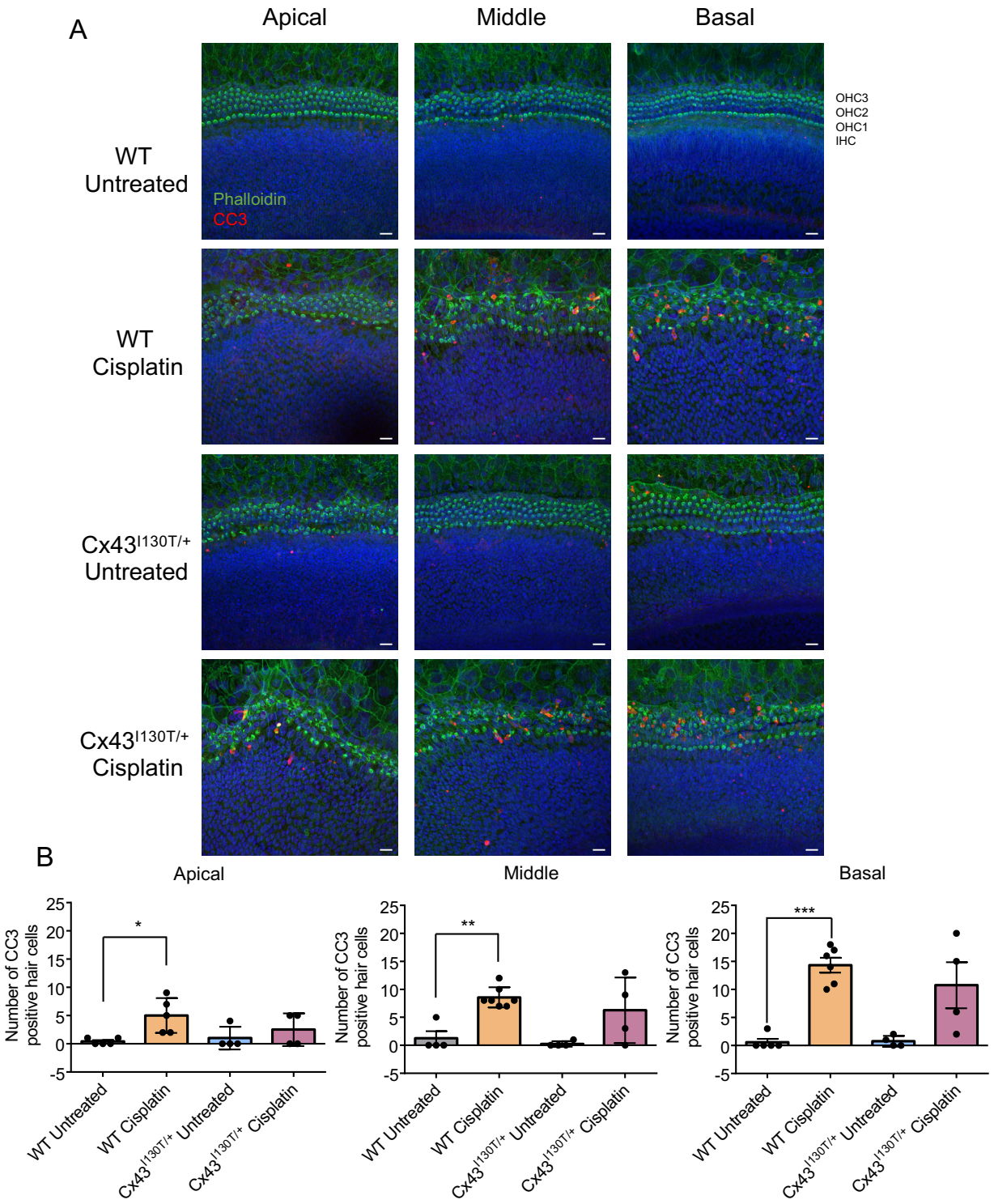
A
Apical
Middle
Basal
WT
Untreated
WT
Cisplatin
Cx43I130T/+
Untreated
Cx43I130T/+
Cisplatin
Phalloidin
CC3
OHC3
OHC2
OHC1
IHC
B
Apical
Middle
Basal
Number of CC3 positive hair cells
25
20
15
10
5
0
-5
*
**
***
WT Untreated
WT Cisplatin
Cx43I130T/+ Untreated
Cx43I130T/+ Cisplatin

Figure S 5.2. Assessment of Cx26 and Cx30 levels in organotypic cochlear cultures after cisplatin treatment.

Double-labeled immunofluorescence for Cx26 and Cx30 was performed in WT and $Cx43^{G60S/+}$ mutant mice before and after cisplatin treatment. Particle analysis plugin on ImageJ was used to quantify the expression and number of gap junctions in the inner sulcus region of littermate mice. (A) Cx30 and Cx26 average intensity levels were analyzed in $Cx43^{G60S/+}$ mutant mice and their WT littermates in control cultures and after 20μM cisplatin treatment for 48 hours. (B) The number of Cx30 and Cx26 gap junction plaques were quantified. (C) Average gap junction plaque size was quantified. N values; WT untreated= 5, WT cisplatin= 4, $Cx43^{G60S/+}$ untreated=6-7, $Cx43^{G60S/+}$ cisplatin= 3-4. Means represent mean ± standard error.

Figure S 5.2.

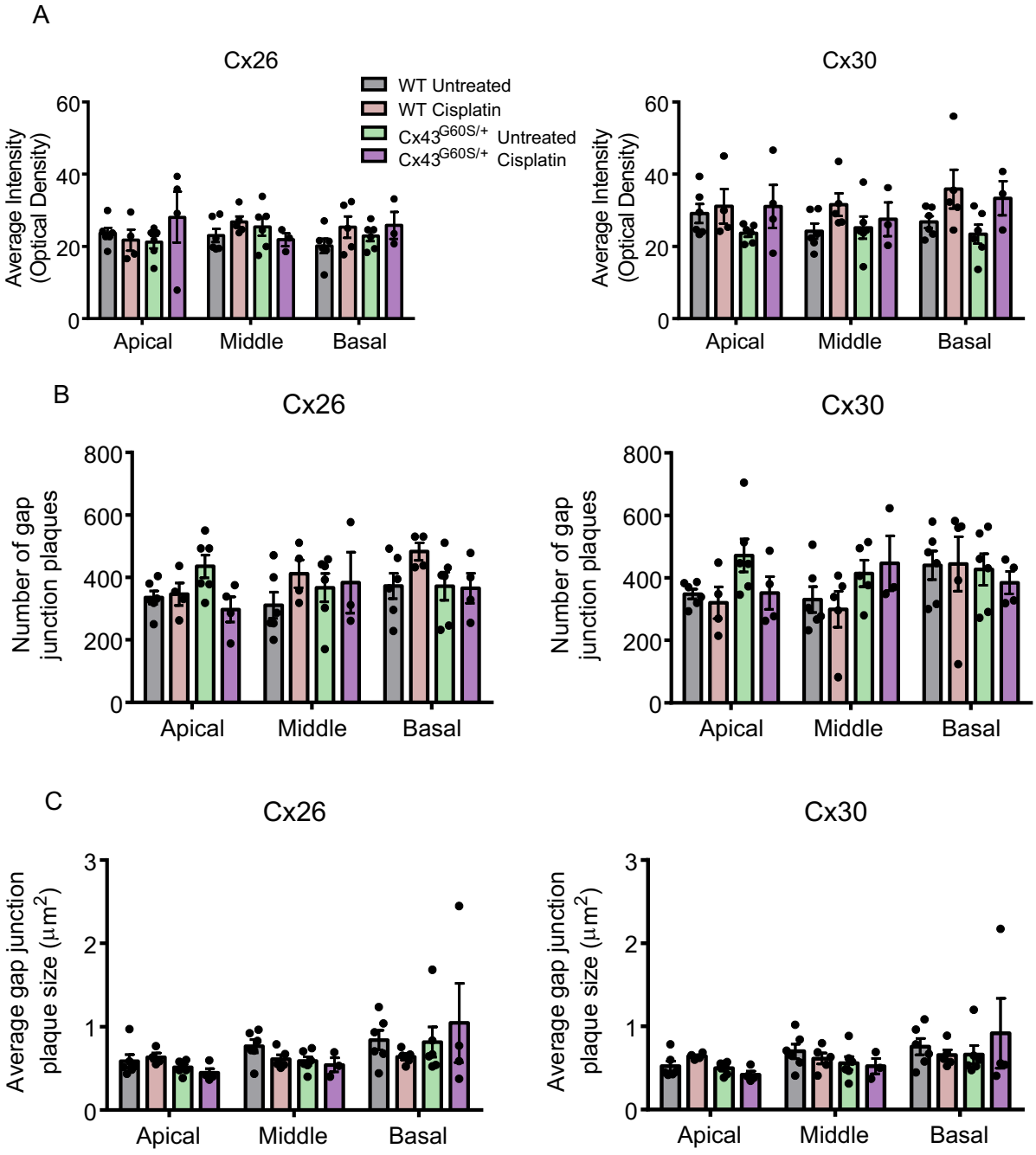
A
Cx26
Cx30
WT Untreated
WT Cisplatin
Cx43G60S/+ Untreated
Cx43G60S/+ Cisplatin
Average Intensity (Optical Density)
0
20
40
60
Apical
Middle
Basal
B
Number of gap junction plaques
0
200
400
600
800
C
Average gap junction plaque size (μm2)
0
1
2
3

Figure S 5.3. Carbenoxolone reduced the number of Cx26 and Cx30 gap junctions in cochlear supporting cells.

(A) Double-immunofluorescent labeling for Cx26 and Cx30 was performed on the basal region of organotypic cochlear cultures before and after carbenoxolone (CBX) and/or cisplatin treatment. (B) Higher magnification images of Cx30 and Cx26 in supporting cells of the inner sulcus region (C) outer sulcus region. Cx30 is denoted in green, Cx26 is in red, phalloidin is in white, and nuclei are in blue. Scale bars= 20μm.

Figure S 5.3.

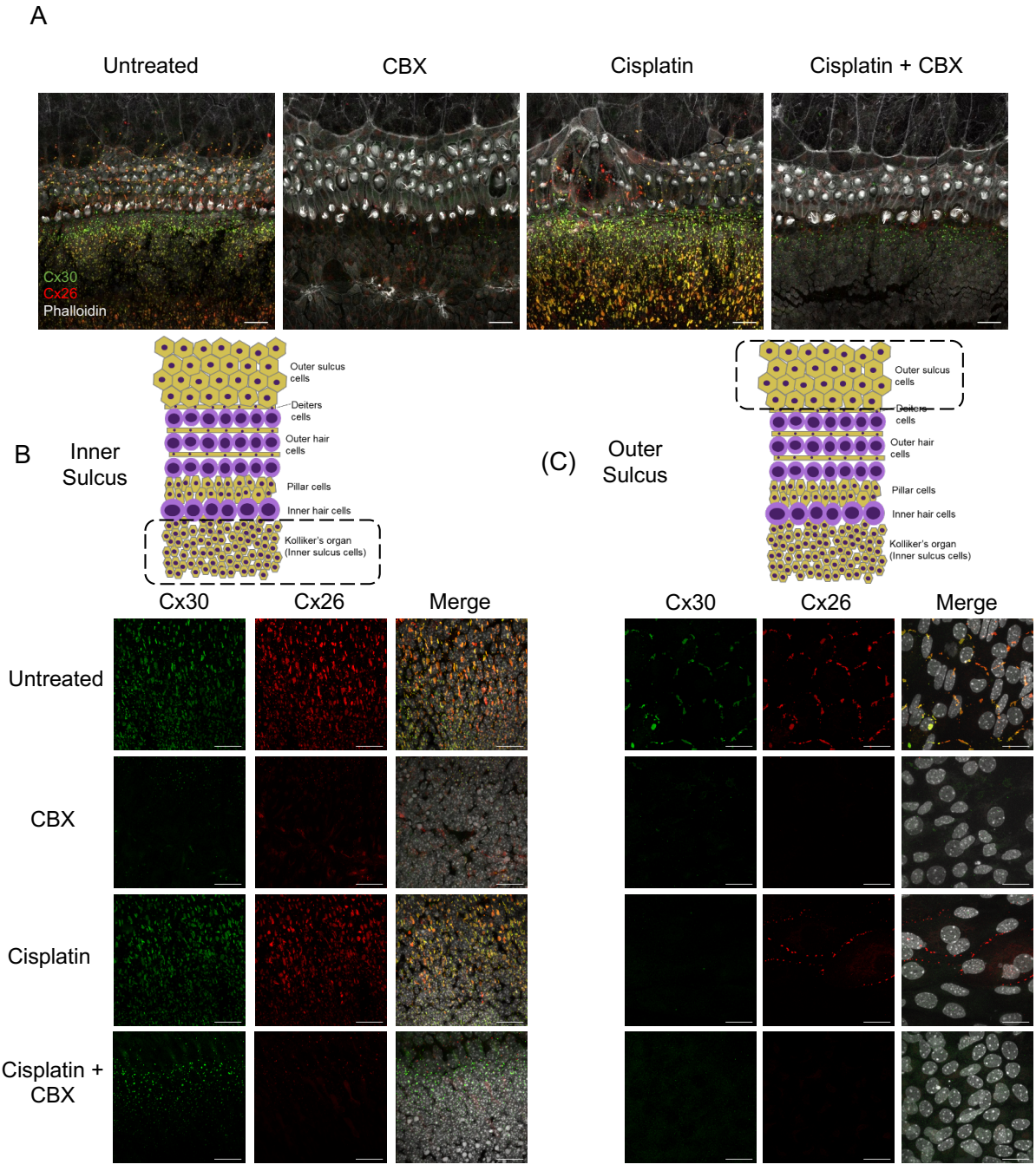
A
Untreated
CBX
Cisplatin
Cisplatin + CBX
Cx30
Cx26
Phalloidin
B
Inner Sulcus
Outer sulcus cells
Deiters cells
Outer hair cells
Pillar cells
Inner hair cells
Kolliker's organ (Inner sulcus cells)
(C)
Outer Sulcus
Cx30
Cx26
Merge
Untreated
CBX
Cisplatin
Cisplatin + CBX

Figure S 5.4 Cx43-ablated HEI-OC1 cells have increased mRNA expression of antioxidant enzymes after cisplatin treatment.

(A) Quantitative real time polymerase chain reaction (qRT-PCR) of antioxidant enzymes: manganese superoxide dismutase (MnSOD), catalase, and glutathione peroxidase (GPx1) from control and Cx43-ablated HEI-OC1 cells after cisplatin treatment. The ratio of proapoptotic Bax to anti-apoptotic Bcl-2 mRNA levels were also calculated. Bars represent mean ± standard error from four independent experiments comprised of two independent Cx43 KO clones. N values; WT: N=4, Cx43 KO: N=7. (B, C) Western blot and quantification of Bax protein expression. GAPDH was used as a protein loading control. N values; WT: N=4, Cx43KO: N=5-7. Two-way ANOVA with Tukey's posthoc test, *$p<0.05$, **$p<0.01$, ***$p<0.001$. $P<0.05$ Represents one-way ANOVA and subsequent Tukey's post hoc test performed.

Figure S 5.4.

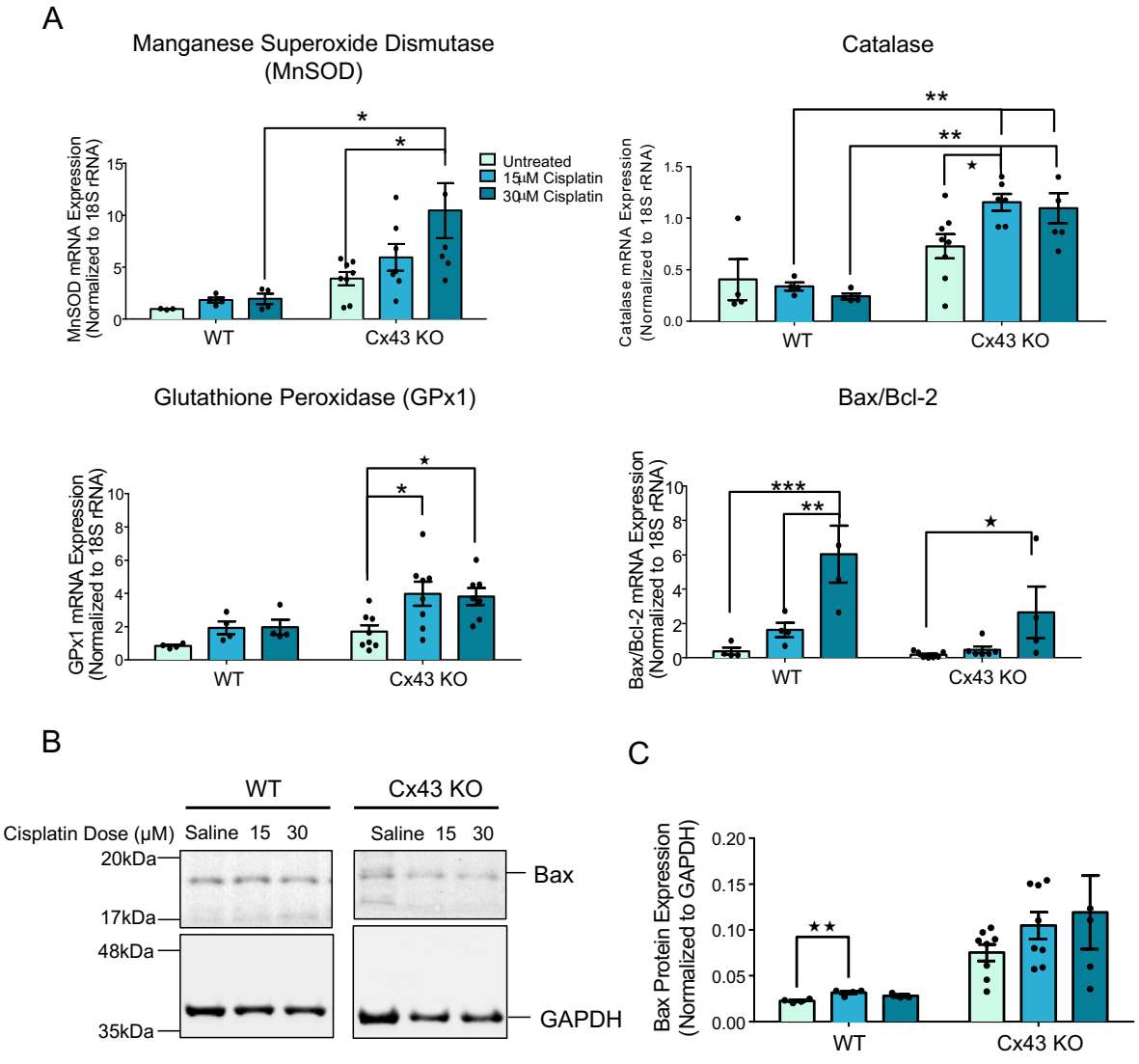
A
Manganese Superoxide Dismutase (MnSOD)
MnSOD mRNA Expression (Normalized to 18S rRNA)
Untreated
15 μM Cisplatin
30 μM Cisplatin
WT
Cx43 KO
Catalase
Catalase mRNA Expression (Normalized to 18S rRNA)
Glutathione Peroxidase (GPx1)
GPx1 mRNA Expression (Normalized to 18S rRNA)
Bax/Bcl-2
Bax/Bcl-2 mRNA Expression (Normalized to 18S rRNA)
B
WT
Cx43 KO
Cisplatin Dose (μM) Saline 15 30
Saline 15 30
20kDa
17kDa
48kDa
35kDa
Bax
GAPDH
C
Bax Protein Expression (Normalized to GAPDH)

Figure S 5.5. HEI-OC1 cells lacking Cx43 preferentially undergo an ER stress response after cisplatin treatment

(A) Representative confocal images of BiP expression and localization in WT and Cx43KO HEI-OC1 cells treated with saline, 15μM, or 30μM cisplatin for 48 hours. BiP is in green, PDI (an ER resident marker) is in red, and blue are nuclei. WT HEI-OC1 cells treated with thapsigargin, a known activator of ER stress were used as a positive control. (B) Western blot for BiP protein expression in untreated and cisplatin-treated cells. GAPDH was used as a loading control. (C) Quantification of BiP protein expression in cells treated with saline (untreated), 15μM, or 30μM cisplatin for 48 hours. Bars represent mean ± standard error from four independent experiments comprised of two independent Cx43 KO clones. N values; WT: N=3-4, Cx43KO: N=5-8. Scale bars=10μm. Two-way ANOVA, *$p<0.05$. $P<0.05$ represents one way-ANOVA followed by a Tukey's post hoc test.

Figure S 5.5.

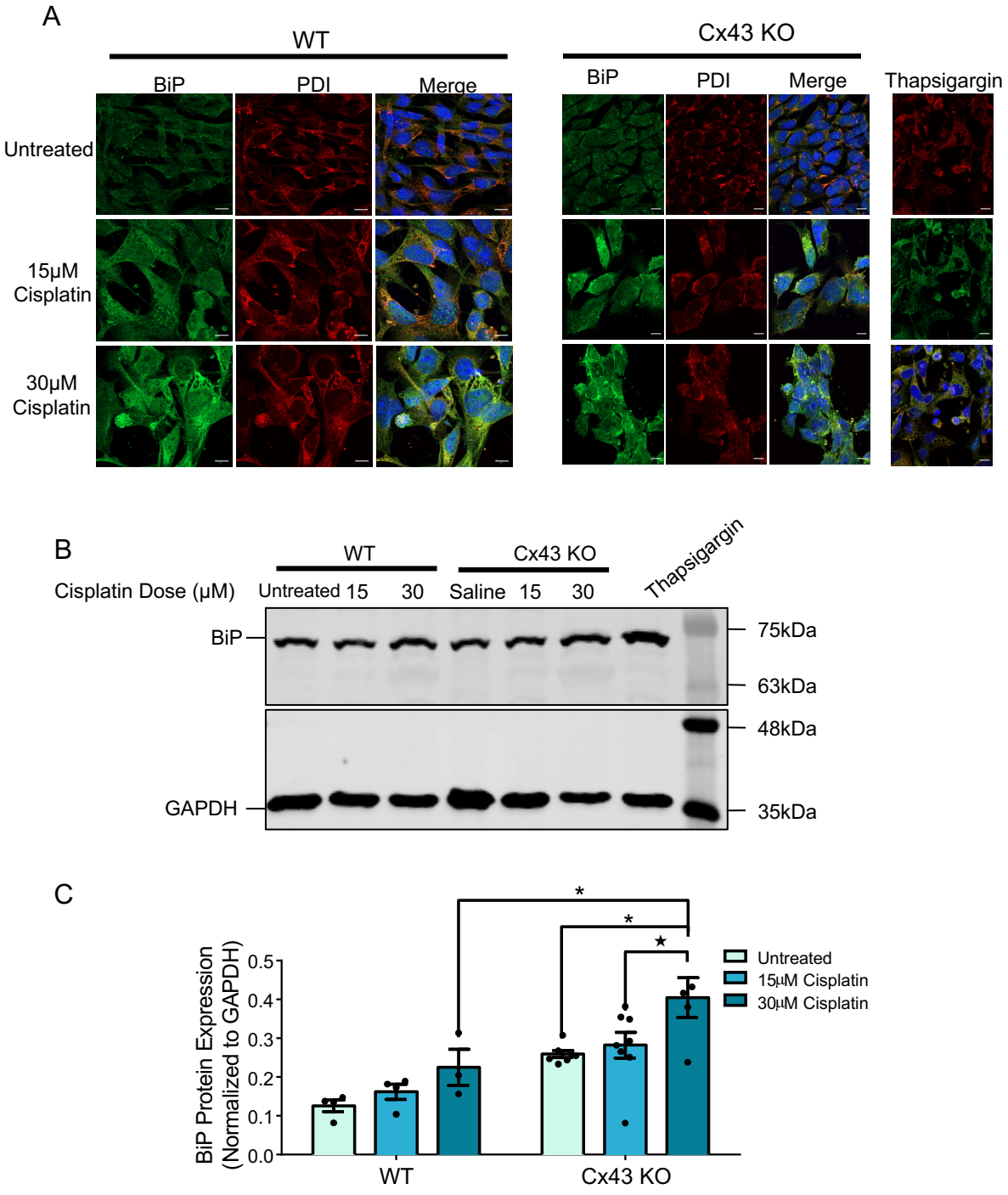
A
WT
Cx43 KO
BiP
PDI
Merge
BiP
PDI
Merge
Thapsigargin
Untreated
15μM Cisplatin
30μM Cisplatin
B
WT
Cx43 KO
Thapsigargin
Cisplatin Dose (μM)
Untreated 15 30
Saline 15 30
BiP
GAPDH
75kDa
63kDa
48kDa
35kDa
C
BiP Protein Expression (Normalized to GAPDH)
0.5
0.4
0.3
0.2
0.1
0.0
WT
Cx43 KO
Untreated
15μM Cisplatin
30μM Cisplatin
*
*
★

5.4. Discussion

Cisplatin is one of the most effective and commonly used chemotherapeutic drugs to treat solid cancer tumors but causes hearing loss in approximately 75-100% of patients [25]. The reason(s) why this sensory organ is so highly susceptible to cisplatin damage is not entirely clear but may be related to the organ of Corti being highly enriched with gap junctions that mediate small molecule (potentially toxic) exchange between connecting cells. Related studies have shown that Cx43-mediated GJIC plays a bystander role in cancer cell lines where downregulating Cx43 leads to protection against cisplatin-induced cell death [34–36]. Although the role of Cx43 in hearing and its localization pattern in the cochlea remain controversial, we have shown for the first time that Cx43 is expressed in organotypic cochlear cultures of neonatal mice. Interestingly, both Cx26 and Cx30 expression were more pronounced in the apical (low frequency) region of organotypic cochlear cultures compared to the basal (high frequency) region, a finding that has also been reported in guinea pigs [37]. This is of particular interest due to the fact that hearing loss generally occurs primarily in the high frequency areas [38,39], a phenomenon that could be due to lowered Cx26 and Cx30 expression within this region.

Although Cx43 has been reported to exacerbate cisplatin-induced cell death, these studies have primarily been examined in cancer cell lines including: testicular [30,36], lung [34][40], ovarian, [34], prostate, and breast [41]. Recently, a study showed that although Cx43 increased cell death in cisplatin-treated testicular cancer cells, this effect was reversed in non-cancerous testicular cells where Cx43 downregulation led to enhanced cisplatin-induced cell death [30]. This suggests that Cx43 may play distinct roles with either propagation of death signals (bystander) or beneficial signals (Good Samaritan) in cisplatin treatment depending on the cell status. To further examine the role of Cx43 in cisplatin-induced ototoxicity, $Cx43^{I130T/+}$ and $Cx43^{G60S/+}$ mutant mice harboring a moderate and severe reduction of Cx43-mediated GJIC, respectively, were used. In the case of $Cx43^{I130T/+}$ mutant mice, we have established that the expected level of Cx43-mediated GJIC is ~50% while $Cx43^{G60S/+}$ mutant mice have only ~20% functional Cx43 [32,33]. We know that $Cx43^{G60S/+}$ mice exhibit severe hearing loss, thereby linking Cx43 to hearing function [23]. Organotypic cochlear cultures from these mutant mice provide an ideal setting to assess Cx43 function on cisplatin-induced hair cell death. Clinically,

the plasma concentration range of cisplatin achieved during most cancer treatments is approximately 1.7 μM- 25 μM [42][43], thus concentrations used in our study are comparable to the clinical setting. We found that although cisplatin treatment caused significant outer hair cell loss compared to untreated cultures, neither mutant mouse showed any differences in hair cell loss compared to WT littermates. Interestingly, cultures from $Cx43^{G60S/+}$ mutant mice had a significantly increased number of CC3-positive hair cells suggesting that these hair cells may be undergoing enhanced apoptosis possibly at a later time point due to the reduced level of functional Cx43 [32,33]. Cx43 KO HEI-OC1 cells had significantly higher cell viability compared to WT cells only when treated with 10 μM cisplatin for 24 hours, which is consistent with another report where the levels of Cx43 in HEI-OC1 cells were reduced using siRNA [44]. However, higher cisplatin concentrations eliminated this protection suggesting that cisplatin toxicity caused cell death irrespective of GJIC. Further supporting the notion that GJIC plays a minimal role in cisplatin-induced cell death, we found that pharmacological blockage of all gap junction channels with CBX had no effect on either resistance or sensitivity of organotypic cultured hair cells to cell death.

Connexins are expressed in cochlear supporting cells and not in hair cells *in vivo*, [45–47], thus blocking gap junctions may not have a direct effect on cisplatin entry and/or propagation in hair cells themselves. Hair cells express many uptake transporters for cisplatin such as Ctr1, OCT1, and OCT2 [48–50], allowing cisplatin to directly enter hair cells. Two copper transporting ATPases, ATP7A and ATP7B mediate cisplatin efflux from cells and are expressed in pillar cells and hair cells, respectively [50]. Although hair cells are suggested to be the primary target of cisplatin, damage to supporting cells may also play a role in cisplatin-induced cell death through indirect mechanisms. A previous study showed that after *in vivo* administration of cisplatin in rats, supporting cell morphology was altered prior to hair cell loss [51]; supporting our findings that altered architecture of the supporting cells may play a key role. It has been well documented that when the cochlea is injured, nearby supporting cells expand, extrude and eventually phagocytose the injured hair cells [52][53]. Cisplatin also disrupts the actin cytoskeleton in supporting cells where they form a “glial scar” to maintain the proper integrity of the sensory epithelium [53,54]. Taken together, these data suggest that although hair cell loss has been mostly documented as a consequence of cisplatin treatment, supporting cells in proximity to hair cells have altered morphology that may impact hair cell

death. In addition, architectural changes in supporting cells occur independent of Cx43-based GJIC suggesting the toxic or beneficial signals do not pass through the gap junction-rich supporting cells.

In the cochlea, Cx26 and Cx30 have been shown to form heteromeric and/or heterotypic gap junction channels in most cochlear supporting cells [29][55][56]. Our study showed that cisplatin caused a reorganization of Cx26 and Cx30 in all organotypic cochlear cultures, reducing the number of hybrid gap junction channels which may give rise to distinct changes in the metabolome that can spread amongst the supporting cells, including propagation of cell death related toxic signals [57]. For example, a previous study showed that heteromeric Cx26/Cx30 cochlear channels had faster Ca^{2+} wave propagation than their homomeric counterparts [55]. Thus, we suspect that cisplatin alters the biochemical coupling status of cochlear supporting cells through the production of fewer heteromeric channels.

Carbenoxolone (CBX) has been widely used as a non-specific gap junction blocker in many different tissues and cell lines including resident cells of the inner ear [58–62]. However, the mechanism of action remains unclear. In rat liver epithelial cells, CBX was shown to dephosphorylate Cx43, leading to a decrease in GJIC [63]. The current study showed that organotypic cochlear cultures treated with CBX had significantly decreased GJIC and Cx26 and Cx30 protein expression, suggesting a novel mechanism of action for CBX in the inner ear. In support of our findings that connexin levels are reduced after CBX treatment, previous studies showed that CBX caused a decrease in Cx43 levels in the prefrontal cortex of rats [64], human glioma cells [65], and human cerebral endothelial cells [66]. In contrast, bovine aortic endothelial cells (BAECs) treated with CBX had elevated levels of Cx43 mRNA and protein [67]. To our knowledge our study is the first to show that CBX attenuates the protein levels of Cx26 and Cx30, suggesting a mode of action that may extend beyond blocking the function of gap junction channels.

Cisplatin causes DNA damage leading to activation of various cell death pathways, including the intrinsic mitochondrial pathway via the permeabilization of the mitochondrial outer membrane and subsequent caspase activation [68]. This in turn generates ROS while depleting antioxidants, leaving cochlear cells unable to rapidly excrete toxins due to its anatomically closed structure [69]. The ER stress pathway, whereby a buildup of misfolded proteins causes

cellular dysfunction, has also been shown to be involved in cisplatin induced cell death [70]. To examine these pathways we evaluated the levels of various antioxidants, Bax (pro-apoptotic protein), and BiP (ER chaperone binding protein) as markers of mitochondrial apoptosis and ER stress, respectively. We showed that both WT and Cx43 KO cells underwent signature changes of the intrinsic mitochondrial pathway upon cisplatin treatment, albeit Cx43 KO cells had increased levels of antioxidant mRNA expression, possibly making them more resistant to ROS. In general, WT HEI-OC1 cells had significantly increased Bax protein expression (i.e. mitochondrial) whereas Cx43 KO HEI-OC1 cells had significantly increased BiP protein expression (i.e. ER) after cisplatin treatment. It is important to note that the cytoplasmic tail of Cx43 has been shown to bind Bax [71], and thus, WT HEI-OC1 cells may undergo enhanced mitochondrial dysfunction because they have the capacity to bind to Bax. Taken together, these data suggest that WT cells had enhanced mitochondria dysfunction while Cx43 KO cells favored an ER stress response pathway.

5.5. Conclusions

In summary, the current study sought to examine the role of GJIC in cisplatin-induced ototoxicity in two different cochlear relevant models. Collectively, we found that GJIC did not influence the amount of cisplatin-induced hair cell death but did cause alterations in cochlear supporting cell morphology and reorganization of Cx26 and Cx30 gap junctions. This is the first study to show that HEI-OC1 cells were highly sensitive to cisplatin-induced cell death regardless of the presence of Cx43, although the absence of Cx43 leads to more cisplatin-induced ER stress. Future studies examining the roles of GJIC in cisplatin-induced ototoxicity in the *in vivo* inner should be evaluated to further understand the molecular processes involved. Overall, our studies are consistent with the notion that patients that harbor any one of several hundred connexin gene mutations are not at increased risk of cisplatin-linked hair cell loss and deafness than patients lacking these mutations.

5.6. Acknowledgements

The authors would like to thank Dr. Glenn Fishman and Dr. Janet Rossant for providing the original Cx43 mutant mice. The authors would also like to thank Dr. Federico Kalinec for providing HEI-OC1 cells. This work was supported by the Canadian Institutes of Health

Research (148584) to DWL and BLA. JMA and RB were supported by Natural Sciences and Engineering Research Council of Canada scholarships.

5.7. References

1 Bruzzone, R., White, T. W. and Paul, D. L. (1996) Connections with Connexins: the Molecular Basis of Direct Intercellular Signaling. Eur. J. Biochem. **238**, 1–27.

2 Laird, D. W. (1996) The life cycle of a connexin: Gap junction formation, removal, and degradation. J. Bioenerg. Biomembr. **28**, 311–318.

3 Verselis, V. K. (2017) Connexin hemichannels and cochlear function. Neurosci. Lett., 0–1.

4 Laird, D. W., Naus, C. C. and Lampe, P. D. (2017) SnapShot: Connexins and Disease. Cell, Elsevier **170**, 1260-1260.e1.

5 Kelsell, D. P., Dunlop, J., Stevens, H. P., Lench, N. J., Liang, J. N., Parry, G., Mueller, R. F. and Leigh, I. M. (1997) Connexin 26 mutations in hereditary non-syndromic sensorineural deafness. Nature.

6 Tritsch, N. X., Yi, E., Gale, J. E., Glowatzki, E. and Bergles, D. E. (2007) The origin of spontaneous activity in the developing auditory system. Nature **450**, 50–55.

7 Cohen-Salmon, M., Ott, T., Michel, V., Hardelin, J. P., Perfettini, I., Eybalin, M., Wu, T., Marcus, D. C., Wangemann, P., Willecke, K., et al. (2002) Targeted ablation of connexin26 in the inner ear epithelial gap junction network causes hearing impairment and cell death. Curr. Biol. **12**, 1106–1111.

8 Sun, Y., Tang, W., Chang, Q., Wang, Y., Kong, W. and Lin, X. (2009) Connexin30 null and conditional connexin26 null mice display distinct pattern and time course of cellular degeneration in the cochlea. J. Comp. Neurol. **516**, 569–579.

9 Crispino, G., Di Pasquale, G., Scimemi, P., Rodriguez, L., Ramirez, F. G., de Siati, R. D., Santarelli, R. M., Arslan, E., Bortolozzi, M., Chiorini, J. A., et al. (2011) BAAV mediated GJB2 gene transfer restores gap junction coupling in cochlear organotypic cultures from deaf Cx26Sox10Cre mice. PLoS One **6**.

10 Chang, Q., Tang, W., Kim, Y. and Lin, X. (2015) Timed conditional null of connexin26 in mice reveals temporary requirements of connexin26 in key cochlear developmental events before the onset of hearing. Neurobiol. Dis., **73**, 418–427.

11 Chen, S., Sun, Y., Lin, X. and Kong, W. (2014) Down regulated connexin26 at different postnatal stage displayed different types of cellular degeneration and formation of organ of Corti. Biochem. Biophys. Res. Commun., **445**, 71–77.

12 Chen, S., Xie, L., Xu, K., Cao, H.-Y., Wu, X., Xu, X.-X., Sun, Y. and Kong, W.-J. (2018) Developmental abnormalities in supporting cell phalangeal processes and cytoskeleton in the *Gjb2* knockdown mouse model. Dis. Model. Mech. **11**, dmm033019.

13 Xie, L., Chen, S., Xu, K., Cao, H.-Y., Du, A.-N., Bai, X., Sun, Y. and Kong, W.-J. (2019) Reduced postnatal expression of cochlear Connexin26 induces hearing loss and affects the developmental status of pillar cells in a dose-dependent manner. Neurochem. Int. **128**, 196–205.

14 Lautermann, J., Frank, H. G., Jahnke, K., Traub, O. and Winterhager, E. (1999) Developmental expression patterns of connexin26 and-30 in the rat cochlea. Dev. Genet. **25**, 306–311.

15 Suzuki, T., Takamatsu, T. and Oyamada, M. (2003) Expression of Gap Junction Protein Connexin43 in the Adult Rat Cochlea: Comparison with Connexin26. J. Histochem. Cytochem. **51**, 903–912.

16 Cohen-Salmon, M., Maxeiner, S., Krüger, O., Theis, M., Willecke, K. and Petit, C. (2004) Expression of the connexin43- and connexin45-encoding genes in the developing and mature mouse inner ear. Cell Tissue Res. **316**, 15–22.

17 Liu, X. Z., Xia, X. J., Adams, J., Chen, Z. Y., Welch, K. O., Tekin, M., Ouyang, X. M., Kristiansen, A., Pandya, A., Balkany, T., et al. (2001) Mutations in GJA1 (connexin 43) are associated with non-syndromic autosomal recessive deafness. Hum. Mol. Genet. **10**, 2945–2951.

18 Liu, W., Boström, M., Kinnefors, A. and Rask-Andersen, H. (2009) Unique expression of connexins in the human cochlea. Hear. Res., Elsevier B.V. **250**, 55–62.

19 Liu, W. J. and Yang, J. (2015) Preferentially regulated expression of connexin 43 in the developing spiral ganglion neurons and afferent terminals in post-natal rat cochlea. Eur. J. Histochem. **59**, 17–29.

20 Liu, W., Glueckert, R., Linthicum, F. H., Rieger, G., Blumer, M., Bitsche, M., Pechriggl, E., Rask-Andersen, H. and Schrott-Fischer, A. (2014) Possible role of gap junction intercellular channels and connexin 43 in satellite glial cells (SGCs) for preservation of human spiral ganglion neurons: A comparative study with clinical implications. Cell Tissue Res. **355**, 267–278.

21 Locher, H., de Groot, J. C. M. J., van Iperen, L., Huisman, M. A., Frijns, J. H. M. and Chuva de Sousa Lopes, S. M. (2015) Development of the stria vascularis and potassium regulation in the human fetal cochlea: Insights into hereditary sensorineural hearing loss. Dev. Neurobiol. **75**, 1219–1240.

22 Kim, A. H., Nahm, E., Sollas, A., Mattiace, L. and Rozental, R. (2013) Connexin 43 and hearing: Possible implications for retrocochlear auditory processing. Laryngoscope **123**, 3185–3193.

23 Abitbol, J. M., Kelly, J. J., Barr, K. J., Allman, B. L. and Laird, D. W. (2018) Mice harbouring an oculodentodigital dysplasia-linked Cx43 G60S mutation have severe hearing loss.

24 Rybak, L. P., Whitworth, C. A., Mukherjea, D. and Ramkumar, V. (2007) Mechanisms of cisplatin-induced ototoxicity and prevention. Hear. Res. **226**, 157–167.

25 McKeage, M. J. (1995) Comparative Adverse Effect Profiles of Platinum Drugs. Drug Saf. **13**, 228–244.

26 Brock, P. R., Knight, K. R., Freyer, D. R., Campbell, K. C. M., Steyger, P. S., Blakley, B. W., Rassekh, S. R., Chang, K. W., Fligor, B. J., Rajput, K., et al. (2012) Platinum-induced ototoxicity in children: A consensus review on mechanisms, predisposition, and protection, including a new International Society of Pediatric Oncology Boston ototoxicity scale. J. Clin. Oncol. **30**, 2408–2417.

27 Knight, K. R. G., Kraemer, D. F. and Neuwelt, E. A. (2005) Ototoxicity in children receiving platinum chemotherapy: Underestimating a commonly occurring toxicity that may influence academic and social development. J. Clin. Oncol. **23**, 8588–8596.

28 Breglio, A. M., Rusheen, A. E., Shide, E. D., Fernandez, K. A., Spielbauer, K. K., McLachlin, K. M., Hall, M. D., Amable, L. and Cunningham, L. L. (2017) Cisplatin is retained in the cochlea indefinitely following chemotherapy. Nat. Commun., US **8**.

29 Forge, A., Marziano, N. K., Casalotti, S. O., Becker, D. L. and Jagger, D. (2003) The inner ear contains heteromeric channels composed of cx26 and cx30 and deafness-related mutations in cx26 have a dominant negative effect on cx30. Cell Commun. Adhes. **10**, 341–346.

30 Tong, X., Hong, X., Yang, Y., Tao, L., Harris, A. L., Zheng, S., Zhang, S. and Wang, Q. (2011) Gap junctions propagate opposite effects in normal and tumor testicular cells in response to cisplatin. Cancer Lett., **317**, 165–171.

31 Kalinec, G. M., Webster, P., Lim, D. J. and Kalinec, F. (2003) A cochlear cell line as an in vitro system for drug ototoxicity screening. Audiol. Neuro-Otology **8**, 177–189.

32 Kalcheva, N., Qu, J., Sandeep, N., Garcia, L., Zhang, J., Wang, Z., Lampe, P. D., Suadicani, S. O., Spray, D. C. and Fishman, G. I. (2007) Gap junction remodeling and cardiac arrhythmogenesis in a murine model of oculodentodigital dysplasia. Proc. Natl. Acad. Sci. U. S. A. **104**, 20512–20516.

33 Flenniken, A. M., Osborne, L. R., Anderson, N., Ciliberti, N., Fleming, C., Gittens, J. E. I., Gong, X.-Q., Kelsey, L. B., Lounsbury, C., Moreno, L., et al. (2005) A Gja1 missense mutation in a mouse model of oculodentodigital dysplasia. Development **132**, 4375–86.

34 Arora, S., Heyza, J., Chalfin, E., Ruch, R. and Patrick, S. (2018) Gap Junction Intercellular Communication Positively Regulates Cisplatin Toxicity by Inducing DNA Damage through Bystander Signaling. Cancers (Basel). **10**, 368.

35 Jensen, R. and Glazer, P. M. (2004) Cell-interdependent cisplatin killing by Ku/DNA-dependent protein kinase signaling transduced through gap junctions. Proc. Natl.

Acad. Sci. **101**, 6134–6139.

36 Wu, D., Li, B., Liu, H., Yuan, M., Yu, M., Tao, L., Dong, S. and Tong, X. (2018) In vitro inhibited effect of gap junction composed of Cx43 in the invasion and metastasis of testicular cancer resistanced to cisplatin. Biomed. Pharmacother., **98**, 826–833.

37 Ning, H.-B. Z. and Y. (2006) Distinct and Gradient Distributions of Connexin26 and Connexin30 in the Cochlear Sensory Epithelium of Guinea Pigs. J. Comp. Neurol. **499**, 506–518.

38 Paken, J., Govender, C. D., Pillay, M. and Sewram, V. (2016) Cisplatin-Associated Ototoxicity: A Review for the Health Professional. J. Toxicol., **2016**.

39 Abujamra, A., Escosteguy, J.R.,Celso, D.,, Manica, D., Cigana, L.F., Coradini, P., Brunetto, A., GregiaAna, L., Abujamra, L., and Rib, J. P. (1996) The Use of High-Frequency Audiometry Increases the Diagnosis of Asymptomatic Hearing Loss in Pediatric Patients Treated With Cisplatin-Based Chemotherapy. J. Clin. Oncol. **14**, 1526–1531.

40 Ruch, R. (2019) Connexin43 Suppresses Lung Cancer Stem Cells. Cancers (Basel). **11**, 175.

41 Ding, Y., 1, And, Nguyen, T. A. and 2. (2012) Gap Junction Enhancer Potentiates Cytotoxicity of Cisplatin in Breast Cancer Cells. J Cancer Sci **6**, 2166–2171.

42 Erdlenbruch, B., Nier, M., Kern, W., Hiddemann, W., Pekrun, A. and Lakomek, M. (2001) Pharmacokinetics of cisplatin and relation to nephrotoxicity in paediatric patients. Eur. J. Clin. Pharmacol. **57**, 393–402.

43 Qin Wang, Tianhui You, Dongdong Yuan, Xu Han, Xiaoting Hong, Bo He, Lingzhi Wang, Xuhui Tong, Liang Tao, and A. L. H. (2010) Cisplatin and Oxaliplatin Inhibit Gap Junctional Communication by Direct Action and by Reduction of Connexin Expression, Thereby Counteracting Cytotoxic Efficacy **333**, 903–911.

44 Kim, Y. J., Kim, J., Tian, C., Lim, H. J., Kim, Y. S., Chung, J. H. and Choung, Y. H. (2014) Prevention of cisplatin-induced ototoxicity by the inhibition of gap junctional intercellular communication in auditory cells. Cell. Mol. Life Sci. **71**, 3859–3871.

45 Zhang, Y., Tang, W., Ahmad, S., Sipp, J. a, Chen, P. and Lin, X. (2005) Gap junction-mediated intercellular biochemical coupling in cochlear supporting cells is required for normal cochlear functions. Proc. Natl. Acad. Sci. U. S. A. **102**, 15201–6.

46 Jagger, D. J. (2006) Compartmentalized and Signal-Selective Gap Junctional Coupling in the Hearing Cochlea. J. Neurosci. **26**, 1260–1268.

47 Forge, A., Jagger, D. J., Kelly, J. J. and Taylor, R. R. (2013) Connexin30-mediated intercellular communication plays an essential role in epithelial repair in the cochlea. J. Cell Sci. **126**, 1703–1712.

48 More, S. S., Akil, O., Ianculescu, A. G., Geier, E. G., Lustig, L. R. and Giacomini, K. M. (2010) Role of the copper transporter, CTR1, in platinum-induced ototoxicity. J. Neurosci. **30**, 9500–9.

49 Ciarimboli, G., Deuster, D., Knief, A., Sperling, M., Holtkamp, M., Edemir, B., Pavenstädt, H., Lanvers-Kaminsky, C., Zehnhoff-Dinnesen, A. A., Schinkel, A. H., et al. (2010) Organic cation transporter 2 mediates cisplatin-induced oto- and nephrotoxicity and is a target for protective interventions. Am. J. Pathol. **176**, 1169–1180.

50 Ding, D., Allman, B. L. and Salvi, R. (2012) Review: Ototoxic Characteristics of Platinum Antitumor Drugs. Anat. Rec. **295**, 1851–1867.

51 Ramírez-Camacho, R., García-Berrocal, J. R., Buján, J., Martín-Marero, A. and Trinidad, A. (2004) Supporting Cells As A Target of Cisplatin-Induced Inner Ear Damage: Therapeutic Implications. Laryngoscope **114**, 533–537.

52 Forge, A. (1985) Outer hair cell loss and supporting cell expansion following chronic gentamicin treatment. Hear Res **19**, 171–182.

53 Leonova, E. V. and Raphael, Y. (1997) Organization of cell junctions and cytoskeleton in the reticular lamina in normal and ototoxically damaged organ of Corti. Hear. Res., Elsevier Science B.V. **113**, 14–28.

54 Slattery, E. L. and Warchol, M. E. (2010) Cisplatin Ototoxicity Blocks Sensory Regeneration in the Avian Inner Ear **30**, 3473–3481.

55 Sun, J., Ahmad, S., Chen, S., Tang, W., Zhang, Y., Chen, P. and Lin, X. (2005) Cochlear gap junctions coassembled from Cx26 and 30 show faster intercellular Ca2+ signaling than homomeric counterparts. Am. J. Physiol. Cell Physiol. **288**, C613–C623.

56 Santos, Z. and. (2000) Voltage Gating of Gap Junctions in Cochlear Supporting Cells: Evidence for Nonhomotypic Channel **24**, 17–24.

57 Weber, P. A., Chang, H. C., Spaeth, K. E., Nitsche, J. M. and Nicholson, B. J. (2004) The permeability of gap junction channels to probes of different size is dependent on connexin composition and permeant-pore affinities. Biophys. J. **87**, 958–973.

58 Goldberg, G. S., Moreno, A. P., Bechberger, J. F., Hearn, S. S., Shivers, R. R., Macphee, D. J., Zhang, Y. C. and Naus, C. C. G. (1996) Evidence that disruption of connexon particle arrangements in gap junction plaques is associated with inhibition of gap junctional communication by a glycyrrhetinic acid derivative. Exp. Cell Res. **222**, 48–53.

59 Schütz, M., Scimemi, P., Majumder, P., de Siati, R. D., Crispino, G., Rodriguez, L., Bortolozzi, M., Santarelli, R., Seydel, A., Sonntag, S., et al. (2010) The human deafness-associated connexin 30 T5M mutation causes mild hearing loss and reduces

biochemical coupling among cochlear non-sensory cells in knock-in mice. Hum. Mol. Genet. **19**, 4759–4773.

60 Zhu, Y., Zong, L., Mei, L. and Zhao, H. B. (2015) Connexin26 gap junction mediates miRNA intercellular genetic communication in the cochlea and is required for inner ear development. Sci. Rep., Nature Publishing Group **5**, 1–8.

61 Nickel, R., Becker, D. and Forge, A. (2006) Molecular and functional characterization of gap junctions in the avian inner ear. J. Neurosci. **26**, 6190–9.

62 Nishiyama, N., Yamaguchi, T., Yoneyama, M., Onaka, Y. and Ogita, K. (2019) Disruption of Gap Junction-Mediated Intercellular Communication in the Spiral Ligament Causes Hearing and Outer Hair Cell Loss in the Cochlea of Mice **42**, 73–80.

63 Guan, X., Wilson, S., Schlender, K. K. and Ruch, R. J. (1996) Gap-junction disassembly and connexin 43 dephosphorylation induced by 18β-glycyrrhetinic acid. Mol. Carcinog. **16**, 157–164.

64 Sun, J. D., Liu, Y., Yuan, Y. H., Li, J. and Chen, N. H. (2012) Gap junction dysfunction in the prefrontal cortex induces depressive-like behaviors in rats. Neuropsychopharmacology, Nature Publishing Group **37**, 1305–1320.

65 Yulyana, Y., Endaya, B. B., Ng, W. H., Guo, C. M., Hui, K. M., Lam, P. Y. P. and Ho, I. A. W. (2013) Carbenoxolone Enhances TRAIL -Induced Apoptosis Through the Upregulation of Death Receptor 5 and Inhibition of Gap Junction Intercellular Communication in Human Glioma . Stem Cells Dev. **22**, 1870–1882.

66 Kim, Y., Griffin, J. M., Harris, P. W. R., Chan, S. H. C., Nicholson, L. F. B., Brimble, M. A., O'Carroll, S. J. and Green, C. R. (2017) Characterizing the mode of action of extracellular Connexin43 channel blocking mimetic peptides in an in vitro ischemia injury model. Biochim. Biophys. Acta - Gen. Subj. **1861**, 68–78.

67 Sagar, G. D. V. and Larson, D. M. (2006) Carbenoxolone inhibits junctional transfer and upregulates Connexin43 expression by a protein kinase A-dependent pathway. J. Cell. Biochem. **98**, 1543–1551.

68 Rybak, L. P. (2007) Mechanisms of cisplatin ototoxicity and progress in otoprotection. Curr. Opin. Otolaryngol. Head Neck Surg. **15**, 364–369.

69 Rybak, L. P., Husain, K., Morris, C., Whitworth, C. and Somani, S. (2000) Effect of protective agents against cisplatin ototoxicity. Am. J. Otol. **21**, 513–520.

70 Mandic, A., Hansson, J., Linder, S. and Shoshan, M. C. (2003) Cisplatin induces endoplasmic reticulum stress and nucleus-independent apoptotic signaling. J. Biol. Chem. **278**, 9100–9106.

71 Sun, Y., Zhao, X., Yao, Y., Qi, X., Yuan, Y. and Hu, Y. (2012) Connexin 43 interacts with Bax to regulate apoptosis of pancreatic cancer through a gap junction-independent pathway. Int. J. Oncol. **41**, 941–948.

Chapter 6 Discussion

6.1. Summary of main findings

It has been known for nearly two decades that *GJB2* and/or *GJB6* gene mutations, encoding Cx26 and Cx30, respectively, cause a large proportion of congenitally acquired hearing loss [1,2]. Using a combination of five different genetically-modified mice, this thesis focuses on the importance of other related large-pore channels; Cx43, Panx1, and Panx3, in auditory function. In chapter 2, we show that both Panx1 and Panx3 are not involved in proper hearing function. In chapter 3, we used a double knock-out mouse to show that Panx1 and Panx3 were not compensating for one another in the auditory system. In chapter 4, we found that a severe but not moderate reduction of Cx43 gap junctional intercellular communication (GJIC) resulted in severe hearing loss where the defect was mapped to the higher-order auditory brainstem regions. In chapter 5, we found that GJIC did not influence the impact of cisplatin-induced cell death in both organotypic cochlear cultures and cochlear relevant immortalized cells. Table 6.1. summarizes the main findings of this thesis. In this section I will further discuss how these findings are relevant to the molecular understanding of hearing with an emphasis on connexins and pannexins and the potential for therapeutic strategies to rescue hearing loss.

6.1.1. Differential effects of pannexins on noise-induced hearing loss

Hearing loss, including noise-induced hearing loss (NIHL), is highly prevalent and severely hinders an individual's quality of life, yet many of the mechanisms that cause hearing loss are unknown [3,4]. Recently, the involvement of Cx channels in NIHL have been investigated; however, whether Panxs also play a role in this process has yet to be examined. As this thesis aimed to evaluate the roles of large pore channels in NIHL, we assessed hearing in globally ablated pannexin1 ($Panx1^{-/-}$) and pannexin3 ($Panx3^{-/-}$) knock-out mice at both baseline and after a loud noise-exposure. The Panx channel proteins, Panx1 and Panx3, are regionally expressed in many cell types along the auditory pathway, and mice lacking Panx1 in specific cells of the inner ear have been reported to exhibit hearing loss [5,6], suggesting a vital role for Panxs in hearing. We proposed that Panx1 and/or Panx3 null mice would exhibit severe hearing loss and increased susceptibility to noise-induced hearing loss.

Table 6.1. Summary of main findings

	Genetically Acquired Hearing Loss	Noise-Induced Hearing Loss (NIHL)	Cisplatin-Induced Hearing Loss
Panx1	Normal hearing when ablated	Loss of Panx1 leads to similar NIHL as WT	N/A
Panx3	Normal hearing when ablated	Loss of Panx3 leads to mild protection against NIHL	N/A
Cx43	Severe hearing loss when Cx43 function is less than 20%, but normal when 50% is maintained	Reduction of Cx43 function leads to similar NIHL as WT	Reduced Cx43 function does not lead to differential susceptibility to cisplatin-induced ototoxicity

Using the auditory brainstem response, we surprisingly found that Panx1$^{-/-}$ and Panx3$^{-/-}$ mice did not harbor hearing or cochlear nerve deficits. Furthermore, while Panx1$^{-/-}$ mice displayed no protection against loud noise-induced hearing loss, Panx3$^{-/-}$ mice exhibited enhanced 16- and 24 kHz hearing recovery seven days after a loud noise exposure (NE; 12 kHz tone, 115 dB sound pressure level for one hour). Interestingly, Cx26, Cx30, Cx43, and Panx2 were up-regulated in Panx3$^{-/-}$ mice compared with wild-type and/or Panx1$^{-/-}$ mice, and assessment of the auditory tract revealed small but detectable morphological changes in the middle ear bones of Panx3$^{-/-}$ mice. It is unclear if these changes alone are sufficient to provide protection against loud noise-induced hearing loss. Contrary to what we expected, these data suggest that Panx1 and Panx3 are not essential for baseline hearing in mice tested, but the therapeutic targeting of Panx3 may prove protective against mid-high-frequency hearing loss caused by loud NE.

6.1.2. Double deletion of *Panx1* and *Panx3* affects skin and bone but not hearing

To date, the use of single knock-out mouse models of both Panx1 and/or Panx3 have demonstrated their roles in skin development, bone formation, and auditory phenotypes [6–9]. Due to sequence homology between Panx1 and Panx3, when one Panx is ablated from germline cells, the other may be upregulated in a compensatory mechanism to maintain tissue homeostasis and function as has been demonstrated for skin, blood vessels, and the vomeronasal organ [7, 10-11]. To evaluate the roles of Panx1 and Panx3 in the skin, bone, and cochlea, we created the first Panx1/Panx3 double knock-out mouse model (dKO) where both isoforms were ablated. Profiling of the auditory system revealed that dKO mice did not exhibit hearing loss and were even slightly protected against noise-induced hearing damage at mid-frequency regions, phenocopying what was found in Panx3$^{-/-}$ mice. Taken together, our findings suggest that Panx1 and Panx3 are expendable in the auditory system which is supported by other studies [12,13]. The expendability of Panx channels in the auditory system may be largely due to the fact that connexins are crucial for hearing and serve many functional similarities as Panx channels such as ATP release, Ca^{2+} wave propagation, and passage of small molecules and ions through the intracellular and extracellular space.

6.1.3. Mice harbouring an oculodentodigital dysplasia-linked Cx43 G60S mutation have severe hearing loss

Given the importance of connexin43 (Cx43, encoded by *GJA1*) function in the central nervous system and sensory organ processing, we proposed that it would also be crucial in auditory function. In addition, since both Cx26 and Cx30 mutations are highly prevalent in congenitally acquired hearing loss, this raised the question as to whether Cx43 was also crucial in hearing. To that end, hearing was examined in two different mouse models of oculodentodigital dysplasia that globally express *GJA1* mutations resulting in moderate or severe loss of Cx43 function. Although $Cx43^{I130T/+}$ mutant mice, with ~50% Cx43 channel function, did not have any hearing loss, $Cx43^{G60S/+}$ mutant mice, with ~20% Cx43 channel function, had severe hearing loss. There was no evidence of inner ear sensory hair cell loss, suggesting that the mechanism for Cx43-linked hearing loss lies downstream in the higher-order auditory pathway. Specifically, $Cx43^{G60S/+}$ mutant mice had decreased ABR waveform amplitudes compared to WTs, consistent with an auditory neuropathy phenotype (i.e. higher-order auditory deficits). Auditory neuropathy has been previously associated with other connexin mutations such as Cx32 causing Charcot Marie Tooth disease harbouring auditory neuropathy [14,15]. Additionally, Cx29 that is exclusively expressed in mice and is localized to Schwann cells around the spiral ganglion neurons in the cochlea has been associated with auditory neuropathy where Cx29 knock-out mice had hearing loss also associated with distortion of auditory brainstem waveforms [16]. Since evidence suggests that Cx26 function is essential for hearing and may be protective against noise-induced hearing loss [17], we challenged $Cx43^{I130T/+}$ mice with a loud noise and found that they had a similar susceptibility to noise-induced hearing loss to that found in controls, suggesting that decreased Cx43 function does not sensitize the mice for environmentally induced hearing loss. Taken together, this study suggests that Cx43 plays an important role in baseline hearing and is essential for auditory processing, however, a residual amount of Cx43 GJIC is enough to maintain proper hearing function.

6.1.4. Cisplatin-induced ototoxicity occurs independent of gap junctional intercellular communication

Cisplatin is a very effective chemotherapeutic, but severe and permanent hearing loss remains a prevalent side effect. The processes underlining cisplatin-induced ototoxicity are not well

understood. Gap junction channels composed of connexin (Cx) subunits allow for the passage of small molecules and ions between contacting neighboring cells. These specialized channels have been postulated to enhance cisplatin-induced cell death by spreading "death signals" throughout the supporting cells of the organ of Corti [18]. This study sought to investigate the role of Cx43 in cisplatin-induced ototoxicity using organotypic cochlear cultures from control and two different Cx43 mutant mouse strains harbouring either a moderate ($Cx43^{I130T/+}$) or severe ($Cx43^{G60S/+}$) reduction of Cx43 function. Cochlear cultures from Cx43 mutant mice with a severe reduction in Cx43-based GJIC had an enhanced number of hair cells that were positive for cleaved caspase 3 after cisplatin treatment. In cisplatin-treated organotypic cochlear cultures, there was a decrease in the co-localization of Cx26 and Cx30 compared to untreated cultures, suggesting that cisplatin causes reorganization of connexin composition in supporting cells. Both Cx26 and Cx30 protein expression as well as GJIC were decreased in organotypic cochlear cultures treated with the gap junction blocker carbenoxolone. When cisplatin and carbenoxolone were co-administered there were no differences in hair cell loss compared to cisplatin treatment alone. Using cisplatin-treated control and Cx43-ablated organ of Corti derived HEI-OC1 cells, we found that greatly reducing GJIC led to preferential induction of an ER stress pathway. Taken together, this study strongly suggests that inhibition of GJIC in organ of Corti cells does not lead to differential susceptibility to cisplatin-induced ototoxicity. Although cisplatin causes the same degree of cell death in gap junction competent and incompetent cochlear cells, the engagement of the mitochondrial dysregulation and ER stress differs.

6.2. Experimental limitations

6.2.1. Limitations in distinguishing between connexin and pannexin channels

Due to the functional similarity of connexin and pannexin channels it is sometimes difficult to fully elucidate their individual roles in physiological processes. Connexin hemichannels are thought to have similar roles as pannexins in regulating different processes such as ATP release [10]. It has become well known that connexin hemichannels are preferentially opened under low extracellular Ca^{2+} concentrations [19,20]. In contrast, pannexins are thought to be opened under normal physiological extracellular Ca^{2+} concentrations [21]. Due to these distinct differences it is possible to selectively examine connexin hemichannel function by lowering

the extracellular Ca^{2+} concentration in order to preferentially induce their opening. However, caution is needed when interpreting these results as there is the potential of connexin and pannexin channel function cross-over.

The use of pharmacological blockers for connexin and pannexin channels have been widely used to assess their functions where different agents can have preferential blocking efficiencies. For example, heptanol has been reported to block connexin hemichannel and gap junction channels with little effect on Panx1 channels [22–24]. Similarly, flufenamic acid (FFA) inhibited connexin hemichannels and Panx channels, albeit the later was inhibited at much lower concentrations [24]. A widely used drug for inhibition of Panx1 channels, probenecid, has been reported to block Panx1 channel currents and dye uptake in oocytes with no changes in connexin currents [25]. In chapter 4 we used carbenoxolone (CBX) as a gap junction blocker which inhibits both connexin and pannexin channels. Previous studies have used low concentrations of CBX (i.e. 5-10 μM) to more selectively block Panx channels [24]. On the other hand, higher concentrations (i.e. 50-300 μM) of CBX have been used to block connexin channels, allowing for some distinction between the two channel types [24,26]. For all of our studies in chapter 4, we used 100 μM CBX to block connexin channels but at this concentration any Panx channels present would also likely be inhibited. Therefore, the use of more targeted blockers would be beneficial to develop and use in future studies.

The use of peptide mimetics designed to bind specific regions of the Cx43 polypeptide have been used to address some of these problems. Gap26 and Gap27 are two peptide mimetics that bind to specific amino acid regions on the first and second extracellular domains of Cx43, respectively, and have been shown to inhibit Cx43 hemichannels in HeLa cells [27–29]. Even so, Gap26 also inhibited Panx1 currents in oocytes [30], suggesting that these mimetics may not function by solely mimicking the protein sequence since Panx1 and Cx43 do not share similar sequences at the region where the peptide binds. In addition, two other peptides that mimic sequences in the intracellular loop of Cx43 were created, Gap19 and TAT-L2. Previous studies have shown that Gap19 does not inhibit GJIC but blocks Cx43 hemichannel activity in the cardiac system and astroglial network of the brain, therefore enabling a peptide that preferentially blocks connexin hemichannels versus gap junction channels [31–33]. Similarly, the TAT-L2 Cx43 peptide has previously been reported to have no effect on gap junctions but inhibited Cx43 hemichannel function [34]. These peptides have no reported function on Panx1

activity, allowing for preferential blocking of connexin channels [32,35]. A mimetic peptide of the first extracellular loop of Panx1, 10panx1, significantly attenuates Panx1 channel current, dye uptake, and ATP release [36–38].

Taken together, due to the similar structure and functions of connexins and pannexins, it is important to consider the experimental limitations in trying to distinguish between these two channels. Caution is also necessary in interpreting studies using connexin and pannexin blockers. In chapter 4, we used CBX at an appropriate concentration to block connexin channels, however whether this involved gap junctions or hemichannels remains unknown. Future studies could use specific connexin peptides that may preferentially block hemichannels versus gap junctions (such as Gap19) on organotypic cochlear cultures to examine whether cisplatin treatment causes any differential regulation to connexin hemichannels.

6.2.2. Limitations of genetically-modified mice

The use of genetically modified mouse models has provided us with novel insights into the functions of connexins and pannexins in various disease processes. The work in this thesis comprises the compilation of data from five different mouse models (three Panx knock-out mice and two different Cx43 mutant mice). When one isoform of a large pore channel is lost, another isoform may be upregulated to allow for compensatory upregulation. Thus, it is possible that other connexins and/or pannexins may have been altered as a consequence of knocking out an entire gene (Panxs) or creating a mutant (Cx43); ultimately allowing for compensation of the altered gene. In the inner ear specifically, the original Cx30 knock-out mouse was reported to have severe hearing loss and did not form an endocochlear potential, which is necessary for proper hearing [39]. Shortly after the generation of this mouse, however, it was reported that the Cx26 protein levels were also significantly reduced [40,41]. Subsequently, another independent Cx30 knock-out mouse model was created that did not alter the expression of Cx26 and these mice were found to have normal hearing function and development of the cochlea [42]. Together these studies suggest that Cx26 may compensate for the loss of Cx30 in the cochlea and that changes in the cochlear expression of one Cx isoform (ex. Cx30) may impact the expression of another isoform (ex. Cx26). Thus, when assessing the consequences of connexin or pannexin ablation it is crucial that other related members in the tissue of interest also be investigated for any potential alterations. In Chapter

4 of this thesis we assessed the potential compensation of Cx26 and Cx30 in the cochlea of the two different Cx43 mutant mice, and found that neither Cx43 mutant mice had differential mRNA transcript levels expression levels of Cx26 or Cx30, suggesting that Cx26 and/or Cx30 are not compensating for the loss of Cx43 gap junction function. To support our findings this was also found in another system where both Cx26 and Cx30 protein expression remained unchanged in mammary glands of $Cx43^{I130T/+}$ mice compared to WT littermates [43]. Although the mRNA transcript levels of Cx26 and Cx30 in the cochlea of both Cx43 mutant mice were similar, the functional status of Cx26 and Cx30 gap junction function in the cochlea of $Cx43^{I130T/+}$ mutant mice remain unknown.

Prior to the completion of Chapter 2, it was reported that two independent mouse models harbouring conditional ablations of Panx1 in the cochlea had hearing loss and cell degeneration in the cochlea [6,9]. Hence, we hypothesized that global ablation of Panx1 would also have hearing deficits which may even be enhanced due to the ubiquitous expression of Panx1 in the auditory tract. However, we found that the global Panx1 knock-out mice used in our study did not have hearing loss, which was consistent with another report where a second Panx1 global knock-out mouse was used [13,44]. Using cochlear organotypic cultures of $Panx1^{-/-}$ mice it was shown that ATP-release remained intact [12]. To address the potential issue of Panx compensation, in Chapter 3 we found that Panx1 and Panx3 double knock-out mice also did not have hearing loss, eliminating the potential of compensation between the two Panx channels. The two studies using conditional ablation of Panx1 in the cochlea used two different cre- mice and bred them to $Panx1^{tm1a(KOMP)Wtsi}$ mice, in which exon 2 of Panx1 is floxed with loxPs, ultimately creating tissue specific knock-outs of Panx1 within cochlear specific regions. A recent study evaluating the utility of $Panx1^{-/-}$ mice (distinct from the one used in our studies) showed that $Panx1^{tm1a(KOMP)Wtsi}$ mice were hypomorphic and $Panx1^{-/-}$ mice derived from these mice still had approximately 30% residual Panx1 mRNA transcript in various tissues including the brain, kidney and liver [45]. Further, the Foxg1-conditional Panx1 knock-out mouse that was reported to have hearing loss exhibited strong immunoreactivity for Panx1 in the organ of Corti as revealed by staining with a chicken anti-human Panx1 antibody which has been shown to have questionable specificity for Panx1 [46]. One noticeable difference between our study and the two conditional Panx1 knock-out mice were the frequencies tested. In Chapter 2 and 3 we used a broadband click stimulus to examine general hearing function as well as 4-, 8-, 16-

and 24 kHz specific frequency stimuli while the studies using conditional Panx1 knock-out mice used 8-, 16-, 24-, 32-, and 40 kHz tonal frequencies. Since the mouse hearing range extends from 1 kHz to approximately 100 kHz [47], the conditional Panx1 knockout studies included testing higher frequency ranges where hearing loss was more evident. However, in support of our findings that hearing is maintained when Panx1 is ablated, a more recent study using a different Panx1 global knock-out mouse found no significant differences in hearing thresholds even at 32 kHz tones [13]. This suggests that the frequency range tested was not the sole reason for the discrepancies between these studies however, it could be a contributing factor. Furthermore, all the above studies using Panx1 knock-out mice have been created on a C57BL/6 background, however it is unknown how many times, or even if, these mice were further backcrossed on other mouse strains, and thus the exact background strain of the mice could account for some of the discrepancies between studies.

Another consideration for the discrepancies between studies are the transcription factors, Foxg1 and Pax2, used for the generation of the conditional Panx1 knock-out mice. Both of these transcription factors are involved in embryonic development not only of the cochlea but also for proper brain development during embryogenesis [48–52]. Importantly, Panx1 is abundantly expressed in the central nervous system particularly in neurons [53,54]. Therefore, by breeding Panx1 floxed mice with cre mice that use transcription factors involved in embryonic development, brain development could also be impaired leading to potential damage in the higher-order auditory regions. In addition, the Foxg1 and Pax2 strains must express a cre recombinase whereas the global mice do not [13]. Cre expression in mammalian cells can produce chromosomal abnormalities depending on cre activity as well as passenger mutations [55]. Although genetically modified mice provide us with the tools to assess genes of interest in the cochlea, the differences observed in hearing phenotypes with the use of Panx1 conditional versus global knock-out mice warrants further investigation. With more advanced technologies in the generation of genetically modified mice the use of CRISPR-Cas9 to make a Panx1 knock-out mouse model may serve to resolve the discrepancies between the current published studies.

6.3. Screening of connexins in congenital hearing loss

In most developed countries shortly after children are born, they undergo newborn hearing screening to examine their auditory function to ensure that all hearing impaired babies are identified as soon as possible. Since age of identification of hearing loss is a critical factor in the development of a child's speech the "Universal Newborn Hearing Screening" program where all babies have the opportunity to be screened for hearing impairment has been the standard of care in the United States, United Kingdom, and most of Canada [56]. Otoacoustic emissions (OAE) tests and/or auditory brainstem responses (ABRs) are used to measure the integrity of the hair cells, and general hearing function, respectively [57]. These tests are minimally invasive as they are completed while the baby is asleep and gives an indication of whether there are any signs of hearing loss. Collectively, approximately 1 in 1000 newborns have hearing loss making it one of the most common congenital disorder [58]. When hearing loss is suspected, they will be genotyped for various common genes involved in hearing loss using DNA samples acquired from either the blood or from oral cavity swabs. Subsequently, *GJB2* and/or *GJB6* are fully sequenced as a first pass test since over 135 mutations in these genes account for most congenitally acquired cases of hearing loss [1,59,60].

In Chapter 4 we examined auditory function in Cx43 mutant mice harbouring both a moderate ($Cx43^{I130T/+}$) and severe ($Cx43^{G60S/+}$) reduction of Cx43 gap junctional intercellular communication and found that only mice with a severe reduction in Cx43 function led to hearing impairment. A previous study examining auditory function in Cx43 heterozygous mouse found similar phenotypes where hearing was normal and was only slightly elevated by approximately 10 dB at 10 months of age [61]. Patients with ODDD often have many additional morbidities with variable severities and approximately 10-15% of patients with ODDD have the comorbidity of hearing loss [62,63], although it is not known why some patients do while others do not. Our findings suggest that newborn screening of hearing loss-linked genes should perhaps extend to include *GJA1*, encoding Cx43. Importantly, while the I130T mutation has been found in the human population, the G60S mutation has not. It would be interesting to assess whether some patients with idiopathic congenitally acquired hearing loss is potentially due to a G60S mutation or possibly another gene mutation that severely compromises Cx43 function. Our studies also suggest that screening newborns for *PANX1* or

PANX3 gene mutations would not be beneficial as our studies collectively present the notion that Panxs are not essential for normal hearing.

6.4. Advances in genetic therapies to correct hearing loss-linked *GJB2* mutations

Treatment of hearing loss currently consists of either hearing aids for mild to moderate hearing loss or cochlear implants for more severe hearing impairments. Although cochlear implants can help most deaf patients understand speech, there are many limitations such as poor pitch perception and difficulty with tonal discrimination under noisy environments [64,65]. Thus, the need for molecular therapies to treat genetically acquired hearing loss has been a major focus in the auditory field.

6.4.1. Routes of drug delivery to the inner ear

One of the most pressing challenges for advancing molecular therapeutics for hearing loss is the development of methodologies for safe and efficient drug delivery to the inner ear. Routes of drug administration to the inner ear include; systemic, intratympanic, and intracochlear routes where local administration becomes imperative in alleviating off target effects [66–69]. In many cases, systemic drug delivery has been used for cochlear interventions, however, the blood labyrinth barrier (BLB) decreases the effectiveness of drug delivery to the inner ear [70–72]. In addition, drug toxicity and off target effects within other tissues are also of concern [69]. Thus, the need for local administration techniques are required for the efficient drug delivery strategies such as intratympanic and intracochlear routes.

Intratympanic injections involves administration of drugs into the middle ear through the tympanic membrane which allows for the direct drug entry into the cochlea [73,74]. Although these injections offer an advantage of being mildly invasive, they rely on proper drug diffusion through the round and/or oval windows of the cochlea. Thus, exact drug concentrations that enter the inner ear can vary [69]. Further, as this route of drug delivery relies mostly on drug diffusion that starts at the base of the cochlea, there may be little or no drug delivery to the apex of the cochlea. This can be used to the patient's advantage depending on the specific disease. For example, patients with Meniere’s disease are treated with a one-shot application of gentamicin through intratympanic injections [75]. This route of drug administration would

allow for maximal treatment along the base of the cochlea and minimize the gentamicin concentrations in the regions that guide the acquisition of speech (i.e. middle region). More invasive intracochlear delivery methods such as injection into the semicircular canal, round window membrane, or the scala media have greatly enhanced the efficiency of drug delivery to the inner ear [67]. These routes require surgery, are highly invasive, and extremely risky as the surgical techniques needed can sometimes induce hearing loss. Therefore, the benefits must outweigh the consequences when considering treatment of restoring hearing loss in human patients.

6.4.2. Cochlear *GJB2* restoration with adeno-associated viruses

Adeno associated viruses (AAVs) are prime candidates for gene therapy as this virus harbors no known adverse pathogenicity and is small (less than 20 nm) which helps diffusion across the cell membrane [76]. In addition, AAVs have been successfully used in human clinical trials for ocular diseases [77]. One of the largest obstacles to overcome in cochlear gene therapy is to deliver a viral vector into the cochlea without causing hearing loss or damage to the cochlea itself. Animal models have shown successful AAV-GFP viral transduction into cochlear cells after injection into different entry points including the posterior semicircular canal, round window, or scala media with little to no cochlear damage [78,79]. Further, CRISPR-Cas9 genome-editing to correct a dominant deafness mutant caused by a mutation in transmembrane channel-like gene family 1 gene (*Tmc1*, Beethoven) was injected into the neonatal cochlea and significantly reduced progressive hearing loss [80].

GJB2 hearing loss linked mutants are uniquely positioned to be rescued by viral induction of AAVs due to their small packing size (limit of 5 kb) where the entire coding exon of connexins can be packed into a single AAV [81]. Additionally, since most *GJB2* hearing loss linked mutants are recessive, it leaves a therapeutic window available whereby only one WT Cx26 allele may be required for significant hearing recovery [1,82]. There is no evidence to suggest that Cx26 plays a role in hair cell fate or differentiation, however, *GJB2* mutants that cause hearing loss result in hair cell loss in early postnatal development [83,84]. AAV viral delivery of WT Cx26 into the scala media of neonatal Cx26 conditional knock-out mice restored the gap junctional intercellular network of cochlear supporting cells and resulted in partial improvement in the morphology of the organ of Corti [85]. However, no functional

improvement in hearing thresholds were observed after viral delivery, limiting the potential therapeutic value [85]. Another study injecting WT Cx26 packed AAVs into the perilymph through the oval window at P0 in Cx26 conditional knock-out mice showed proper formation of the organ of Corti and significant hearing preservation [86]. However, when the injection was performed in mice at P42 no cochlear morphology or hearing improvement was observed, suggesting that one limiting factor of successful hearing restoration is early gene delivery.

These studies are a promising start to the potential of personalized gene therapy for individual *GJB2* mutations that may have different mechanisms of action in the *in vivo* cochlea. However, it is also important to note the different developmental stages of hearing in mice versus humans where mice acquire mature hearing at P14 while humans can hear at approximately four months in utero [87–89]. While most successful AAV deliveries in mice have been performed in P0-P1 cochlea, this would translate to a "pre-hearing" phenotype in mice. In humans, to treat the fetus as a similar stage of hearing acquisition would require in utero viral delivery; a procedure that would require extreme precision and could cause potential damage. Consequently, this approach is somewhat daunting to consider. Preclinical work has shown that overexpression of Atoh1 (transcription factor involved in hair cell differentiation) is sufficient to rescue hearing impairment by regenerating hair cells [90,91]. A clinical trial involving an AAV containing Atoh1-cDNA for the treatment of hearing loss was started in 2014 and expected to be completed 2021 (clinicaltrials.org). This trial will give us novel insight as to the translational capacity of using AAVs to treat hearing loss in human patients.

6.4.3. Targeted antibodies for *GJB2* related hearing loss mutants

The use of antibodies to block and downregulate specific proteins of interest has proven to be a useful approach in therapeutics. There are at least eight different gain-of function syndromic *GJB2* mutations causing skin disorders that exhibit hyperactive or "leaky" hemichannels (G11E, G12R, N14K, N14Y, A40V, G45E, D50A, D50N, A88V) [92]. For these particular mutations, downregulating Cx26 function may prove to be beneficial. Another study recently identified a human recombinant antibody that binds a peptide derived from the first extracellular loop of Cx26 and perturbs hemichannel function [93]. This study found that the antibody was non-toxic to cells, and reversibly inhibited Cx26 hemichannel currents while strongly reducing hemichannel activity of some Cx26 hyperactive mutants. In organotypic

cochlear cultures of P5 mice, incubation of the antibody (abEC1.1) for 15-20 minutes significantly reduced spontaneous Ca^{2+} events, a process that is known to involve connexins. However, microinjection of Lucifer yellow into cultures showed that pre-incubation of this antibody did not affect dye transfer, suggesting that this antibody specifically inhibited connexin hemichannel, but not gap junction, function [93]. The antibody also reduced the activity of hyperactive hemichannels of Cx26 G45E and D50N in a keratinocyte cell line [93]. Further studies using connexin targeted antibodies delivered specifically to the inner ear are needed to evaluate whether they provide a novel potential therapeutic strategy in treating hearing loss.

6.5. Potential therapeutic targets of connexins and pannexins

Collectively our studies show that pannexins are not involved in auditory function, suggesting there is limited utility in developing potential therapies for pannexins in auditory function. However, it is important to note that the first human patient with a *PANX1* variant was recently found to have multiple symptoms including hearing loss leading to a cochlear implant [94]. It is unclear if hearing loss is directly correlated to the variant itself or due to one of the other many symptoms incurred such as brain developmental deformities. Nonetheless, the need for connexin therapeutics whereby increasing GJIC may help to restore normal cochlear function would be useful for hearing loss-linked connexin mutations. Many therapeutic targets including antisense oligonucleotides and peptide mimetics have been used to alter Cx43 expression [95]. For example, an oligonucleotide (AsODN) from CoDa Therapeutics has been used to treat skin wounds since it is known that decreasing Cx43 expression enhances wound healing [96,97]. A promising peptide mimetic produced by First String Research, aCT1, was originally shown to decrease scar formation and promote wound healing in preclinical studies [98]. In clinical trials, aCT1 reduced the ulcer area and enhanced wound closure in diabetic patients [97]. Previous studies have shown that aCT1 prevents the interaction between Cx43 and ZO-1, ultimately leading to larger gap junctions which may increase communication between cells [99,100]. aCT1 has also been shown to promote the incorporation of Cx43 hemichannels to gap junction plaques, which may in turn lead to enhanced cellular communication [100].

The potential of drug therapeutics for treatment of hearing loss is theoretically promising due documented successes of some key preclinical and clinical trials. The therapeutic approach of Cx43 targeted strategies may be useful for patients with ODDD that have sensorineural hearing loss as an additional comorbidity. In Chapter 4 we showed that $Cx43^{G60S/+}$ mutant mice had significant hearing loss while $Cx43^{I130T/+}$ mutant mice did not, where the G60S mutation retains only 15-20% of GJIC while the I130T mutant retains approximately 50% [101,102]. Importantly, some patients with ODDD have hearing loss while others do not, thus, we propose that this phenomenon may be due to the functional level of Cx43 in the auditory system. These findings support the notion that Cx43 function in the auditory tract is essential, however, there is a therapeutic window where only 50% function is enough to maintain proper hearing. Using a peptide, such as aCT1, that would promote Cx43 GJIC could in theory be beneficial in treating hearing loss linked patients with ODDD.

6.6. Future directions

In Chapter 4 we found that $Cx43^{G60S/+}$ had significant hearing loss which was mapped to decreases in the neural firing of the auditory brainstem regions (i.e. higher order auditory regions). Additionally, we found Cx43 to be localized to the cochlear nerve region where the nerves contact the brain region. Since Cx43 is abundantly expressed in astrocytes of the brain, it would be beneficial to conduct more higher-order auditory processing tasks to see if these mutant mice also have dysfunction in the auditory cortex region. This is of particular importance because typically higher-order auditory testing is not generally performed as a first pass screening and thus, patients with these mutations could have processing disorders that will remain undetected. With future studies examining the role of Cx43 in these regions, more insight will be shed on its' precise role in hearing.

In Chapter 5 we found that GJIC did not influence the level of cisplatin-induced ototoxicity in Cx43 mutant mice and a cochlear relevant cell line. The use of organotypic cochlear cultures is useful in maintaining the three-dimensional aspect of the cochlea for the use of drug treatments, however, it is not the same environment as is in the *in vivo* inner ear. For example, we and others have found that carbenoxolone treatment did not cause hair cell loss in organotypic cochlear cultures [103]. However, when CBX was administered into the *in vivo* cochlea directly, CBX causes significant hair cell loss [103]. This emphasizes the fact that the

model may not fully mimic the *in vivo* setting. Therefore, future directions of this study could involve administering cisplatin to Cx43 mutant mice through intravenous injection, as is performed in humans, and examine whether loss of Cx43 GJIC impacts cisplatin-induced ototoxicity *in vivo*. Further, because we examined reorganization of Cx26 and Cx30 gap junction channels after cisplatin treatment in our organotypic cochlear cultures, it would be interesting to see if this also occurred in cochlear supporting cells when cisplatin was administered to the mouse directly. Continuing on with these studies, cisplatin administration to hearing loss-linked Cx26 mutant mice would provide us with insight as to whether patients with Cx-induced hearing loss would be more or less susceptible to drug-induced hearing loss. Collectively, these studies would provide us with information that would be informative in a translational capacity to patients with hearing loss and undergoing cancer treatment.

6.7. Overall conclusions

The compilation of studies presented in this thesis were performed to assess the importance of large pore channels, connexins and pannexins, in auditory function. To accomplish this we examined three main categories of hearing loss including; genetically acquired-, noise- and drug-induced hearing loss. Using both genetically modified mice harboring either global ablations of pannexins and point mutations of connexins we were able to phenotype the auditory profile of these mice under baseline hearing as well as after exposure to loud noise-exposure. Finally, to evaluate the molecular processes involved in drug-induced hearing loss we used organotypic cochlear cultures treated with cisplatin in connexin mutant mice to examine whether connexins exacerbated or prevented cisplatin-induced cell death. The work presented in this thesis outlines the first comprehensive evaluation of connexins and pannexins in a wide range of hearing loss.

6.8. References

1 Kelsell, D. P., Dunlop, J., Stevens, H. P., Lench, N. J., Liang, J. N., Parry, G., Mueller, R. F. and Leigh, I. M. (1997) Connexin 26 mutations in hereditary non-syndromic sensorineural deafness. Nature.

2 Kelley, P. M., Abe, S., Askew, J. W., Smith, S. D., Usami, S. I. and Kimberling, W. J. (1999) Human connexin 30 (GJB6), a candidate gene for nonsyndromic hearing loss: Molecular cloning, tissue-specific expression, and assignment to chromosome 13q12. Genomics **62**, 172–176.

3 Le, T. N., Straatman, L. V., Lea, J. and Westerberg, B. (2017) Current insights in noise-induced hearing loss: a literature review of the underlying mechanism, pathophysiology, asymmetry, and management options. J. Otolaryngol. - Head Neck Surg., Journal of Otolaryngology - Head & Neck Surgery **46**.

4 Kurabi, A., Keithley, E. M., Housley, G. D., Ryan, A. F. and Wong, A. C. Y. (2017) Cellular mechanisms of noise-induced hearing loss. Hear. Res., **349**, 129–137.

5 Zhao, H.-B., Zhu, Y., Liang, C. and Chen, J. (2015) Pannexin 1 deficiency can induce hearing loss. Biochem. Biophys. Res. Commun. 1–5.

6 Chen, J., Zhu, Y., Liang, C., Chen, J. and Zhao, H.-B. (2015) Pannexin1 channels dominate ATP release in the cochlea ensuring endocochlear potential and auditory receptor potential generation and hearing. Sci. Rep., **5**, 10762.

7 Penuela, S., Kelly, J. J., Churko, J. M., Barr, K. J., Berger, A. C. and Laird, D. W. (2014) Panx1 regulates cellular properties of keratinocytes and dermal fibroblasts in skin development and wound healing. J. Invest. Dermatol., Nature Publishing Group **134**, 2026–35.

8 Moon, P. M., Penuela, S., Barr, K., Khan, S., Pin, C. L., Welch, I., Attur, M., Abramson, S. B., Laird, D. W. and Beier, F. (2015) Deletion of Panx3 Prevents the Development of Surgically Induced Osteoarthritis. J. Mol. Med. 845–856.

9 Zhao, H.-B., Zhu, Y., Liang, C. and Chen, J. (2015) Pannexin 1 deficiency can induce hearing loss. Biochem. Biophys. Res. Commun. 1–5.

10 Lohman, A.W and Isakson, B,E. (2014) Differentiating connexin hemichannels and pannexin channels in cellular ATP release **588**, 1379–1388.

11 Whyte-fagundes, P., Kurtenbach, S., Zoidl, C., Shestopalov, V. I., Carlen, P. L. and Zoidl, G. (2018) A Potential Compensatory Role of Panx3 in the VNO of a Panx1 Knock Out Mouse Model **11**, 1–16.

12 Anselmi, F., Hernandez, V. H., Crispino, G., Seydel, A., Ortolano, S., Roper, S. D., Kessaris, N., Richardson, W., Rickheit, G., Filippov, M. A., et al. (2008) ATP release through connexin hemichannels and gap junction transfer of second messengers

propagate Ca2+ signals across the inner ear. Proc. Natl. Acad. Sci. **105**, 18770–18775.

13 Zorzi, V., Paciello, F., Ziraldo, G., Peres, C., Mazzarda, F., Nardin, C., Pasquini, M., Chiani, F., Raspa, M., Scavizzi, F., et al. (2017) Mouse Panx1 is dispensable for hearing acquisition and auditory function. Front. Mol. Neurosci. **10**, 379.

14 Rance, G., Ryan, M. M., Bayliss, K., Gill, K., O'Sullivan, C. and Whitechurch, M. (2012) Auditory function in children with Charcot-Marie-Tooth disease. Brain **135**, 1412–1422.

15 Choi, J. E., Seok, J. M., Ahn, J., Ji, Y. S., Lee, K. M., Hong, S. H., Choi, B. O. and Moon, I. J. (2018) Hidden hearing loss in patients with Charcot-Marie-Tooth disease type 1A. Sci. Rep., **8**, 1–8.

16 Tang, W., Zhang, Y., Chang, Q., Ahmad, S., Dahlke, I., Yi, H., Chen, P., Paul, D. L. and Lin, X. (2006) Connexin29 Is Highly Expressed in Cochlear Schwann Cells, and It Is Required for the Normal Development and Function of the Auditory Nerve of Mice. J. Neurosci. **26**, 1991.

17 Zhou, X. X., Chen, S., Xie, L., Ji, Y. Z., Wu, X., Wang, W. W., Yang, Q., Yu, J. T., Sun, Y., Lin, X., et al. (2016) Reduced connexin26 in the mature cochlea increases susceptibility to noise-induced hearing lossin mice. Int. J. Mol. Sci. **17**.

18 Dilber, M. S., Abedi, M. R., Christensson, B., Bjrkstrand, B., Kidder, G. M., Naus, C. C. G., Gahrton, G. and Smith, C. I. E. (1997) Gap junctions promote the bystander effect of herpes simplex virus thymidine kinase in vivo. Cancer Res. **57**, 1523–1528.

19 Quist, A. P., Rhee, S. K., Lin, H. and Lal, R. (2000) Physiological role of gap-junctional hemichannels: Extracellular calcium-dependent isosmotic volume regulation. J. Cell Biol. **148**, 1063–1074.

20 Lopez, W., Ramachandran, J., Alsamarah, A., Luo, Y., Harris, A. L. and Contreras, J. E. (2016) Mechanism of gating by calcium in connexin hemichannels. Proc. Natl. Acad. Sci. U. S. A. **113**, E7986–E7995.

21 Bruzzone, R., Barbe, M. T., Jakob, N. J. and Monyer, H. (2005) Pharmacological properties of homomeric and heteromeric pannexin hemichannels expressed in Xenopus oocytes. J. Neurochem. **92**, 1033–1043.

22 Eskandari, S., Zampighi, G. A., Leung, D. W., Wright, E. M. and Loo, D. D. F. (2002) Inhibition of gap junction hemichannels by chloride channel blockers. J. Membr. Biol. **185**, 93–102.

23 Srinivas, M. and Spray, D. C. (2003) Closure of gap junction channels by arylaminobenzoates. Mol. Pharmacol. **63**, 1389–1397.

24 Bruzzone, R., Barbe, M. T., Jakob, N. J. and Monyer, H. (2005) Pharmacological properties of homomeric and heteromeric pannexin hemichannels expressed in

Xenopus oocytes. J. Neurochem. **92**, 1033–1043.

25 Silverman, W., Locovei, S. and Dahl, G. (2008) Probenecid, a gout remedy, inhibits pannexin 1 channels. AJP Cell Physiol. **295**, C761–C767.

26 Ye, Z. C., Wyeth, M. S., Baltan-Tekkok, S. and Ransom, B. R. (2003) Functional hemichannels in astrocytes: A novel mechanism of glutamate release. J. Neurosci. **23**, 3588–3596.

27 Wang, N., De Bock, M., Antoons, G., Gadicherla, A. K., Bol, M., Decrock, E., Evans, W. H., Sipido, K. R., Bukauskas, F. F. and Leybaert, L. (2012) Connexin mimetic peptides inhibit Cx43 hemichannel opening triggered by voltage and intracellular Ca2+ elevation. Basic Res. Cardiol. **107**, 17.

28 Desplantez, T., Verma, V., Leybaert, L., Evans, W. H. and Weingart, R. (2012) Gap26, a connexin mimetic peptide, inhibits currents carried by connexin43 hemichannels and gap junction channels. Pharmacol. Res., **65**, 546–552.

29 Warner, A., Clements, D. K., Parikh, S., Evans, W. H. and DeHaan, R. L. (1995) Specific motifs in the external loops of connexin proteins can determine gap junction formation between chick heart myocytes. J. Physiol. **488**, 721–728.

30 Wang, J., Ma, M., Locovei, S., Keane, R. W. and Dahl, G. (2007) Modulation of membrane channel currents by gap junction protein mimetic peptides: size matters. Am J Physiol Cell Physiol **293**, C1112-9.

31 Howard Evans, W. and Leybaert, L. (2007) Mimetic peptides as blockers of connexin channel-facilitated intercellular communication. Cell Commun. Adhes. **14**, 265–273.

32 Wang, N., De Vuyst, E., Ponsaerts, R., Boengler, K., Palacios-Prado, N., Wauman, J., Lai, C. P., De Bock, M., Decrock, E., Bol, M., et al. (2013) Selective inhibition of Cx43 hemichannels by Gap19 and its impact on myocardial ischemia/reperfusion injury. Basic Res. Cardiol. **108**.

33 Abudara, V., Bechberger, J., Freitas-Andrade, M., De Bock, M., Wang, N., Bultynck, G., Naus, C. C., Leybaert, L. and Giaume, C. (2014) The connexin43 mimetic peptide Gap19 inhibits hemichannels without altering gap junctional communication in astrocytes. Front. Cell. Neurosci. **8**, 1–8.

34 D'hondt, C., Iyyathurai, J., Himpens, B., Leybaert, L. and Bultynck, G. (2014) Cx43-hemichannel function and regulation in physiology and pathophysiology: insights from the bovine corneal endothelial cell system and beyond. Front. Physiol. **5**, 1–13.

35 Ponsaerts, R., De Vuyst, E., Retamal, M., D'hondt, C., Vermeire, D., Wang, N., De Smedt, H., Zimmermann, P., Himpens, B., Vereecke, J., et al. (2010) Intramolecular loop/tail interactions are essential for connexin 43-hemichannel activity. FASEB J. **24**, 4378–4395.

36 Seminario-Vidal, L., Okada, S. F., Sesma, J. I., Kreda, S. M., Van Heusden, C. A., Zhu, Y., Jones, L. C., O'Neal, W. K., Penuela, S., Laird, D. W., et al. (2011) Rho signaling regulates pannexin 1-mediated ATP release from airway epithelia. J. Biol. Chem. **286**, 26277–26286.

37 Pelegrin, P. and Surprenant, A. (2007) Pannexin-1 couples to maitotoxin- and nigericin-induced interleukin-1β release through a dye uptake-independent pathway. J. Biol. Chem. **282**, 2386–2394.

38 Manohar, M., Hirsh, M. I., Chen, Y., Woehrle, T., Karande, A. A. and Junger, W. G. (2012) ATP release and autocrine signaling through P2X4 receptors regulate γδ T cell activation. J. Leukoc. Biol. **92**, 787–794.

39 Teubner, B., Michel, V., Pesch, J., Lautermann, J., Cohen-Salmon, M., Söhl, G., Jahnke, K., Winterhager, E., Herberhold, C., Hardelin, J. P., et al. (2003) Connexin30 (Gjb6)-deficiency causes severe hearing impairment and lack of endocochlear potential. Hum. Mol. Genet. **12**, 13–21.

40 Boulay, A.-C., Del Castillo, F. J., Giraudet, F., Hamard, G., Giaume, C., Petit, C., Avan, P. and Cohen-Salmon, M. (2013) Hearing Is Normal without Connexin30 **33**, 430–434.

41 Ortolano, S., Di Pasquale, G., Crispino, G., Anselmi, F., Mammano, F. and Chiorini, J. A. (2008) Coordinated control of connexin 26 and connexin 30 at the regulatory and functional level in the inner ear. Proc. Natl. Acad. Sci. **105**, 18776–18781.

42 Ahmad, S., Tang, W., Chang, Q., Qu, Y., Hibshman, J., Li, Y., Söhl, G., Willecke, K., Chen, P. and Lin, X. (2007) Restoration of connexin26 protein level in the cochlea completely rescues hearing in a mouse model of human connexin30-linked deafness. Proc. Natl. Acad. Sci. U. S. A. **104**, 1337–41.

43 Stewart, M. K. G., Gong, X.-Q., Barr, K. J., Bai, D., Fishman, G. I. and Laird, D. W. (2013) The severity of mammary gland developmental defects is linked to the overall functional status of Cx43 as revealed by genetically modified mice. Biochem. J. **449**, 401–13.

44 Abitbol, J. M., Kelly, J. J., Barr, K., Schormans, A. L., Laird, D. W. and Allman, B. L. (2016) Differential effects of pannexins on noise-induced hearing loss. Biochem. J. **473**, 4665–4680.

45 Hanstein, R., Negoro, H., Patel, N. K., Charollais, A., Meda, P., Spray, D. C., Suadicani, S. O. and Scemes, E. (2013) Promises and pitfalls of a Pannexin1 transgenic mouse line. Front. Pharmacol. **4**

46 Bargiotas, P., Krenz, A., Hormuzdi, S. G., Ridder, D. A., Herb, A., Barakat, W., Penuela, S., von Engelhardt, J., Monyer, H. and Schwaninger, M. (2011) Pannexins in ischemia-induced neurodegeneration. Proc. Natl. Acad. Sci. U. S. A. **108**, 20772–7.

47 Heffner, H. E. and Heffner, R. S. (2007) Hearing ranges of laboratory animals. J. Am. Assoc. Lab. Anim. Sci. **46**, 20–22.

48 Lawoko-Kerali, G., Rivolta, M. N. and Holley, M. (2002) Expression of the transcription factors GATA3 and Pax2 during development of the mammalian inner ear. J. Comp. Neurol. **442**, 378–391.

49 Manuel, M., Martynoga, B., Yu, T., West, J. D., Mason, J. O. and Price, D. J. (2010) The transcription factor Foxg1 regulates the competence of telencephalic cells to adopt subpallial fates in mice. Development **137**, 487–497.

50 Kumamoto, T. and Hanashima, C. (2017) Evolutionary conservation and conversion of Foxg1 function in brain development. Dev. Growth Differ. **59**, 258–269.

51 Urbánek, P., Fetka, I., Meisler, M. H. and Busslinger, M. (1997) Cooperation of Pax2 and Pax5 in midbrain and cerebellum development. Proc. Natl. Acad. Sci. U. S. A. **94**, 5703–5708.

52 Fotaki, V., Price, D. J. and Mason, J. O. (2008) Newly identified patterns of Pax2 expression in the developing mouse forebrain. BMC Dev. Biol. **8**, 1–11.

53 Vogt, A., Hormuzdi, S. G. and Monyer, H. (2005) Pannexin1 and Pannexin2 expression in the developing and mature rat brain. Mol. Brain Res. **141**, 113–120.

54 Penuela, S., Gehi, R. and Laird, D. W. (2013) The biochemistry and function of pannexin channels. Biochim. Biophys. Acta, Elsevier B.V. **1828**, 15–22.

55 Loonstra, A., Vooijs, M., Beverloo, H. B., Allak, B. Al, Van Drunen, E., Kanaar, R., Berns, A. and Jonkers, J. (2001) Growth inhibition and DNA damage induced by Cre recombinase in mammalian cells. Proc. Natl. Acad. Sci. U. S. A. **98**, 9209–9214.

56 Patel, H. and Feldman, M. (2011) Universal Newborn HS - H.Patel. Paediatr Child Heal. **16**, 301–305.

57 Nazir, T., Gupta, S., Mir, G., Jamwal, A., Kalsotra, P. and Singh, K. (2016) Evaluation of otoacoustic emissions and auditory brainstem responses for hearing screening of high risk infants. Indian J. Otol. **22**, 221–230.

58 Korver, A. M. H., Smith, R. J. H., Camp, G. Van, Schleiss, M. R., Bitner-Glindzicz, M. A. K., Lustig, L. R., Usami, S.-I. and Boudewyns, A. N. (2018) Congenital hearing loss HHS Public Access.

59 Erbe, C. B., Harris, K. C., Runge-Samuelson, C. L., Flanary, V. A. and Wackym, P. A. (2004) Connexin 26 and Connexin 30 Mutations in Children with Nonsyndromic Hearing Loss. Laryngoscope **114**, 607–611.

60 Laird, D. W., Naus, C. C. and Lampe, P. D. (2017) SnapShot: Connexins and Disease. Cell, **170**, 1260-1260.e1.

61 Kim, A. H., Nahm, E., Sollas, A., Mattiace, L. and Rozental, R. (2013) Connexin 43 and hearing: Possible implications for retrocochlear auditory processing. Laryngoscope **123**, 3185–3193.

62 Paznekas, W. A., Boyadjiev, S. A., Shapiro, R. E., Daniels, O., Wollnik, B., Keegan, C. E., Innis, J. W., Dinulos, M. B., Christian, C., Hannibal, M. C., et al. (2003) Connexin 43 (GJA1) mutations cause the pleiotropic phenotype of oculodentodigital dysplasia. Am. J. Hum. Genet. **72**, 408–18.

63 Paznekas, W. A., Karczeski, B., Vermeer, S., Lowry, R. B., Delatycki, M., Laurence, F., Koivisto, P. A., Van Maldergem, L., Boyadjiev, S. A., Bodurtha, J. N., et al. (2009) GJA1 mutations, variants, and connexin 43 dysfunction as it relates to the oculodentodigital dysplasia phenotype. Hum. Mutat. **30**, 724–733.

64 Zeng, F. G., Tang, Q. and Lu, T. (2014) Abnormal pitch perception produced by cochlear implant stimulation. PLoS One **9**.

65 Dillon, M. T., Buss, E., Rooth, M. A., King, E. R., Pillsbury, H. C. and Brown, K. D. (2019) Low-Frequency Pitch Perception in Cochlear Implant Recipients With Normal Hearing in the Contralateral Ear. J. Speech, Lang. Hear. Res. **62**, 1–12.

66 Salt, A. N. and Plontke, S. K. (2009) Principles of local drug delivery to the inner ear. Audiol. Neurotol. **14**, 350–360.

67 Hao, J. and Li, S. K. (2018) Inner ear drug delivery: Recent advances, challenges, and perspective. Eur. J. Pharm. Sci.,

68 Liu, H., Hao, J. and Li, K. S. (2013) Current strategies for drug delivery to the inner ear. Acta Pharm. Sin. B, Elsevier **3**, 86–96.

69 Rybak, L. P., Dhukhwa, A., Mukherjea, D. and Ramkumar, V. (2019) Local Drug Delivery for Prevention of Hearing Loss. Front. Cell. Neurosci. **13**, 1–14.

70 Okano, T. (2014) Immune system of the inner ear as a novel therapeutic target for sensorineural hearing loss. Front. Pharmacol. **5**, 1–8.

71 Nyberg, S., Joan Abbott, N., Shi, X., Steyger, P. S. and Dabdoub, A. (2019) Delivery of therapeutics to the inner ear: The challenge of the blood-labyrinth barrier. Sci. Transl. Med. **11**, 1–12.

72 Glueckert, R., Johnson Chacko, L., Rask-Andersen, H., Liu, W., Handschuh, S. and Schrott-Fischer, A. (2018) Anatomical basis of drug delivery to the inner ear. Hear. Res., The Authors **368**, 10–27.

73 Patel, J., Szczupak, M., Rajguru, S., Balaban, C. and Hoffer, M. E. (2019) Inner ear therapeutics: An overview of middle ear delivery. Front. Cell. Neurosci. **13**, 1–8.

74 Mäder, K., Lehner, E., Liebau, A. and Plontke, S. K. (2018) Controlled drug release to

the inner ear: Concepts, materials, mechanisms, and performance. Hear. Res. **368**, 49–66.

75 Naples, J. G., Henry, L., Brant, J. A., Eliades, S. J. and Ruckenstein, M. J. (2019) Intratympanic Therapies in Ménière Disease: Evaluation of Outcomes and Early Vertigo Control. Laryngoscope **129**, 216–221.

76 Xie, Q., Bu, W., Bhatia, S., Hare, J., Somasundaram, T., Azzi, A. and Chapman, M. S. (2002) The atomic structure of adeno-associated virus **99**.

77 Dalkara, D., Byrne, L. C., Klimczak, R. R., Visel, M., Yin, L., Merigan, W. H., Flannery, J. G. and Schaffer, D. V. (2013) In vivo-directed evolution of a new adeno-associated virus for therapeutic outer retinal gene delivery from the vitreous. Sci. Transl. Med. **5**.

78 Zhang, W., Kim, S. M., Wang, W., Cai, C., Feng, Y., Kong, W. and Lin, X. (2018) Cochlear Gene Therapy for Sensorineural Hearing Loss: Current Status and Major Remaining Hurdles for Translational Success. Front. Mol. Neurosci. **11**.

79 Landegger, L. D., Pan, B., Askew, C., Wassmer, S., Galvin, A., Taylor, R., Forge, A., Stankovic, K. M., Holt, J. R., Vandenberghe, L. H., et al. (2017) A synthetic AAV vector enables safe and efficient gene transfer to the mammalian inner ear Lukas **35**, 280–284.

80 Gao, X., Tao, Y., Lamas, V., Huang, M., Yeh, W.-H., Pan, B., Hu, Y.-J., Hu, J. H., Thompson, D. B., Shu, Y., et al. (2017) Treatment of autosomal dominant hearing loss by in vivo delivery of genome editing agents. Nature, Nature Publishing Group.

81 Maeda, S., Nakagawa, S., Suga, M., Yamashita, E., Oshima, A., Fujiyoshi, Y. and Tsukihara, T. (2009) Structure of the connexin 26 gap junction channel at 3.5 Å resolution. Nature, Nature Publishing Group **458**, 597–602.

82 Kemperman, M. H., Hoefsloot, L. H. and Cremers, C. W. R. J. (2002) Hearing loss and connexin 26. J. R. Soc. Med. **95**, 171–177.

83 Cohen-Salmon, M., Ott, T., Michel, V., Hardelin, J. P., Perfettini, I., Eybalin, M., Wu, T., Marcus, D. C., Wangemann, P., Willecke, K., et al. (2002) Targeted ablation of connexin26 in the inner ear epithelial gap junction network causes hearing impairment and cell death. Curr. Biol. **12**, 1106–1111.

84 Maeda, Y., Fukushima, K., Kawasaki, A., Nishizaki, K. and Smith, R. J. H. (2007) Cochlear expression of a dominant-negative GJB2 R75W construct delivered through the round window membrane in mice **58**, 250–254.

85 Yu, Q., Wang, Y., Chang, Q., Wang, J., Gong, S., Li, H. and Lin, X. (2014) Virally expressed connexin26 restores gap junction function in the cochlea of conditional Gjb2 knockout mice. Gene Ther. **21**, 71–80.

86 Iizuka, T., Kamiya, K., Gotoh, S., Sugitani, Y., Suzuki, M., Noda, T., Minowa, O. and Ikeda, K. (2015) Perinatal GJB2 gene transfer rescues hearing in a mouse model of hereditary deafness. Hum. Mol. Genet. **24**, 3651–3661.

87 Sonntag, M., Englitz, B., Kopp-Scheinpflug, C. and Rübsamen, R. (2009) Early postnatal development of spontaneous and acoustically evoked discharge activity of principal cells of the medial nucleus of the trapezoid body: An in vivo study in mice. J. Neurosci. **29**, 9510–9520.

88 Querleu, D., Renard, X., Versyp, F., Paris-Delrue, L. and Crèpin, G. (1988) Fetal hearing. Eur. J. Obstet. Gynecol. Reprod. Biol. **28**, 191–212.

89 Tritsch, N. X., Yi, E., Gale, J. E., Glowatzki, E. and Bergles, D. E. (2007) The origin of spontaneous activity in the developing auditory system. Nature **450**, 50–55.

90 Yang, S. M., Chen, W., Guo, W. W., Jia, S., Sun, J. H., Liu, H. Z., Young, W. Y. and He, D. Z. Z. (2012) Regeneration of Stereocilia of Hair Cells by Forced Atoh1 Expression in the Adult Mammalian Cochlea. PLoS One **7**, 1–8.

91 Lee, S., Jeong, H.-S. and Cho, H.-H. (2017) Atoh1 as a Coordinator of Sensory Hair Cell Development and Regeneration in the Cochlea. Chonnam Med. J. **53**, 37.

92 Retamal, M. A., Reyes, E. P., GarcÃ-a, I. E., Pinto, B., MartÃ-nez, A. D. and GonzÃ¡lez, C. (2015) Diseases associated with leaky hemichannels. Front. Cell. Neurosci. **9**, 1–10.

93 Xu, L., Carrer, A., Zonta, F., Qu, Z., Ma, P., Li, S., Ceriani, F., Buratto, D., Crispino, G., Zorzi, V., et al. (2017) Design and Characterization of a Human Monoclonal Antibody that Modulates Mutant Connexin 26 Hemichannels Implicated in Deafness and Skin Disorders. Front. Mol. Neurosci. **10**.

94 Shao, Q., Lindstrom, K., Shi, R., Kelly, J., Schroeder, A., Juusola, J., Levine, K. L., Esseltine, J. L., Penuela, S., Jackson, M. F., et al. (2016) A germline variant in PANX1 has reduced channel function and is associated with multisystem dysfunction. J. Biol. Chem. jbc.M116.717934.

95 Laird, D. W. and Lampe, P. D. (2018) Therapeutic strategies targeting connexins. Nat. Rev. Drug Discov.

96 Wong, P., Tan, T., Chan, C., Laxton, V., Chan, Y. W. F., Liu, T., Wong, W. T. and Tse, G. (2016) The role of connexins in wound healing and repair: Novel therapeutic approaches. Front. Physiol. **7**, 1–11.

97 Montgomery, J., Ghatnekar, G. S., Grek, C. L., Moyer, K. E. and Gourdie, R. G. (2018) Connexin 43-based therapeutics for dermal wound healing. Int. J. Mol. Sci. **19**.

98 Ghatnekar, G. S., Quinn, M. P. O., Jourdan, L. J., Gurjarpadhye, A. A., Draughn, R. L. and Gourdie, R. G. (2010) and Promote Regenerative Healing Following Skin

Wounding **4**, 205–223.

99 Hunter, A. W. and , Ralph J. Barker, Ching Zhu, and R. G. G. (2005) Zonula Occludens-1 Alters Connexin43 Gap Junction Size and Organization by Influencing Channel Accretion. Mol. Biol. Cell **16**, 4341–4349.

100 Rhett, J. M., Jourdan, J. and Gourdie, R. G. (2011) Connexin 43 connexon to gap junction transition is regulated by zonula occludens-1. Mol. Biol. Cell **22**, 1516–1528.

101 Kalcheva, N., Qu, J., Sandeep, N., Garcia, L., Zhang, J., Wang, Z., Lampe, P. D., Suadicani, S. O., Spray, D. C. and Fishman, G. I. (2007) Gap junction remodeling and cardiac arrhythmogenesis in a murine model of oculodentodigital dysplasia. Proc. Natl. Acad. Sci. U. S. A. **104**, 20512–20516.

102 Flenniken, A. M., Osborne, L. R., Anderson, N., Ciliberti, N., Fleming, C., Gittens, J. E. I., Gong, X.-Q., Kelsey, L. B., Lounsbury, C., Moreno, L., et al. (2005) A Gja1 missense mutation in a mouse model of oculodentodigital dysplasia. Development **132**, 4375–86.

103 Nishiyama, N., Yamaguchi, T., Yoneyama, M., Onaka, Y. and Ogita, K. (2019) Disruption of Gap Junction-Mediated Intercellular Communication in the Spiral Ligament Causes Hearing and Outer Hair Cell Loss in the Cochlea of Mice **42**, 73–80.

Appendix 1 Copyrights

SPRINGER NATURE LICENSE
TERMS AND CONDITIONS

Sep 05, 2019

This Agreement between Miss. Julia Abitbol ("You") and Springer Nature ("Springer Nature") consists of your license details and the terms and conditions provided by Springer Nature and Copyright Clearance Center.

License Number	4660860920756
License date	Sep 02, 2019
Licensed Content Publisher	Springer Nature
Licensed Content Publication	Nature Reviews Drug Discovery
Licensed Content Title	Therapeutic strategies targeting connexins
Licensed Content Author	Dale W. Laird, Paul D. Lampe
Licensed Content Date	Oct 12, 2018
Licensed Content Volume	17
Licensed Content Issue	12
Type of Use	Thesis/Dissertation
Requestor type	academic/university or research institute
Format	electronic
Portion	figures/tables/illustrations
Number of figures/tables/illustrations	1
High-res required	no
Will you be translating?	no
Circulation/distribution	1 - 29
Author of this Springer Nature content	no
Title	The role of connexins and pannexins in hearing
Institution name	The University of Western Ontario
Expected presentation date	Nov 2019
Portions	Figure 1A&B
Requestor Location	Miss. Julia Abitbol 2200 South Lane Road Sudbury, ON P3G 1C8 Canada Attn: Miss. Julia Abitbol
Total	0.00 CAD
Terms and Conditions	

Springer Nature Customer Service Centre GmbH
Terms and Conditions

This agreement sets out the terms and conditions of the licence (the **Licence**) between you and **Springer Nature Customer Service Centre GmbH** (the **Licensor**). By clicking

ELSEVIER LICENSE
TERMS AND CONDITIONS

Sep 10, 2019

This Agreement between Miss. Julia Abitbol ("You") and Elsevier ("Elsevier") consists of your license details and the terms and conditions provided by Elsevier and Copyright Clearance Center.

License Number	4665590336628
License date	Sep 10, 2019
Licensed Content Publisher	Elsevier
Licensed Content Publication	Biochimica et Biophysica Acta (BBA) - Biomembranes
Licensed Content Title	The biochemistry and function of pannexin channels
Licensed Content Author	Silvia Penuela,Ruchi Gehi,Dale W. Laird
Licensed Content Date	Jan 1, 2013
Licensed Content Volume	1828
Licensed Content Issue	1
Licensed Content Pages	8
Start Page	15
End Page	22
Type of Use	reuse in a thesis/dissertation
Portion	figures/tables/illustrations
Number of figures/tables/illustrations	1
Format	electronic
Are you the author of this Elsevier article?	No
Will you be translating?	No
Original figure numbers	Figure 1
Title of your thesis/dissertation	The role of connexins and pannexins in hearing
Publisher of new work	The University of Western Ontario
Expected completion date	Nov 2019
Estimated size (number of pages)	1
Requestor Location	Miss. Julia Abitbol

Publisher Tax ID	GB 494 6272 12
Total	0.00 CAD
Terms and Conditions	

SPRINGER NATURE LICENSE
TERMS AND CONDITIONS

Sep 05, 2019

This Agreement between Miss. Julia Abitbol ("You") and Springer Nature ("Springer Nature") consists of your license details and the terms and conditions provided by Springer Nature and Copyright Clearance Center.

License Number	4660861191683
License date	Sep 02, 2019
Licensed Content Publisher	Springer Nature
Licensed Content Publication	JARO - Journal of the Association for Research in Otolaryngology
Licensed Content Title	The Membrane Properties of Cochlear Root Cells are Consistent with Roles in Potassium Recirculation and Spatial Buffering
Licensed Content Author	Daniel J. Jagger, Graham Nevill, Andrew Forge
Licensed Content Date	Jan 1, 2010
Licensed Content Volume	11
Licensed Content Issue	3
Type of Use	Thesis/Dissertation
Requestor type	academic/university or research institute
Format	electronic
Portion	figures/tables/illustrations
Number of figures/tables/illustrations	1
Will you be translating?	no
Circulation/distribution	1 - 29
Author of this Springer Nature content	no
Title	The role of connexins and pannexins in hearing
Institution name	The University of Western Ontario
Expected presentation date	Nov 2019
Portions	Figure 1A
Requestor Location	Miss. Julia Abitbol

Total	0.00 USD

Terms and Conditions

Springer Nature Customer Service Centre GmbH
Terms and Conditions

This agreement sets out the terms and conditions of the licence (the **Licence**) between you and **Springer Nature Customer Service Centre GmbH** (the **Licensor**). By clicking

Appendix 2 Animal use protocol approval

AUP Number: 2019-009
PI Name: Laird, Dale W
AUP Title: The role of connexin and pannexin channels in health and disease
Approval Date: 05/01/2019

Official Notice of Animal Care Committee (ACC) Approval:
Your new Animal Use Protocol (AUP) 2019-009:1: entitled " The role of connexin and pannexin channels in health and disease "
has been APPROVED by the Animal Care Committee of the University Council on Animal Care. This approval, although valid for up to four years, is subject to annual Protocol Renewal.

Prior to commencing animal work, please review your AUP with your research team to ensure full understanding by everyone listed within this AUP.

As per your declaration within this approved AUP, you are obligated to ensure that:

1) Animals used in this research project will be cared for in alignment with:
   a) Western's Senate MAPPs 7.12, 7.10, and 7.15
   http://www.uwo.ca/univsec/policies_procedures/research.html

   b) University Council on Animal Care Policies and related Animal Care Committee procedures
   http://uwo.ca/research/services/animalethics/animal_care_and_use_policies.htm
2) As per UCAC's Animal Use Protocols Policy,
   a) this AUP accurately represents intended animal use;
   b) external approvals associated with this AUP, including permits and scientific/departmental peer approvals, are complete and accurate;
   c) any divergence from this AUP will not be undertaken until the related Protocol Modification is approved by the ACC; and
   d) AUP form submissions - Annual Protocol Renewals and Full AUP Renewals - will be submitted and attended to within timeframes outlined by the ACC.
   e) http://uwo.ca/research/services/animalethics/animal_use_protocols.html

3) As per MAPP 7.10 all individuals listed within this AUP as having any hands-on animal contact will
   a) be made familiar with and have direct access to this AUP;
   b) complete all required CCAC mandatory training (training@uwo.ca); and
   c) be overseen by me to ensure appropriate care and use of animals.
4) As per MAPP 7.15,
   a) Practice will align with approved AUP elements;
   b) Unrestricted access to all animal areas will be given to ACVS Veterinarians and ACC Leaders;
   c) UCAC policies and related ACC procedures will be followed, including but not limited to:
      i) Research Animal Procurement
      ii) Animal Care and Use Records

iii) Sick Animal Response
iv) Continuing Care Visits

5) As per institutional OH&S policies, all individuals listed within this AUP who will be using or potentially exposed to hazardous materials will have completed in advance the appropriate institutional OH&S training, facility-level training, and reviewed related (M)SDS Sheets, http://www.uwo.ca/hr/learning/required/index.html

Submitted by: Copeman, Laura
on behalf of the Animal Care Committee
University Council on Animal Care

Dr.Timothy Regnault,
Animal Care Committee Chair

The University of Western Ontario
Animal Care Committee / University Council on Animal Care

Curriculum Vitae

Education

2014 – Present **University of Western Ontario – London, ON**
PhD Candidate 2019 (transferred from masters)

2010 – 2014 **University of Western Ontario – London, ON**
Bachelor of Science

- Bachelor Honours Specialization in Biology, minor in Medical Cell Biology
- Dean's Honours list (Fall/2012, Winter/2012)
- The Western Scholarship of Distinction (2010)

Academic Accomplishments/ Research Contributions:

Publications:

Julia M. Abitbol, Rianne Beach, Jessica Esseltine, Kevin Barr, Brian L. Allman, and Dale W. Laird. Cisplatin-induced ototoxicity occurs independent of gap junctional intercellular communication. Submitted to *Cell death and Differentiation.*

Julia M. Abitbol, Brooke L. O'Donnell, Brent B. Wakefield, Elizabeth Jewlal, John J. Kelly, Kevin Barr, Katherine E. Willmore, Brian L. Allman, Silvia Penuela. Double deletion of *Panx1* and *Panx3* affects skin and bone but not hearing. *Journal of Molecular Medicine.* May 2019. 97(5):723-736.

John J. Kelly, Julia M. Abitbol, Stephanie Hulme, Eric R. Press, Dale W. Laird, and Brian L. Allman. The connexin 30 A88V mutant reduces cochlear gap junction expression and confers long-term protection against hearing loss. *Journal of Cell Science*, Jan 2019. 132(2):224097.

Julia M. Abitbol, John J. Kelly, Kevin J. Barr, Brian L. Allman, and Dale W. Laird. Mice harbouring an oculodentodigital dysplasia-linked Cx43 G60S mutation have severe hearing loss. *Journal of Cell Science*, May 2018, 131(9):214635.

Julia M. Abitbol, John J. Kelly, Kevin Barr, Ashley L. Schormans, Dale W. Laird, and Brian L. Allman. Differential effects of Pannexins on noise-induced hearing loss. *Biochemical Journal*, December 2016, 473(24): 4665-4680.

Oral Presentations

- The role of gap junctional intercellular communication in cisplatin-induced ototoxicity as revealed in organotypic cochlear cultures. London Health Research Day, London Convention Center, London, Ontario. (April 2019).

- The role of gap junctional intercellular communication in cisplatin-induced ototoxicity as revealed in organotypic cochlear cultures. Nexin Forum Research Day, University of Western Ontario, London, Ontario. (March 2019).

- Bridging gaps between connexins, pannexins, and hearing loss. Anatomy and Cell Biology Departmental seminar, University of Western Ontario, London, Ontario. (April 2018).

- Severe loss-of-function Cx43 leads to hearing loss in a mouse model of oculodentodigital dysplasia. Nexin Forum Research Day, University of Western Ontario, London, Ontario. (May 2017).

- Large-pore channels in hearing and noise-induced hearing loss. Poster Blitz in Association for Otolaryngology, Baltimore. (February 2017).

- Utilizing genetically modified mice to investigate large-pore channels in hearing. Anatomy and Cell Biology research day. University of Western Ontario, London, Canada. (October 2016).

- The role of Pannexin3 in the auditory system and its contributions to noise-induced hearing damage. Nexin Forum Research Day, University of Western Ontario, London, Ontario. (February 2016).

Poster Presentations

Julia M. Abitbol, Rianne Beach, Kevin Barr, Brian L. Allman, and Dale W. Laird. The role of Cx43 in cisplatin-induced ototoxicity of organotypic cochlear cultures. Anatomy and Cell Biology research day, University of Western Ontario, Canada. (October 2018).

Julia M. Abitbol, John J. Kelly, Kevin Barr, Brian L. Allman, Dale W. Laird. Severe loss-of-function Cx43 leads to hearing loss in a mouse model of oculodentodigital dysplasia. London health research day, London convention center, London, Canada. (May 2018).

Julia M. Abitbol, John J. Kelly, Kevin Barr, Brian L. Allman, Dale W. Laird. Severe loss-of-function Cx43 leads to hearing loss in a mouse model of oculodentodigital dysplasia. Anatomy and Cell Biology research day, University of Western Ontario, London, Canada. (October 2017).

Julia M. Abitbol, John J. Kelly, Kevin Barr, Brian L. Allman, Dale W. Laird. Severe loss-of-function Cx43 leads to hearing loss in a mouse model of oculodentodigital dysplasia. International gap junction meeting, Glasgow, Scotland. (August 2017).

Julia M. Abitbol, John J. Kelly, Kevin Barr, Brian L. Allman, Dale W. Laird. Large-Pore channels in hearing and noise-induced hearing loss. Association for research in Otolaryngology, Baltimore, Maryland, United States. (February 2017).

Julia M. Abitbol, John J. Kelly, Kevin Barr, Brian L. Allman, Dale W. Laird. The Role of Pannexin1 and Pannexin3 in the Auditory System. JAX mouse auditory research workshop. Bar Harbour, Maine, United States. (September 2016).

Julia M. Abitbol, John J. Kelly, Kevin Barr, Brian L. Allman, Dale W. Laird. The Role of Pannexin1 and Pannexin3 in the auditory system. London Health Research Day, London, Canada. (2016).

Julia M. Abitbol, John J. Kelly, Kevin Barr, Brian L. Allman, Dale W. Laird. The Role of Pannexin1 and Pannexin3 in the auditory system. American Society of Cell Biology, San Diego, California, United States (2015).

Julia M. Abitbol, John J. Kelly, Kevin Barr, Ashley Schormans, Brian L. Allman, Dale W. Laird. The Role of Pannexin 3 in Auditory Ossicle Development and Hearing**.** Southern Ontario Neuroscience Association (SONA), London, Ontario, Canada. (2015).

Julia M. Abitbol, Ashley L. Schormans, Marei Typlt, Brian L. Allman. The Effects of Chronic Stress on Noise-Induced Hearing Loss. London Health Research Day, London Convention Center, London, Canada. (2013).

Awards, Honours, and Scholarships

2019/06	Suzanne M. Bernier publication award 2019 for paper "Mice harbouring an oculodentodigital dysplasia-linked Cx43 G60S mutation have severe hearing loss"
2019/05	Marine Biology Laboratory travel award to attend "The Biology of the Inner Ear" workshop, $1200 USD
2019/05	Selected cover image from figure 5f from paper "Double deletion of *Panx1* and *Panx3* affects skin and bone but not hearing". *Journal of Molecular Medicine*, May cover
2019/04	Feature platform presentation winner, London Health Research Day 2019, $650 CAD
2018/05	Selected cover image for Volume 131, Issue 9 in the *Journal of Cell Science*
2018/04	First authour interview feature in the *Journal of Cell Science* (http://jcs.biologists.org/content/131/9/jcs219196)
2017/10	Best Poster Presentation Award, Anatomy and Cell Biology research day, $150
2017/07	Best Poster Presentation Award, International Gap Junction Meeting, $150 (Euro)
2017	Travel Scholarship, International Gap Junction Meeting, $250 (Euro)
2017-2020	NSERC CGS doctoral Scholarship, $35,000/yr
2017-2018	Ontario Graduate Scholarship, University of Western Ontario, $15,000 (declined)
2017-2019	Western Graduate Research Scholarship, value $7,000/yr
2016/11	Publication of the month; Schulich Medicine and Dentistry's Current Affairs
2016	JAX Lab mouse research travel scholarship, Bar Harbour Maine,

	$1,500 (USD)
2016-2017	Ontario Graduate Scholarship, University of Western Ontario, $15,000
2016/04	Anatomy and Cell Biology Travel Award, University of Western Ontario, $500
2014-2017	Western Graduate Research Scholarship, value $4,500/yr

Teaching Assistant Positions:

2016-2017	Teaching assistant for first year graduate course in Neuroscience 9500
2015-2016	Teaching assistant for third year undergraduate Anatomy and Cell Biology 3319 Systemic Human Anatomy course
2014-2015	Teaching assistant for third year undergraduate Anatomy and Cell Biology 4451 Integrative Neuroscience course